



SCUOLA DOTTORALE IN  
GEOLOGIA DELL'AMBIENTE E DELLE RISORSE  
(SDIGAR)

Ciclo XXIII

*RECONSTRUCTION OF BURIAL AND EXHUMATION HISTORY OF THE  
APENNINIC-MAGHREBIAN FOLD-AND-THRUST BELT IN EASTERN SICILY  
BY MEANS OF INTEGRATED STUDIES OF THERMAL AND  
THERMOCHRONOLOGICAL CONSTRAINS*

Lea Di Paolo

A.A. 2010/2011

**Tutor**

Prof.ssa Sveva Corrado

**Direttore SDIGAR**

Prof. Domenico Cosentino

**Correlatori**

Dott. Luca Aldega

Dott.ssa Maria Laura Balestrieri

**Revisori**

Prof. Stefano Mazzoli

Università di Napoli Federico II  
Dipartimento di Scienze della Terra

Prof. Massimiliano Zattin

Università degli Studi di Padova  
Dipartimento di Geoscienze

## ACKNOWLEDGEMENTS

First of all, I would like to express my gratitude to my supervisor, Prof. Sveva Corrado, whose constant guidance and support, enthusiasm and inspiration, enabled me to develop this research project.

I am extremely indebted to Dr. Luca Aldega for his irreplaceable daily help that enhanced every single page of this thesis.

I am grateful to Dr. Sabina Bigi for her encouragement to undertake the PhD doctorate and for the confidence she put in me.

Dr. Maria Laura Balestrieri and Dr. Valerio Olivetti are acknowledged for giving me the possibility to use their thermochronological data and for the discussion on the burial and exhumation history results on the Eastern Sicily fold-and-thrust belt.

I would also like to thank Dr. Roberta Somma and Dr. Rosanna Maniscalco who have contributed significantly to the results presented in Chapter 3 of this thesis and also for their help and hospitality during the fieldwork.

I am thankful to the Indiana Geological Survey, to Dr. Maria Mastalerz and Dr. Arndt Schimmelmann for the facilities given for conducting the research on organic matter by means of FTIR analysis while in Bloomington and for their kind hospitality.

Thanks are also due to Prof. Stefano Mazzoli and Prof. Massimiliano Zattin who provided stimulating and helpful reviews of my Thesis.

I also want to thank Dr. Sergio Lo Mastro for the time spent on XRD samples scanning.

Thanks to all that have orbited the “Io e la geologia...” PhD study room, Matteo, Chiara, Lilli, Massimetto, Luca, Gianluca, Giorgia... and in particular, Sandro and Danilo for keeping me in a good mood even when it was very difficult and for the time spent to discuss anything but my thesis work.

Thanks also to all the international mix of PhD students and to the Italian brain drain I met in Bloomington, in particular my roommate Dani, Hongji and Aga with whom I had the pleasure to explore the Sunshine State and the Midwest and Ling for the pleasant chats green tea-based.

Thanks to Irene for embarking with me on these last delirious months and to my old roommates, Dalila, Giorgio, Ileana and Naida.

A special thanks goes to Damiano for the lifts to the airport, the English translations, the four-leaf clover he found for me and many other reasons... to him, I would like to dedicate the Chapter 3 of this thesis.

Finally, many thanks to my parents, my sister and my dear friends Fabio, Fabrizio, Lele, Mario and Nicoletta... sui quali posso sempre contare...

## TABLE OF CONTENTS

ABSTRACT	6
RIASSUNTO	9
<b>CHAPTER 1 - INTRODUCTION</b>	<b>12</b>
1.1. Aims and methodologies	12
1.2. Outline of the thesis	13
1.3. Evolution of this study	14
1.4. Geological setting of Eastern Sicily	16
1.4.1 Previous studies	19
<b>CHAPTER II- METHODS</b>	<b>22</b>
2.1. Optical study of organic matter dispersed in sediments aimed at the analysis of the thermal evolution of sedimentary basins	22
2.1.1. Generalities: Organic Matter dispersed in sediments and its thermal evolution	22
2.1.2. Thermal maturity parameters used in this Thesis	25
2.1.2.1. Vitrinite Reflectance	25
Sample preparation and analysis	26
2.1.2.2. Fourier transform infra red spectroscopy (FTIR) analysis	27
Concentration of kerogen	29
2.2. XRD study of clay minerals for thermal evolution of sedimentary basins	30
2.2.1. Generalities: clay minerals and their thermal evolution	30
Sample preparation and analysis	33
2.3. Low temperature thermo-chronology for exhumation of sedimentary successions	34
2.3.1. Generalities	34
2.4. Thermo-structural modelling	37
2.5. GIS analysis	38
<b>CHAPTER III - INTERNAL ZONE (PELORITANI MTS.)</b>	<b>40</b>
3.1. Introduction	40
3.2. Geological and structural setting	41
3.3. Geological features of sampled lithostratigraphic units	45
3.4.1. Organic matter data	46
3.4.1.1. Stilo Capo d'Orlando Formation	46
3.4.1.2. Antisicilide Unit	47



3.4.1.3. Serravallian-Messinian siliciclastic deposits	50
3.4.2. Clay mineralogy data	50
3.4.2.1. Stilo Capo d'Orlando Formation	50
3.4.2.2. Antisicilide Unit	51
3.4.2.3. Serravallian-Messinian siliciclastic deposits	52
3.4.3. Structural data	52
3.4.3.1. Stilo Capo d'Orlando Formation	52
3.4.3.2. Antisicilide Unit	54
3.4.3.3. Serravallian-Messinian siliciclastic deposits	54
3.5. Discussion	55
3.5.1. Isopach and paleoisopach map reconstruction of the Stilo-Capo d'Orlando Basin	55
3.5.2. Reconstruction of the paleogeothermal gradient during Oligocene Miocene time	56
3.5.3. Burial and thermal history of the Stilo Capo d'Orlando depocentre	58
3.5.4. Sedimentary vs. tectonic burial of the Peloritani Mts. northern sector	59
3.6. Conclusion	64
<b>CHAPTER IV - EXTERNAL ZONE (MT. JUDICA UNIT)</b>	<b>65</b>
4.1. Introduction	65
4.2. Geological setting	67
4.3. Results	73
4.3.1 - FTIR on organic matter	73
4.3.2. XRD on clay minerals	76
4.4. Discussion	79
4.4.1. Thermal evolution of Mt. Judica succession	79
4.4.1a. Extracting information on thermal maturity from FTIR spectra	79
4.4.1b. Thermal modelling	81
4.4.2. Along-strike variations of the Gela nappe front	84
4.4.3. Application of critical taper analysis to the eastern Sicily fold-and-thrust belt	87
4.5. Conclusion	91
<b>CHAPTER V - EARLY FOREDEEP DEPOSITS ("NUMIDIAN FLYSCH")</b>	<b>92</b>
5.1. Introduction: Geological setting of the Numidian Flysch Basin in the Mediterranean area	92
5.2. Geological and structural setting of the Numidian Flysch in Eastern Sicily	93
5.3. Results	99
5.3.1. Maragone Unit	99
5.3.2. Nicosia Unit	102
5.3.3. Mt. Salici Unit	105
5.3.4. Clays and Glauconitic Sandstones of the Mt. Judica Unit	105

5.4. Discussion	105
Thermal interpretation of the tectono-stratigraphic units	105
5.4.1. Maragone Unit	105
5.4.2. Nicosia Unit	106
5.4.3. Mt. Salici Unit	106
5.5. Conclusion	106
<b>CHAPTER VI - BURIAL AND EXHUMATION ALONG THE OROGENIC TRANSECT</b>	<b>108</b>
REFERENCES CITED	121
APPENDIX	

## ABSTRACT

The reconstruction of burial and exhumation history of sedimentary rocks can provide, when linked with the structural and stratigraphic records, important time-temperature constraints to the thrust belt dynamics. The purpose of this study has been to decipher the maximum paleo-temperatures and the exhumation rates of the sedimentary successions constituting the Eastern Sicily fold-and-thrust belt through a multidisciplinary approach based on the integration of different thermal and thermo-chronological methodologies.

In particular, three sectors of the Eastern Sicily fold-and-thrust belt were investigated: the Internal Zone of the Peloritani Mts., the frontal part of the thrust belt in the Mt. Judica area and the outcropping area of the Numidian Flysch.

In the Peloritani Mts., the integration of Vitrinite reflectance and mixed-layered clay minerals with published apatite fission-track and (U-Th)/He ages allowed to reconstruct the paleo-geothermal gradient of the Stilo-Capo d'Orlando basin in Oligocene-Miocene times, to constrain its burial evolution and discriminate between areas where it has been affected by sedimentary and/or tectonic load. In the southern area of the basin, organic and inorganic thermal parameters increase as function of depth suggesting that their evolution is ruled by sedimentary burial. They recorded a decrease in paleo-geothermal gradient values which marked the evolution of the basin from a fore-arc to a thrust-top setting during the convergence-collision process between the Calabria-Peloritani Arc and the African plate. Differently, in the northern edge of the basin, high vitrinite reflectance values (0.46-0.58%) indicate that the thermal evolution of this area was controlled by tectonic burial related to a late Langhian-early Serravallian out-of-sequence thrusting. The tectonic overburden has been totally removed by extensional tectonics and/or erosion since Late Miocene. The short time span at maximum temperature (<2 Ma) elapsing between thrust stack emplacement and the beginning of its removal have allowed only vitrinite reflectance and thermo-chronological indicators to record this compressive reactivation.

In the Mt. Judica area, the integration of X-ray diffraction (XRD) data concerning the illite content in mixed layer illite-smectite with data derived from Fourier Transform Infrared spectroscopy (FTIR) on H-rich organic matter allowed to constrain the burial-

exhumation path of the Mt. Judica sedimentary succession cropping out in tectonic window in Eastern Sicily.

Thermal constraints showed that the Mt. Judica succession experienced paleotemperatures in the range of 100-130 °C in late diagenetic conditions and early mature stage of hydrocarbon generation with a general depth-dependent thermal maturity feature. Specifically, the illite content in mixed layer I-S increases from 50 to 76% and FTIR-derived indexes suggest a thermal maturity equivalent to  $VR_o$  values of at least 0.5-0.7%. As a whole, the Mt. Judica succession experienced maximum tectonic burial (ranging between 2.4 and 3.2 km) during the Middle Miocene as a result of the emplacement of the Allochthonous Units atop it. The subsequent breaching phase characterized by up-thrust geometries, and erosion during Pliocene times ruled out the Mt. Judica exhumation. This last tectonic phase did not overprint thermal maturity because the extent of overthrusting was negligible when compared with the magnitude of vertical movements. Restoration of balanced cross-sections revealed an increase of shortening from the salient to the Mt. Judica recess with values from 12.3 to 23.9 km, consistent with the increase of tectonic thickening of the fold-and-thrust belt. Integration of maximum burial and shortening values along the strike of the Sicilian fold-and-thrust belt allowed to reconstruct the wedge paleo-geometry in the Mt. Judica recess area, to investigate the along-strike variations of the tectonic overburden, and to discuss the geodynamic causes of these changes. These results were compared with theoretical models of wedge dynamics.

For the Numidian Flysch thrust stack an increasing level of diagenesis from the uppermost to the lowermost tectono-stratigraphic units has been observed. From the top to the bottom of the tectonic pile, the Nicosia Unit showed the lowest % I values in I-S mixed layers in the range of 20-50% and vitrinite reflectance data between 0.36-0.42% in the immature stages of hydrocarbon generation. The Mt. Salici Unit displayed random ordered mixed layers I-S with an illite content of 50-55%. These data correlated to slightly higher levels of diagenesis than those recorded in the Nicosia Unit, suggesting that sedimentary burial is the main factor affecting the thermal maturity of both units. The lowermost of the Numidian tectonic pile (Maragone Unit) revealed mixed-layered ordered structures with % of I in I-S between 66 and 79% indicating the highest levels of thermal maturity for the Numidian Flysch.

The integration of organic and inorganic thermal parameters with thermo-chronological data performed for my PhD project on the main outcropping tectono-stratigraphic Units in Eastern Sicily, contributed to the reconstruction of the burial and exhumation history of the Peloritani Mts. and the Apenninic-Maghrebian fold-and-thrust belt between the Nebrodi Mts. and the Hyblean Foreland.

## RIASSUNTO

La ricostruzione dei carichi tettonico/sedimentari e dell'esumazione delle successioni sedimentarie che costituiscono le catene orogeniche, integrata con dati stratigrafico-strutturali, può fornire importanti vincoli termici e temporali alla dinamica delle catene orogeniche. L'obiettivo di questa Tesi è stato quello di ricostruire l'evoluzione termica e termo-cronologica delle successioni sedimentarie, costituenti le unità della catena Appenninico-Maghrebide affioranti in Sicilia orientale, per porre nuovi vincoli quantitativi alla definizione di un modello di evoluzione geodinamica neogenico-quadernaria dell'orogene.

E' stato utilizzato un approccio multidisciplinare basato sull'integrazione di differenti metodologie di analisi termica e termocronologica tipiche dell'Analisi di Bacino. Lo studio ottico e all'infrarosso della materia organica dispersa nei sedimenti e lo studio ai raggi x dei minerali delle argille, sostanzialmente dall'analisi delle tracce di fissione in apatite, ha permesso di quantificare i massimi carichi sedimentari e/o tettonici subiti dalle successioni sedimentarie studiate. L'analisi delle tracce di fissione in apatite inoltre, ha permesso di definire i tassi e l'entità dell'esumazione. I dati termici e termocronologici ottenuti sono stati utilizzati per calibrare modelli termici e di seppellimento monodimensionale attraverso l'utilizzo del software Basin mod 1D e per creare un database in QuantumGIS software che ha consentito la realizzazione di carte tematiche. Le informazioni derivanti dai diversi settori sono state integrate, insieme con ricostruzioni già esistenti per altre porzioni della catena (p.e., prisma di accrezione sicilide) per ricostruire la storia esumativa dell'intero sistema orogenico affiorante in Sicilia orientale.

In particolare sono stati indagati tre settori della catena orogenica: la Zona Interna dei Monti Peloritani, il fronte orogenico nell'area di Monte Judica e l'area di affioramento del Flysch Numidico.

Nei Monti Peloritani, l'integrazione della riflettanza della vitrinite con gli strati misti dei minerali delle argille e con dati pubblicati di tracce di fissione in apatite ed età (U-Th)/He hanno permesso di ricostruire il gradiente paleogeotermico del bacino di Stilo-Capo d'Orlando nell'Oligo-Miocene e di vincolarne la storia di seppellimento, distinguendo tra aree affette da carico tettonico e/o sedimentario. Nell'area meridionale del bacino, i parametri termici organici ed inorganici aumentano in funzione della profondità suggerendo un'evoluzione termica e di seppellimento regolata dal carico sedimentario. E' stata osservata una diminuzione dei valori di gradiente paleogeotermico che marca l'evoluzione del bacino di Stilo-Capo d'Orlando da un assetto di fore-arc nell'Oligocene ad uno di thrust-top nel Miocene in seguito alla collisione tra l'arco Calabro-Peloritano e la placca Africana.

Differentemente, nel settore più settentrionale del bacino, alti valori di riflettanza della vitrinite (0.46-0.58%) indicano che l'evoluzione termica di questa area è stata regolata dalla messa in posto di un carico tettonico relativo ad una riattivazione in fuori sequenza delle zone più interne avvenuta tra il Langhiano superiore e il Serravalliano inferiore.

Il carico tettonico è stato velocemente rimosso, a partire dal Miocene Superiore, per erosione e per tettonica estensionale che ha accomodato la deposizione delle marne serravalliane-messiniane sui blocchi del complesso metamorfico ribassati.

I minerali delle argille non hanno registrato la riattivazione in compressione dei settori interni della catena a causa del breve intervallo di tempo alle massime temperature (<2Ma), intercorso tra la messa in posto del carico tettonico e l'inizio della sua rimozione.

Nell'area di Monte Judica al fronte della catena orogenica, l'integrazione di dati derivanti dall'analisi quantitativa in diffrazione ai raggi X riguardanti il contenuto di illite nell'interstratificato misto illite-smectite con dati derivanti dalla Spettroscopia all'Infrarosso in Trasformata di Fourier (FTIR) su materia organica ricca in idrogeno, ha permesso di vincolare la storia di seppellimento ed esumazione della successione sedimentaria di Monte Judica affiorante in finestra tettonica.

I vincoli termici hanno permesso di determinare per la successione di Monte Judica paleotemperature massime raggiunte tra 100 e 130 °C corrispondenti a condizioni diagenetiche tardive ed ad un primo stadio maturo di generazione degli idrocarburi con un generale aumento della maturità termica in funzione della profondità. Nel dettaglio, il contenuto di illite nell'interstratificato misto I-S aumenta dal 50 al 76% e gli indici di maturità derivati dall' FTIR suggeriscono una maturità termica equivalente a valori di almeno 0.5-0.7% di VR<sub>0</sub>. In definitiva, la successione di Monte Judica ha subito il seppellimento tettonico massimo (tra 2.4 e 3.2 km) nel Miocene Medio a causa dell'accavallamento dell'Unità Alloctona Superiore (complesso Sicilide e Flysch Numidico).

La successiva fase deformativa nel Pliocene, caratterizzata da sovrascorrimenti ad alto angolo ed erosione, ha regolato l'esumazione dell'Unità di Monte Judica non influenzando la storia termica. La ricostruzione delle sezioni bilanciate ha mostrato un aumento del raccorciamento dal saliente di Gela al recesso di Monte Judica con valori da 12.3 a 23.9 km, in accordo con l'aumento dell'ispessimento tettonico della catena a pieghe e sovrascorrimenti. L'integrazione del massimo seppellimento con i valori di raccorciamento calcolati lungo lo strike della catena a pieghe e sovrascorrimenti in Sicilia

orientale, ha permesso di ricostruire la paleogeometria del cuneo orogenico nell'area di recesso, di investigare le variazioni del carico tettonico lungo lo strike della catena e di discuterne le cause geodinamiche.

Per l'impilamento tettonico del Flysch Numidico è stato osservato un aumento della maturità termica dalle Unità tettono-stratigrafiche sommitali a quelle basali. Dal top alla base della pila tettonica, l'Unità di Nicosia ha mostrato i valori più bassi di percentuale di illite nell'interstratificato misto I-S (tra il 20 e il 50%) e di riflettanza della vitrinite (tra 0.36 e 0.42%) corrispondenti allo stadio immaturo di generazione degli idrocarburi. L'Unità di Mt. Salici ha rivelato un contenuto di I nell'interstratificato misto I-S di 50-55%. Questi dati sono stati correlati con livelli diagenetici leggermente più alti rispetto all'Unità di Nicosia suggerendo che il fattore principale che ha influito sulla maturità termica di entrambe le unità è stato il carico sedimentario. L'Unità tettonica strutturalmente più bassa (l'Unità di Maragone) ha mostrato una percentuale di illite nell'interstratificato misto I-S tra il 66 e il 79% indicando i livelli più alti di maturità per il Flysch Numidico.

L'integrazione di parametri termici organici ed inorganici con dati termocronologici prodotti durante il dottorato di ricerca sulle principali Unità tettono-stratigrafiche affioranti in Sicilia orientale, hanno contribuito alla ricostruzione della storia di seppellimento ed esumazione dei Monti Peloritani e della catena a pieghe e sovrascorrimenti Appenninico-Magrebide tra i Monti Nebrodi e l'avampaese Ibleo.



## CHAPTER 1 - INTRODUCTION

### 1.1. Aims and methodologies

Characterizing the timing and magnitude of vertical motions of rocks within thrust belts is critical for understanding their development and evolution. Although structural and metamorphic studies have begun to address these fundamental issues, remarkably little is known of the timing, duration, and rates of thrust belt construction, thickening, and unroofing. Deciphering thermal-burial histories and exhumation rates of sedimentary rocks can provide, when linked with the structural record, critical time-temperature constraints necessary for a more complete understanding of thrust belt dynamics.

The aim of this Thesis is the reconstruction of the burial and exhumation history of the tectono-stratigraphic Units and syn-orogenic sediments outcropping in Eastern Sicily (Fig. 1.1). This region is particularly suitable for these kinds of studies because it is a well-known portion of the orogen from a stratigraphic and structural point of view and it is also peculiar for the presence of the boundary between the Internal and External Zones constituting the orogen. In addition, the bibliography in this sense is very poor.

A multidisciplinary approach based on the integration of different thermal and thermochronological methodologies was used to achieve this aim. The used methods are typical of Basin Analysis, developed for oil exploration and then applied to geodynamic issues.

The optical and infra-red study of the organic matter dispersed in sediments and the X-ray diffraction study of clay minerals, substantiated by apatite fission track analyses, allowed the quantification of maximum sedimentary and/or tectonic loads the studied successions underwent. Furthermore, the apatite fission track analysis provided the definition of the exhumation timing, rates and magnitudes of exposed successions.

Basin Mod 1D software applications, that jointly elaborate data from stratigraphic-structural and paleo-thermometric databases, allowed the creation of mono-dimensional thermo-burial models, while QuantumGis and ArcGIS softwares allowed the creation of database of geological and paleo-geothermal data obtained from literature, fieldwork and laboratory and the construction of thematic maps.

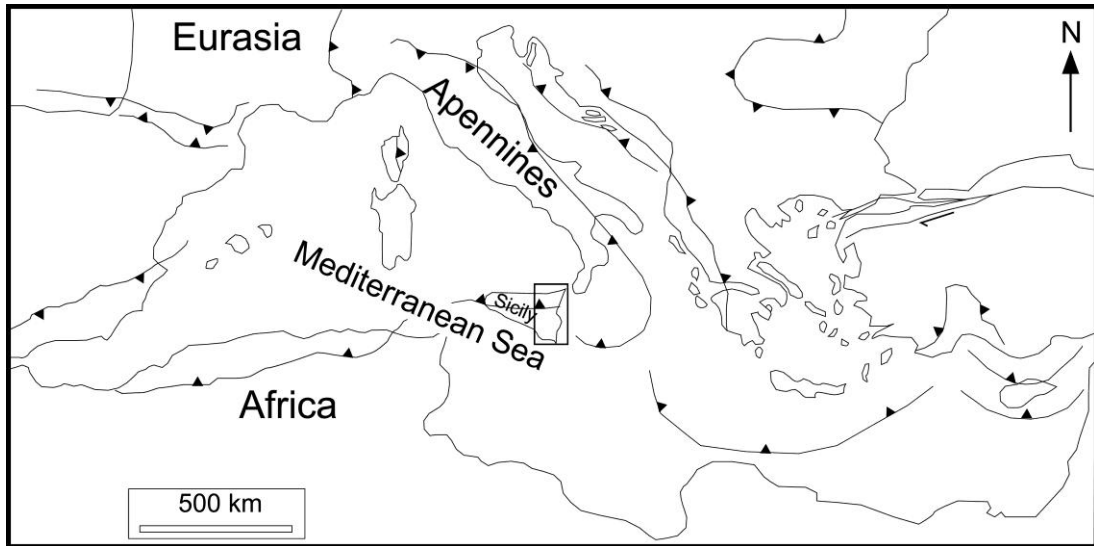


Figure 1.1 - Tectonic sketch map of the Mediterranean area. Rectangle shows the studied area.

## 1.2. Outline of the thesis

Chapter 1 is the present general introduction to aims, methodologies and evolution (Fig. 1.2) of this research. In addition, it offers a description of the geological setting and previous thermal and thermo-chronological studies of the investigated area.

Chapter 2 introduces theoretical aspects and analytical procedures of the applied methodologies and a description of the used software.

Chapter 3 focuses on the thermal and structural evolution of the Internal zones of the Eastern Sicily fold-and-thrust belt (Peloritani Mts.).

Chapter 4 treats the thermal and structural evolution of the Mt. Judica Unit at the front of the orogen.

Chapter 5 presents the thermal results of the Early foredeep deposits (Numidian Flysch).

In the chapter 6, which represents a key part of this thesis, the results coming from the different studied areas are integrated with previous studies to reconstruct the burial and exhumation history along the eastern Sicily transect.

### 1.3. Evolution of this study

The first few months were spent reviewing the literature of the sedimentary successions outcropping in the Eastern Sicily. The research was focused on the study of the most recent bibliography of the analytical Techniques and theory on thermal evolution of sedimentary basins used and on the existing geological mapping, geological-structural, stratigraphic-sedimentological, biostratigraphical and petrographic data of Eastern Sicily.

Following a critical review of bibliographic data, three key sectors for structural investigation and sampling for thermal and thermo-chronological analysis were identified.

Samples for organic matter optical analysis and clay mineralogy were collected in the field and prepared for lab analysis. The Vitrinite Reflectance data, were performed and processed, evaluating the interpretative problems related to alteration and rearrangement of fragments, and correlated with data derived from the analysis of clay mineralogy and apatite fission tracks.

In the first half of the second year, the reconstruction of the thermal evolution of the sedimentary successions cropping out in the Peloritani Mts. was performed and a geological interpretation was proposed.

The second half was spent both on the studies of the Mt. Judica Unit and Numidian Flysch, and on a bibliographic research about further methods of organic matter thermal analysis. Several field geological campaign were carried on to collect samples and for structural analysis.

The first three months of the third year were spent at the Indiana Geological Survey and Department of Geology of the Indiana University, Bloomington, USA, as a visiting scholar. Collected samples of the Mt. Judica Unit were analyzed with FTIR instrumentation in collaboration with Dr. M. Mastalerz and Dr. A. Schimmelmann.

The rest of the time was spent in unravelling the thermal evolution of the Mt. Judica Unit and of the Numidian Flysch and to construct a model of geodynamic evolution of the orogen.

Throughout the duration of this study, poster and oral presentations were given at national and international conferences:

1. *Meeting in Memory of Angelo di Grande and Mario Grasso*, Catania, June 2008;
2. *EAGE Conference & Exhibition*, Rome, June 2008;
3. *Geoitalia 2009, VII Forum italiano di Scienze della Terra*, Rimini, September 2009;
4. *EAGE Conference & Exhibition*, Barcellona, June 2010.

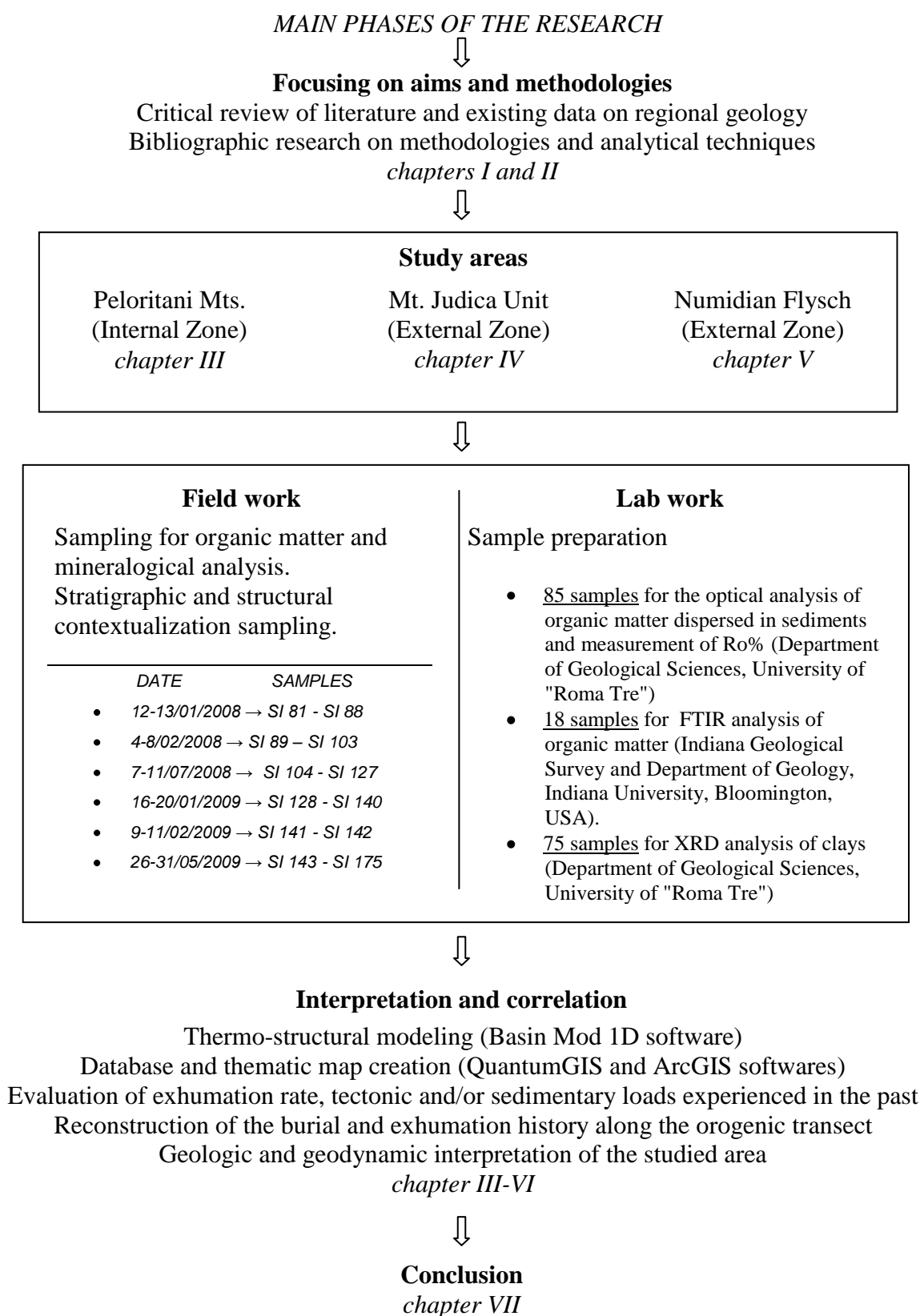


Figure 1.2 - Diagram showing the study evolution and thesis organization.

## 1.4. Geological setting of Eastern Sicily

In the western Mediterranean area (Fig. 1.3), the convergence and continental collision between the European, Iberian, African and Adria plates have been leading since the Late Cretaceous to the formation of thousands of kilometers long arcuate Alpine orogen (Dewey et al., 1989; Faccenna et al., 2001). Particularly, the western Peri-Mediterranean Alpine orogen is classically subdivided into two main structural zones indicated as Internal and External Zones (Fig. 1.3; Martín-Algarra et al., 2000; Vera, 2004; Perrone et al., 2006 and references therein). The Internal Zones, cropping out in the hinterland of the Betic Cordillera, Rif, Kabylies, Northern Apennines, and in the Calabria-Peloritani Arc, consist of nappes deriving from the deformation of original paleo-geographic domains belonging to the European plate paleo-margin (Bouillin, 1984) or, according to recent reconstructions, to a small continental crust block -the Mesomediteranean Block- (Martín-Algarra and Vera, 2004). Differently, the External Zones, exposed on the outer portions of the Betic Cordillera, African and Sicilian Maghrebids, Northern and Southern Apennines, are made up of tectono-stratigraphic units deriving from the deformation of paleo-geographic domains belonging to the south Iberian, African and western Adria paleo-margins (Martín-Algarra et al., 2000). Jurassic to Miocene clastic deposits, sedimented in the original Flysch Basin (Guerrera et al., 2005), form the tectono-stratigraphic units interposed between the Internal and External Zones (Fig. 1.3).

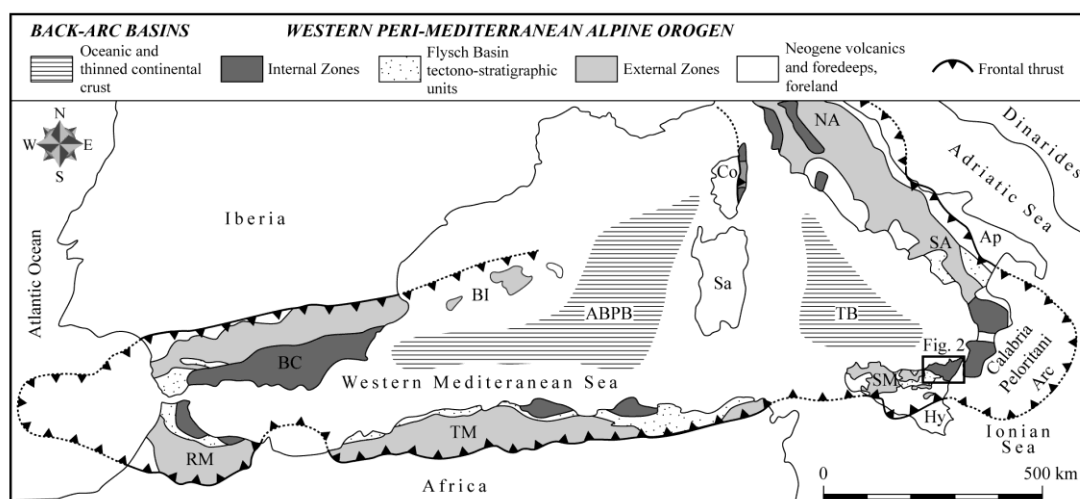


Figure 1.3 - Tectonic sketch map of the western Mediterranean region. Acronyms - ABPB: Algero-Balearic-Provençal Basin; Ap: Apulia Plateau; BC: Betic Cordillera; BI: Balearic Islands; Co: Corsica; Hy: Hyblean Plateau; NA: Northern Apennines; RM: Rifian Maghrebids; Sa: Sardinia; SA: Southern Apennines; SM: Sicilian Maghrebids; TB: Tyrrhenian Basin; TM: Tellian Maghrebids.

In Eastern Sicily the thrust belt is formed by both the two main structural zones: the Internal Zone to the north and the External Zone to the south.

The Internal Zone consists of south-verging thin crystalline nappes and Late Oligocene-Messinian syn-orogenic deposits of the Peloritani Mts. (Kablian-Peloritan-Calabrian Units sensu Lentini et al. 1996; Fig. 1.4).

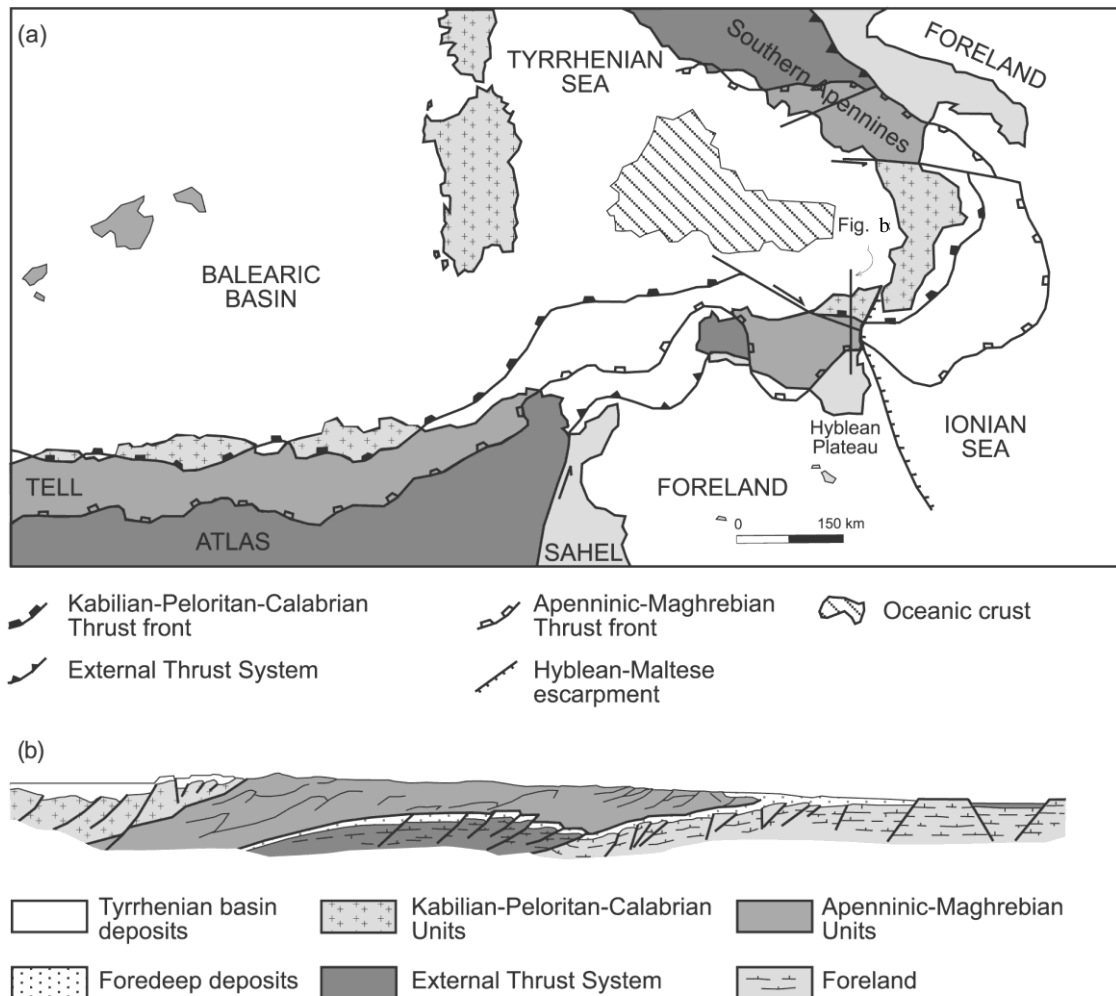


Figure 1.4 – (a) Tectonic map of Sicily, Tyrrhenian Sea, and adjacent areas; (b) Schematic regional cross section across Eastern Sicily reworked and modified after Bianchi et al. 1996.

The External Zone is made up of two main tectono-stratigraphic domains: the Apenninic-Maghrebian belt and the External Thrust System (Fig. 1.4).

The crystalline nappes of the Kabilian-Peloritan-Calabrian belt still widely preserve the Variscan signature (De Gregorio et al., 2003; Somma et al., 2005). Some nappes record Alpine metamorphism (Atzori et al., 1994), followed by substantial exhumation prior to

their final emplacement atop the Apenninic-Maghrebian Units, as indicated by zircon and apatite fission-track data (Thomson, 1994). This early exhumation is controlled by synorogenic extension (Cutrupia and Russo, 2005; Somma et al., 2005), predating the overthrusting onto the Apenninic-Maghrebian belt in Early Miocene times (Amodio-Morelli et al., 1976).

The Apenninic-Maghrebian belt is made up of imbricate sheets of Mesozoic-Tertiary rocks (Lentini et al., 1995). Its structurally highest tectono-stratigraphic units, well exposed in the Nebrodi Mts., are represented by the remnants of the Neotethyan accretionary wedge, made up of part of the Sicilide Complex (Mt. Soro, Troina, and far-travelled Sicilide Units) consisting of a Late Cretaceous to Early Miocene pelagic succession and by the Oligocene-Langhian foredeep deposits of the Numidian Flysch (Carbone et al., 1990; Lentini et al. 2000).

Tectonically beneath these units, the more external Imerese-Sicano Unit is present. It crops out in the tectonic window of Mt. Judica area at the front of the Eastern Sicily fold-and-thrust belt. These two Allochthonous Units form a thin-skinned thrust system that rest on a more External Thrust System (ETS) (Fig. 1.4). This system derived from the imbrication of a thick carbonate platform sequence with interleaved marls and mafic volcanic levels (Bianchi et al., 1989; Billi et al., 2006) detached from the flexure continental sectors of the Africa foreland (Lentini et al., 1996, Fig. 1.4).

The present-day structural setting of the orogen is the result of a poliphasic deformation started since Early Miocene times with the emplacement of the allochthonous Units (Numidian Flysch, Sicilide Complex and the Imerese-Sicano Unit) onto the Hyblean foreland through low angle regional thrusts (Bello et al., 2000) and with the overthrusting of the metamorphic massif of the Peloritani Mts. onto the innermost sedimentary units of the Eastern Sicily fold-and-thrust belt (Amodio-Morelli et al. 1976).

During Upper Miocene–early Pliocene times the development of the External Thrust System strongly modified the geometric relationships of the Allochthonous Units, producing the internal stacking of the Mt. Judica succession (Bello et al. 2000) and break-back, out of sequence, propagation of back-thrusts in central-north Sicily (Carbone et al. 1990; Grasso et al. 1995).

#### *1.4.1 Previous studies*

In recent years there have been several contribution aiming at defining maximum burial depths and exhumation rates of the sedimentary successions and tectonic units forming the Eastern Sicily fold-and-thrust belt.

Thomson (1994) and Olivetti et al. (2010), studying the Internal Zone of the Eastern Sicily fold-and-thrust belt by means of apatite fission-track (AFT) and (U-Th)/He analyses, have been reconstructed in the crystalline rocks of the Peloritani Mts. two main cooling phases since Oligocene times.

Thomson (1994) ascribed the older exhumation phase of the Peloritani Mts. between 35 and 15 Ma and Olivetti et al. (2010), recognized a second exhumation phase (AFT ages < 15 Ma) with a rate of 0.3 mm/yr calculated from the difference between young AFT and (U-Th)/He ages (AFT ages range between  $29.0 \pm 5.5$  Ma and  $5.5 \pm 0.9$  Ma while (U-Th)/He ages vary from 19.4 Ma to 3.3 Ma) post-dating the Stilo-Capo d'Orlando deposition.

Several Authors have studied the External Zone. The thermal state of the Mt. Judica Unit was investigated by Roure et al. (1990) and their burial evaluation, about 3 km, was confirmed by Aldega et al. (2007), although Larroque et al. (1996) and Dewever et al. (2006), observed homogenization temperatures of fluid inclusions ( $235 \pm 10$  °C in the calcite veins for the deep sole thrust) that suggest deeper burial and/or hot fluid circulation.

Aldega et al. (2007) proposed a first thermal quantitative characterization for most of the units of the eastern sicily fold-and-thrust belt on the basis of optical organic matter maturity and X-ray diffraction clay-mineralogy data, observing a general trend of decreasing thermal maturity of sediments moving from hinterland to foreland and from older to younger stratigraphic units (Fig. 1.5).

Corrado et al. (2009) providing new thermal and thermo-chronological constraints, recognize a warmer core made up of the Mt. Soro and Troina Units and two colder rims constituted by the far-travelled Sicilide and Antisicilide Units. The former is characterized by vitrinite reflectance values ranging between 0.6 and 0.96% and illite content in mixed layer I-S between 60 and 85%, the second by vitrinite reflectance ranging between 0.41 and 0.56% and illite content in mixed layer I-S between 25 and 50%. AFT data indicate that fission tracks were partially to totally annealed during wedge accretion and that the subsequent exhumation occurred mainly in Burdigalian times (17.7-



20.2 Ma). AFT data from Antisicilide Unit indicate low levels of thermal maturity in early diagenetic conditions because of no annealing of tracks. The Mt. Soro and Troina Units were involved into trench development before Early Miocene times and acquired a late diagenetic signature due to thrust-stacking at deep levels whereas the far-travelled Sicilide and Antisicilide Units kept their early diagenetic signature at shallower or outer structural levels of the accretionary wedge and were remobilized since late Burdigalian-Langhian times by gravity-driven processes (Fig. 1.6).

Barbera et al. (2009), using XRD clay mineralogy analysis, chemical composition and multivariate analysis on shales belonging to several tectono-stratigraphic units of the Apenninic-Maghrebian confirmed the diagenetic conditions of the Sicilide accretionary wedge. In particular the diagenetic grade increases from the south-west, where the external Numidian Flysch (NS) and the VS underwent low diagenetic conditions, to the north-east where the originally inner and structurally highest units (CSS; Monte Soro and Upper Scagliose shales) reached high-grade diagenetic stages in agreement with Aldega (2007) and Corrado (2009).

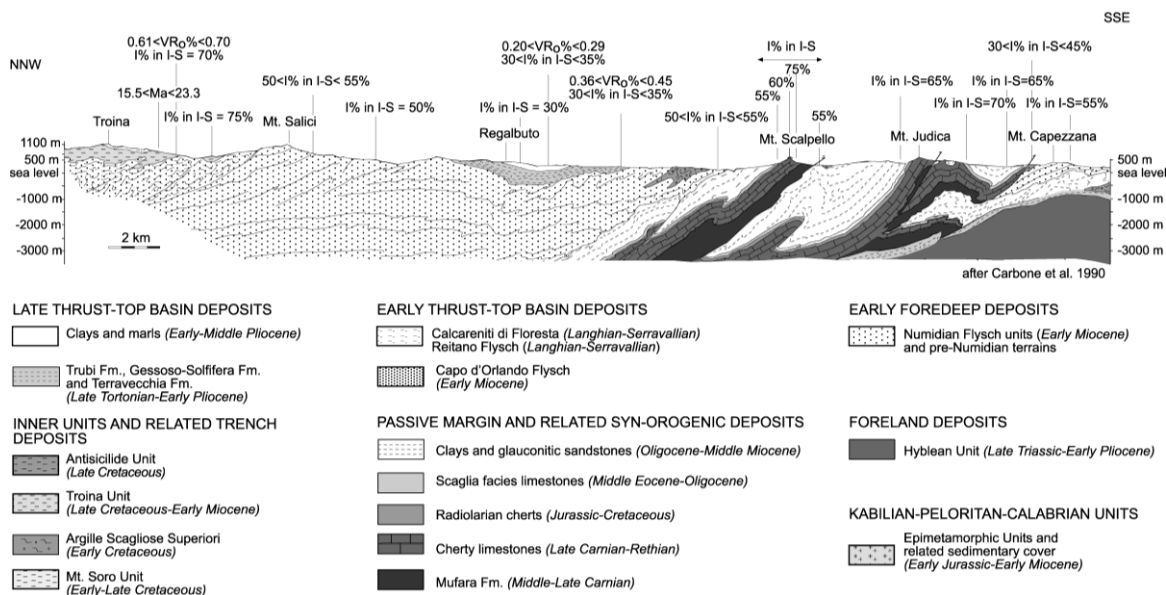


Figure 1.5 – Schematic geological cross section between Troina village and Mt. Judica with main thermal data from Aldega et al. (2007).

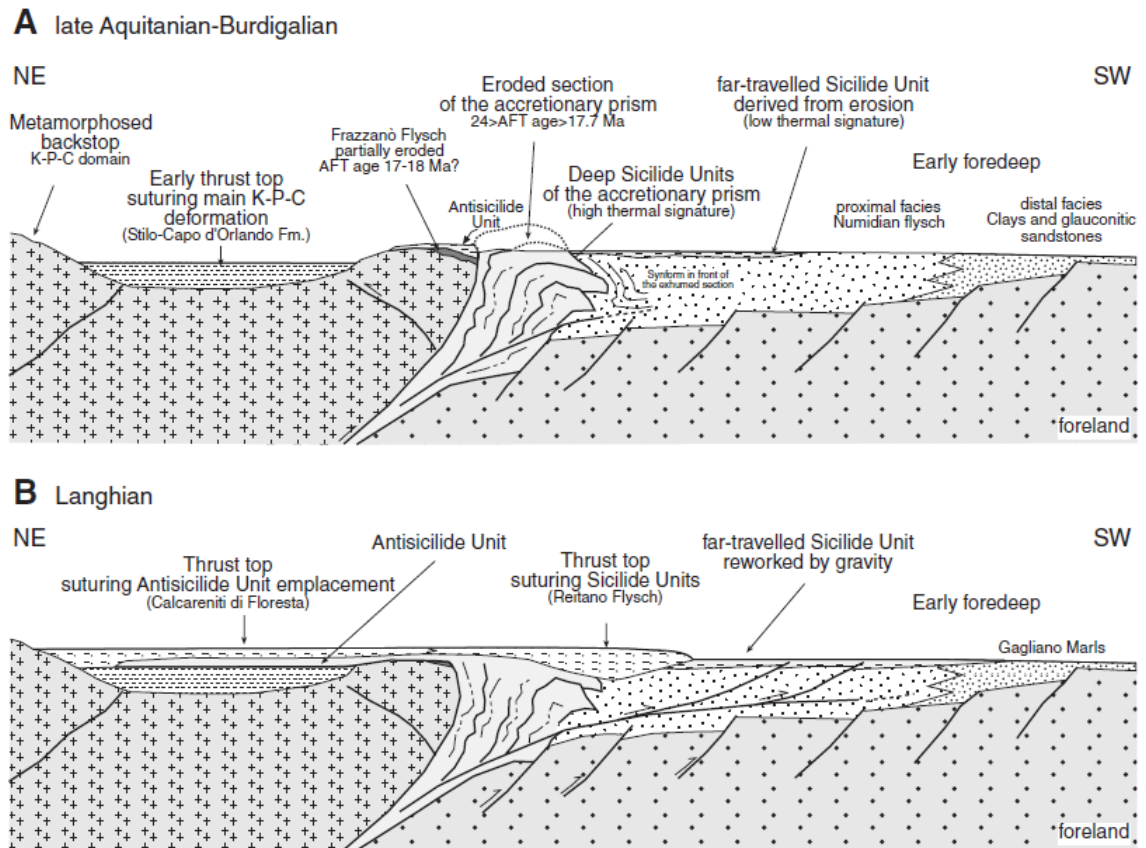


Figure 1.6 – Schematic evolution of burial-exhumation of the accretionary wedge of the Apenninic-Maghrebien orogen in Eastern Sicily in Aquitanian-Langhian times from Corrado et al. (2009).

## CHAPTER II- METHODS

Methods described in this section are those directly used to derive pieces of information on thermal evolution of studied sedimentary successions or adopted to elaborate new and pre-existing data for geological interpretation.

### **2.1. Optical study of organic matter dispersed in sediments aimed at the analysis of the thermal evolution of sedimentary basins**

#### *2.1.1. Generalities: Organic Matter dispersed in sediments and its thermal evolution*

The organic matter (OM) dispersed in sediments is composed of a mixture of organic compounds of various origin and composition. Aquatic organisms contribute mainly proteins, lipids and carbohydrates; higher plants contribute resins, waxes, lignins and carbohydrates in the form of cellulose (Barnes et al., 1990).

In the starting phases of sediment burial, the OM sustains irreversible physical and chemical variations that are extremely sensitive to temperature changes concerning the re-organization of carbon-hydrogen bonds. These transformations will produce an organic macromolecule called kerogen that progressively will convert into hydrocarbons with increasing burial and temperature.

Kerogens are commonly characterized by the use of bulk parameters, such as the H/C and O/C atomic ratios, obtained from elemental analyses (Fig. 2.1).

On the basis of these ratios, four types of kerogen have been defined which appear to follow distinct diagenetic pathways. This division of kerogen in four types has been supported by another independent scheme of classification using transmitted-light microscopy, so that kerogen types are defined by the morphologies of the kerogen particles called macerals.

Type I kerogen has high initial H/C and low O/C ratios. The source material is mainly algal, or a combination of algal lipids and waxes from higher plants. It forms part of the liptinite macerals in coal (Fig. 2.2).

Type II kerogen has intermediate initial H/C and O/C ratios, and larger contributions by aromatic and carboxylic acid groups than the type I kerogens. Ester bonds are abundant, as are medium-length aliphatic hydrocarbon chains and naphthenic rings. Both algal and higher plant sources appear to contribute to type II kerogens (liptinite macerals).

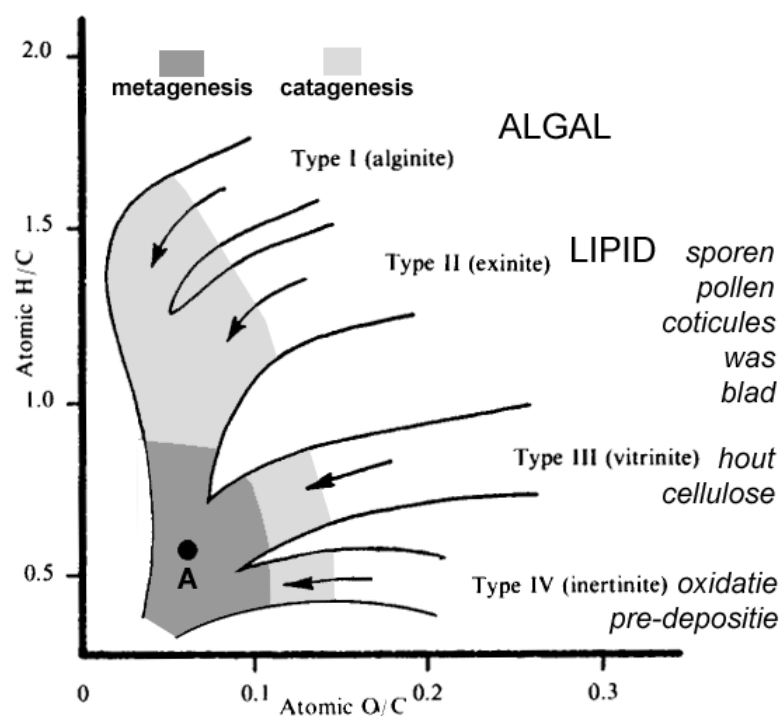


Figure 2.1 - Van Krevelen diagram showing maturation pathways for Types I to IV kerogen as traced by changes in atomic H/C and O/C ratios. The progressively darker shaded areas approximately represent diagenesis, catagenesis, and metagenesis stages, respectively (from [http://www.falw.vu/~rondeel/grondstof/oil/oil-total-web.html#\\_Toc531067567](http://www.falw.vu/~rondeel/grondstof/oil/oil-total-web.html#_Toc531067567)).

Type III kerogen has an initial H/C ratio less than 1, an initial O/C ratio of 0.2 to 0.3, and is derived dominantly from terrestrial plants. It consists mainly of aromatic groups formed from lignins and humic compounds, and represents the huminite/vitrinite fractions of coal petrography. Oxygen is present as carboxylic acids, ketones and ethers rather than in ester bonds.

Type IV kerogen has the H/C ratio less than 0.5 and contains mostly decomposed organic matter and highly oxidized material of various origins and represents the inertinite group (Fig. 2.2).

With increasing maturity, kerogen loses first preferentially O to produce CO<sub>2</sub> and H<sub>2</sub>O, then H to produce hydrocarbons. Changes in the molecular structure have effect in the petrographic appearance of the vitrinite macerals with a strong increase of their capacity to reflect light.

Reflectance of vitrinite is one of the most commonly used indicators of thermal maturity and is correlated to the stages of hydrocarbon generation and other thermal parameters in sedimentary environments (Hunt, 1986; Scotti, 2003; Fig. 2.3).

Thus, it is one of the most widely used parameter to calibrate basin modelling (Dow, 1977; Mukhopadhyay, 1994). The method relies on the presence of the huminite-vitrinite maceral group that is derived from cellulose, lignin and tannins in OM from terrestrial woody plants.

<i>Kerogen Type (according to IFP)</i>	<i>Principal biomass</i>	<i>Environment (general)</i>	<i>Original Hydrogen Index</i>	<i>Sulphur incorporation</i>	<i>Hydrocarbons generated and expelled (1)</i>
<b>Type I</b>	algae, bacteria	tectonic non-marine basin	<b>&gt; 700</b>	low	<b>oils</b>
<b>Type II</b>	marine algae, bacteria	marine	<b>400-700</b>	moderate	<b>oils</b>
<b>Type II S (sulphur rich)</b>	marine algae, bacteria	marine, carbonatic environment	<b>400-700</b>	high	<b>oils</b>
<b>Type III “H”</b>	spores, pollens, cuticles, resin, lignin, bacteria	fluvial-lacustrine, coastal plains	<b>300-600</b>	low	<b>waxy oils</b>
<b>Type III</b>	lignin	coastal plains, deltaic, turbiditic	<b>50-250</b>	low	<b>gas and light oils</b> ( <b>gas</b> traces when HI < 100)
<b>Type IV</b>	lignin	coastal plains, deltaic	<b>&lt; 50</b>	low	none

(1) Also depending by kerogen maturity level.

Figure 2.2 – The main kerogen types from Scotti (2005).

Maturation rank		Paleo Temp. (1) (°C)	Microscopic parameters					Chemical parameters		
Kerogen	Coal		Vitrinite Reflectance (Ro %)	TAI (2)	SCI (2)	CAI	Fluorescence of alginite	T <sub>max</sub>	Biomarker Isomerization Sterane Hopane	Hydrocarbon main products
Immature	Peat	50	0.2	1 Yellow	1	1 Yellow	Bue-green	420	0,10	Bacterial gas
	Lignite		0.3				Greenish -yellow			
	Sub-bituminous Coal		0.4				Golden yellow			
Mature Very Mature High Maturity	Bituminous Coal	100	0.5 – 0.55	2 Orange	3 4 5 6 7	2 Light brown	Dull yellow	430	0,10 0,50	Immature heavy oil (3)
			0.7							
			0.8							
			1.0							
			1.35							
Overmature	Semi Anthracite	150	1.5	3 Brown	8	3 Brown	Orange	450	None	Oil (3) and wet gas
			2.0							
			2.5							
Organic Metamorphisme	Anthracite	200	3.0	4 Brown/ Black	9	4 Dark brown	Red	465	None	Wet gas
			4.0							
			5.0							
	Meta Anthracite	250	4.0	5 Black	10	5 Black	Nonfluorescent	500	None	Dry gas
			5.0							

(1) Depending by duration

(2) International standard is not available - a lot of correlation scales are present in literature

(3) Depending also by kerogen type

Figure 2.3 - Correlation chart among the most important organic maturity parameters from Scotti (2005).

### 2.1.2. Thermal maturity parameters used in this Thesis

#### 2.1.2.1. Vitrinite Reflectance

Mean vitrinite reflectance (VRo%) is measured as the percentage of the incident light intensity which is reflected from the polished surface of vitrinite macerals fragments relative to a standard substance (e.g glass, sapphire, etc.). This measurement uses immersion oil and is related to the refractive index and absorptive index of immersion oil and standards which follows the Fresnel-Beer equation:

$$R_o = (\mu - \mu_o)^2 + \mu^2 k^2 / (\mu + \mu_o)^2 + \mu^2 k_o^2$$

where:  $\mu$ ,  $\mu_o$  = refractive index of vitrinite and immersion oil, respectively;  $k$ ,  $k_o$  = absorption index of vitrinite and immersion oil, respectively.

These indexes are wavelength dependent, thus a green monochromatic non-polarised light ( $\lambda = 526$  nm) is chosen for Ro% measurements.

In diagenesis and in the first stages of catagenesis ( $R_o\% < 1.5$ ), vitrinite is optically isotropic and the aromatic clusters present in the organic structure have no preferred orientations. In metagenesis instead, vitrinite behaves like an anisotropic material because of the orientation of aromatic clusters (Oberlin et al., 1980). When tectonic stress affects the thermal maturity of sediments, vitrinite macerals can turn out to be biaxial (Levine and Davis, 1989).

The indigenous vitrinite fragments are generally more abundant than altered or reworked woody material and show a gaussian distribution (see histogram of Fig. 2.4). In the example of Figure 2.6, where reflectance step are 0.05%, mean vitrinite reflectance derives from the arithmetic mean of the indigenous vitrinite population (in orange), and standard deviation is calculated on these fragments alone.

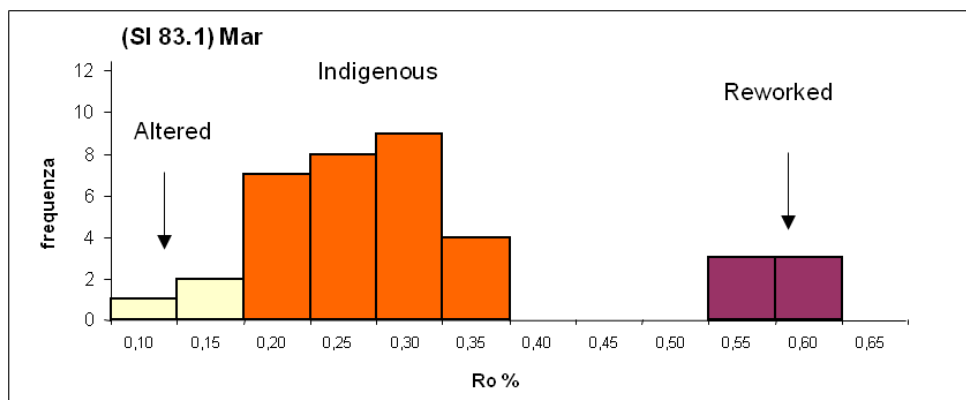


Figure 2.4 – An example of histogram of vitrinite reflectance readings is shown.

Most of the methodological limitations are due to:

- the lack of information on macerals different from the vitrinite group;
- a lower reliability for  $Ro\% < 0.3$ ;
- the presence of re-worked organic material;
- the whole-rock composition of the hosting rocks.

$Ro\%$  data, measured on subsurface samples and on outcropping sedimentary successions, usually allow to reconstruct the organic matter thermal maturity trend as a function of time and depth. These values used together with other geological pieces of information related to the sedimentary basin allow to deduce the thermal evolution of the sedimentary succession filling the basin. In particular, it is possible to use  $Ro\%$  data for:

- reconstructing burial and thermal history calibrating the time-temperature models by the calculation of paleo-geothermal gradient, erosion and/or exhumation rates (Van Hinte, 1978);
- identifying the hydrocarbons generation stages reached by vitrinite-bearing rocks;
- correlating with other organic (e.g. thermal alteration index, conodont alteration index, biomarkers) and inorganic (e.g. %I in I-S, Kübler index, fluid inclusions) paleotemperature indicators in diagenesis and in very low-grade metamorphism environments (Fig. 2.2).

#### *Sample preparation and analysis*

The analysed samples were prepared according to standardized procedures described in Bustin et al. (1990). Grounded material and extracted kerogen particles were englobe into an epoxy resin block. The samples were polished using an automated polishing system, 250, 500, 1000 carborundum papers and isopropanol as lubricant. After washing the sample in order to remove debris, three polishing laps are loaded with alumina powders of decreasing grain size (1, 0.3, 0.01  $\mu\text{m}$ ) and the sample polished.

Organic matter optical analysis were performed in Rome Tre and Bloomington (Indiana, USA) laboratories using a Zeiss Axioplan microscope, under oil immersion ( $n = 1.518$ ,  $23^\circ\text{C}$ ) in reflected monochromatic non-polarised light ( $\lambda = 546 \text{ nm}$ ).

On each sample, minimum twenty measurements were performed on vitrinite fragments never smaller than 5  $\mu\text{m}$  and only slightly fractured. Mean reflectance values were calculated from the arithmetic mean of these measurements on indigenous fragments.

#### 2.1.2.2. Fourier transform infra red spectroscopy (FTIR) analysis

Fourier transform infra red spectroscopy (FTIR) has been widely used to provide insight into the chemical composition and structure of coal (Painter et al., 1981; Sobkowiak and Painter, 1992; Mastalerz and Bustin, 1993; Iglesias et al., 1995; Ibarra et al., 1996; Guo and Bustin, 1998) and kerogen (Ganz and Kalkreuth, 1987; Kister et al., 1990; Lin and Ritz, 1993a).

FTIR studies assigned specific bands to chemical structures in complex kerogen molecules (Painter et al., 1981, 1983; Baruah, 1986) and proved the diagnostic value for maturity and kerogen type (Ganz et al., 1990; Christy et al., 1989; Kister et al., 1990; Lin and Ritz, 1993b; Chen et al., 1998; Lis et al., 2005) (Fig. 2.5).

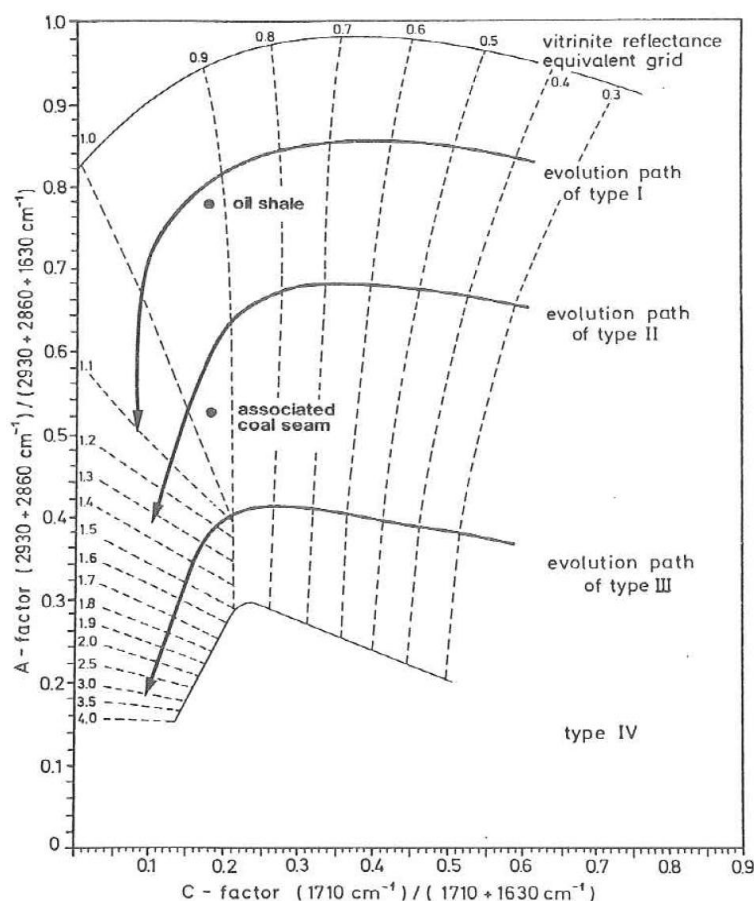


Figure 2.5 – Classification of kerogen-types and maturation according to FTIR ratio of the intensities of aliphatic/aromatic bands (A-Factor) and FTIR ratio of the intensities of carboxyl and carbonyl/aromatic bands (C-Factor) and the vitrinite reflectance equivalent grid from Ganz et al. (1990).

FTIR experiments were carried out at the Indiana Geological Survey using a Nicolet 6700 spectrometer equipped with a DTGS detector. Ground kerogen was mixed with potassium bromide in the proportion of 1 mg/ 100 mg and was analyzed as KBr pellets. Two hundred scans per sample were recorded in absorption mode from 4000 to 500 cm<sup>-1</sup>



with a 4 cm<sup>-1</sup> resolution. Bands were identified by comparison with published spectra (Painter et al., 1981; Wang and Griffith, 1985; Sobkowiak and Painter, 1992) and their assignments were performed according to Drobnik and Mastalerz, 2006 (Table 1.1).

Integrated band areas were measured using Omnic spectral analysis software. In particular they are: aromatic C-H stretching region (3,000-3,100 cm<sup>-1</sup>), aliphatic C-H stretching region (2,800-3,000 cm<sup>-1</sup>), oxygenated groups and aromatic/olefinic region (1,550-1,750 cm<sup>-1</sup>), CH<sub>2</sub> and CH<sub>3</sub> bending modes (complex peak at 1,450 cm<sup>-1</sup>), CH<sub>3</sub> absorption band (peak at 1,375 cm<sup>-1</sup>), and aromatic out-of-plane C-H deformation region (700-900 cm<sup>-1</sup>) (Fig. 2.6).

The aliphatic C-H stretching region (2,800-3,000cm<sup>-1</sup>) was resolved using Fourier deconvolution (Lin and Ritz, 1993a) into five spectral bands at 2,955 (asymmetrical CH<sub>3</sub> stretching), 2,925 (asymmetrical CH<sub>2</sub> stretching), 2,890 (CH stretching), 2,865 (symmetrical CH<sub>3</sub> stretching), and 2,850 cm<sup>-1</sup> (symmetrical CH<sub>2</sub> stretching).

The CH<sub>2</sub>/CH<sub>3</sub> ratio was calculated using asymmetrical stretching of these bands (2,925/2,955 cm<sup>-1</sup>) according to Lin and Ritz (1993a). Bands in the 1,550-1,750 cm<sup>-1</sup> region were resolved into two peaks representing carbonyl/carboxyl absorption at 1,700 cm<sup>-1</sup> and an olefinic/aromatic region at 1,600 cm<sup>-1</sup>.

FTIR band assignments	
Absorption band (cm <sup>-1</sup> )	Band assignment
3000-3100	Aromatic C-H stretching
2960	Aliphatic C-H stretching vibrations-methyl (CH <sub>3</sub> )
2920	Aliphatic C-H stretching vibrations-methylene (CH <sub>2</sub> )
2880	Aliphatic C-H stretching vibrations-methyl (CH <sub>3</sub> )
2850	Aliphatic C-H stretching vibrations-methylene (CH <sub>2</sub> )
1710	C=O stretching vibrations-carbonyl groups
1650	C=O stretching vibrations conjugated with aromatic rings
1600	C=C aromatic ring
1445-1454	Asymmetric aliphatic C-H deformation of methylene and methoxyl
1370	Symmetric aliphatic C-H bending of methyl groups
880	Aromatic out-of-plane-aryl ring with isolated C-H groups
815	Aromatic out-of-plane-rings with 2 neighboring C-H groups
750	Aromatic out-of-plane-4 neighboring C-H groups

Table 1.1 – FTIR band assignments of the main functional groups.

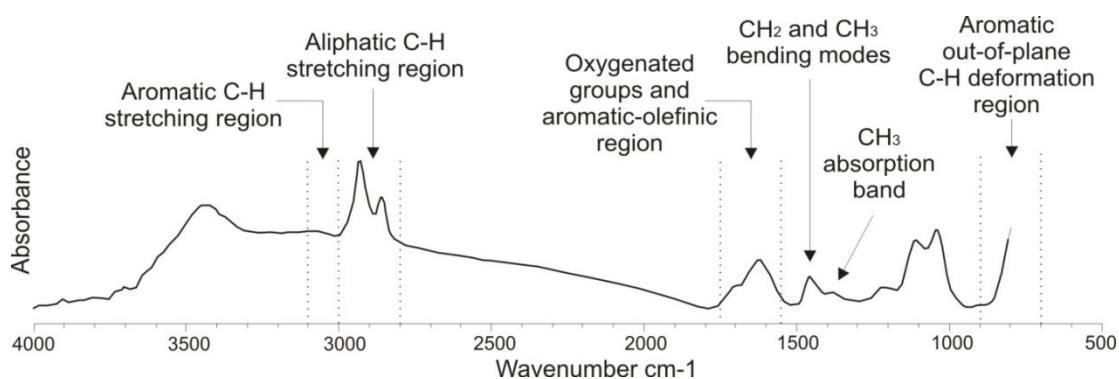


Figure 2.6 – FTIR spectrum of a concentrated kerogen. Measured band areas and peaks.

Identified band areas were used to calculate 10 FTIR parameters: nine aromaticity parameters (ratios of aromatic absorptions to aliphatic absorptions) and one aliphaticity parameter ( $\text{CH}_2/\text{CH}_3$  aliphatic stretching modes) as indices of organic matter thermal maturity in type-II kerogens (Lis et al., 2005).

### Concentration of kerogen

In this thesis kerogens were extracted using wet-chemical acid demineralization according to Robl and Davis (1993) and Schimmelmann et al. (1999).

Samples were crushed using the mixer ball mill. Three grams of powder sample were put into a glass extraction vial to remove the hydrophobic organic material coating inorganic grains and to expose inorganic grains to subsequent acid digestion. The extraction was performed using dichloromethane (DCM). Three-four times more dichloromethane (DCM) volume than volume of rock sample was added. The glass vial was shaken and placed into an ultrasonic bath for 20' and left upright in a rack overnight. The procedure with new DCM was repeated until the extract was transparent. DCM was removed with a pipette after sample's centrifugation.

Removal of carbonates was done adding HCl on the dried samples. The HCl was added in small increments to prevent excessive foaming. The acid digestion process was done at 50-60°C in a water bath to facilitate removal of carbonates. The acid was removed with pipette and disposed in plastic containers with neutralizing limestone gravel under a fume hood.

Digestion of inorganic matter was done by hydrofluoric acid (HF). For 3 g of powder sample a mixture of 50% distilled water and 50% HF was added (45 ml). Samples were

placed on a shaker table for 2 hours at regular intervals. The samples were pre-chilled in an ice bath and 9 g per sample of crystalline boric acid ( $\text{H}_3\text{BO}_3$ ) was added in two steps to prevent overheating. The samples were then washed 5-6 times with distilled water.

## **2.2. XRD study of clay minerals for thermal evolution of sedimentary basins**

### *2.2.1. Generalities: clay minerals and their thermal evolution*

The study of clay mineralogy has provided several useful tools for diagenesis and very low-grade metamorphism by furnishing information on the burial and thermal history of sedimentary sequences (Botti et al., 2004, Corrado et al., 2005)

Clay minerals in shales and sandstones undergo diagenetic and very low-grade metamorphic reactions in response to sedimentary and/or tectonic burial. Reactions in clay minerals are irreversible under normal diagenetic and anchizonal conditions, so that exhumed sequences generally retain indices and fabrics indicative of their maximum maturity and burial (Merriman and Frey 1999).

An important reaction occurring in shales during burial diagenesis and in hydrothermal settings is the gradual conversion of smectite to illite through I-S mixed layers as intermediate phases. The progressive trend ranging from early diagenesis to the epizonal setting includes the following series: dioctahedral smectite - disordered mixed layers (R0) - ordered mixed layers (R1 and R3) - illite - dioctahedral white K-mica (muscovite). This prograde series is characterized by various crystal structural changes as the decrease of proportions of swelling phases and the increase of ordering in mixed layers. The layers are stacked along a direction parallel to the c-axis in random, partially regular, or regular sequences. The classical terminology for the stacking order is based on the term R (Reichweite; Jadgozinski, 1949) that expresses the probability, given a layer A, of finding the next layer to be B. The R parameter may range from 0 to 3. R=0 means that there is no stacking order and illite and smectite layers are stacked randomly along the c-axis, R=1 indicates that a smectite layer is followed by an illite layer and a stacking order appears in the interstratification sequence, R=3 means that each smectite layer is surrounded by at least three illite layers on each side.

In this thesis, I-S structures will be described by means of the Reichweite nomenclature using R1 to mean R=1, R3 for R=3, etc. (Fig. 2.7).

The most common approaches utilizing I-S “geothermometer” in diagenetic studies are vertical profiles from wells and outcrops and thermal maturity mapping at local and regional scale. In the first case, illitization reaction profiles are generally produced. They are compared to the present geothermal gradient profile and organic matter maturity profiles in order to determine the temperature range in a particular point of the well correlating them to hydrocarbon generation phases (Pollastro, 1993; Merryman and Frey, 1999, Fig. 2.8).

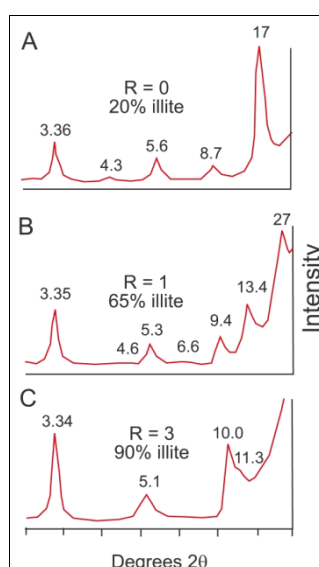


Figure 2.7 – Calculated XRD patterns of illite-smectite mixed layers with different illite content and stacking order: A) random ordered I-S, B) short range ordered I-S, C) long range ordered I-S (after Pollastro, 1990).

In the second case, I-S mixed layers of a particular unit or a stratigraphic succession are studied to detect variations in the area distribution of the thermal evolution of sediments and to reconstruct the tectonic loading those units have experienced during the evolution of fold-and-thrust belts (Botti et al., 2004; Corrado et al., 2005).

Although the conversion to paleotemperatures depends on more than one factor (e.g., heating rate, protolith, fluid composition, permeability, fluid flow), Pollastro (1990; 1993) summarized the application of two simple time-temperature models for I-S geothermometry studies based primarily on the duration of heating (or residence time) at critical I-S reaction temperatures. The first model was developed by Hoffman and Hower (1979) for long-term, burial diagenetic settings that can be applied to most geologic and petroleum studies of sedimentary rocks and basins of Miocene age or older. In this model the major changes from R0 to R1 and from R1 to R3 occur in the temperature range of

about 100-110 °C and of 170 °C-180 °C respectively and a minimum heating duration of 2 My is generally placed (Hoffman and Hower, 1979).

The second model, which was developed for short-lived heating events, applies to young basins or areas characterized by relatively recent thermal activity with high geothermal gradients, or to recent hydrothermal environments. Such settings are those where relatively young rocks were subject to burial temperatures in excess of 100 °C for <2 My. In this model the conversion from R0 to R1 and from R1 to R3 ordering occurs at about 130-140 °C and 170-180 °C respectively (Jennings and Thompson, 1986).

Many authors have studied the use of illite-smectite reaction as a measurement of temperature. Bibliographic data of approximative temperatures for changes in mixed layer illite/smectite, relative to different geological settings, are reported in Table 1.2.

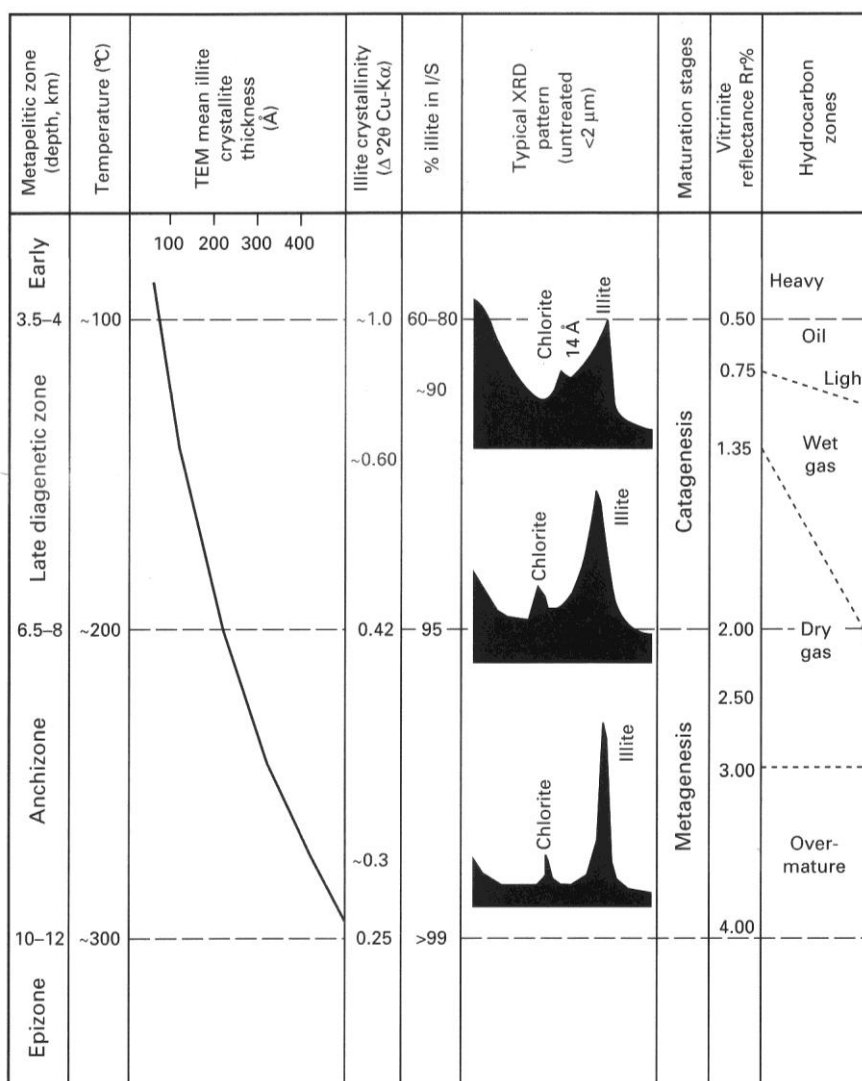


Figure 2.8 – Correlation scheme among clay mineral geothermometers, vitrinite reflectance data, hydrocarbon zones, metapelitic zones and palaeotemperatures according to Merriman and Frey (1999).

	% I in I-S (Reichweite parameter)	0-20% (Smectite to R0)	30-60% (R0)	60-80% (R0 to R1)	80-90% (R1 to R3)	90-95% (R3)	100% illite
Authors	Hoffman & Hower, 1979	50-60 °C		100-110 °C	170-180 °C		210 °C
	Jennings & Thompson, 1986			130-140 °C	170-180 °C		
	Weaver <i>et al.</i> , 1994		90-140 °C (only 40%)		200 °C	250-280 °C	
	Merriman & Frey, 1999	<100 °C		100 °C		200 °C	300 °C
	Jaboyedoff & Thelin, 1999	<100 °C		100-130 °C		200-250 °C	
	Uysal <i>et al.</i> , 2000			115-120 °C			

Table 1.2 – Approximate temperatures for changes in mixed layer illite/smectite proposed by different models from Aldega (personal communication).

### Sample preparation and analysis

Samples were analyzed by XRD using a Scintag X1 system (CuK $\alpha$  radiation) at 40 kV and 45 mA. Randomly-oriented whole-rock powders were run in the 2-70 °2 $\theta$  interval with a step size of 0.05 °2 $\theta$  and a counting time of 3 s per step.

Oriented air-dried and ethylene-glycol solvated samples were scanned from 1 to 48 °2 $\theta$  and from 1 to 30 °2 $\theta$  respectively with a step size of 0.05 °2 $\theta$  and a count time of 4 s per step. Oriented slides of the <2  $\mu$ m grain-size fraction were prepared by the pipette-on-slide method, keeping the specimen thickness as constant as possible, within the range of 1 to 3 mg of clay per cm<sup>2</sup> of glass slide. The illite content in the mixed layer I-S was determined according to Moore and Reynolds (1997) using the delta two-theta method after decomposing the composite peaks between 9-10 °2 $\theta$  and 16-17 °2 $\theta$ . Peaks in relative close position were selected for clay mineral quantitative analysis of the <2  $\mu$ m (equivalent spherical diameter) in order to minimize the angle-dependent intensity effect. Composite peaks were decomposed using Pearson VII functions and the DMSNT Scintag associated program.

## **2.3. Low temperature thermo-chronology for exhumation of sedimentary successions**

### ***2.3.1. Generalities***

Apatite fission-track analysis on sedimentary successions has been the object of many studies since the last years because of its implications with hydrocarbon geology (Gleadow et al., 1983). This methodology provides an evaluation of the thermal history, giving information on burial depths and on the structural setting of the sedimentary successions involved in the chain building (Zattin et al., 2002). The most important difference with other low-temperature indicators (such as vitrinite reflectance and I-S mixed layers) is that this methodology provides both temperature and time information. The other difference is that apatite fission-track (FT) analysis is a reversible indicator because the sample age and the track length distribution can reflect multiple cooling and heating events.

FT dating is based on the spontaneous fission of  $^{238}\text{U}$  which produces a damaged zone or a linear defect (spontaneous track) in the crystal lattice (Fleischer et al., 1965).

FT dating is very similar to other isotopic dating methods based on the decay of an unstable parent to a stable daughter atom. The age is function of the proportion between the abundance of the new stable isotope and the parent unstable atom. In FT dating methodology, these two quantities are substituted by the number of observable tracks and the amount of uranium present in the sample. The uranium content is determined by the number of induced tracks obtained by irradiation with a known dose of thermal neutrons in a nuclear reactor. This irradiation causes the fission of  $^{235}\text{U}$  which isotopic ratio with  $^{238}\text{U}$  is constant in nature. Therefore, the age of the sample can be estimated by the ratio between spontaneous and induced tracks.

The most important parameter affecting the stability of tracks is temperature. As temperature increases, a decreasing of the number of tracks and a reduction of their length is visible. This process is known as annealing. The FT annealing rate depends on the chemical composition of apatite (Green et al., 1986) and on cooling or heating rate (Gleadow and Duddy, 1981). It generally occurs between about 60 °C and 125 °C for heating time of about 10 My and can be used to reconstruct the thermal history of basins, from deposition and burial of sediments through subsequent cooling related to uplift and erosion.

The temperature range in which reduction of lengths occurs is known as Partial Annealing Zone (PAZ; Wagner and Van den Haute, 1992). According to this concept, temperatures of any geological setting can be divided into three zones with respect to fission-track annealing:

- the total annealing zone, in which spontaneous tracks are immediately erased after any fission event;
- the partial annealing zone, in which reduction of lengths occurs with the increase of temperature;
- the stability zone, where tracks are stable.

FT record the age of cooling and the exhumation rate of rocks from the total annealing zone, evaluate the thermal history of a sedimentary succession in the partial annealing zone and assess the age of the source rock in the stability zone giving information on the provenance of the sediments.

As it is possible to see in the Arrhenius diagram (Fig. 2.9), the annealing temperatures depend on the rate of the geological process and the PAZ temperature range can not be univocally defined.

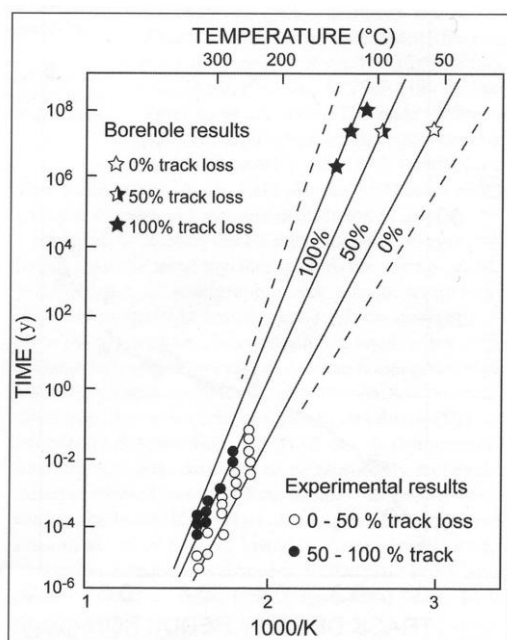


Figure 2.9 - Reduction of the FT density as a function of temperature in drill-hole samples from the Otway Group sandstones after Gleadow and Duddy (1981).

For apatite, temperatures between 140 and 120 °C are cited for the bottom whereas 70 to 40 °C for the top of the PAZ. More precisely, Gleadow and Duddy (1981), on the basis of



data obtained from drill holes samples in the Otway basin, suggest a PAZ between 145 and 80 °C for heating events 1 My long, and between 110 and 45 °C for events 1 Gy long.

The cooling range in the PAZ has been simplified in a single temperature value to which the age has to be referred. This temperature value was defined by Dodson (1973) as the closure temperature. Wagner and Reimer (1972) suggest that the closure temperature correspond to temperature at which 50% of the track are retained. In conclusion, the best assessments of the closure temperature are 128 °C, 112 °C, 98 °C and 85 °C for cooling rates of 100 °C/My, 10 °C/My, 1 °C/My and 0.01 °C/My, respectively (Brandon et al., 1998).

Most of the methodological limitations are due to the young age of sediments (less than 10 My). In fact in this short period of time, the accumulation time of tracks can be too short to produce a good number of measurable tracks with a “normal” uranium content (about 35 ppm) causing relevant errors in the age determination (Zattin, 2003). A different problem derives from the relationships between the apatite chemistry and the annealing degree. In terrigenous rocks, it is very probable to analyse, in the same sample, apatites coming from different source rocks with different chemical composition. Finally, different source areas may have different cooling times and, as a consequence, the pre-depositional history of detrital apatites cannot be the same for the single grains in the samples and therefore quantitative modelling of data can be very difficult given the heterogeneity in the thermal history of single grains.

Radial plots and/or peak-fitting statistical method can be used to discriminate different inherited populations and overcome this problem (Gailbraith, 1988; Brandon and Vance, 1992; Brandon et al., 1998; Fig. 2.10).

Thermochronological contribution to this thesis come from a collaboration with Dr. Maria Laura Balestrieri (CNR, Florence) who provided AFT data of the Peloritani Mts. area and a huge support in integrating organic matter and clay mineralogy data with low temperature thermochronology.

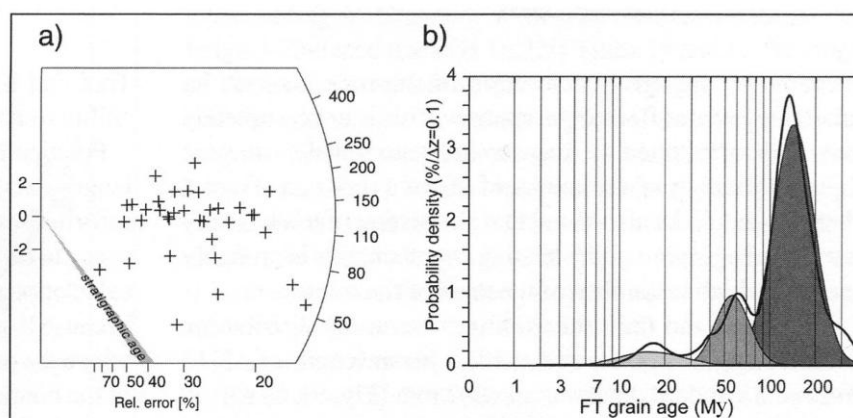


Figure 2.10 - Graphical methods for visualization of FT data. a) Radial plot: each single cross represents a crystal; age can be read on the intersection between the line linking the origin with the point and the arc; the x coordinate is the precision of the age which increases towards the arc; the error  $\pm 2$ , represented by the bar on the origin, is easily detected superimposing the bar on the selected point. b) Probability density plot: the thicker line represents the observed distribution whereas different tones of grey are assigned to the individual peaks obtained by binomial peak-fitting method from Zattin (2003).

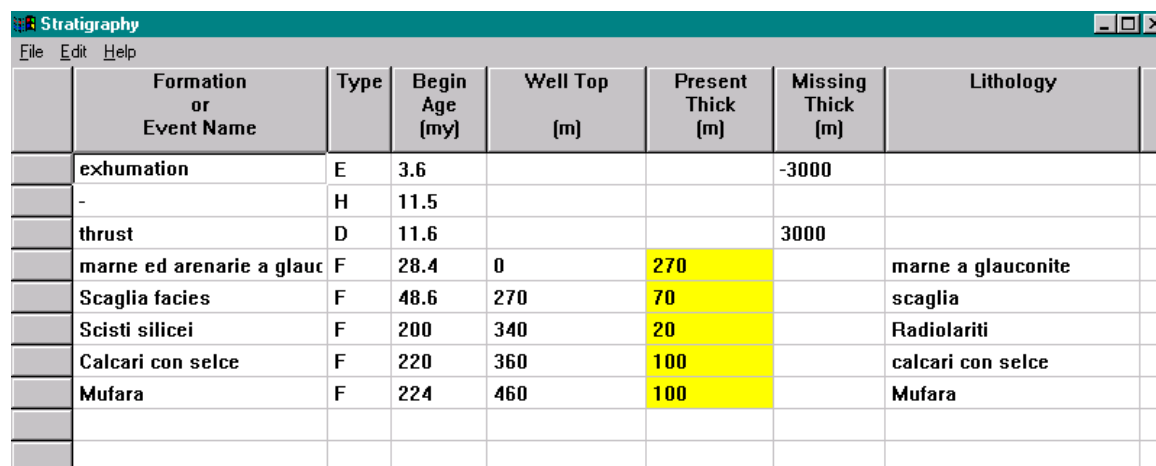
## 2.4. Thermo-structural modelling

Thermo-structural modelling was performed using Basin Mod-1D software for Windows (1996). This software allows reconstructing the burial and thermal evolution of sedimentary sequences both in undeformed and deformed conditions from geological data (e.g., age of sedimentary sequences and tectonic/erosional events, pure and mixed lithologies, thicknesses, porosity, permeability and thermal conductivity of sedimentary sequences, Fig. 2.11).

These data derive from the integration between the database of physical features provided by the libraries available of the modelling software and the geological information coming from the regional literature and the stratigraphic and structural data collected in the field.

Burial curves were corrected for decompaction according to the Sclater and Christie's method (1980). Sea level changes were neglected, as sediments thickness, more than water column controls and thermal evolution (Butler, 1992). Thermal modelling was performed through LLNL Easy %Ro method (Sweeney and Burnham, 1990) adopting different geothermal gradients for sedimentation, thrusting, exhumation events and a surface temperature of 10°C. Thrusting was modelled as instantaneous when compared with the duration of sedimentation, as generally suggested in theoretical models

(Endignoux and Wolf, 1990). Burial curves were generally calibrated with Ro% and I% in I-S, according to the geothermometer's correlation proposed by Pollastro (1993).



	Formation or Event Name	Type	Begin Age (my)	Well Top (m)	Present Thick (m)	Missing Thick (m)	Lithology
	exhumation	E	3.6			-3000	
	-	H	11.5				
	thrust	D	11.6			3000	
	marne ed arenarie a glauc	F	28.4	0	270		marne a glauconite
	Scaglia facies	F	48.6	270	70		scaglia
	Scisti silicei	F	200	340	20		Radiolariti
	Calcari con selce	F	220	360	100		calcari con selce
	Mufara	F	224	460	100		Mufara

Figure 2.11 - Input data used in worked example of burial history reconstructions.

## 2.5. GIS analysis

Geographic information systems (GIS) or geospatial information systems is a set of tools that captures, stores, analyzes, manages, and presents data that are linked to locations. In the simplest terms, GIS is the merging of cartography, statistical analysis, and database technology. GIS systems are used in cartography, land surveying, public utility management, natural resource management, geography, emergency management, and for many other purposes. GIS applications are tools that allow users to create interactive queries (user-created searches), analyze spatial information, edit data and maps.

In this thesis QuantumGIS software (Fig. 2.12) were used to create a database of paleo-geo-thermal data derived from literature (stratigraphic sections, geological cross-sections, thickness of the studied formations) and from field and lab work (vitrinite reflectance, percentage of illite in I-S and apatite fission tracks data) and to create thematic maps.

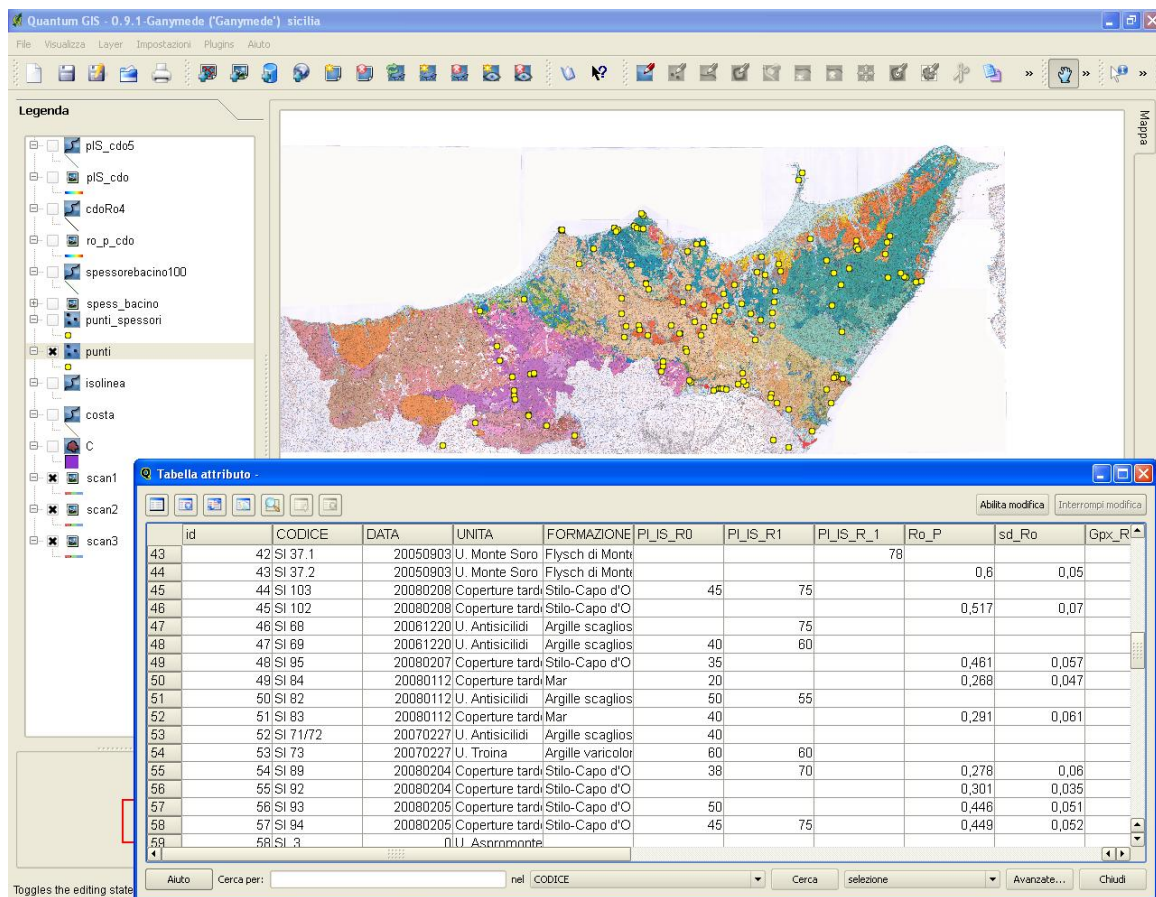


Figure 2.12 – QuantumGIS main screen and attribute table.

## CHAPTER III - INTERNAL ZONE (PELORITANI MTS.)

### 3.1. Introduction

Internal Zones of the Peri-Mediterranean orogen (Fig. 1.3; Vera, 2004 and references therein; Jolivet et al., 2008) are dominated by Alpine metamorphism and complex ductile to brittle deformation structures related to subduction, collision and exhumation processes. Out-of-sequence compressive reactivation may represent a typical way the orogenic system has to accommodate changes in boundary conditions especially in post-collisional settings that may be followed by late stages of exhumation (Jolivet et al., 2007 and references therein). Great attention has often been dedicated to the reconstruction of thermo-baric evolution (P-T-t paths) of the metamorphic units constituting the orogens (Brun and Faccenna, 2008) whereas less emphasis has been given to compressive reactivation (in brittle regime), in terms of tectonic burial and exhumation. This lack of information is generally due to the amount of tectonic burial, that generally is in the order of a few kilometers. As a matter of fact very few methodologies may be applied to both sedimentary and crystalline rocks (Corcoran and Dorè, 2005) to detect such renewed tectonic burial. Furthermore exhumation, through either erosion or tectonics, may contribute to remove the tectonic overburden (Ring et al., 1999; Dorè et al., 2002) and the record of its development may be totally lost in the evolutionary reconstruction of the orogen.

A portion of the Alpine Internal Zones is widely exposed on the Peloritani Mts. (NE Sicily; Fig. 3.1). The Peloritani Alpine orogen is mainly made up of thin crystalline nappes unconformably overlain by upper Oligocene-lower Miocene sedimentary successions post-dating nappe emplacement and the main exhumation phase. Since Oligocene times, two main cooling phases have been reconstructed in the crystalline rocks of the Peloritani Mts. by means of apatite fission-track (AFT) and (U-Th-Sm)/He analyses (Thomson, 1998; Balestrieri et al., 2008). The older phase, Oligocene in age, relates to regional cooling at shallow depths, the second one to brittle conditions after collision, starting in Serravallian-Tortonian times.

The causes of the first cooling phase have been extensively discussed (Platt and Compagnoni, 1990; Wallis et al., 1993; Messina et al., 1996; Bonardi et al., 2001;

Rossetti et al., 2001; Iannace et al., 2007), while causes and mechanisms of the second one have never been investigated.

Therefore the Peloritani orogen represents an excellent natural lab where to investigate the burial-exhumation path during the late orogenic evolutionary stages. In order to contribute to this issue, we performed XRD, structural and organic matter optical analyses on the siliciclastic sequences post-dating the Oligocene cooling phase. Vitrinite reflectance (VRo%) and illite content in mixed-layer illite-smectite (%I in I-S) that are sensible indicators of maximum paleo-temperatures in diagenetic conditions (Hoffman and Hower, 1979; Underwood et al., 1988; Bustin et al., 1990; Pollastro, 1990; Botti et al., 2004; Aldega et al., 2007a, b), were used to define the paleo-thermal conditions of the: (i) upper Oligocene-middle Burdigalian siliciclastic sediments (Stilo-Capo d'Orlando Fm., hereafter SCO) unconformably overlying the Peloritani nappes and filling a long-lived fore-arc basin which evolves during collision into a thrust-top basin; (ii) Upper Cretaceous varicoloured clays of the Antisicilide Unit, filling the top of the aforementioned basin and deriving from the unroofing of the Sicilide accretionary wedge interposed between the Peloritani Mts. and the Africa-derived units, mainly exhumed in Burdigalian times (Corrado et al., 2009); (iii) Serravallian-Messinian siliciclastic deposits filling normal fault-controlled basins stretched along the Tyrrhenian and Ionian flanks of the Peloritani orogen.

This multi-method approach allowed us to reconstruct the paleo-geothermal gradient values during Oligocene-Miocene times, to constrain the burial evolution of the Paleogene and Neogene sedimentary sequences of the Peloritani Mts. and discriminate between areas where these successions have been affected by sedimentary and/or tectonic load.

### **3.2. Geological and structural setting**

The Peloritani Mts. constitute the W-ward termination of the Calabria-Peloritani Arc of southern Italy, an orogenic segment connecting the sedimentary thrust systems of the Apennines and the Maghrebids of the western Mediterranean region (Amodio-Morelli et al., 1976; Cifelli et al., 2008; Fig. 1.3).

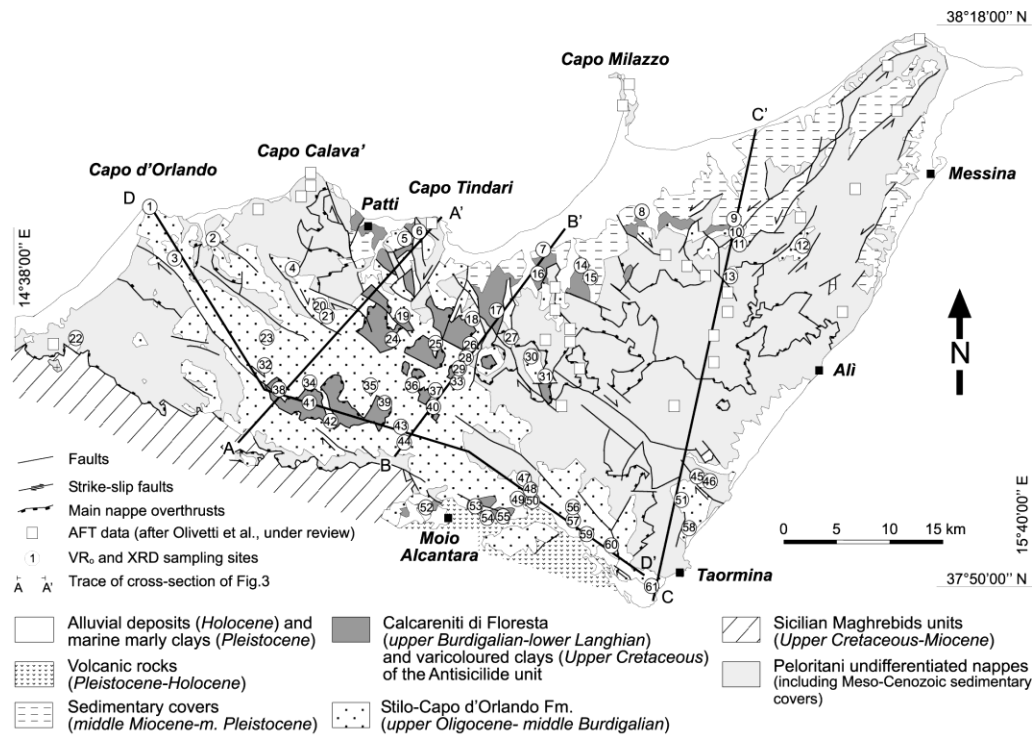


Figure 3.1- Geological sketch map of the Peloritani Mts. with sampling sites and traces of cross sections, redrawn and modified after Lentini et al. (2000) and Messina et al. (2004).

They are made up of a series of south-verging thin continental crustal nappes bounded by low-temperature cataclastic to mylonitic shear zones (Messina et al., 2004). These nappes are formed by different lithodemic units mainly consisting of Variscan metamorphic rocks (314 Ma from Rb/Sr dating, Bonardi et al., 2001), locally intruded by late-Variscan plutonites (292 Ma, from Rb/Sr dating, Rottura et al., 1990) and capped by Mesozoic-Cenozoic sedimentary covers (Lentini et al., 2000; Fig. 3.2). In detail, the crystalline nappes are made up of cata- to epizone continental crustal rocks showing a decrease of metamorphic grade from top to bottom of the nappe pile (Bonardi et al., 1976; Messina et al., 2004). The uppermost nappes (Aspromonte and Mela Units; Fig. 3.1 and 3.2) consist of high to medium grade Variscan crystalline rocks without sedimentary cover.

The nappes below (Piraino, Mandanici, Alì-Montagnareale, Fondachelli and Longi-Taormina Units; Fig. 3.1 and 3.2), are made up of medium to very low-grade metamorphic rocks covered by the remnants of the Mesozoic-Cenozoic sedimentary rocks (Somma et al., 2005a, b; Somma, 2006). Evidence for the occurrence of Alpine metamorphism is shown by the Alì-Montagnareale and Aspromonte Units. In the latter, metamorphism has been dated 28-22 Ma (Rb/Sr dating; Bonardi et al., 1987, 1992). The SCO sedimentary sequence (Bonardi, et al., 1980), late Oligocene-early Burdigalian

according to Lentini et al., 1995 or Burdigalian according to De Capoa et al., 1997, 2000, 2004, post-dates the main nappes emplacement. Paleogene to Recent sedimentary covers deposited in unconformity above the crystalline nappes (Fig. 3.3). The Oligocene-Miocene tectonic evolution of the area was controlled by compressive tectonics which caused regional subsidence and local uplifts. Regional subsidence controlled deposition within the basin which was completely filled and determined progressive north-ward transgression onto former structurally high areas of the orogen (Lentini et al., 1995).

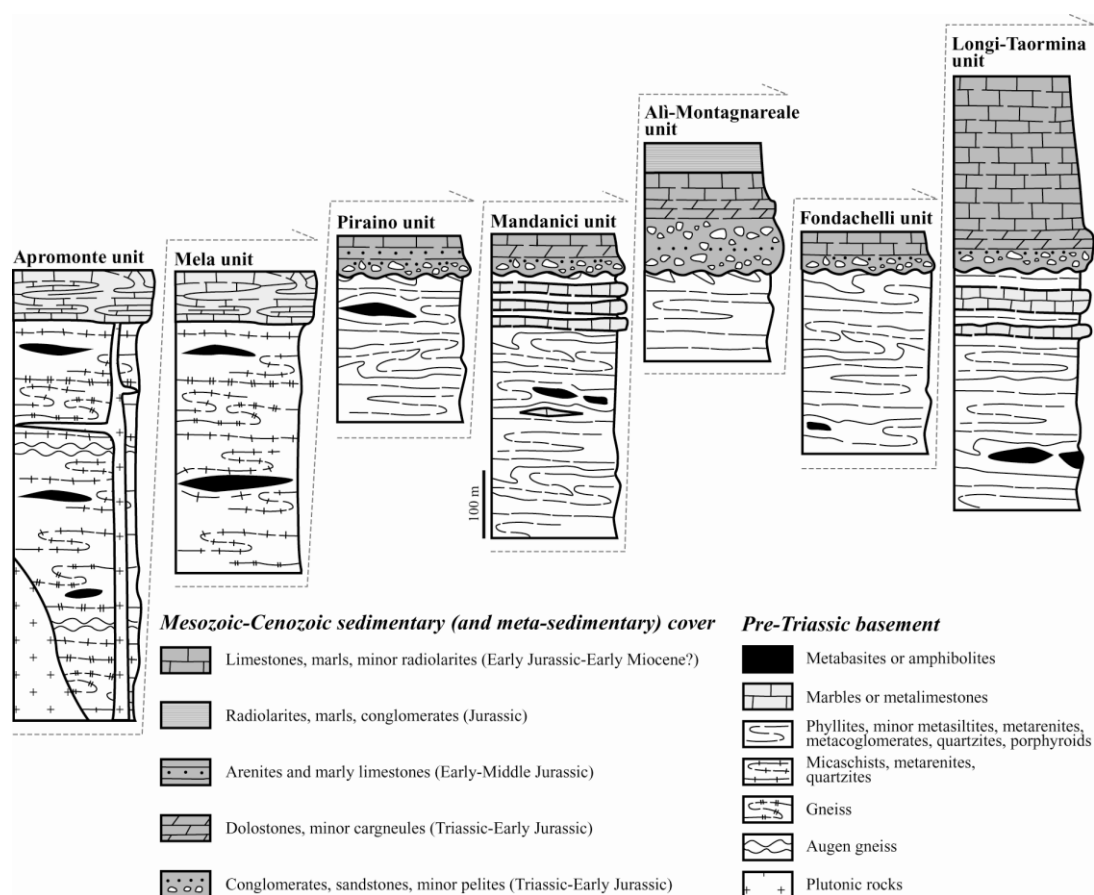


Figure 3.2 - Schematic stratigraphic setting of the Peloritani Mts. Units.

The collision between the southern edge of the Calabria-Peloritani Arc and the African plate, that started in middle to late Burdigalian and continued into Langhian time, caused back-thrusting of the Antisicilide Unit (Lentini and Vezzani, 1978; Cavazza and Barone, 2010) on top of the SCO, interrupting the turbiditic sedimentation. Collision caused intense deformation and translation of this subduction-related mélangé from the Sicilide accretionary wedge (Bonardi et al., 2001).



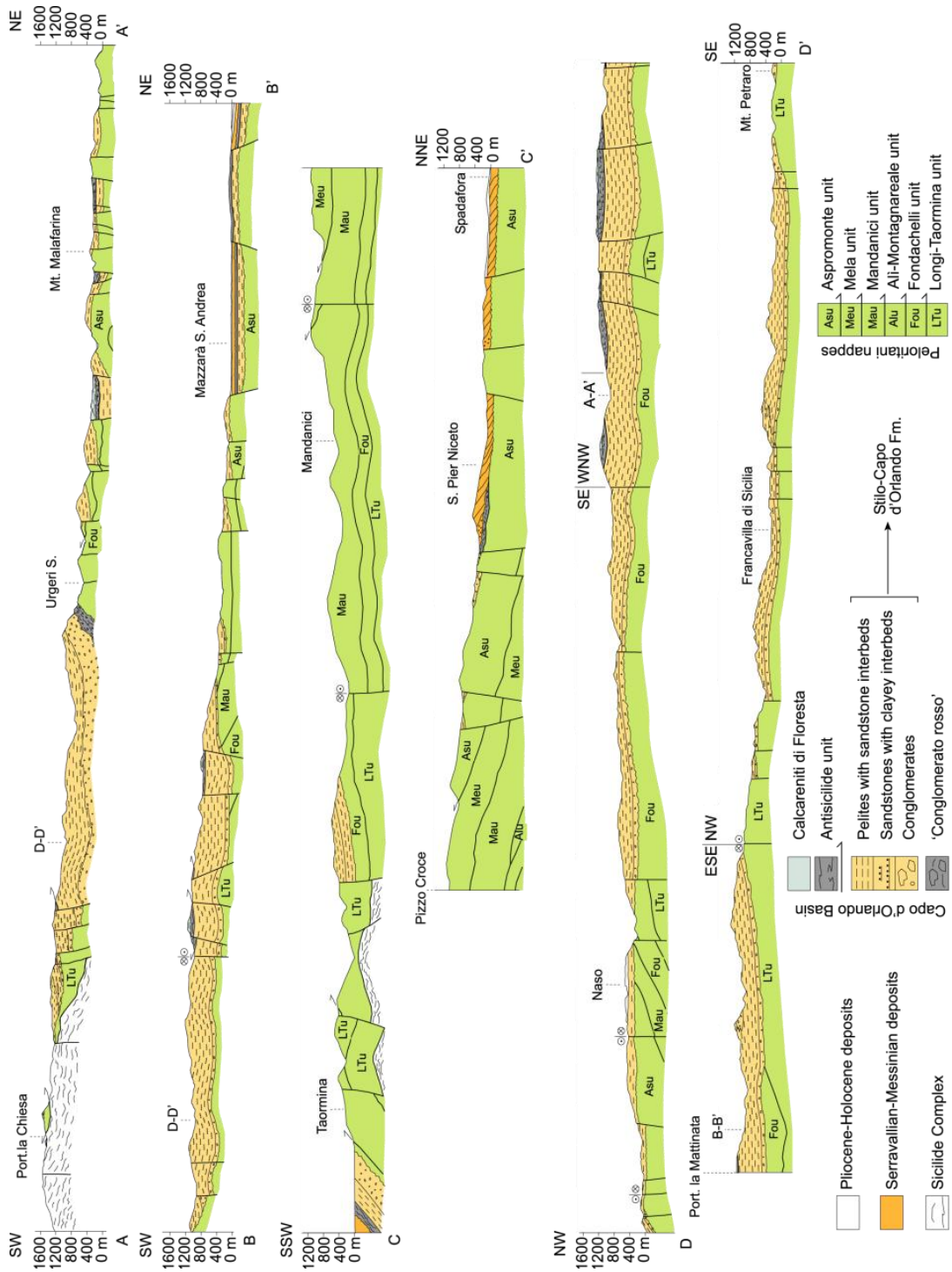


Figure 3.3  
- Geological cross sections. Sampling sites (in brackets), vitrinite reflectance, illite content in mixed layers I-S and apatite fission tracks data are plotted. Traces of cross sections in figure 3.1. Section A-A' reworked and modified after Lentini et al. (2000)

Gravity-driven mechanisms contributed to the final emplacement of the Antisicilide Unit in perched basins (Ogniben, 1969; Corrado et al., 2009; Cavazza and Barone, 2010).

The deposition of the Calcareni di Floresta (late Burdigalian-early Langhian) post-dated the emplacement of the Antisicilide Unit and covered the suture between the Calabria-Peloritani Arc and the Sicilide accretionary wedge. Sea level variation and extensional tectonics controlled facies distribution and the extent of Serravallian-Messinian siliciclastic rocks which cover with a down-lap geometry the Peloritani nappes and the above-mentioned sedimentary deposits. The entire succession deposited within normal fault-controlled basins while incomplete and/or condensed series sedimented on top of horst-like structures in response to the strong uplift of the Peloritani Mts. (Lentini et al., 2000).

### **3.3. Geological features of sampled lithostratigraphic units**

A suite of 42 samples for organic matter optical analysis and 62 samples for XRD study was collected from the SCO, the overlying varicoloured clays of the Antisicilide Unit and the Serravallian-Messinian deposits (Fig. 3.1).

The SCO (Bonardi et al., 1980), up to 600-900 m thick, crops out extensively along a NW-SE oriented belt, about 70 km-long and 20 km-wide, stretched from Capo d'Orlando to Taormina villages, and along a N-S trending graben located in the surroundings of Patti village. Small outcrops are also preserved in the north-eastern area of the Peloritani Mts. (Fig. 3.1). The SCO is subdivided into three main lithofacies (Carmisciano and Puglisi, 1982). The lowermost is composed of coarse-grained sandstones intercalated with large conglomeratic bodies (lithofacies c). It evolves upwards to thin-bedded sandy turbidites with clayey interbeds (lithofacies b) and to thick-bedded coarse-grained sandstones, occasionally intercalated with micro-conglomerates (lithofacies a). Locally, a red conglomerate with huge calcareous olistolithes is present at the SCO base (Bonardi et al., 1982; Fig. 3.3, cross section A-A'). These lithofacies are arranged in a transgressive-regressive depositional sequence with onlap termination on the Peloritani Mts. In detail, lithofacies c has been interpreted as debris flow deposited along marine paleo-canyons (Bonardi et al., 1980). The other two lithofacies have been considered as slope sediments cut by channel fills and turbiditic flows. Nannofossils dating indicates a late Oligocene (Lentini et al., 1995) and a middle Burdigalian (De Capoa et al., 2000, 2004) age for the lowermost and uppermost part of the succession respectively.

The Antisicilide Unit is formed by Upper Cretaceous varicoloured clays (Argille Scagliose Auct.) containing blocks of limestones and quartzarenites. Black shales and radiolarites are occasionally present (Truillet, 1969). This unit tectonically lies on the SCO and locally on the Peloritani nappes. It is unconformably overlain by upper Burdigalian-lower Langhian bioclastic calcarenites and arkoses of the Calcareni di Floresta.

The Serravallian-Messinian deposits (Selli, 1978; Ghisetti, 1979; corresponding to the “Motta Flysch” of Barrier et al., 1987) are siliciclastic rocks that mainly crop out along the Tyrrhenian piedmont belt and subordinately along the Ionian side covering the Peloritani nappes, the SCO, the Antisicilide Unit and the Calcareni di Floresta (Fig. 3.1). Three main lithofacies have been distinguished and dated on the basis of foraminifera and nannofossils assemblages (Lentini et al., 2000). The lowermost lithofacies (lowermost Serravallian) is formed by clayey marls and clays intercalated with sandstones. This lithofacies evolves upwards to large conglomeratic bodies in a sand matrix and it is overlain by thin-bedded sandstones alternated with pelites (Lentini et al., 2000). These deposits, sedimented in a fluvial-deltaic environment, show clinoforms dipping toward N-NW and W along the Tyrrhenian and Ionian side, respectively.

### **3.4. Results**

#### *3.4.1. Organic matter data*

##### 3.4.1.1. Stilo Capo d'Orlando Formation

Organic matter dispersed in the SCO sediments is generally abundant, homogeneous and mainly made up of well-preserved macerals. They mainly belong to the huminite-vitrinite group, with predominant collotelinite and telinite fragments and subordinate amounts of inertinite group macerals. Data generally show one main cluster identifiable by a Gaussian distribution which represents the indigenous population of huminite-vitrinite macerals. Pyrite either finely dispersed or in small globular aggregates is locally present along the rims of huminite-vitrinite macerals.  $VR_o\%$  values range from 0.21 (site 1 in Fig. 3.1) to 0.58% (site 13), indicating the immature and early mature stages of hydrocarbon generation. An increase of  $VR_o\%$  values as function of depth has been recognized in the southern area of the Peloritani Mts. (in the surroundings of Floresta and Taormina villages). In this area, values increase from 0.28% at the top of the succession

(Fig. 3.4A) up to 0.47-0.48% at the bottom (Fig. 3.4E). In the north-eastern zone of the Peloritani Mts., where the SCO thickness does not exceed 100 m, high  $VR_o\%$  values (0.46-0.58%; sites 5, 12 and 13; Fig. 3.5a) have been identified (see discussion).

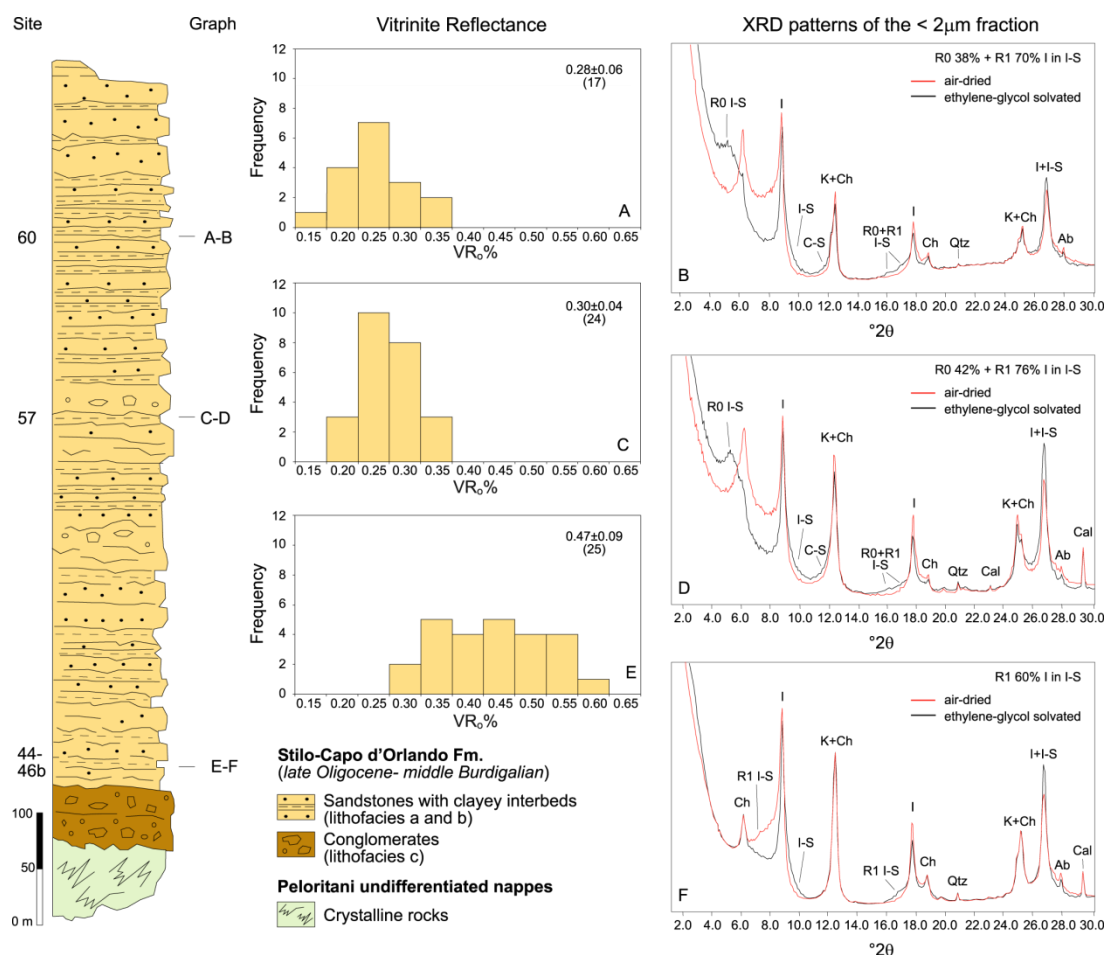


Figure 3.4 - Synthetic stratigraphic log of the Stilo-Capo d'Orlando Fm. with selected vitrinite reflectance histograms (A-C-E) and XRD oriented patterns of the <2  $\mu$ m grain-size fraction (B-D-F).

Acronyms - Ab: albite; Cal: calcite; Ch: chlorite; C-S: mixed layer chlorite-smectite; I: illite; I-S: mixed layer illite-smectite; K: kaolinite; Qtz: quartz.

### 3.4.1.2. Antisicilide Unit

Only four samples provided reliable  $VR_o$  results for the varicoloured clays of the Antisicilide Unit. Kerogen is generally scarce. Among the others it contains macerals of the huminite-vitrinite group (collinite and telinite) with two generations (one indigenous and one reworked) and subordinate of the inertinite group (fusinite).  $VR_o\%$  values range from 0.41 (site 16a) to 0.56% (site 53b), indicating the immature and early mature stages of hydrocarbon generation (Tab. 3.1 and Fig. 3.6).

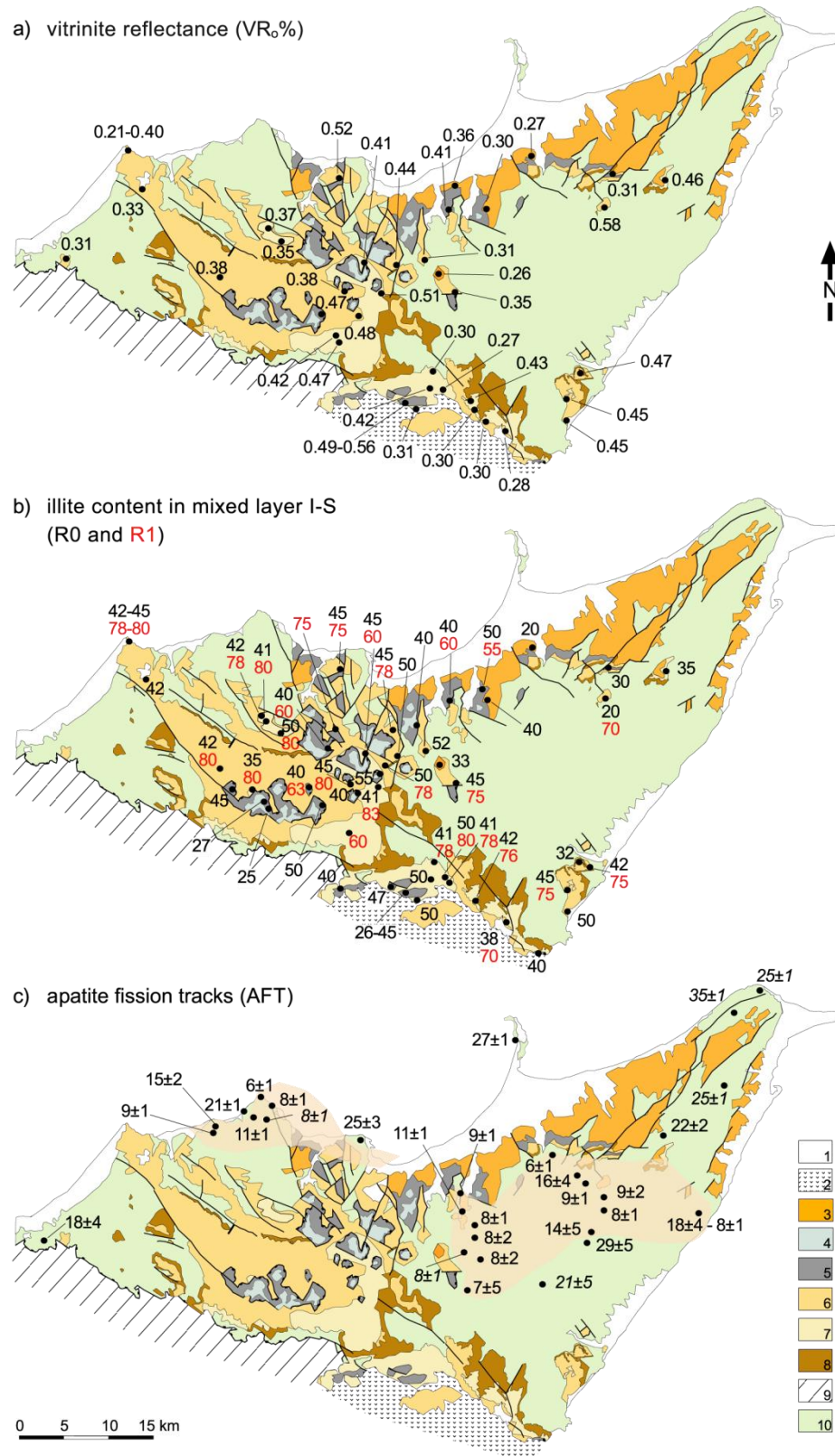


Figure 3.5 - Sketch maps of the Peloritani Mts. with distribution of vitrinite reflectance (a), illite content in mixed-layer I-S (b) and apatite fission-track data (c) from Thomson, 1994 (*italics*) and Balestrieri et al., 2008 (*regular*). The shaded area in (c) characterized by young (<15 Ma) fission-track ages is affected by a post-SCO deposition thermal event. 1: alluvial deposits and marine marly clays; 2: volcanic rocks; 3: Serravallian-Messinian siliciclastic deposits; 4: Calcareni di Floresta; 5: Antisicilide Unit; 6: Stilo-Capo d'Orlando Fm.; 7: Sicilian Maghrebrids Units; 8: Undifferentiated nappes of the Peloritani orogen.

Sample	Stratigraphic and (Structural) Unit	VR <sub>0</sub> % (n. measurements)	%I in I-S (R parameter)	%C in C-S	XRD Analyses	
					<2 µm	Whole-rock
7	Serravallian-Messinian siliciclastic deposits	0.36±0.08 (22)	N.D.	N.D.	N.D.	N.D.
8		0.27±0.05 (5)	20 (R0)	65	I52I-S2C-S7K33Ch6	Qtz16Cal2Kfs3Ab33Ph46
9		barren	N.D.	N.D.	N.D.	N.D.
15		0.30±0.06 (22)	40 (R0)	65	I44I-S12C-S12K28Ch4	Qtz15Cal4Kfs3Ab32Ph46
30		0.26±0.07 (24)	33 (R0)	N.D.	I64I-S32Ch4	Qtz9Cal22Kfs1Ab14Ph54
11		N.D.	30 (R0)	N.D.	I17I-S34K46Ch3	Qtz16Kfs1Ab4Ph79
14a		N.D.	50;55 (R0;R1)	N.D.	I24I-S20K23Ch33	Qtz17Ab2Ph81
14b		N.D.	50 (R0)	N.D.	I37I-S20K25Ch18	Qtz11Ab2Ph84Ank3
16a		0.41±0.09 (26)	40;60 (R0;R1)	N.D.	I21I-S14K23Ch42	Qtz14Ab3Ph83
16b		N.D.	40;60 (R0;R1)	N.D.	I14I-S20K39Ch27	Qtz14Ab1Ph85
17	Argille scagliose (Antiscilide Unit)	N.D.	40 (R0)	N.D.	I17I-S33K32Ch18	Qtz9Ab2Ph87Hem2
19		N.D.	75 (R1)	N.D.	I40I-S14K13Ch33	Qtz15Ab4Ph81
24		N.D.	40;60 (R0;R1)	N.D.	I10I-S32K36Ch22	Qtz13Cal2Ab2Ph74Hem9
29		N.D.	55 (R0)	N.D.	I19I-S10K57Ch14	Qtz9Ab3Ph79Hem9
35		N.D.	40;63 (R0;R1)	N.D.	I17I-S7K42Ch34	Qtz14Ab3Ph83
37a		N.D.	40 (R0)	N.D.	I21I-S22K49Ch8	Qtz4Ab2Ph94
37b		N.D.	50 (R0)	N.D.	I34I-S15K48Ch3	Qtz4Ab2Ph93Hem1
38		N.D.	45 (R0)	80	I61I-S22C-S12Ch5	Qtz14Ab3Ph83
39		0.47±0.08 (23)	50 (R0)	60	I15I-S34C-S24K24Ch3	Qtz13Ab3Ph84
41		N.D.	27 (R0)	N.D.	I56I-S43K1	Qtz21Ab2Ph75Jar2
42		N.D.	25 (R0)	N.D.	I34I-S25Ch41	Qtz28Ab2Ph72
45a		N.D.	32 (R0)	N.D.	I10I-S31K54Ch5	Qtz28Cal3Ab2Ph87
45b		N.D.	20 (R0)	N.D.	I29I-S62K2Ch7	Qtz28Cal4Ab1Ph87
52a		N.D.	40 (R0)	70	I40I-S35C-S9Ch16	Qtz9Ab2Ph82Ank4Hem3
52b		N.D.	40 (R0)	70	I44I-S19C-S10Ch27	Qtz10Ab2Ph82Ank6
53a		N.D.	47 (R0)	70	I9I-S35C-S16K34Ch6	Qtz12Ph88
53b		0.56±0.05 (21)	40 (R0)	N.D.	I20I-S22K58	Qtz11Ab3Ph81Hem5
53c		N.D.	50 (R0)	60	I7I-S36C-S10Ch47	N.D.
54a		N.D.	45 (R0)	N.D.	I27I-S11K57Ch5	Qtz6Ab4Ph90
54b		N.D.	26 (R0)	N.D.	I9I-S15K64Ch12	Qtz6Ab3Ph89Ank2
54c		0.49±0.01 (3)	45 (R0)	70	I7I-S4C-S10K10Ch69	Qtz24Ab1Ph71Hem4
61a		N.D.	40 (R0)	N.D.	I30I-S31K15Ch4	Qtz10Cal9Ab2Ph77Ank2
61b		N.D.	40 (R0)	N.D.	I12I-S39K35Ch14	Qtz28Cal1Ab3Ph88
1a	Stilo-Capo d'Orlando Fm.	0.33±0.04 (39)	N.D.	N.D.	N.D.	N.D.
1b		0.21±0.05 (24)	N.D.	N.D.	N.D.	N.D.
1c		0.52±0.05 (7)	45;76 (R0;R1)	N.D.	I64I-S15K14Ch7	Qtz10Cal2Kfs2Ab21Ph85
1d		0.32±0.04 (27)	40;78 (R0;R1)	N.D.	I41I-S14K27Ch18	Qtz11Cal9Kfs2Ab23Ph55
1e		0.40±0.05 (28)	42;80 (R0;R1)	N.D.	I45I-S17K18Ch20	Qtz28Cal18Kfs1Ab12Ph61
2		barren	N.D.	N.D.	N.D.	N.D.
3		0.33±0.06 (7)	42 (R0)	N.D.	I53I-S27K15Ch5	Qtz9Kfs1Ab22Ph68
4		barren	N.D.	N.D.	N.D.	N.D.
5		0.52±0.07 (23)	N.D.	N.D.	N.D.	N.D.
6		N.D.	45;75 (R0;R1)	N.D.	I69I-S19K7Ch5	Qtz10Kfs1Ab20Ph68Hem1
10		0.31±0.05 (19)	N.D.	N.D.	N.D.	N.D.
12		0.46±0.06 (20)	35 (R0)	N.D.	I43I-S3K22Ch32	Qtz13Cal2Kfs2Ab28Ph55
13		0.58±0.08 (22)	20;70 (R0;R1)	N.D.	I63I-S9Ch28	Qtz16Kfs1Ab5Ph78
18		N.D.	45;78 (R0;R1)	N.D.	I53I-S27K17Ch3	Qtz14Kfs2Ab24Ph60
20a		N.D.	42;78 (R0;R1)	N.D.	I45I-S22Ch33	Qtz11Kfs1Ab27Ph59
20b		0.37±0.06 (17)	41;80 (R0;R1)	N.D.	I46I-S25K22Ch7	Qtz10Kfs1Ab21Ph68
21		0.35±0.03 (7)	50;80 (R0;R1)	N.D.	I42I-S30K22Ch6	Qtz11Kfs1Ab11Ph77
22		0.31±0.03 (6)	N.D.	N.D.	N.D.	N.D.
23		barren	N.D.	N.D.	N.D.	N.D.
25		0.41±0.05 (38)	45;60 (R0;R1)	N.D.	I45I-S14K25Ch16	Qtz15Cal5Kfs3Ab30Ph47
26		0.44±0.05 (30)	50 (R0)	N.D.	I52I-S5K14Ch29	Qtz26Cal29Kfs1Ab11Ph50Hem3
27		0.31±0.05 (17)	52 (R0)	N.D.	I67I-S8K17Ch8	Qtz28Cal14Ab10Ph68
28		N.D.	50;78 (R0;R1)	N.D.	I53I-S10K12Ch25	Qtz14Kfs2Ab30Ph54
31a		0.35±0.04 (100)	N.D.	N.D.	N.D.	N.D.
31b		N.D.	45;75 (R0;R1)	N.D.	I46I-S17K24Ch13	Qtz12Kfs1Ab17Ph70
32		0.38±0.05 (12)	42;80 (R0;R1)	N.D.	I38I-S34Ch28	Qtz12Kfs3Ab31Ph54
33		0.51±0.06 (36)	41;83 (R0;R1)	N.D.	I35I-S16K25Ch24	Qtz19Cal6Kfs2Ab31Ph42
34		N.D.	35;80 (R0;R1)	N.D.	I37I-S18K22Ch23	Qtz12Kfs1Ab18Ph69
36		0.38±0.07 (53)	45;80 (R0;R1)	N.D.	I39I-S31K23Ch6	Qtz28Kfs1Ab12Ph79
40		0.48±0.06 (21)	N.D.	N.D.	N.D.	N.D.
43		0.42±0.07 (16)	N.D.	N.D.	N.D.	N.D.
44		0.47±0.08 (39)	60 (R1)	N.D.	I50I-S8K12Ch30	Qtz17Cal12Kfs1Ab25Ph45
46a		N.D.	42;75 (R0;R1)	50	I48I-S9C-S21K9Ch13	Qtz12Kfs2Ab23Ph63
46b		0.47±0.09 (25)	N.D.	N.D.	N.D.	N.D.
47		0.30±0.05 (33)	41;78 (R0;R1)	N.D.	I61I-S9K13Ch17	Qtz11Cal6Kfs1Ab16Ph66
48		N.D.	50;80 (R0;R1)	N.D.	I58I-S9K18Ch15	Qtz14Kfs2Ab20Ph64
49		0.42±0.06 (26)	50 (R0)	N.D.	I49I-S5K26Ch20	Qtz28Cal4Kfs1Ab17Ph70
50		0.27±0.02 (8)	41;78 (R0;R1)	N.D.	I46I-S11K24Ch19	Qtz29Cal2Kfs2Ab19Ph68
51		0.45±0.05 (51)	45;75 (R0;R1)	N.D.	I48I-S7K28Ch17	Qtz28Cal13Kfs1Ab14Ph64
55		0.31±0.05 (34)	50 (R0)	N.D.	I49I-S4K21Ch26	Qtz15Cal1Kfs3Ab30Ph51
56		0.43±0.06 (9)	N.D.	N.D.	N.D.	N.D.
57		0.30±0.04 (24)	42;76 (R0;R1)	65	I48I-S7C-S16K22Ch7	Qtz28Cal12Kfs1Ab15Ph64
58		0.45±0.05 (61)	50 (R0)	N.D.	I49I-S2K19Ch30	Qtz26Cal4Kfs2Ab12Ph76
59		0.30±0.04 (30)	N.D.	N.D.	N.D.	N.D.
60		0.28±0.06 (17)	38;70 (R0;R1)	65	I46I-S24C-S5K9Ch16	Qtz26Kfs1Ab15Ph78

Table 3.1 – Summary of inorganic and organic thermal parameters and XRD quantitative analysis.



### 3.4.1.3. Serravallian-Messinian siliciclastic deposits

In the Serravallian-Messinian siliciclastic deposits, kerogen is of terrestrial origin with predominant macerals of the huminite-vitrinite group and subordinate of the inertinite group. Pyrite is frequently associated with both groups. VR<sub>0</sub>% data range from 0.26 (site 30) to 0.36% (site 7), indicating the immature stage of hydrocarbon generation (Tab. 3.1 and Fig. 3.6).

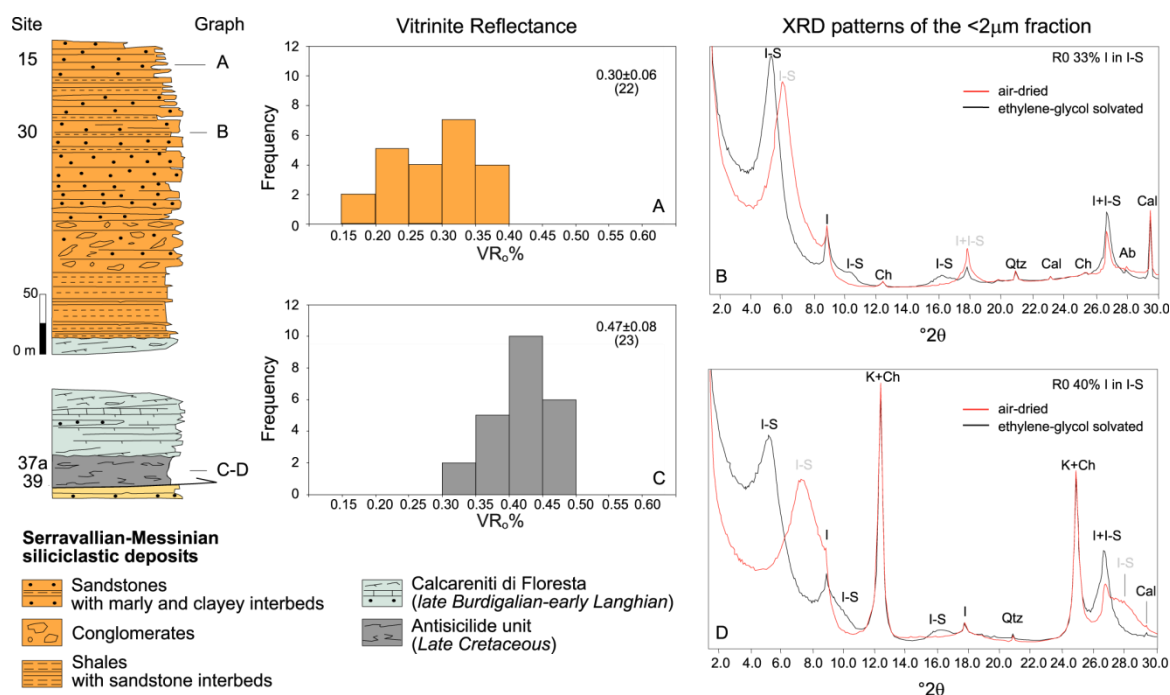


Figure 3.6 - Synthetic stratigraphic logs of the Serravallian-Messinian deposits and the Antisicilide Unit + Calcareni di Floresta pair with selected vitrinite reflectance histograms (A-C) and XRD oriented patterns of the <2 μm grain-size fraction (B-D). Acronyms - Ab: albite; Cal: calcite; Ch: chlorite; I: illite; I-S: mixed layer illite-smectite; K: kaolinite; Qtz: quartz.

### 3.4.2. Clay mineralogy data

#### 3.4.2.1. Stilo Capo d'Orlando Formation

Analysis of randomly-oriented whole-rock powder patterns shows that fine-grained sandstones of the SCO are mainly composed of phyllosilicates (mica and clay minerals), quartz, albite, calcite and minor amounts of K-feldspar (Tab. 3.1). Oriented mounts of the <2 μm grain-size fraction display illite-rich assemblages which constitute at least 40% of the overall composition, chlorite, kaolinite and subordinate amounts of mixed-layered minerals (Tab.3.1 and Fig. 3.4B, D, F).

Although the XRD peaks of mixed-layered minerals are not much visible and their abundance usually does not exceed 20% of the clay fraction, three different interstratified

minerals can be distinguished comparing ethylene-glycol and air-dried patterns and using modeling procedures.

The decomposition of the complex peaks between 9-10 °2 $\theta$  and 16-17 °2 $\theta$  points out the presence of a 10 Å phase (~8.87 °2 $\theta$ ) corresponding to illite and/or K-white mica which are unaffected by glycolation and two mixed-layers illite-smectite (I-S) of different composition and stacking order. Mixed-layered I-S with no preferred sequence in stacking of layers have an illite content of 38-52%, whereas ordered R1 structures have contents higher than 70%. The decomposition of the peak at ~12.40 °2 $\theta$  confirms the superimposition of kaolinite (001) and chlorite (002) reflections together with mixed-layers chlorite-smectite (C-S) which cause the asymmetry of the peak tail in the low angle region. Averaged chlorite content in mixed-layers C-S is 60%.

In the southern area of the Peloritani Mts., mixed layers I-S display a trend similar to that shown by vitrinite reflectance. Random-ordered I-S disappears as function of depth and converts into short-ordered structure with a progressive increase of illite layers from 38% (Fig. 3.4B) to 60% (Fig. 3.4F). In the north-eastern zone of the Peloritani Mts., the SCO exhibits illite contents in I-S lower than 35%. The heterogeneous mixed-layer clay minerals assemblage (R0+R1 I-S) in the uppermost part of the succession is interpreted as a mix of diagenetic and detrital phases (see discussion).

#### 3.4.2.2. Antisicilide Unit

The Upper Cretaceous varicoloured clays of the Antisicilide Unit are generally composed of phyllosilicates and quartz which constitute the 87-98% of the overall composition (Tab. 3.1). Calcite, albite, ankerite and hematite occur as minor phases. Jarosite has been detected only in one sample (site 41).

Illite and mixed layer I-S are the most abundant minerals in the <2 µm grain-size fraction. Kaolinite, chlorite and mixed layers C-S irregularly occur in subordinate amounts. Non-clay minerals such as quartz, calcite and albite are also observed in this fraction. Mixed-layered clay minerals generally consist of random ordered I-S with an illite content between 20 and 55% and mixed layer C-S where the chlorite content ranges from 60 to 80%. Occasionally, ordered and random ordered I-S have been observed together in the same sample. In these cases, three distinct sub-populations of illitic assemblages have been identified by using a profile-fitting method (Lanson, 1997). They correspond to discrete illite, R1 I-S with smectite layers that do not exceed 45% and R0 I-S with smectite content in the range of 50-60% (Tab. 3.1).



#### 3.4.2.3. Serravallian-Messinian siliciclastic deposits

Only three samples from the Serravallian-Messinian siliciclastic deposits were studied by XRD analysis (Fig. 3.6B). Two out of three samples were selected from marly and clayey interbeds of fine-grained sandstones whereas the remnant is from sandstones. Clay-rich lithologies show a mineralogical assemblage composed of phyllosilicates, quartz and albite with minor amounts of K-feldspar and calcite. The <2 µm grain-size fraction contains illite and chlorite as major minerals and subordinate amounts of mixed layers I-S, C-S and chlorite (Tab. 3.1). The lack of kaolinite and mixed layer C-S in the fine fraction and a greater amount of calcite in the whole-rock composition are the main differences observed in site 30 compared with clayey rocks. Mixed-layer clay minerals are random ordered I-S with an illite content between 20 and 40% and mixed layer C-S where the chlorite content is 65%.

#### 3.4.3. Structural data

##### 3.4.3.1. Stilo Capo d'Orlando Formation

Structural analysis of the SCO indicates the occurrence of two main compressive deformation styles. Shortening is quite mild with ENE-WSW fold axis in the southern area of the Peloritani Mts. and severe with E-W fold axis to the north. In the southern sector, structures are represented by hectometer to kilometer ENE-WSW-trending open folds (Fig. 3.3, cross sections A-A', B-B', D-D') locally with en-échelon arrangement (Somma, 2006). The youngest rocks affected by these folds are the Calcareni di Floresta (upper Burdigalian-lower Langhian) and probably also the upper Langhian-lowermost Serravallian clayey and marly lithofacies. As the overlying lower Serravallian-lower Messinian siliciclastic deposits are not involved in this compressive deformation (Fig. 3.3, cross sections B-B' and C-C'), the fold age should be post-late Langhian and pre-(?)early Serravallian.

To the north, on the Tyrrhenian coast, the SCO is highly deformed, being affected by rare high angle reverse faults and folds (Fig. 3.7f). Reverse faults, mainly observed in Burdigalian sandstones with siltite interbeds, are E-W trending and dip north-wards with angles of 70-80°. Kinematics indicators (striae) and decimeter horse-like structures indicate a south-ward tectonic transport direction. The cross-cutting relationships between bedding and reverse faults define angles lower than 30-40°.

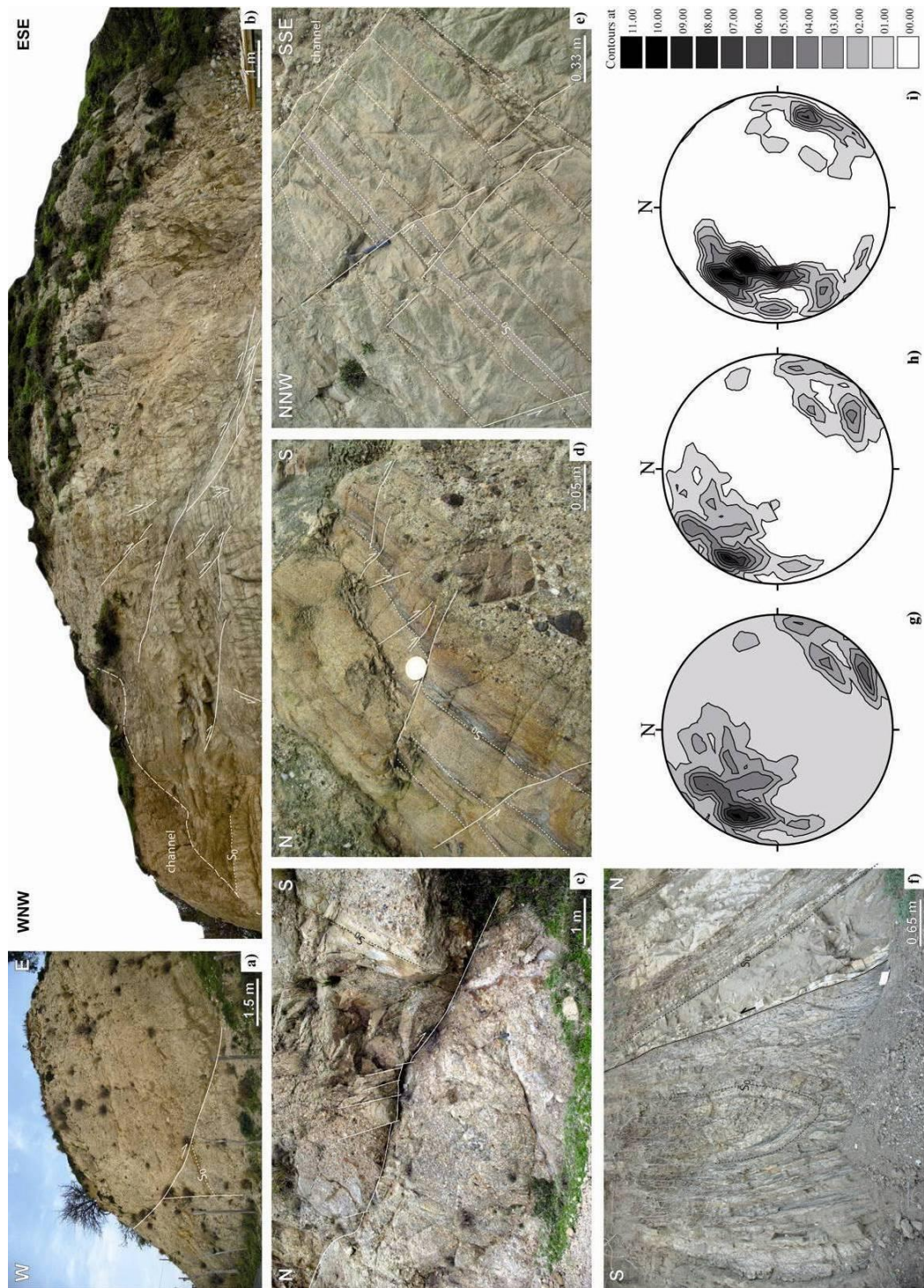


Figure 3.7 - Low- (a-d), high-angle normal faults and apparent reverse faults (e) in the Serravallian-Messinian deposits. Reverse fault and syncline in the Burdigalian deposits of the Stilo-Capo d'Orlando Fm. (f). Orientation data of normal faults in the Serravallian-Messinian conglomerates (g-i) (density stereogram, equal area projection, lower hemisphere). Present-day orientation data (g) (n=109). Orientation data after rotation (h) (zenithal angle 14° around an axis 80/0) to restore bedding (mean plunge: 350 and inclination: 54° to clinoforms with a mean inclination value of 40° (gravels internal friction angle). Present-day orientation data (i) (n=47).

Fault footwall is occasionally affected by south-verging meter scale folds with E-W axis and axial surfaces dipping towards north with angles of 70-80° (Fig. 3.7f). Folds are similar with interlimb angles ranging from 30 to 80°. They are associated with an axial plane cleavage, characterized by cm-thick lithons and intersection lineation (between cleavage and bedding) parallel to the fold axis. The above-mentioned structures are absent in the overlying Serravallian-lower Messinian conglomeratic and arenitic lithofacies. Consequently, this compressive tectonics should be post-Burdigalian and pre-(?)early Serravallian. The high dip angles of the reverse faults, fold axial planes and cleavages are probably due to later rotation around horizontal axis. This rotation might be Serravallian-early Messinian in age, as similar syn-sedimentary rotational deformation has been identified in the Serravallian-lower Messinian conglomerates and sandstones (see below). Consequently, reverse faults and folds should represent tilted original thrusts and folds.

#### 3.4.3.2. Antisicilide Unit

Deformation is rarely observable in the varicoloured clays of the Antisicilide Unit. Structures consist of rare meter to decameter SSE-vergent buckling folds with ENE-WSW axis (Moio Alcantara area). These folds are open and upright, and show curved hinges. A similar deformation style has been also identified in the siliciclastic deposits of the Sicilide Units exposed close to the edge of the Peloritani Mts.

#### 3.4.3.3. Serravallian-Messinian siliciclastic deposits

The conglomeratic lithofacies of the Serravallian-Messinian siliciclastic deposits is strongly affected by extensional brittle tectonics (Fig. 3.7). It consists of NE-SW and NNE-SSW oriented fault systems showing extremely variable angles of dip that range from 20-30° to 70-85° (Fig. 3.7g-i). Typical kinematics indicators are striae and drag folds. Sub-vertical faults are generally ENE-WSW trending and show a lateral component of the movement. SE- and SSE-dipping normal faults with a mean angle of dip of 30-45° (Fig. 8a-d) and a local dextral component of the movement are widely developed. The conglomerate layers cut by these faults show downlap terminations of the strata characterized by N- to NW-dips with angles up to 70° (Fig. 3.7c). The cross-cutting relationships between faults and clinoforms are characterized by angles up to 80-90°. Most faults display low displacements ranging from 0.01 to 0.33 m (Fig. 3.7a-e). The associated damage zones are from 0.001 to 0.01 m wide. C-S structures and fault gouge

generally develop in the footwall. Conglomerates show pebbles and boulders (diameter ranging from 0.004 to 1 m) cross-cut by joints and normal faults with displacements from 0.01 to 0.1 m. Occasionally, reverse and/or oblique faults affect the pebbles. Considering the afore-mentioned angular relationships between bedding and NE-SW oriented faults, as well as the elevated values of the clinoform dip-angles, the low dip-angle of most of the normal faults and (apparent) high-angle reverse faults (Fig. 3.7g) can be interpreted as due to tilting of previous high angle normal faults (Fig. 3.7d). Restoration of structural data (Fig. 3.7g), performed by a clockwise rotation about a horizontal axis parallel to the bedding strike, corroborates this hypothesis, as restored faults (Fig. 3.7h) show attitudes analogous to those of the deposits not affected by rotation (Fig. 3.7i), the bedding being with dip-angles lower than 30°. The age of inception of extensional tectonics in this area is still debated, and has been proposed to be Serravallian (Lentini et al., 1995) or late Tortonian (Catalano et al., 1996; Pepe et al., 2000).

At regional scale, these faults probably belong to the NW- and SE-dipping normal fault systems stretched along the Tyrrhenian and Ionian side respectively, putting in contact the crystalline rocks (in the footwall) with the Paleogene and Neogene sedimentary covers (in the hanging wall) of the Peloritani Mts.

### **3.5. Discussion**

#### *3.5.1. Isopach and paleoisopach map reconstruction of the Stilo-Capo d'Orlando Basin*

As temperature, time, fluid composition and some chemical variables can change simultaneously, it is difficult to discriminate which parameter affects most the proportion of illite layers in mixed layers I-S during burial diagenesis. Variability of illite content in I-S in rocks of similar age, origin and lithology can only be attributed to different maximum paleo-temperatures as result of differences in uplift, erosion rate and sedimentary/tectonic loading. For this reason, the reconstruction of basin geometry and the definition of sedimentary units thicknesses are essential to distinguish the effect of burial diagenesis and tectonic loading on thermal maturity of sediments.

We reconstructed the basin architecture and the SCO thickness variation through field mapping studies and using measured stratigraphic sections (Carmisciano and Puglisi, 1978; Bonardi et al. 1980; Caliri et al., 1993; Catalano and Di Stefano, 1996; Carbone et

al., 1998, 2008; Giunta and Nigro, 1999; Lentini et al., 2000; Messina et al., 2004; Fig. 3.8).

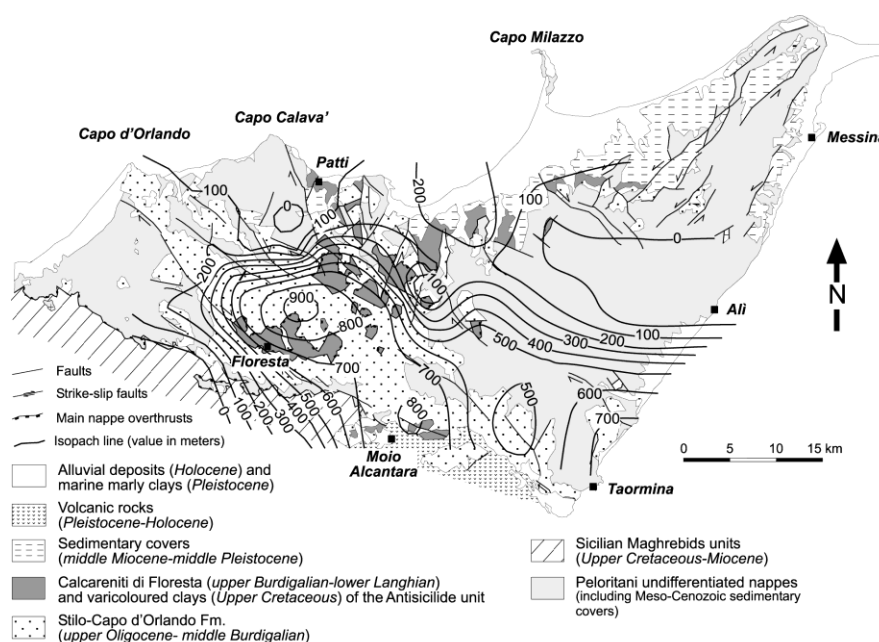


Figure 3.8 - Isopach map of the paleo-distribution of the Stilo-Capo d'Orlando Fm. Thickness data are from Carmisciano and Puglisi (1978); Bonardi et al. (1980); Caliri et al. (1993); Catalano and Di Stefano (1996); Carbone et al. (1998, 2008); Giunta and Nigro (1999); Lentini et al. (2000) and Messina et al. (2004).

The syn-orogenic succession is covered by the widespread remnants of the Antisicilide Unit which preserves the original thickness of the SCO throughout the basin. The depocenter is a NW-SE elongated area stretched from Floresta to Taormina villages (in the southern area of Peloritani Mts.) with thicknesses exceeding 900 m (Fig. 3.8). The succession abruptly thins towards Patti to the N and Peloritani Mts. to the NE (in the northern area of the Peloritani Mts.). In these areas, erosion of the SCO is negligible, because the youngest portion (Burdigalian) of the SCO crops out (Carbone et al., 2008).

### 3.5.2. Reconstruction of the paleogeothermal gradient during Oligocene Miocene time

We reconstructed the paleo-geothermal gradient during the deposition of the SCO and traced its thermal evolution through time using the following equation: geothermal gradient ( $^{\circ}\text{C}/\text{km}$ ) = heating rate ( $^{\circ}\text{C}/\text{Ma}$ )/burial rate ( $\text{km}/\text{Ma}$ ). The heating rate value was extracted from the correlation of vitrinite reflectance and expandability (reverse of illite content in I-S) data based on the kinetic model of vitrinite maturation of Burnham and Sweeney (1989) and the kinetics of the I-S reaction determined by Hillier et al. (1995).

Figure 3.9 shows two main data clusters. One group (blue circles) corresponding to Miocene samples yields heating rates lower than 1.5 °C/Ma. The other group (green circles) corresponds to upper Oligocene and deeper strata indicating heating rates between 1.5 and 6°C/Ma. Just one sample (red circle) correlates to anomalous heating rates.

Calculated paleo-geothermal gradients for the two data clusters are in the range of 17-23 °C/km for low heating rates (Miocene deposits) and 55-60 °C/km for the second group (Oligocene deposits) considering burial rates of 0.06 Km/Ma for the Miocene and 0.09 Km/Ma for the Oligocene. These last data derive from sections dated by Catalano and Di Stefano (1996).

The decrease of the heating rates from late Oligocene to Miocene times can be interpreted in terms of geodynamics of the SCO basin, being related to the evolution from the subduction to collision stage. As a matter of fact, since late Oligocene, the SCO filled a fore-arc basin located on the crystalline nappes of the Peloritani Mts. that evolved later on into a thrust-top basin. Geothermal gradients of 36-64 °C/km (most likely 50 °C/km) and 54-72 °C/Km for hot fore-arcs (Bachman et al., 1983; Miller and Macdonald, 2004) and of 22-24 °C/km for thrust-top basins (Allen and Allen, 1993) are in reasonable agreement with those calculated by organic and inorganic thermal indicators for the SCO basin.

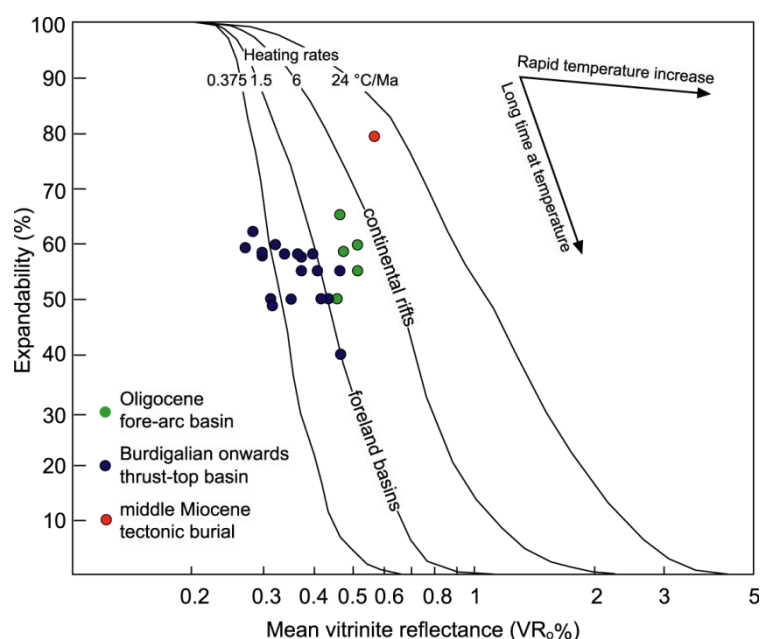


Figure 3.9 - Heating rates values for the Stilo-Capo d'Orlando Fm. extracted from the correlation of vitrinite reflectance and expandability (reverse of illite content in I-S) data based on the kinetic model of vitrinite maturation of Burnham and Sweeney (1989) and the kinetics of the I-S reaction determined by Hillier et al. (1995).



### 3.5.3. *Burial and thermal history of the Stilo Capo d'Orlando depocentre*

Mineralogical thermal indicators reflect the reconstructed basin architecture and a burial diagenesis trend can be traced in the basin depocenter. The diagenetic signal is always blurred by high illite content detrital I-S in the uppermost beds while is more clear in the deepest strata where the random to short ordered I-S conversion occurs (Fig. 3.4B-F). The slight increase of illite layers as function of depth is supported by organic matter optical data which show a single population of indigenous vitrinite macerals and vitrinite reflectance values increasing from 0.28 to 0.47-0.48%. The observed maturity trend of ~0.2% VR<sub>o</sub>/km and the corresponding increase of 22% illite layers in I/S per km is the result of a complex summation of sedimentary burial and variable heating rates. Back-thrusting of the Antisicilide Unit and the sedimentation of the Calcareni di Floresta (total maximum thickness of about 250 m) contributed in minor amounts to the acquisition of the thermal maturity trend.

A simplified reconstruction of the burial and thermal history of the SCO in the basin depocenter was performed using the software package Basin Mod<sup>®</sup> 1-D (1996; Fig. 3.10). The main assumptions for modeling are that: (i) rock decompaction factors apply only to clastic deposits (i.e., SCO and Calcareni di Floresta) according to Sclater and Christie's method (1980) and (ii) a variable geothermal gradient has been adopted according to our calculation. The results of burial and thermal modeling are shown in figure 3.10A.

The reconstructed evolution begins with the deposition of the SCO in a fore-arc basin in late Oligocene times. The collision between the southern edge of the Calabria-Peloritani Arc and the African plate caused back-thrusting of the Antisicilide Unit (Lentini and Vezzani, 1978; Cavazza and Barone, 2010) on top of the SCO. This phase brought to a shallow tectonic burial of the SCO. Syn-orogenic sedimentation continued in thrust-top basins during the late Langhian and up to the early Serravallian. During this time span the Calcareni di Floresta deposited and evolved into a succession of marls and marly clays with interbedded sands capping the suture between the Calabria-Peloritani Arc and the Sicilide accretionary prism. The SCO deepened at maximum depths of ~1200 m recording maximum temperatures of about 70-75°C. The type of evolution outlined here, allowed an acceptable calibration against measured data, as shown by the resulting maturity curve of figure 3.10B. The SCO experienced low temperature evolution in the

early diagenetic zone and in the immature stage of hydrocarbon generation (Merriman and Frey, 1999).

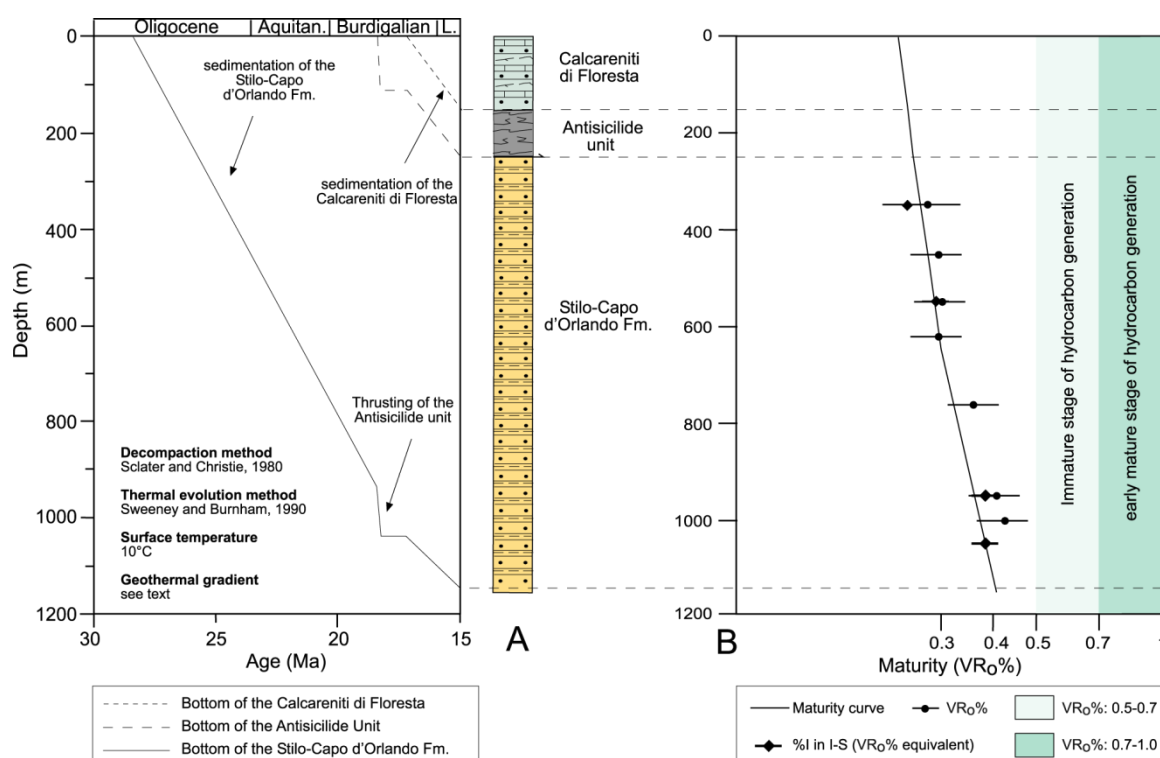


Figure 3.10 - A) Representative 1-D burial and thermal modeling of the Stilo-Capo d'Orlando Fm. in the basin depocenter; B) Present-day maturity data plotted against calculated maturity curve. Depth for each sample based on outcrop distribution.

### 3.5.4. Sedimentary vs. tectonic burial of the Peloritani Mts. northern sector

Contrasting thermal information can be derived from organic and inorganic indicators for the north-eastern sector of the Peloritani Mts. and the Patti area where the SCO reduces its thickness to zero and is generally less than 100 m (Fig. 3.8). As a matter of fact, in some localities the Antisicilide Unit directly lies on top of the Peloritani nappes testifying the closure of the SCO basin towards the north. Mineralogical analyses of the <2 µm fraction display the coexistence of random and short ordered I-S and the lowest illite content (20-35%; Fig. 3.4b) for R<sub>0</sub> I-S, suggesting that clay minerals assemblage is a mix of mostly detrital and diagenetic phases. On the contrary, vitrinite reflectance values (0.46-0.58%; Fig. 3.4a) are too high considering the SCO thickness and they suggest a greater thermal imprint for this sector. This result is strongly supported by a companion study where apatite fission-track and (U-Th-Sm)/He analysis have been



applied on the crystalline substratum of the basin (Balestrieri et al., 2008). Fission-track analysis indicates for an intermediate portion of the Peloritani Mts. (shaded area in Fig. 3.4c) temperatures of 80-120 °C partially to totally annealing the fission tracks after the SCO sedimentation. It is worth to note as the area affected by this late thermal event constrained by young (<15 Ma) fission-track age (Fig. 3.4c) is superimposing on the high vitrinite reflectance values not justified by sedimentary load. Additionally, (U-Th-Sm)/He ages indicate a fast cooling since Messinian-Pliocene times. In this time span (~2 Ma), temperature turns down quickly from 80-100 to 65 °C.

Thus the heating event was too short to overprint clay minerals indicators whose kinetic response is much lower than organic matter for short term and low temperature heating events (Hillier et al., 1995). This is the reason why clay minerals record early diagenetic conditions reflecting the basin architecture instead of the thermal anomaly in the north-eastern area of the Peloritani Mts.

Hence, the young thermal event we have identified is characterised by: a short duration as pointed out by the integration of AFT, (U-Th-Sm)/He ages, organic and clay minerals parameters; and a localized area of influence. On the basis of regional data, the causes that could be invoked to justify this thermal anomaly may be at least three: (i) back-thrusting of the Antisicilide Unit on the hinterland generating a tectonic load; (ii) lateral changes in heat flow due to lithosphere configuration; (iii) compressive reactivation at the rear of the chain with emplacement of an out-of-sequence S-verging thrust stack.

The first hypothesis might be supported by substantial pieces of regional evidence. As a matter of fact back-thrusting of more external units (Tellian nappe) onto the hinterland (Kabylies) is a distinctive feature in the Algerian portion of the orogen (Roca et al., 2004) as well as in Sicily where the Antisicilide Unit have been backthrust onto the Peloritani Mts. in Burdigalian times (Corrado et al. 2009 and references therein). Nevertheless, this cause can be excluded as major factor responsible for the high thermal maturity in the NE area of the Peloritani Mts. because the original thickness of the Antisicilide Unit is negligible (max 200 m) when totally preserved by the Calcareni di Floresta Fm. and tends to reduce to zero moving from the depocenter towards the north.

The hypothesis of a lateral increase in heat flow should be considered in the regional context in which the Peloritani Mts. are part of the Calabria-Peloritani Arc whose complex geodynamic evolution has been recently revised from a geophysical, structural and paleo-magnetic point of view (Faccenna et al., 2004 and references therein; Cifelli et al., 2007 and references therein). As a matter of fact, the mechanism of the SE-ward

retreat migration of the Ionian slab in the Neogene and Quaternary times and the related formation of the arc suggests that slab deformation was driven, not only by the presence of an oceanic (deep sea) Mesozoic seaway but also by lateral mantle flow that may account first-order lateral heat flow variations. Nevertheless the short duration and the localized effects of the heating event highlighted in this paper seem to be too limited in space and time to account for thermal variations linked to first-order processes due to lithosphere configuration and slab dynamics. These processes in a first approximation should involve the entire Peloritani Mts. in a wider time span. However, we cannot exclude this hypothesis and only a fully developed 2-D (or 3-D) modeling integrating plate configuration as well as a detailed distribution of loads, analogously to what proposed by Hardebol et al. (2009) in the Rocky Mts., could provide a further contribution to this point.

The third hypothesis seems to satisfy both regional and local constraints. Lentini et al. (1995) and Catalano and Di Stefano (1996) underlined that active thrusting represented one of the major factors, together with regional subsidence and sea level changes, controlling the depositional architecture of terrigenous units in the Peloritani Mts. between late Oligocene and late Langhian. Furthermore, Carbone et al. (1993) outlined a syn-sedimentary thrust activity between late Burdigalian and Langhian based on a detailed analysis of facies distribution, depositional geometries and biostratigraphic record of the Calcareni di Floresta. Additionally, Giunta and Nigro (1999) invoked compressive reactivation in the Peloritani Mts. during Burdigalian-Langhian times on the basis of local structural data and Vignaroli et al. (2008) testify a S-verging compressive deformation of the SCO.

Therefore, we consider the emplacement of an out-of-sequence thrust stack, nowadays eroded, the most probable key process causing the partial to total annealing of fission-tracks and the enhancement of vitrinite reflectance values. The eroded structure thickness calculated through 1-D modeling is ~3.5 kilometers.

This reconstruction is also supported by our structural investigation. The two field evidence that strengthen our hypothesis are: (i) the compressive tectonics showing different deformation styles in the southern and northern Peloritani Mts. (Fig. 3.11a-b); (ii) the extensional tectonics affecting the Serravallian-lower Messinian successions (Fig. 3.11c).

Concerning the first point, the different style and orientation of folding in the northern and southern areas of the Peloritani Mts. can be ascribed to different tectonic events. In

the southern area, gentle ENE-WSW folds, are compatible with the regional stress field orientation responsible for the activation of WNW-ESE to NNW-SSE right lateral strike-slip faults that occurred at different time intervals since Middle-Late Miocene times (Ghisetti, 1979; Billi et al., 2006; Somma, 2006). The depocenter of the SCO basin should have developed in a such tectonic context, where the exclusive effect of sedimentary burial has been recorded by both organic and inorganic indicators.

On the other hand, in the northern area, severe deformation caused E-W fold and thrust associations during late Langhian-early Serravallian times. In this area, the local heating recorded by vitrinite reflectance and AFT data might depend on the tectonic overburden caused by out-of-sequence thrusting. Vergence of folding may testify a top to the south transport direction of the supposed thrust stack.

This hypothesis is in reasonable agreement with a discrete amount of strain accommodated in Miocene times within the metamorphic belt by breaching thrusts and transpressive faults as summarised by Billi et al. (2007) and evidenced for the first time by Giunta and Nigro (1999).

Concerning the second point, the NNE-striking extensional fault system that affect the Serravallian-Messinian succession along the Tyrrhenian and the Ionian coasts totally coincides with extensional fault pattern analysed by Ghisetti (1992), Di Stefano and Lentini (1995) and Lentini et al. (1995, 1996) in north-eastern Sicily, mostly result of WNW-ESE and NW-SE-oriented stretching processes (Cifelli et al., 2004). Their activity ruled the development of extensional basins both on-shore and in near off-shore areas since Late Miocene (Catalano et al., 1996; Pepe et al., 2000). In particular, the early Serravallian tectonic inversion occurring in the Calabria-Peloritani Arc segment of north-eastern Sicily, which produced extensional structures associated with the uplift of the Peloritani Mts., overprinted the Early Miocene out-ward migrating thrust belt (Lentini et al., 1995). At that time, new drainage patterns were established with sediment transport towards the north (in present-day coordinates) and this new tectonic pattern was probably related to the early Serravallian foundering of a proto-Tyrrhenian depression (Speranza et al., 2003). Thus this syn-sedimentary extensional tectonics contributed at least since middle Miocene to the uplift, exhumation and unroofing of the Peloritani Mts. with the removal of the out-of-sequence thrust stack supposed on the base of organic matter and thermo-chronological signature.

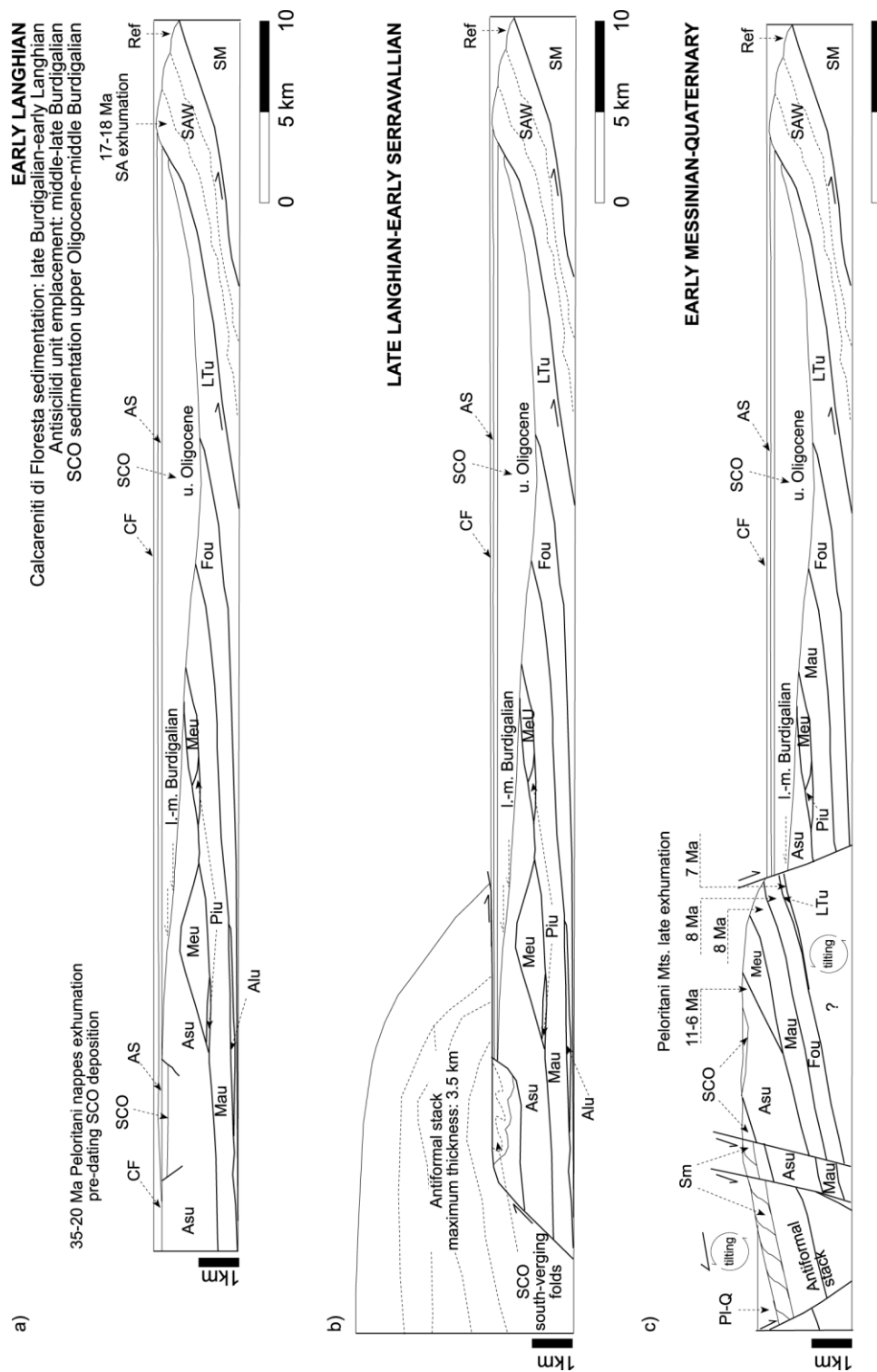


Figure 3.11- Schematic evolution of burial-exhumation of the Peloritani Mts. since middle Miocene. a) early Langhian; b) late Langhian-(?)early Serravallian; c) early Messinian-Quaternary. Acronyms - PL-Q: Pliocene-Quaternary deposits; Ref: Reitano Flysch; SAW: Sicilide Accretionary Wedge; Sm: Serravallian-Messinian siliciclastic deposits; AS: Antiscilide unit; CF: Calcareni di Floresta; SCO: Stilo-Capo d'Orlando Fm.; Internal Zone (nappes from top to base) - Asu: Apromonte unit; MeU: Mela unit; Plu: Piramo unit; Fou: Mandanici unit; Mau: Ali-Montagnareale unit; Alu: Ali-Montanici unit; Ltu: Longi-Taormina unit. External Zone - SM: Sicilian Maghrebids.

### 3.6. Conclusion

Vitrinite reflectance and mixed-layered clay minerals data allowed us to trace the thermal evolution of the Paleogene and Neogene sedimentary sequences of the Peloritani Mts. and record the occurrence of a late Langhian-(?)early Serravallian out-of-sequence thrust tectonics.

In the SCO basin, we indentified two different sectors affected by sedimentary and/or tectonic burial. A southern area, NW-SE oriented, where thermal parameters increase as function of depth indicating that the SCO thermal evolution is ruled by sedimentary burial. Organic and inorganic thermal indicators record the immature stage of hydrocarbon generations and diagenetic conditions revealing a decrease in paleo-geothermal gradient values from fore-arc (55-60 °C/km) to thrust-top (17-23 °C/km) setting. The reconstructed Oligocene-Miocene paleo-geothermal gradient marked the SCO basin evolution from convergence to collision occurred between the Calabria-Peloritani Arc and the African plate in the western Mediterranean area.

Differently, in the northern area of the basin, the thermal evolution was controlled by tectonic burial related to middle Miocene out-of-sequence thrust tectonics. The emplacement of a thrust stack with maximum thickness of ~3.5 km, quickly removed from Late Miocene onwards by extensional tectonics and erosion only affected organic matter thermal maturity. The short time at maximum temperature (<2 Ma) and the slow kinetic response at low temperatures of clay minerals are the reason why mixed layer I-S did not record thrust emplacement and evolved less than organic material.

## CHAPTER IV - EXTERNAL ZONE (MT. JUDICA UNIT)

### 4.1. Introduction

The internal structure of orogenic belts is a result of the interaction between first order processes such as crustal flexure, shortening and exhumation. The frontal part of fold-and-thrust belts is generally nonlinear and characterized by salient and recess features that often are strongly controlled by stratigraphic inhomogeneities in the foreland plate (e.g., Ben Avraham & Grasso, 1990) but may be also linked to the occurrence of mid-crustal basement-involved thrusts (e.g. Billi and Tiberti, 2009). The geologic factors controlling curvature geometry and kinematics in fold-and-thrust belts have been already widely investigated in the literature (e.g., Marshak, 1988 for a review; Paulsen and Marshak, 1999; Marshak, 2004; Sussman and Weil, 2004), but minor attention has been given to the evolution of burial and exhumation processes along the strike of the belt. Moreover, relationships among burial and exhumation amounts, shortening and thrust wedge thickness along strike have not been quantitatively investigated in detail, despite they may have conspicuous implications for thermal maturation of potential source rocks.

In Sicily, the Neogene-Quaternary Apenninic-Maghrebian orogenic front forms a wide salient, convex towards the south, extending offshore along the Sicily Channel in the Mediterranean Sea (Fig. 4.1). This salient evolves onshore towards the east into a recess in the area of Castel di Judica village to the west of Catania. The arcuate origin of the Sicilian thrust front has been related to the piggy-back thrust migration towards the Hyblean foreland with a highly articulated Mesozoic-Cenozoic paleogeography (Lickorish et al., 1999). The main salient developed in front of a Mesozoic thin and well-bedded pelagic succession that favoured thrust propagation whereas the eastern recess developed in front of a few km thick carbonate platform succession (Catalano et al., 2008) of the Hyblean foreland.

In the recess area of Mt. Judica, a Middle Triassic-Early Miocene stratigraphic succession is currently imbricated in three tectonic slices and exposed in a tectonic window. This succession is overthrust by a huge cover of several kilometers thick Allochthonous Units to the north and in the salient area of the fold-and-thrust belt to the west. A few attempts have been made to characterize the thermal and structural evolution

of the Mt. Judica succession: Guilhaumou et al. (1994), on the basis of fluid inclusion microthermometry of tectonic veins and Rock-Eval Pyrolysis and micro-infrared analysis on organic matter, estimated the P-T conditions of the fluid circulating in the sole thrust at the base of the succession with temperatures between 140 and 235 °C and lithostatic pressures of 0.8-1.0 kbar whose origin has been discussed by Larroque et al. (1996) and Dewerer et al. (2006). These data are consistent with a recent paper by Aldega et al. (2007) who performed a first correlation of organic and inorganic parameters estimating a tectonic load of ~3.0 km for the Jurassic-middle Miocene portion of the Mt. Judica Unit. Nevertheless, a study extended to the entire stratigraphic succession cropping out in the Mt. Judica recess comprising its base (Middle Triassic in age) is not available and the along strike space-evolution of tectonic overburden has never been traced from the recess towards the salient.

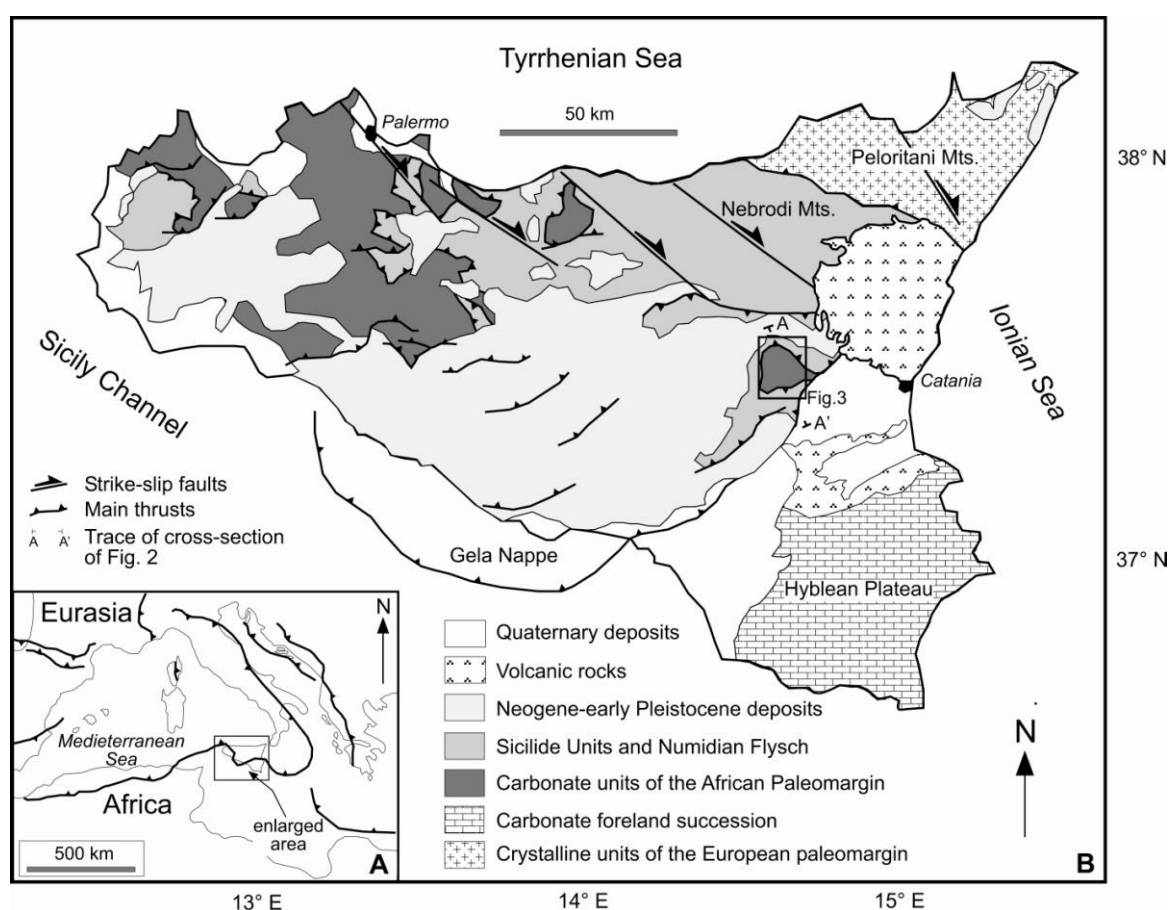


Figure 4.1 – Schematic geological map of Sicily showing the Gela nappe salient and the Mt. Judica (in the box) recess redrawn and modified after Monaco and De Guidi (2006).

In this paper, we integrated XRD data concerning the illite content in mixed layer illite-smectite (I-S) with data derived from FTIR on H-rich organic matter in order to constrain

thermal modelling of the burial-exhumation path of the Mt. Judica sedimentary succession in the recess area. The calculated maximum burial in Mt. Judica area and the restoration of balanced cross-sections along the thrust front allowed us

1. to reconstruct the wedge geometry in the recess area,
2. to investigate the along-strike variations of the tectonic overburden,
3. to discuss the geodynamic causes of these changes.

These regional results have been eventually compared with theoretical models of wedge dynamics, improving the understanding of recess to salient geometries and kinematics of curved fold-and-thrust belts in the Mediterranean area.

#### 4.2. Geological setting

In Eastern Sicily the thrust belt is organized into two main structural zones: Internal Zone to the north and External Zone to the south (Fig. 4.2).

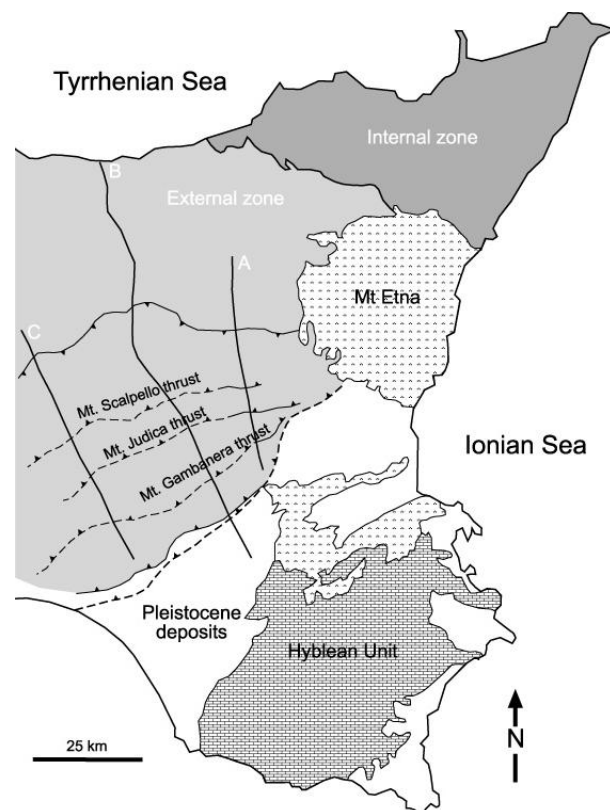


Figure 4.2 – Simplified structural scheme of Eastern Sicily with location of the geological cross-sections modified and redrawn after Bello et al. (2000). A-B-C are cross section traces published by Bello et al. (2000) and used for interpretation of evolution of structures along strike.



The External Zone is made up of three main tectono-stratigraphic units deriving from the deformation of palaeogeographic domains belonging to the African paleo-margin and the present structural setting is illustrated by three regional cross-sections derived from seismic lines (Bello et al. 2000; Fig. 4.3).

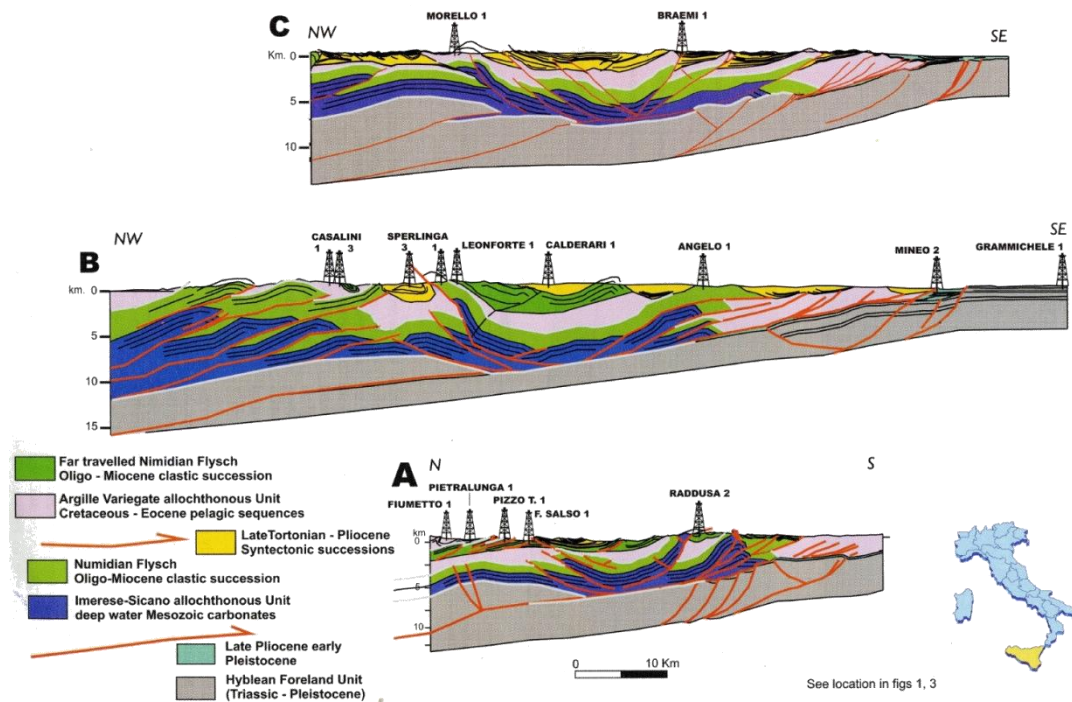


Fig. 4.3 – Regional geological cross-sections from Bello et al. 2000 (see location in Fig. 4.2)

The structurally highest units, well exposed in the Nebrodi Mts., are represented by the remnants of the Neotethyan accretionary wedge (Corrado et al., 2009), made up of a portion of the Sicilide Complex (Ogniben, 1960) consisting of a Late Cretaceous to early Miocene pelagic succession and by the Oligocene-Langhian foredeep deposits of the Numidian Flysch (Carbone et al., 1990; Catalano et al., 2006). Tectonically beneath these units, the more external Imerese-Sicano Unit forms an imbricate thrust system with a backthrust region in the centre of Sicily (Sturiale et al. 2010; Fig. 4.3), and a series of south verging thrusts to the south. It crops out in the tectonic window of Mt. Judica area at the front of the Apenninic-Maghrebian fold-and-thrust belt (Fig. 4.4 and 4.5). The succession is made up of mainly pelagic basin Mesozoic carbonates with radiolarian cherts, overlain by Paleogene marly limestones and younger clastic deposits (Bianchi et al., 1987).

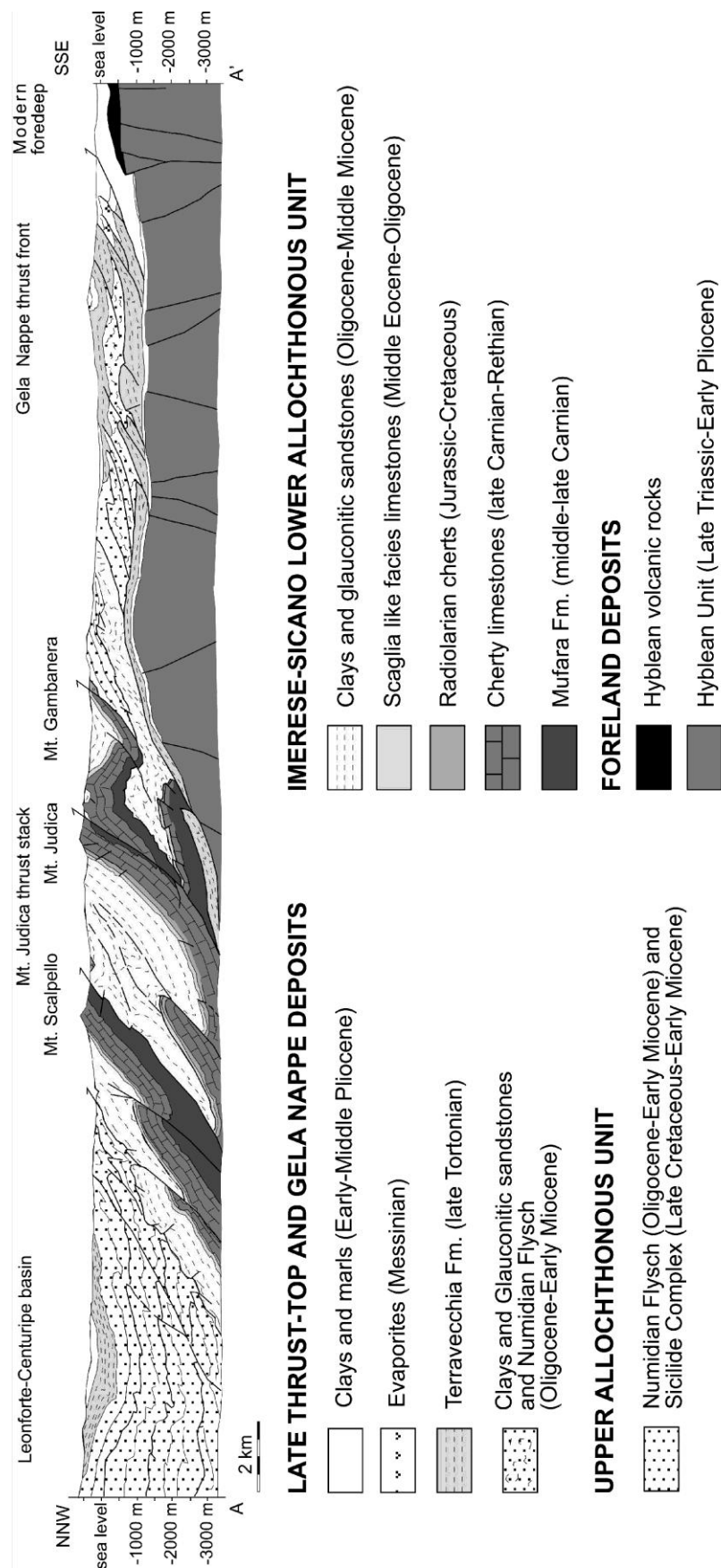


Fig. 4.4 – Cross-section through the frontal part of the Apenninic-Maghrebic fold-and-thrust belt in Eastern Sicily, modified after Bianchi et al. (1989). Trace section is located in Fig. 4.1.

In front of the Mt. Judica thrust stack a deformed wedge of Tertiary sediments lies, the Gela Nappe (Fig. 4.4; Butler et al., 1992). The deepest structural unit of the thrust belt is the Hyblean Unit, which consists of a thick carbonate platform sequence with interleaved marls and mafic volcanic levels (Bianchi et al., 1987) connected to the south to the Hyblean foreland, affected by high angle normal faults, partly reactivated in compression (Bello et al., 2000; Fig. 4.3).

This setting is the result of poliphasic deformation started since early Miocene times with the emplacement of the Allochthonous Units (Numidian Flysch, Sicilide Complex and the Imerese-Sicano Unit) onto the Hyblean foreland through low angle regional thrusts (Bello et al., 2000). During the Late Miocene, deformation caused the breaching of the Imerese-Sicano Unit with up-thrusts which cut the overlying Allochthonous Units and pre-date the late Tortonian deposits (Terravecchia Fm; Fig. 4.4; Butler et al., 1992). This deformation continued until middle Pleistocene times (Lickorish et al., 1999) giving rise to structural ridges cropping out in the Mt. Judica area. At the rear of the structural highs, propagation was accompanied by the development of syntectonic marine basins (e.g., Leonforte-Centuripe basin; Fig. 4.4; Roure et al., 1990).

As a whole, the Mt. Judica area underwent strong clockwise rotations (Speranza et al., 2003) and shortening (either 20 km or 38 km, over a section of about 12 km, according to either Lickorish et al., 1999 or Butler et al., 1992) and was deformed by two superposed fold and reverse fault systems according to Monaco and De Guidi (2006).

In detail, the pre-Tortonian contractional deformation affected the Mesozoic-Serravallian succession by roughly WSW-ENE trending folds and by 70° clockwise rotation with respect to the Hyblean foreland (Speranza et al., 2003). Then the Upper Tortonian to Pliocene clastic deposits subdued 30° clockwise rotation as documented all over Northern Sicily (Guarnieri, 2004; Monaco and De Guidi, 2006) and the Mesozoic-Serravallian succession was further deformed with the development of interference structures and mainly northwards tilting of the pre-existing fold axes. The occurrence of post-Tortonian NW-SE and WNW-ESE en-échelon right lateral strike-slip fault systems (Lentini et al., 1991; Monaco and De Guidi, 2006) may be partially responsible of the youngest structures and rotations.

Our study in the Mt. Judica area, has been concentrated on the imbricate thrust system of the E-W-striking thrust ridges namely from the north to the south, Mt. Scalpello, Mt. Judica-Mt. Turcisi and Mt. Gambanera (Figs. 4.4 and 4.5).

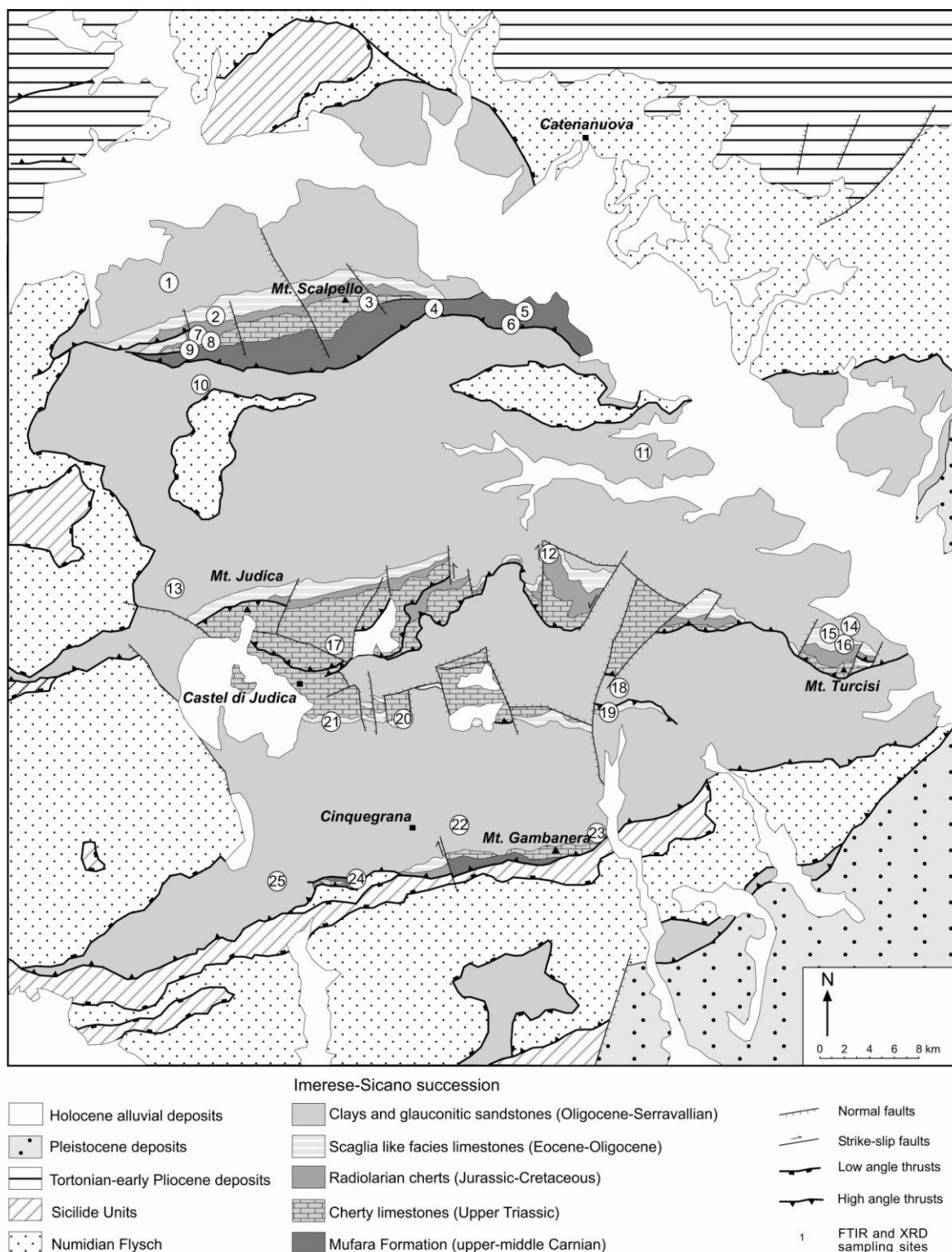


Figure 4.5 – Geological map of the Mt. Judica area with sampling location redrawn and modified after Carbone et al. (1990).

The local stratigraphic succession (Fig. 4.6) consists of Middle Carnian clays, limestones and sandstones (Mufara Fm) grading to Upper Triassic cherty limestones. The Mesozoic carbonates pass to Jurassic-Cretaceous radiolarian cherts and are covered by

Palaeogene marls and marly limestones of the Scaglia like facies. The latter deposits evolve to Upper Oligocene–Serravallian clays and glauconitic sandstones which represent the most external deposits of an early episode of foredeep sedimentation (Numidian Flysch). In the Mt. Gambanera and Mt. Judica thrust sheets the succession thickness ranges from a minimum of 540 m to 840 m respectively. In the Mt. Scalpello thrust sheet the stratigraphic thickness displays maximum values up to 1,200 m.

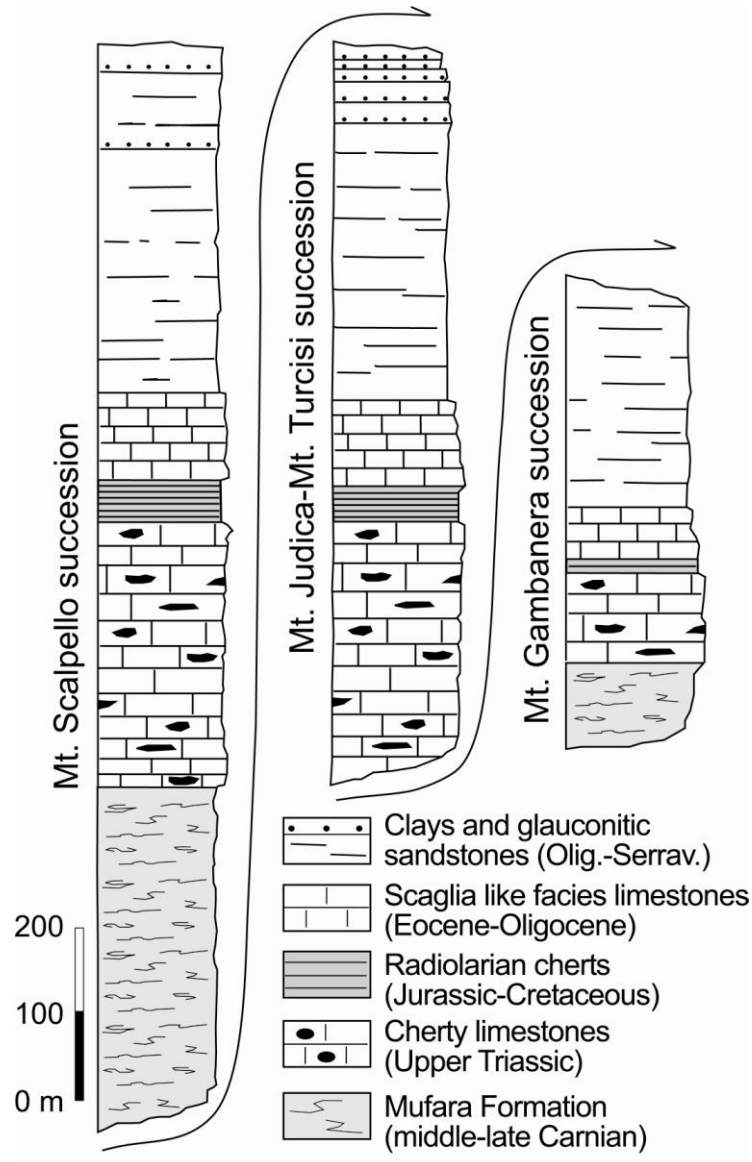


Figure 4.6 – Stratigraphic logs of the Mt. Judica Unit redrawn and modified after Bianchi et al. (1987).

### 4.3. Results

#### 4.3.1 - FTIR on organic matter

Samples analysed through this technique derive from the pre- and syn-orogenic successions cropping out from Mt. Judica to Mt. Gambanera. Sampled units are Clays and Glauconitic sandstones, cherty limestones and Mufara Fm.

Figure 4.7A shows spectra with a low intensity to undetectable aromatic C-H stretching absorption band in the 3,000-3,100  $\text{cm}^{-1}$  region and two distinct peaks in the aliphatic C-H stretching vibration (2,800-3,000  $\text{cm}^{-1}$ ) which are of similar intensity. In the oxygenated groups and aromatic/olefinic region (1,550-1,750  $\text{cm}^{-1}$ ), the carbonyl/carboxyl peak at  $\sim 1,710 \text{ cm}^{-1}$  is lower than the olefinic/aromatic peak which shifts progressively from 1,628  $\text{cm}^{-1}$  (clays and glauconitic sandstones and cherty limestones) to 1,620-1,625  $\text{cm}^{-1}$  (Mufara Fm).

In the aromatic out-of-plane C-H deformation region (700-900  $\text{cm}^{-1}$ ) the exact number and locations of bands still not fully resolved (e.g., Painter et al, 1981) but at least five bands can occur, with three of them (860, 815, and 750  $\text{cm}^{-1}$ ) being commonly assigned to aromatic vibration modes (e.g., Lis et al., 2005). In the spectra related to the Mufara Fm, only the 890  $\text{cm}^{-1}$  peak is resolved and has low intensity (Fig. 4.7A and B). In the other spectra (clays and glauconitic sandstones and cherty limestones), the aromatic out-of-plane C-H modes are not distinguishable.

The spectra in Fig. 4.7B are characterized by the absence of the peaks in the 3,000-3,100  $\text{cm}^{-1}$  region and at 1,375  $\text{cm}^{-1}$ , by the presence of the lower intensity peaks with respect to those in Fig. 5A in the 3,000-2,800  $\text{cm}^{-1}$  region, and by one peak at 1,650  $\text{cm}^{-1}$  (C=O conjugated group) in the 1,550-1,750  $\text{cm}^{-1}$  region.

Three aromaticity ratios involving the aromatic stretching region are correlated with thermal maturity ( $\text{Ar}_{3000-3100}/\text{Al}_{2800-3000}$ ,  $\text{Ar}_{3000-3100}/\text{Al}_{1450}$  and  $\text{Ar}_{3000-3100}/\text{Al}_{1370}$ , Tab. 1) increase as a function of stratigraphic age, being lowest in the youngest formation (see discussion). Ratios between the  $\sim 1,600 \text{ cm}^{-1}$  aromatic band and the three aliphatic band areas ( $\text{Ar}_{1600}/\text{Al}_{2800-3000}$ ,  $\text{Ar}_{1600}/\text{Al}_{1450}$ , and  $\text{Ar}_{1600}/\text{Al}_{1375}$ ) do not increase with depth but range from 0.36 to 1.23, 1.73 to 6.33, and 15.65 to 44.38, respectively.

The last three aromaticity parameters could be calculated only for spectra of the Mufara Fm (Tab. 1). They show values ranging from 0.001 to 0.008 for the  $\text{Ar}_{700-900}/\text{Al}_{2800-3000}$ , from 0.003 to 0.022 for the  $\text{Ar}_{700-900}/\text{Al}_{1450}$  and from 0.027 to 0.867 for the  $\text{Ar}_{700-900}/\text{Al}_{1370}$ .

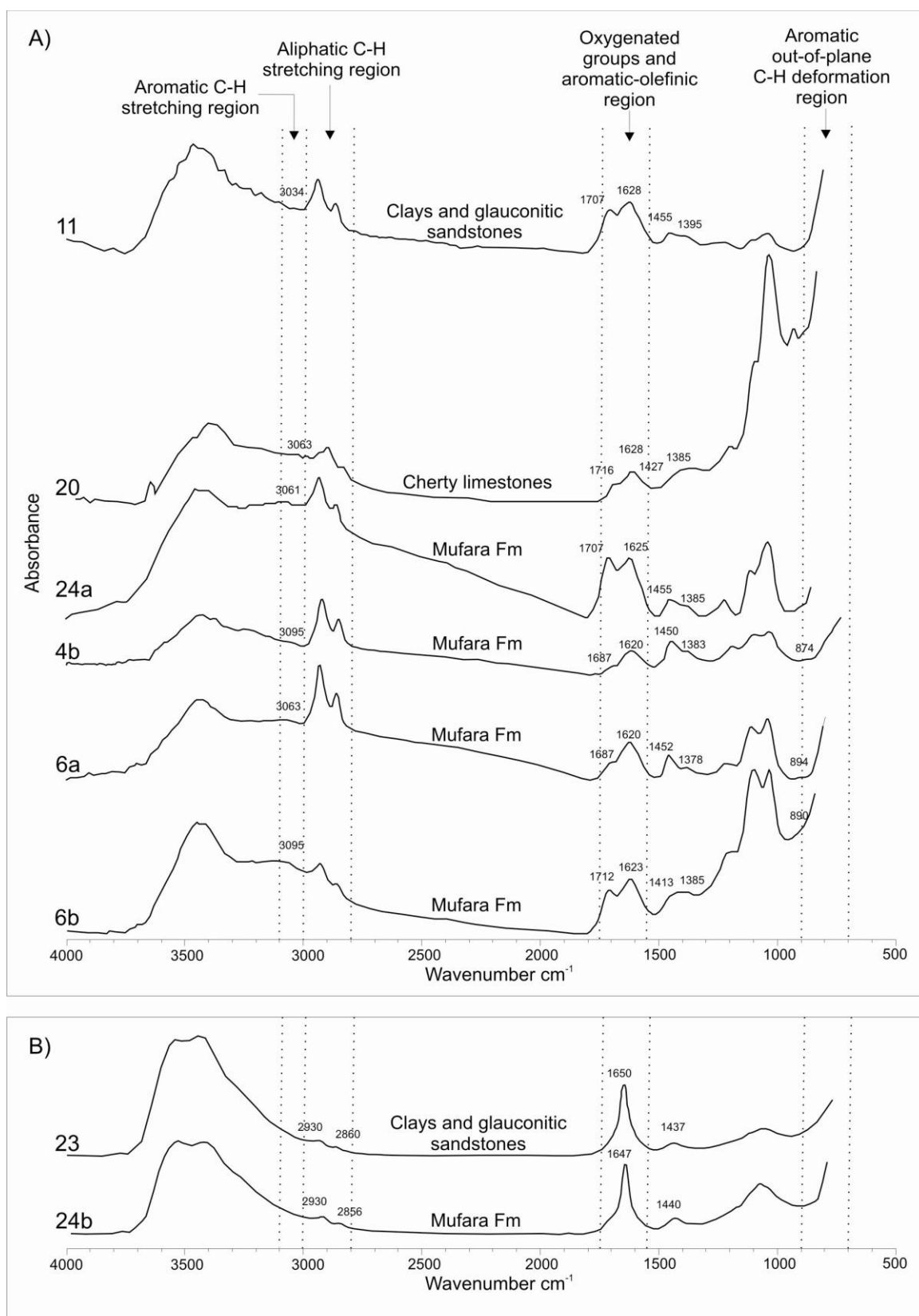


Figure 4.7 – Selected FTIR spectra of concentrated kerogen for unaltered (A) and oxidized (B) samples: Clays and Glauconitic sandstones (11 and 23), cherty limestones (20) and Mufara Fm (4b, 6a, 6b, 23, 24a, 24b). In box A, samples are distributed in stratigraphic order.

Formation	Sample	Ar <sub>3000-3100</sub>		Ar <sub>3000-3100</sub>		Ar <sub>1600</sub>		Ar <sub>1600</sub>		Ar <sub>700-900</sub>		Ar <sub>700-900</sub>		CH <sub>2</sub> CH <sub>3</sub>
		Al <sub>2800-3000</sub>	Al <sub>1450</sub>	Al <sub>1370</sub>	Al <sub>2800-3000</sub>	Al <sub>1450</sub>	Al <sub>1370</sub>	Al <sub>2800-3000</sub>	Al <sub>1450</sub>	Al <sub>2800-3000</sub>	Al <sub>1450</sub>	Al <sub>1370</sub>	Al <sub>1370</sub>	
Clays and glauconitic sandstones	11	0.007	0.072	0.212	0.599	6.331	18.717	—	—	—	—	—	—	2.03
	23	—	—	—	—	—	—	—	—	—	—	—	—	2.13
Cherty limestones	20	0.022	0.146	0.687	0.507	3.318	15.653	—	—	—	—	—	—	1.65
	24a	0.020	0.119	0.821	0.696	4.175	28.878	—	—	—	—	—	—	2.27
	24b	—	—	—	—	—	—	0.008	0.005	—	—	—	—	3.28
	4a	0.020	0.087	3.461	—	—	—	0.005	0.022	0.867	—	—	—	4.69
	4b	0.012	0.060	0.682	0.362	1.730	19.839	0.003	0.014	0.157	—	—	—	2.94
	5	—	—	—	—	—	—	—	—	—	—	—	—	2.84
	6a	0.021	0.124	1.129	0.478	2.866	26.167	0.0005	0.003	0.027	—	—	—	3.15
	6b	0.063	0.250	2.277	1.234	4.863	44.382	0.004	0.016	0.145	—	—	—	3.53

Table 4.1 – Aromaticity (ratios of aromatic versus aliphatic FTIR absorption values) and aliphaticity ratio (CH<sub>2</sub>/CH<sub>3</sub>).



The CH<sub>2</sub>/CH<sub>3</sub> ratio has the lowest value (1.65) in the cherty limestones, about 2.00 in the clays and glauconitic sandstones and ranges between 2.27 and 4.69 in the Mufara Fm.

#### 4.3.2. XRD on clay minerals

Quantitative analysis of the <2 µm grain size fraction displays various clay mineral assemblages related to different lithologies (Tab. 4.2). In general, the Mufara Fm and other clay-rich lithologies from the Oligocene basin fill reveal kaolinite-rich assemblages with subordinate amounts of mixed layer I-S, chlorite and illite. Glauconitic fine-grained sandstones show random ordered mixed-layer I-S (84-86 wt.%), minor amounts of kaolinite (10-12 wt.%), illite (1-5 wt.%) and chlorite (1 wt.%; Fig. 4.8a). Shales from Scaglia like facies (Fig 4.8b) and cherty limestones are characterized by high amount of mixed-layer I-S whereas an illite-rich assemblage is typical for marly samples and radiolarian cherts. Despite these lithology-dependant mineralogical differences which may affect the use of clay-mineral based geothermometers, mixed-layer I-S displays a progressive increase of the proportion of illite layers as function of stratigraphic age. In the northernmost and uppermost thrust sheet (Mt. Scalpello thrust) the illitic content in mixed-layer I-S increases from 55% at the top to 76% at the base of the succession (Fig. 4.9; Tab. 4.2). Within the cherty limestones and Mufara Fm, XRD patterns show the first order superstructure reflection (*d*-spacing: ~2.7 nm; Fig. 4.8c and d) which correspond to mixed-layer clay minerals with alternating layer types of illite and smectite (rectorite). A second population of ordered mixed-layer I-S with a proportion of illite layers of 75-76% is generally associated with rectorite. In the Mt. Judica-Mt. Turcisi ridge, the conversion from random ordered to short-range ordered I-S occurs within the Oligocene clays and glauconitic sandstones and the Scaglia like facies (Fig. 4.9; Tab. 4.2). The observed population of I-S clay minerals has an illite content ranging from 50 to 68%. The deepest and southernmost thrust sheet (Mt. Gambanera thrust) is characterized by short-range ordered I-S with an illite content from 60 to 73% (Fig. 4.9; Tab. 4.2). Also in this succession, the sample from the Mufara Fm shows the presence of rectorite together with low-expandable R1 mixed-layer I-S.

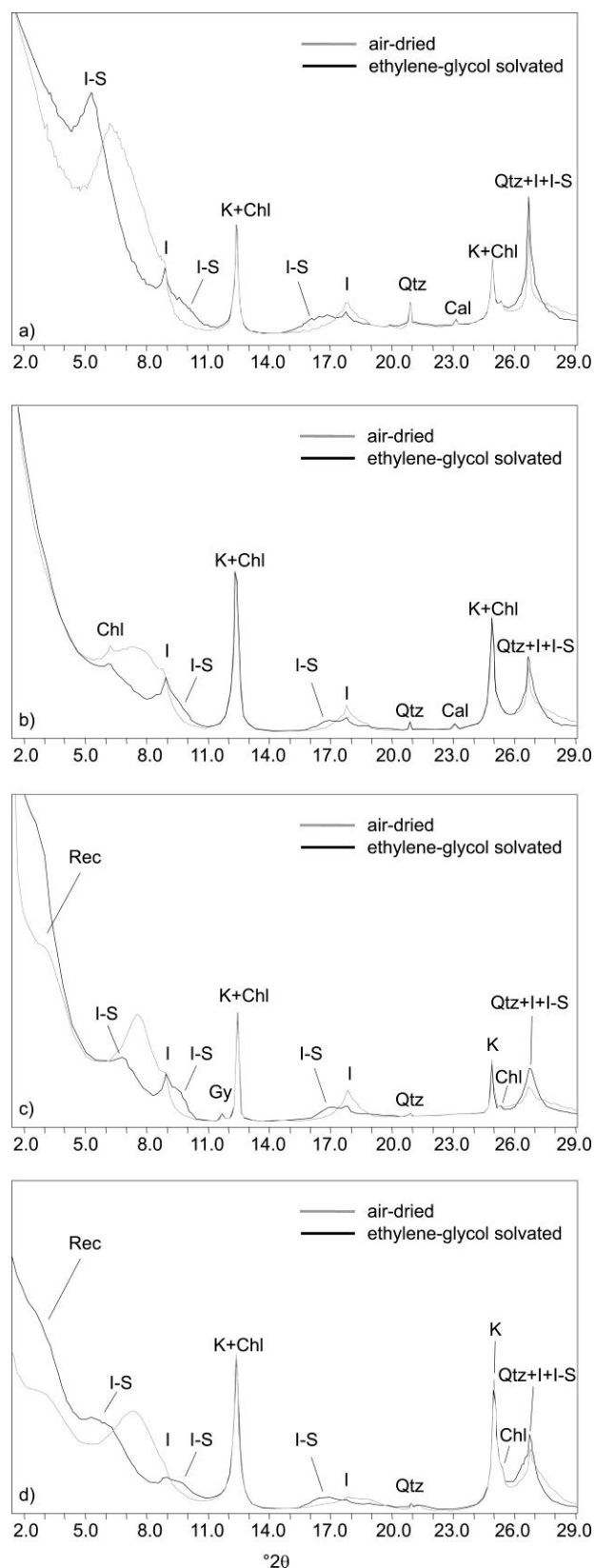


Figure 4.8 – Selected XRD patterns of the  $<2\mu\text{m}$  grain-size fraction. a) Clays and Glauconitic sandstones; b) “Scaglia like facies”; c) Cherty limestones; d) Mufara Fm.

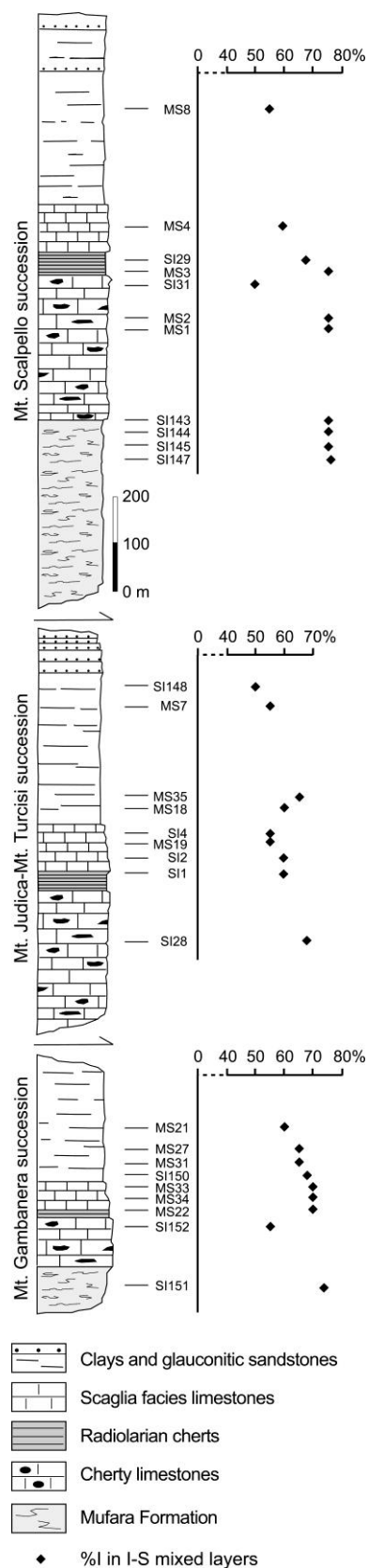


Figure 4.9 – Stratigraphic logs of the Mt. Judica Unit and distribution of illite content in mixed layer I-S with depth redrawn and modified after Bianchi et al. (1987).

Site	sample	thrust sheet	Formation	Rock type	X-ray quantitative analysis of the <2µm grain size fraction (%wt.)					R	%I in I-S
					I	I-S	K	Chl	Non-clay		
1	MS8	Mt. Scalpello	clays and sandstones	sandstone	5	84	10	1	Qtz+Cal	0	55
2	MS4	Mt. Scalpello	Scaglia limestones	marl	73	21	3	3	Qtz+Pl	0	60
3	SI29	Mt. Scalpello	Radiolarian cherts	shale	46	42	11	1	Qtz+Cal+Pl	1	68
7	MS3	Mt. Scalpello	Radiolarian cherts	shale	60	26	0	14	Qtz+Cal	1	75
7	SI31	Mt. Scalpello	Cherty limestones	shale	62	18	11	9	Qtz+Pl	0	50
8	MS1	Mt. Scalpello	Cherty limestones	shale	35	44	19	2	Qtz+Cal	1	75
7	MS2	Mt. Scalpello	Cherty limestones	shale	13	61	24	2	Qtz+Cal	1	75
4	SI143	Mt. Scalpello	Mufara Fm.	shale	4	39	47	10	Qtz	1	75
4	SI144	Mt. Scalpello	Mufara Fm.	shale	9	36	35	20	Qtz+Ank+Pl	1	75
4	SI145	Mt. Scalpello	Mufara Fm.	shale	8	17	51	24	Qtz	1	75
6	SI147	Mt. Scalpello	Mufara Fm.	shale	7	25	47	21	Qtz	1	76
10	MS7	Mt. Judica	clays and sandstones	shale	1	86	12	1	Qtz+Cal+Pl	0	55
11	SI148	Mt. Judica	clays and sandstones	shale	10	15	75	1	Qtz	0	50
14	MS18	Mt. Judica	clays and sandstones	shale	19	13	50	18	Qtz+Cal	0/1	60
13	MS35	Mt. Judica	clays and sandstones	marl	21	18	47	14	Qtz	1	65
16	MS19	Mt. Judica	Scaglia limestones	marl	2	94	3	1	Qtz+Cal	0	55
12	SI2	Mt. Judica	Scaglia limestones	marl	12	88	0	0	Qtz+Cal	0/1	60
15	SI4	Mt. Judica	Scaglia limestones	marl	8	83	8	1	Qtz+Cal	0	55
12	SI1	Mt. Judica	Radiolarian cherts	shale	31	66	2	1	Qtz+Pl	0/1	60
17	SI28	Mt. Judica	Cherty limestones	shale	8	87	5	0	Qtz	1	68
18	MS21	Mt. Gambanera	clays and sandstones	shale	16	15	57	12	Qtz	1	60
22	MS27	Mt. Gambanera	clays and sandstones	marl	22	9	52	17	Qtz+Gy	1	65
25	MS31	Mt. Gambanera	clays and sandstones	marl	12	4	64	20	Qtz	1	65
23	SI150	Mt. Gambanera	clays and sandstones	marl	24	29	37	10	Qtz+Cal+Pl	1	67
19	MS22	Mt. Gambanera	Scaglia limestones	marl	32	27	37	4	Qtz+Cal	1	70
21	MS33	Mt. Gambanera	Scaglia limestones	marl	31	34	29	6	Qtz+Cal	1	70
21	MS34	Mt. Gambanera	Scaglia limestones	marl	16	29	43	13	Qtz+Cal	1	70
20	SI152	Mt. Gambanera	Cherty limestones	shale	67	27	0	6	Qtz+Cal+Pl	0/1	55
24	SI151	Mt. Gambanera	Mufara Fm.	shale	22	27	42	8	Qtz+Cal	1	73

Table 4.2 – X-ray quantitative analysis of the <2µm grain-size fraction. I= illite; I-S= mixed layer illite-smectite; K= kaolinite; Chl= chlorite; Qtz= quartz; Cal= calcite, Pl= plagioclase; Ank= ankerite; Gy= gypsum; R= stacking order; %I in I-S= illite content in mixed layer illite-smectite.

## 4.4. Discussion

### 4.4.1. Thermal evolution of Mt. Judica succession

#### 4.4.1a. Extracting information on thermal maturity from FTIR spectra

The most common proxy used to study thermal maturity of sedimentary rocks is vitrinite reflectance (VR<sub>0</sub>%). This parameter increases as a function of depth and increasing temperature in sediments via a series of irreversible physico-chemical processes which change the macromolecular structure of organic matter of terrestrial origin (huminite-vitrinite group of macerals). Nevertheless, samples from the Mufara Fm, cherty limestones and marls and glauconitic sandstones prepared for organic matter optical analysis contain only H-rich organic matter and not macerals of the huminite-vitrinite group. In the absence of vitrinite, changes of organic matter structure due to increasing temperature may be investigated by other techniques, including FTIR

(Rouxhet and Robin, 1978; Monthieux and Landais, 1988; Schenk et al., 1990; Mastalerz and Bustin, 1993; Ibarra et al. 1994; 1996). In fact, FTIR studies assigning specific bands to chemical bonds in complex kerogen molecules (Painter et al., 1981, 1983; Baruah, 1986), proved to be diagnostic for kerogen type identification and particularly useful for determining the degree of thermal maturity of marine source rocks lacking in vitrinite macerals (Ganz and Kalkreuth, 1987; Christy et al., 1989; Kister et al., 1990; Lin and Ritz, 1993b; Chen et al., 1998; Lis et al., 2005).

In this work, we used FTIR absorption bands and derived parameters as proxies for thermal maturity in order to integrate them with clay minerals based geothermometers in thermal modeling.

The presence of the peaks related to the C-H stretching vibration in the 3,000-3,100  $\text{cm}^{-1}$  region suggests that our samples achieved a coalification stage equivalent to at least 0.5-0.7%  $\text{VR}_o\%$  (Lis et al., 2005).

The progressive shift of the aromatic carbon peak (in the 1,550-1,650  $\text{cm}^{-1}$ ) towards lower frequencies from the youngest (clays and glauconitic sandstones) to the oldest formation (Mufara Fm) documents an increase of coalification rank with depth as indicated by Ibarra et al. (1996) and Ganz et al. (1990).

Other absorption bands and some of their ratios indicate a thermal maturity consistent with that suggested by the peaks in the 3,000-3,100  $\text{cm}^{-1}$  region and near 1,600  $\text{cm}^{-1}$ . For example, the stronger absorption close to 860  $\text{cm}^{-1}$  compared to that near 815  $\text{cm}^{-1}$  in the 700-900 region of our spectra, according to Ibarra et al. (1996) and Riesser et al. (1983), can be observed from the sub-bituminous stage ( $\text{VR}_o$  lower boundary of about 0.37%) whereas the aromatic band near 815  $\text{cm}^{-1}$  is related to peat and lignite.

Many authors have demonstrated that aromaticity and aliphaticity are reliable parameters to indicate the degree of coalification from lignite to anthracite. Our results indicate an increase in aromaticity with depth, expressed by three ratios of aromatic to aliphatic band areas ( $\text{Ar}_{3000-3100}/\text{Al}_{2800-3000}$ ;  $\text{Ar}_{3000-3100}/\text{Al}_{1450}$ ;  $\text{Ar}_{3000-3100}/\text{Al}_{1370}$ ). Other six aromaticity parameters do not show significant differences with depth (Tab. 4.1), suggesting that their utility as thermal maturity indicators for the sediments studied is limited.

The methylene/methyl ratio measured in the 2,800-3,000  $\text{cm}^{-1}$  region ( $\text{CH}_2/\text{CH}_3$ , Tab. 4.1) reflects the length of aliphatic chains (Lin and Ritz, 1993b; Pradier et al., 1992) strongly dependant on maceral type, being higher in the liptinite and lower in the vitrinite group macerals (Mastalerz and Bustin, 1996). This ratio can be also used to extract

thermal information. Lis et al. (2008) observed a decreasing ratio in the maturity interval corresponding to  $VR_o$  range from 0.3 to 1.3  $VR_o\%$ , followed by no further significant change of the ratio for higher  $VR_o\%$  values.

In our results, the increasing  $CH_2/CH_3$  ratio as function of depth in clays and glauconitic sandstones and Mufara Fm is indicative of the increasing proportion of long-chain aliphatic compounds and of a marine depositional environment characterized by a decreasing input of organic matter of terrestrial origin during middle Triassic.

The lack of the peak in the 3,000-3,100  $cm^{-1}$  region and at 1,375  $cm^{-1}$ , the lower intensity of absorption in the 2,800-3,000  $cm^{-1}$  region and the presence of the peak near 1,650  $cm^{-1}$  (C=O conjugated group) common to the spectra in Fig. 4.7B indicate formation of oxygen-containing species in the 1,630-1,850  $cm^{-1}$  region and consumption of  $CH_x$  species in the 2,740-3,100  $cm^{-1}$  region (Calemma et al., 1988; Sobalik et al., 1998). This evidence testified that organic matter in these samples may have suffered oxidation, thus the results were not taken into account for thermal maturity considerations.

In synthesis, FTIR data suggest that the degree of thermal maturity of the Mt. Judica succession increases with depth as already indicated by the increase in illitic content of mixed layer I-S and that sediments experienced at least a coalification stage equivalent to vitrinite reflectance values of 0.5-0.7% which corresponds to temperature ranges of at least 80-110 °C according to Barker & Pawlewicz's equation (1994).

#### 4.4.1b. Thermal modelling

A simplified reconstruction of the burial and thermal history of the three thrust sheets deforming the Mt. Judica succession was performed using the software package Basin Mod<sup>®</sup> 1-D (1996). The main assumptions for modeling are that: (i) rock decompaction factors apply only to clastic deposits according to Sclater and Christie's method (1980); (ii) seawater depth variations in time are not relevant in modeling, because thermal evolution is mainly affected by sediment thickness rather than by water depth (Butler, 1992); (iii) thrusting has been considered instantaneous when compared with the duration of deposition of stratigraphic successions, as generally suggested by theoretical models (Endignoux and Wolf, 1990); (iv) a variable geothermal gradient has been adopted for syn-rift (45 °C/km) and post-rift deposits (30 °C/km); and (v) thicknesses and age inputs are from geological field mapping (Bianchi et al., 1987; Carbone et al., 1990). Geological constraints and modeling results are listed in Table 4.3.

Main tectonic and erosion/deposition events	Timing of events	Thickness of: removed material <sup>a</sup> / tectonic <sup>b</sup> / sedimentary units (m)	Average exhumation <sup>c</sup> / sedimentation <sup>a</sup> rate (mm/y)	Calculated maximum temperatures (°C)	
				Top	Bottom
Erosion	late Pliocene-Holocene (3.6-0 My)	~ 2800 <sup>a</sup> , <sup>b</sup>	~ 0.777 <sup>c</sup>	-	-
		~ 2400 <sup>a</sup> , <sup>b</sup>	~ 0.666 <sup>c</sup>	-	-
		~ 3000 <sup>a</sup> , <sup>c</sup>	~ 0.833 <sup>c</sup>	-	-
Emplacement of the allochthonous units	late Serravallian-late Pliocene <sup>††</sup> (11.6-3.6 My)	~ 2800 <sup>a</sup> , <sup>b</sup>	N.D.	-	-
		~ 2400 <sup>a</sup> , <sup>b</sup>	N.D.	-	-
		~ 3000 <sup>a</sup> , <sup>c</sup>	N.D.	-	-
Late foredeep deposits	late Oligocene-late Serravallian <sup>†††</sup> (28.5-11.6 My)	~ 390 <sup>ss</sup> , <sup>†††</sup> , <sup>a</sup>	~ 0.023 <sup>#</sup>	94	106
		~ 400 <sup>ss</sup> , <sup>†††</sup> , <sup>b</sup>	~ 0.024 <sup>#</sup>	82	94
		~ 270 <sup>ss</sup> , <sup>†††</sup> , <sup>c</sup>	~ 0.016 <sup>#</sup>	103	111
post-rift deposits	Upper Triassic-Oligocene <sup>†††</sup> (224-28.5 My)	~ 450 <sup>ss</sup> , <sup>†††</sup> , <sup>a</sup>	~ 0.023 <sup>#</sup>	106	120
		~ 440 <sup>ss</sup> , <sup>†††</sup> , <sup>b</sup>	~ 0.023 <sup>#</sup>	94	108
		~ 270 <sup>ss</sup> , <sup>†††</sup> , <sup>c</sup>	~ 0.014 <sup>#</sup>	111	117
Syn-rift deposits	middle-upper Camian <sup>†††</sup> (224-220 My)	~ 400 <sup>ss</sup> , <sup>†††</sup> , <sup>a</sup>	~ 0.100 <sup>#</sup>	120	132
		N.D.	N.D.	N.D.	N.D.
		~ 100 <sup>ss</sup> , <sup>†††</sup> , <sup>c</sup>	~ 0.025 <sup>#</sup>	117	132

Notes: thickness of the allochthon and exhumation rates for the Mt. Judica succession obtained by our modeling.

<sup>a</sup> Mt. Scalpello thrust sheet.

<sup>b</sup> Mt. Judica-Turcisi thrust sheet.

<sup>c</sup> Mt. Gambanera thrust sheet.

<sup>††</sup> Data from Butler et al. (1992).

<sup>†††</sup> Data from Bianchi et al. (1987); Carbone et al. (1990).

Table 4.3 – Main depositional and tectonic events related to the modelled tectonic evolution of the Mt. Judica succession.

The reconstructed burial evolution began in middle Carnian times with the deposition of the syn-rift deposits of the Mufara Fm and continued since Upper Triassic with a post-rift basinal succession. From Jurassic to Cretaceous sedimentation took place in the basin at low sedimentation rates and stopped in Paleocene times. Deposition started again during Eocene times with the sedimentation of pelagic limestones of the Scaglia like facies and continued until Serravallian times. During the Middle Miocene collisional event (Butler et al., 1992) the Mt. Judica succession was tectonically overlain by the chaotic terranes of the Sicilide Unit and the Numidian Flysch (case 1 in Fig. 4.9A). This phase brought the Mt. Judica succession to depths of about 4 km recording maximum temperatures of about 132 °C. The calculated tectonic loading for the three ridges is in the range of 2,400 – 3,000 m and persisted for about 8 Ma onto the Mt. Judica succession (Tab. 4.3). The deposition of the late Tortonian Terravecchia Fm contributed in minor amounts to the deepening of the Mt. Judica sedimentary succession. Subsequent imbrications of the buried succession stacked the deep marine carbonates and younger clastics of the Mt. Judica Unit, locally breaching through the tectonically overlying allochthonous units. It is unclear how much of the deformation within the Mt. Judica Unit pre-dates the deposition of the Terravecchia Fm and whether this deposit sedimented atop the structuring ridges. The best constrain we can provide to this topic is that most of deformation is post-Trubi Fm (Lower Pliocene; Butler et al., 1992). Uplift and erosion started in Upper Pliocene, ruled by high angle up-thrusts. An alternative model, which does not take into account the deposition of the Terravecchia Fm atop the Mt. Judica succession has been produced

(case 2 in Fig. 4.9A). This reconstruction, which provides a higher amount of tectonic burial than that of case 1, produces a similar burial evolution without major differences in the final acquired thermal maturity.

Both types of evolution outlined here, allowed an acceptable calibration against measured data, as shown by the resulting thermal maturity curve of figure 4.9B. The comparable tectonic loading among the distinct thrust sheets suggests that the acquired thermal maturity of the Mt. Judica succession is due to the Middle-Miocene thrusting event and pre-dates its internal stacking. Up-thrust geometries indicate that the extent of thrust sheets overlapping is negligible when compared with the magnitude of vertical movements.

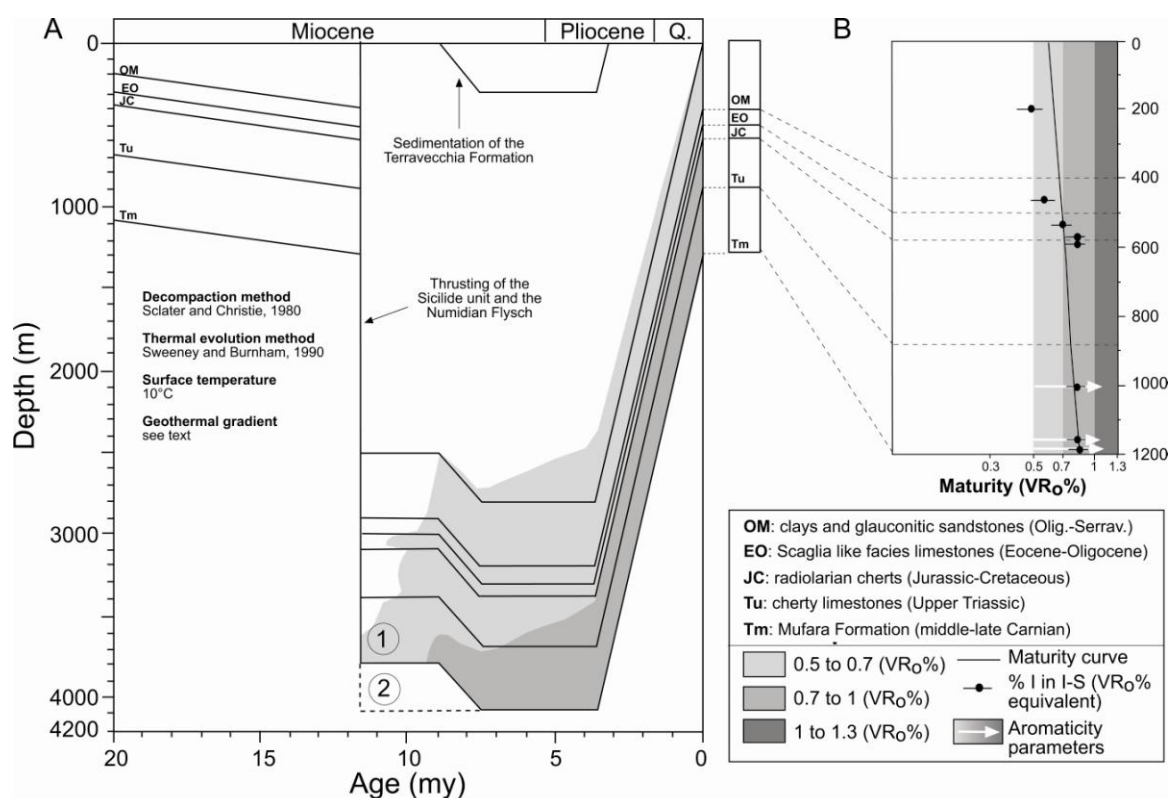


Figure 4.9 – A) 1D burial and thermal history of the Mt. Scalpello thrust sheet with (case 1) and without (case 2) contribution of Terravecchia Fm; B) Maturity curve calibrated by illite content in mixed layer I-S and FTIR data. Thermal maturity is expressed in equivalent values of vitrinite reflectance. The thermal modeling has been performed using LLNL Easy %Ro method based on Burnham and Sweeney (1989) and Sweeney and Burnham (1990).



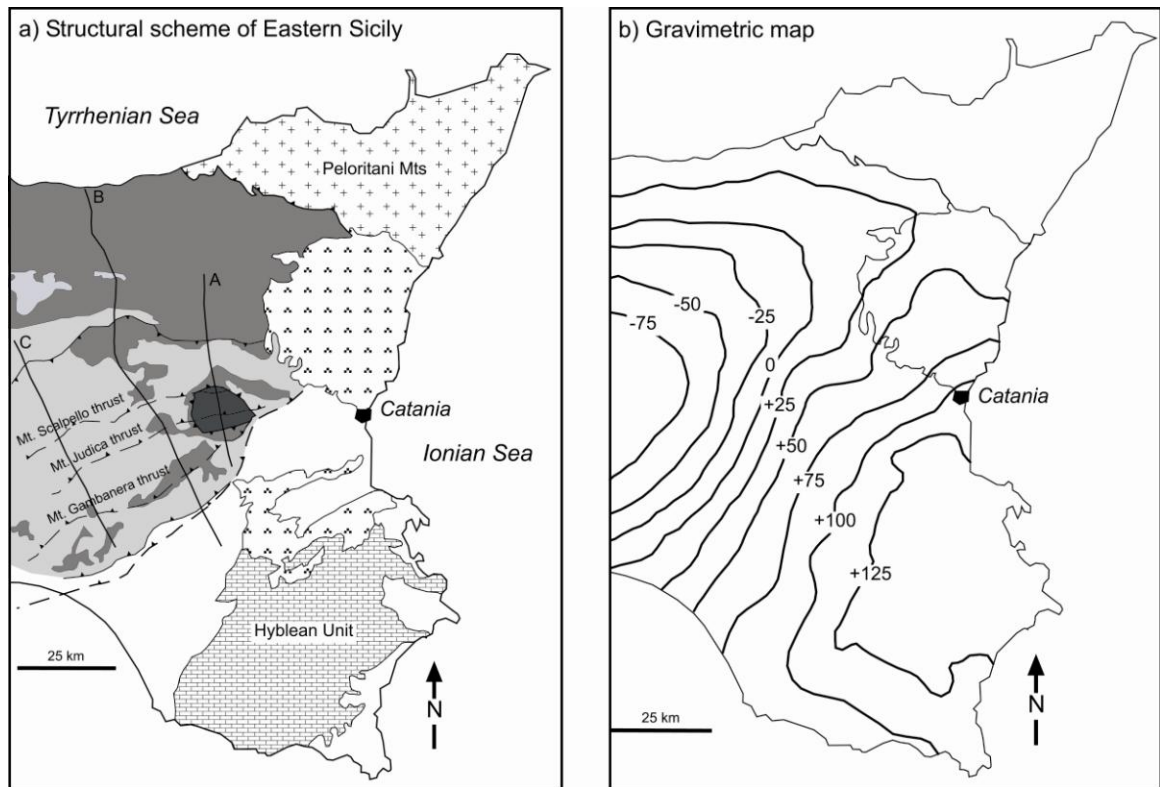
#### 4.4.2. Along-strike variations of the Gela nappe front

The structural evolution of external orogenic zones is controlled by its internal deformation and the flexural bending of the subducting plate (Ford et al. 2005). The interaction between these two factors may change through time and along the strike of the chain as a result of variations in wedge mechanical properties and/or changes in stratigraphical features of the foreland (e.g. Boyer, 1995; Mitra, 1997).

We have studied three sections (Bello et al., 2000; Fig. 4.3) moving from the recess to the salient of the arc-shaped thrust front to evaluate the along strike thickness and shortening variations of the wedge. We measured the thickness of the main stratigraphic-structural units constituting the thrust wedge: the thrust-top deposits, the Upper Allochthonous Unit (Numidian Flysch and Sicilide Complex) and the lower Imerese-Sicano Allochthonous Unit (Fig. 4.10). Thickness measurements were performed along a vertical line from the tip point and following the strike of the three main thrusts both in surface (cross section A) and subsurface (cross-sections B and C, Fig. 4.10a). Apart from their discontinuous distribution along the cross-sections, the thickness of thrust-top deposits decreases from 0.6 to 0.3 km along cross-section C (Fig. 4.10c). The thickness of the Upper Allochthonous Unit decreases of about 1.2 and 2.3 km along cross-section C and B respectively. Moving from the east to the west, the thickness reduction is consistent with that calculated along the cross-sections. For the Imerese-Sicano stratigraphic-structural Unit, thickness decreases of about 1.5-2 km moving from the Mt. Scalpello thrust to the north to the Mt. Gambanera thrust to the south (cross sections A and C) and of about 2-2.5 km from the east to the west (Fig. 4.10c). The Imerese-Sicano Unit has a fairly constant thickness along cross-section B where the unit deepens. These thickness variations can be considered also in terms of crustal shortening by restoring the Imerese-Sicano Unit.

To provide shortening values three balanced cross-sections were reconstructed by the sinuous bed method, where lengths of the layers are preserved (Dahlstrom, 1969). This method assumes that rocks displacement occur only within the cross-section plane and that strike and oblique slips are neglected. A pin line was set in the less deformed layers with a horizontal bedding on the SE end of the cross-sections.

Balanced cross-sections (Fig. 4.11) indicate different shortening amounts: 23.9 km or 45% in cross-section A, 15.4 km or 30% in cross-section B and 12.3 km or 25% in cross-section C with a shortening decrease of 11.6 km from the east to the west.



c) Thickness (in km) of the main stratigraphic-structural Units

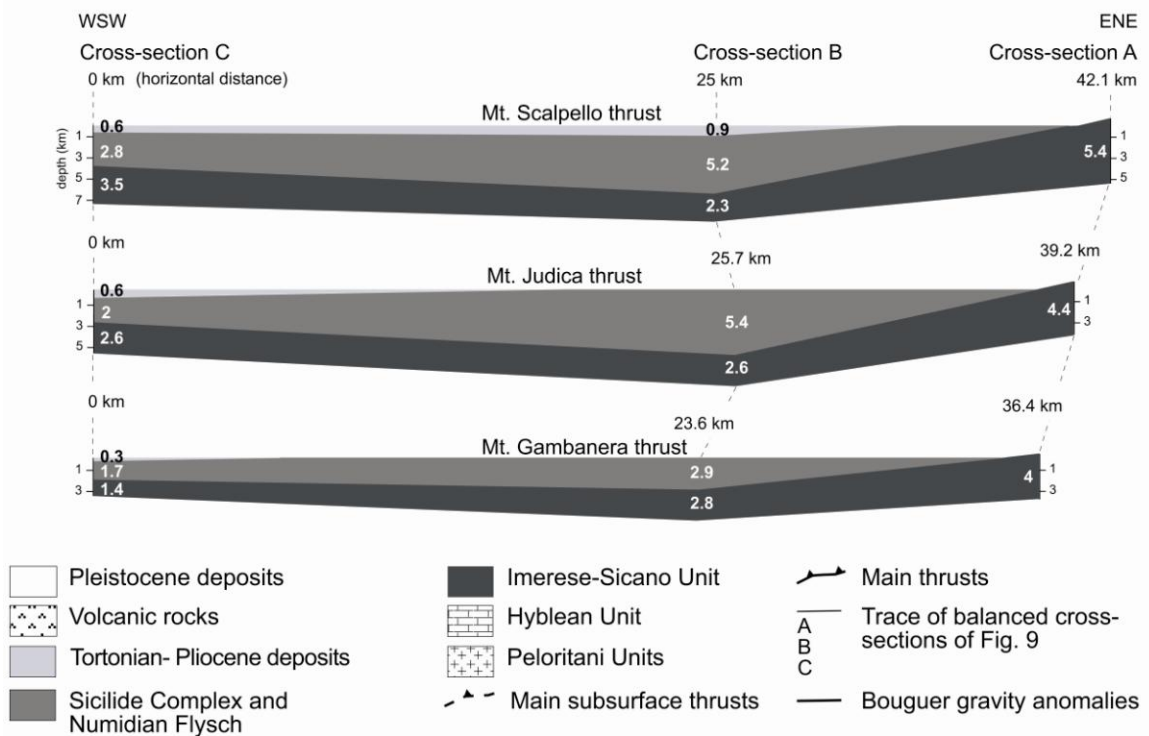


Figure 4.10 – a) Simplified structural scheme of Eastern Sicily with location of the geological cross-sections, redrawn and modified after Bello et al. (2000). A-B-C are section traces published by Bello et al. (2000) in Figure 4.3 and used to describe structures variations along strike; b) Gravimetric map of the Eastern Sicily region. Contour interval 25 mGal simplified after Carozzo et al. (1991); c) Thickness (in km) of the Tortonian-Pliocene deposits, the Upper Allochthonous Unit and the Imerese-Sicano Unit: see text for their variations along strike of the orogen (section traces in fig. 4.10a).

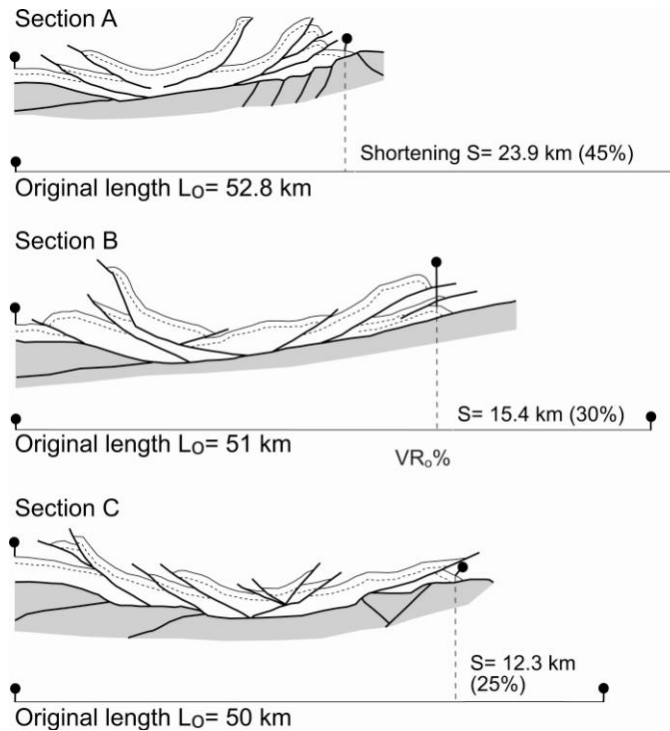


Figure 4.11 – Simplified cross sections A, B and C (Fig. 4.3): in white the Imerese-Sicano Unit, in gray, the Hyblean domain deformed and undeformed. Shortening calculated from the horizontal distance between pin and loose lines based on the line length ( $L_0$ ) of the top of Imerese-Sicano Unit strata.

These differences, either in terms of crustal shortening or thickening, are caused to crustal scale variations of the Hyblean foreland that are envisaged by gravimetric anomalies and Moho geometry (Fig. 4.10b and 4.12). The gravimetric anomalies are positive over the Hyblean Plateau and clearly define its boundaries. On the other hand negative values towards the west probably are due to the large accumulation of syn-orogenic sediments. In this area, according to Ben-Avrham and Grasso (1990), a crustal thickening (up to 35 km) takes place, although the crystalline portion of the crust is probably quite thin.

Since Late Oligocene, the western sectors suffered greater rates of flexural downbending than the eastern sectors. This evidence is attested by the higher thickness of syn-tectonic sediments (Yellin-Dror et al., 1997) and by the deeper regional monocline ( $\beta$ ) that increases from 3-6° to 12° moving from the recess to the salient (Mariotti and Doglioni, 2000). Therefore in the recess area the Hyblean foreland impedes the propagation of deformation more than in the salient area, maintaining the regional monocline angle lower than that in the salient.

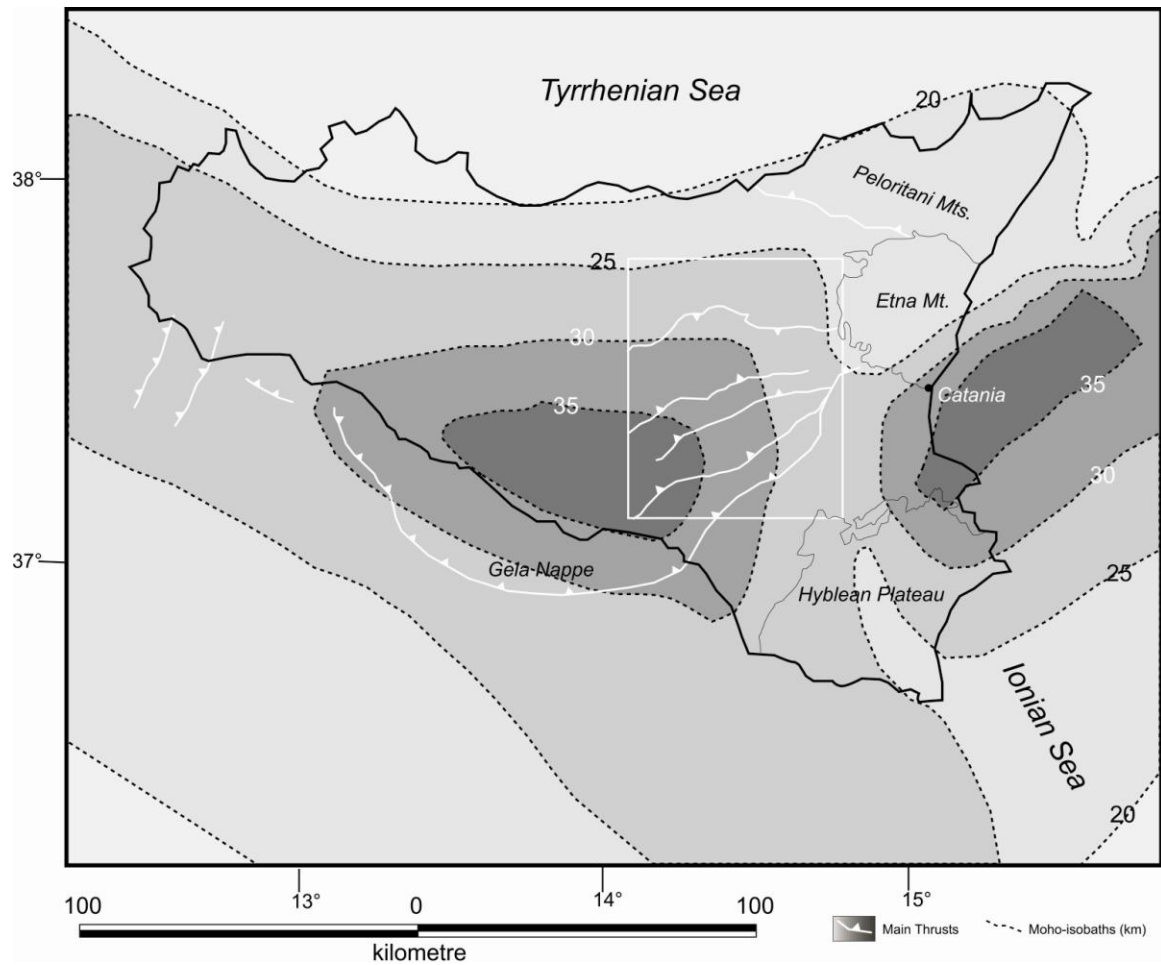


Figure 4.12 – Map of Moho-isobaths of the Sicily region, after Nicolich (2001, redrawn). The main tectonic thrust, discussed in the text, are shown in white.

#### 4.4.3. Application of critical taper analysis to the eastern Sicily fold-and-thrust belt

To explain the dynamic evolution of the eastern Sicily fold-and-thrust belt we applied the critical taper analysis for non-cohesive Coulomb wedges (Davis et al., 1983; Dahlen et al., 1984; Dahlen and Suppe, 1988).

We reconstructed the wedge taper evolution of the orogenic transect in the recess area from Mt. Scalpello to the tip of the wedge using data of maximum burial from this paper and shortening values from Butler et al. (1992) integrating them with cross-sections from the literature (Roure et al. 1990, Bello et al. 2000).

The observed wedge parameters are: the depth of the basal detachment beneath the Mt. Scalpello thrust sheet ( $h$ ); the cross-section length from Mt. Scalpello to the front of the

belt (L); the topographic surface angle ( $\alpha$ ) in the frontal part of the orogenic wedge, measured parallel to the tectonic transport direction, and the dip angle of the foreland monocline ( $\beta$ ) (Fig. 4.13A; Tab. 4.4).

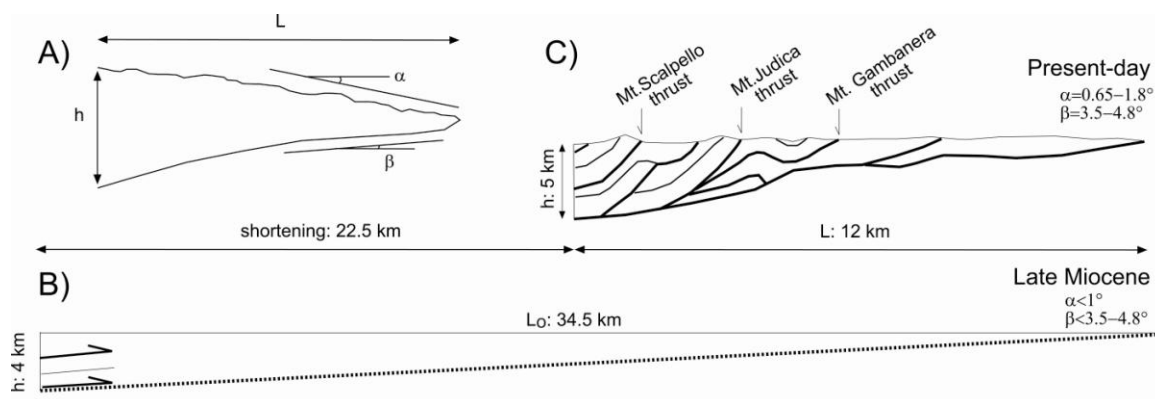


Figure 4.13 – Restoration of the wedge-shape geometry of the orogenic transect from Mt. Scalpello to the tip of the wedge. A) Observed parameters; (B) Simplified wedge shape in Late Miocene time; C) Schematic section showing the present-day internal geometry.

parameters	Mt. Scalpello section (present-day)	Mt. Scalpello restored cross-section (Late Miocene)
$\alpha$ (°)	0.65-1.8 (Adam and Reuther, 1995)	<1
$\beta$ (°)	3.5-4.8 (Adam and Reuther, 1995)	<3.5-4.8
h (km)	5 (Bello et al. 2000, Roure et al. 1990)	4
L (km)	12 (Butler et al., 1992, Roure et al. 1990)	34.5 (Butler et al., 1992)

Table 4.4 – Geometrical parameters of the wedge calculated and derived from literature.

The depth (h) of the basal detachment, corresponding to the calculated maximum burial, is ~4 km in the late Tortonian (Fig. 4.13B; Tab. 4.4) before the breaching of the Mt. Judica Unit, and is ~5 km in the present-day profile (Bello et al. 2000, Roure et al. 1990; Fig. 4.13C; Tab. 4.4).

The estimated maximum shortening of the frontal part of the orogen since the late Tortonian is of about 38 km (17.5 km on the duplicating thrust, 15.5 km on the basal detachment and 5 km internal shortening within the nappe; Butler et al., 1992) on a present-day distance of 12 km. In this restoration, we neglected nappe displacement atop the buried Hyblean platform (15.5 km).

The calculated  $\alpha$  value, based on topographic data, is ~1.3° (between 0.65 and 1.8° according to Adam and Reuther, 1995) and is assumed to be lower than 1° in late

Tortonian times because the wedge top represents the depositional surface of the Terravecchia Fm (according to Ford's general statement, 2005).

The present-day  $\beta$  value, according to Adam and Reuther (1995) is between 3.5 and 4.8°. In late Tortonian times  $\beta$  should be lower than the present-day angle considering that, from a geometrical point of view, the depth of the basal detachment ( $h = \sim 4$  km; Fig. 4.13B) and the length of the restored section ( $L_o = 34.5$  km; Fig. 4.13B) define a wedge with a lower apical angle.

The values of  $\alpha$  and  $\beta$  for the present-day and reconstructed late Tortonian wedge geometry, suggest subcritical condition (Fig. 4.14A, stages 1 and 5) in accordance with the critical taper models of Adam and Reuther (1995) based on the restored sections and kinematic analysis of the Eastern-Sicily fold-and-thrust belt. From late Tortonian up to Messinian the wedge thickened to a critical state through deformation by means of up thrusts of the Mt. Judica succession (Fig. 4.14A and B, stage 2). According to Nigro and Renda (2001) in this deformation phase, the tectonic uplift exceeded the foreland flexural subsidence and therefore the value of  $\alpha$  should increase (Fig. 4.14A, stage 2). At the beginning of the Messinian, the Mt. Judica thrust stack started to propagate onto the Tortonian foredeep sediments which deformed simultaneously and created the Messinian Gela Nappe at the front of the chain (Fig. 4.14B, stage 3). During the Messinian, as documented by Yellin-Dror et al. (1997), the region underwent tectonic uplift coupled with a major sea-level fall. These processes changed the rheological parameters ( $\lambda$  and  $\lambda_b$  between 0.3 and 0.8, Adam and Reuther, 1995) and the Mt. Judica thrust stack continued to be deformed internally to adjust and maintain the critical taper (Fig. 4.14A). In the Early Pliocene the regional subsidence rate exceeded the tectonic uplift rate (Nigro and Renda, 2001) and the marine transgression dropped the critical state ( $\lambda$  and  $\lambda_b = 0.8$ , Adam and Reuther, 1995) keeping the system in supercritical condition (Fig. 4.14A, stage 4). After the Early Pliocene the whole system (Mt. Judica thrust stack and Gela Nappe) propagated forward on top the Trubi Fm undergoing strong erosion and gravity collapse processes.

The upper structural levels of the thrust stack were re-deposited toward the toe of the chain on top the deformed Messinian Gela Nappe structural levels (Fig. 4.4). The topographic slope ( $\alpha$ ) decreased, while as we discussed in the previous paragraph, this sector of the chain did not undergo a large flexural downbending and the  $\beta$  angle remained almost constant (Fig. 4.14A, stage 4). In terms of critical taper, according to Adam and Reuther (1995) and Nigro and Renda (2001), the wedge extended to reduce the

taper with erosion and propagation and this elongation led the system to a subcritical state. Internal deformation of the Mt. Judica Unit continued to achieve the critical state and to accommodate the erosional processes decreasing the topographic wedge slope.

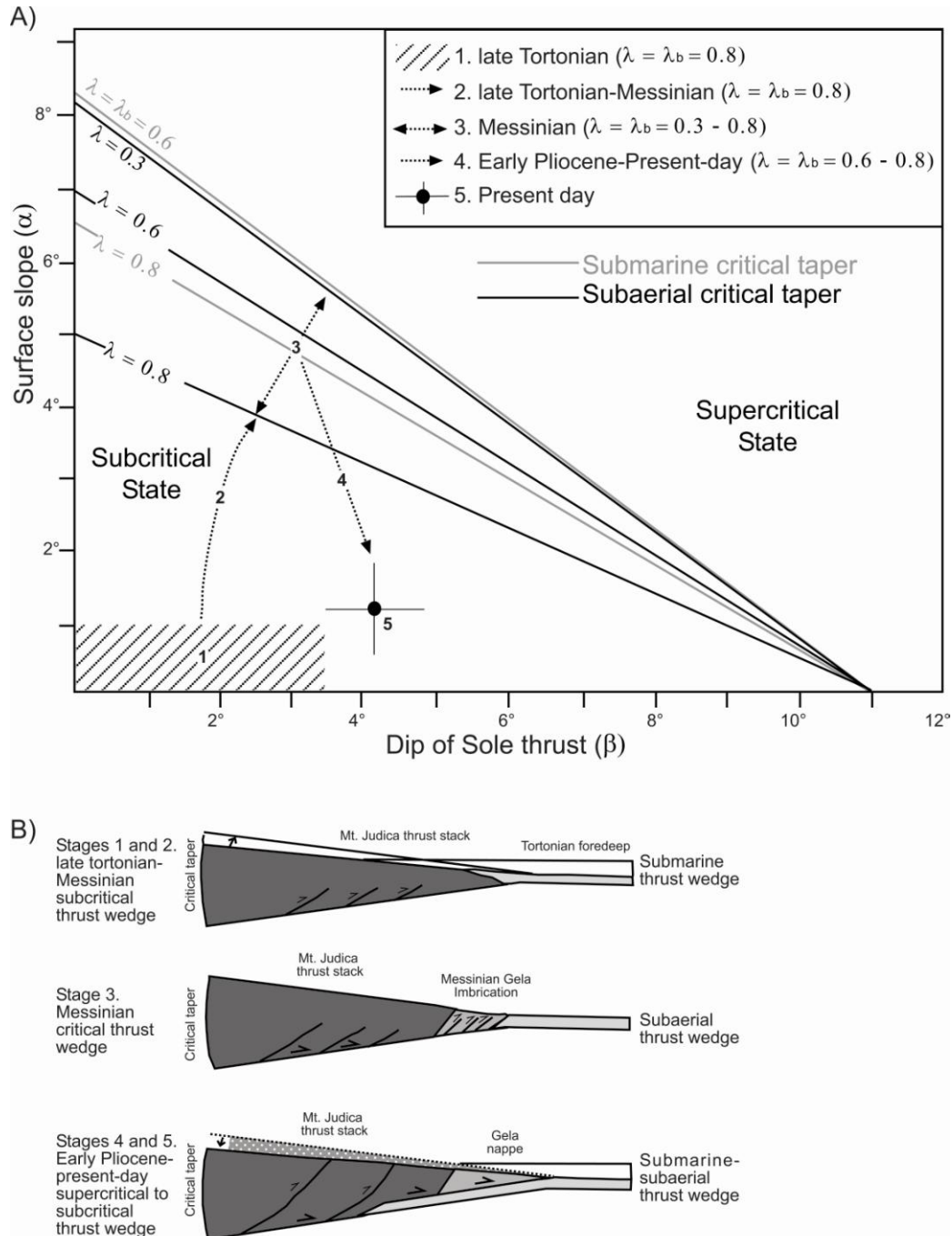


Figure 4.14 – A) Values of  $\alpha$  and  $\beta$  of the front of the Sicilian orogenic wedge derived from published works and analyses from this paper. The lines represent the relationship between pore-fluid pressure ratio ( $\lambda$ ), surface slope ( $\alpha$ ) and basal detachment ( $\beta$ ) for a submarine (grey lines) and subaerial (black lines) orogenic wedges at critical taper assuming value of 1.03 for the effective coefficient of internal friction of the wedge ( $\mu$ ) and 0.85 for the coefficient of internal friction of the basal detachment ( $\mu_b$ ) following Byerlee's law.  $\lambda_b$  is the ratio of pore fluid pressure to lithostatic pressure at the base of the wedge. B) Dynamic thrust wedge models of the external fold-and-thrust belt in Eastern Sicily since Late Miocene redrawn and modified after Adam and Reuther, 1995. Five stages of restoration are shown: 1. late Tortonian, 2. late Tortonian-Messinian, 3. Messinian, 4. Early Pliocene-present-day and 5. Present-day times.

#### 4.5. Conclusion

Thermal and structural analyses of the Sicilian thrust front from the Mt. Judica recess to the salient to the west, allowed us to investigate the final collisional stages during Late Miocene times and its effect on vertical motions along the thrust front. Thermal constraints derived from clay mineral-based geothermometers and FTIR on organic matter showed that the Mt. Judica Unit experienced paleo-temperatures in the range of 94-132 °C in late diagenetic conditions and early mature stage of hydrocarbon generation (according to Scotti, 2003). As a whole, the Mt. Judica Unit experienced maximum burial during the Middle Miocene as a result of the emplacement of the Sicilide Complex and the Numidian Flysch atop the Unit. Structural data based on cross balanced restorations pointed out an increase of shortening of the Imerese-Sicano Unit from the Gela salient to the Mt. Judica recess with values from 12.3 km to 23.9 km and an increase of tectonic thickening. These variations are due to buttressing of the accretionary wedge against the crustal ramp bounding the Hyblean Plateau domain to the chain which produced substantial wedge shortening, recorded by major overthrusting and breaching.

Application of theoretical models to wedge dynamics allowed us to reconstruct the Upper Miocene to present-day wedge evolution for the Mt. Judica area. From late Tortonian to Messinian, the wedge from subcritical condition evolved to a critical state thickening internally. The Pliocene was a fundamental stage in the tectonic evolution of the recess area: the wedge evolved to a supercritical state. Erosion and gravity-driven processes ruled out the last evolutionary stage leading the wedge to the present-day subcritical conditions. At least ~2.4-3.0 km-thick Allocthonous Units were removed off, and the Mt. Judica Unit exhumed by up-thrust geometries (which caused uplift) and erosion. This Pliocene stage of shortening did not overprint thermal maturity because the extent of thrust sheets overlapping is negligible when compared with the extent of vertical movements.



## CHAPTER V - EARLY FOREDEEP DEPOSITS (“NUMIDIAN FLYSCH”)

### 5.1. Introduction: Geological setting of the Numidian Flysch Basin in the Mediterranean area

The Numidian Flysch crops out continuously from Gibraltar through Morocco, Algeria, Tunisia, Sicily and the Southern Apennines (Grasso, 2001; see Fig. 1.3 in chapter I). It is mainly composed of detrital quartz coming from the African Craton (Nubian Sandstone) according to Wezel (1970), and represents the upper Oligocene to middle Miocene filling of the precursor foredeep basins, formed after the collision between the Africa and Europe continental plates. The African source should have provided the sediments that, like the Fortuna sandstones, spread from Tunisia to Sicily Channel and western Sicily, and as turbidity currents as far as Sicily and the southern Apennines (Benomran et alii, 1989). Apart from the African provenance, the other possible sources for the Numidian quartzarenites are areas located west of the Numidian through, as proposed by Durand-Delga (1967).

The term was firstly introduced by Flandrin (1948) to indicate alternating brown clays and quartzarenites of early to middle Miocene age cropping out along the Maghrebian Chain in Sicily (Carbone et al. 1987). A first lithological subdivision of the unit from the Mistretta area is due to Sequenza (1873), who describes a lower pelitic interval of “*argille scagliose grigie o brune*” and an upper quartzarenitic one made of “*arenaria grossolana a granuli di quarzo traslucidi e cemento siliceo*”. Several papers relate the Numidian Flysch to the time interval comprised between the Late Oligocene and the Early Miocene (Baldacci, 1886; Checchia-Rispoli, 1916) and the formation was formally defined by Flandrin (1948). Important contributions are from Accordi (1958) and Schmidt di Friedberg et al. (1960), who respectively defined the Geraci Siculo Fm. (Oligocene-Early Miocene, Aquitanian in age) and Collesano Fm. Ogniben (1960) recognised a lateral continuity with the North African “*Numidien*” and proposed for the formation the name “*Flysch Numidico*”. In northern Sicily, in the Madonie Mts., the Numidian Flysch is tectonically overlain by an allochthonous calcareous-dolomitic succession with thicknesses up to 600 m (Lugeon and Argand, 1906a, b; Fabiani e Trevisan, 1940) of Triassic to Oligocene age. At its front the allochthonous carbonate nappe is characterised by swarms of blocks and mega breccias of platform carbonates embedded with the brown shales of

the Numidian Flysch, interpreted as a Wildflysch by Ogniben (1960). Where preserved, the carbonate nappe is overlain by the upper quartzarenite part of the “Numidian Flysch” (lower to middle Miocene) and a marly succession (Langhian to lower Tortonian, Grasso, 2001). These are, in turn, covered by various allochthonous units including the Sicilides. The autochthonous parts of the Numidian Flysch, which are intercalated between nappes are known in the literature as meso-autochthonous (Selli, 1957; Ogniben, 1960). Broquet et al. (1967) and Broquet (1970) describe two different basins with two distinct numidian successions: a southern autochthonous one (Numidien externe) and a northern allochthonous one (Numidien Interne). The substratum to the two different successions is respectively Varicoloured Clays in the “Numidien Interne” and brown clays in the “Numidien Externe”. Wezel (1970) recognise different facies and depositional environments in the Numidian Flysch of central-north Sicily.

## **5.2. Geological and structural setting of the Numidian Flysch in Eastern Sicily**

The geological setting of the Numidian Flysch suggests deposition over a large basin, the external side of which was represented by the still undeformed Africa plate margin (Grasso, 2001). Along this margin of the basin, as observed in Sicily, the “Numidian Flysch” quartzarenites laterally evolves to glauconitic sandstones and calcarenites. The internal margin of the “Numidian Flysch” basin is more difficult to reconstruct because of intense later Miocene-Pliocene deformation, and crustal shortening occurred during the progressive building of the Maghrebien chain (Grasso, 2001). Although most of the original contacts between the “Numidian Flysch” and its substratum are often overprinted by later tectonic detachments, it is still possible to infer the stratigraphic substratum of the Numidian Flysch. In Sicily, the substratum to the “Numidian Flysch” is represented by both platform and basin carbonates and successions belonging to the Sicilian domain.

The Numidian Flysch is actually made of several south-verging structural slices, detached mainly along Oligocene stratigraphic horizons, even if locally deformation is younger (Pliocene) and the footwall to the thrust is made of Messinian successions (M. Altesina backthrust).

Bianchi et al. (1987) recognize five different tectonic units, that are described from the external zones to the internal ones (Fig. 5.1). They exhibit significant facies variations and are, in turn, deformed into minor thrust sheets to form an imbricate thrust system.



The more external one is the Gagliano Unit: known from subsurface data alone (wells for hydrocarbon exploration). It represents the reservoir of gas, condensate, and light oil (55° API) of the “Gagliano” group fields with main productive depths comprised between 2,800 and 3,000 m in Enna subsurface area (Holton, 1999; Pieri, 2001). This petroleum probably originated from unknown Mesozoic (Mattavelli and Novelli 1988) and probably Tertiary sources rocks (Anelli et al., 1996). The substratum to this unit is a thick Mesozoic succession of the “Imerese” domain, which passes stratigraphically up to a thick succession (more than 1,000 m) of Oligocene grey-brown clays passing to an alternation of clays and quartzarenites and mainly quartzarenites and glauconitic sandstones toward the top of the succession, which is middle Miocene in age.

Serra del Bosco Unit: it is the lowest outcropping unit and can be observed in the areas west of Gagliano. It is present from Serra del Bosco to Monte Boscorotondo, to the north of Leonforte village (Enna area) (Lentini et al. 1987). This unit is tectonically overlain by the Numidian Flysch of Mt. Salici Unit. The Serra del Bosco Unit, cover, in turn, another thick Numidian unit, which is probably tectonically duplicated before reaching the “Imerese” substratum (Fig. 5.1).

Mt. Salici Unit, cropping out in the homonymous localities, tectonically overlies Serra del Bosco Unit, with or without the interposition of Sicilide Unit (Fig. 5.2), and Mt. Judica Unit (Fig. 5.1). locality.

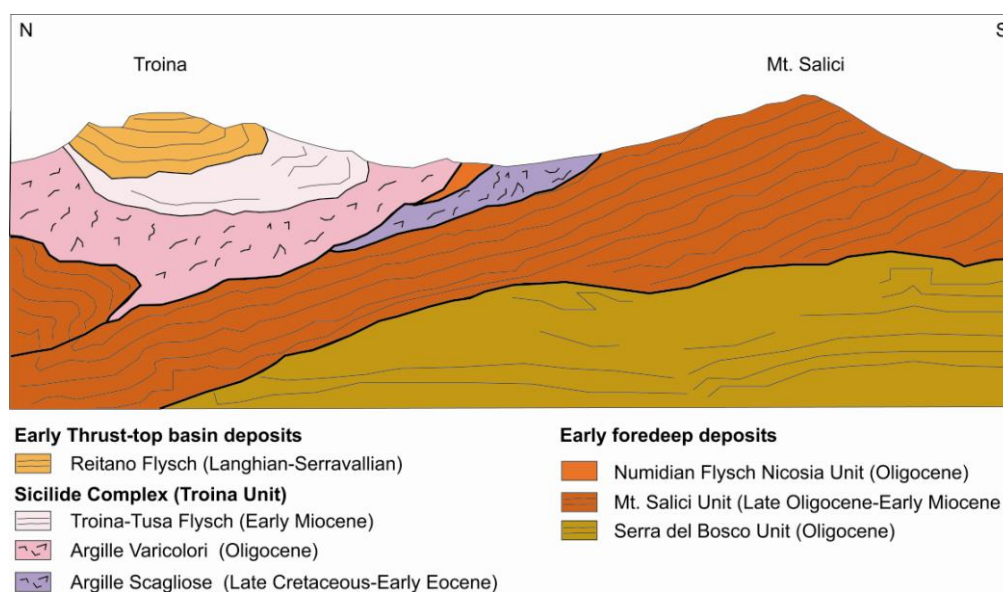
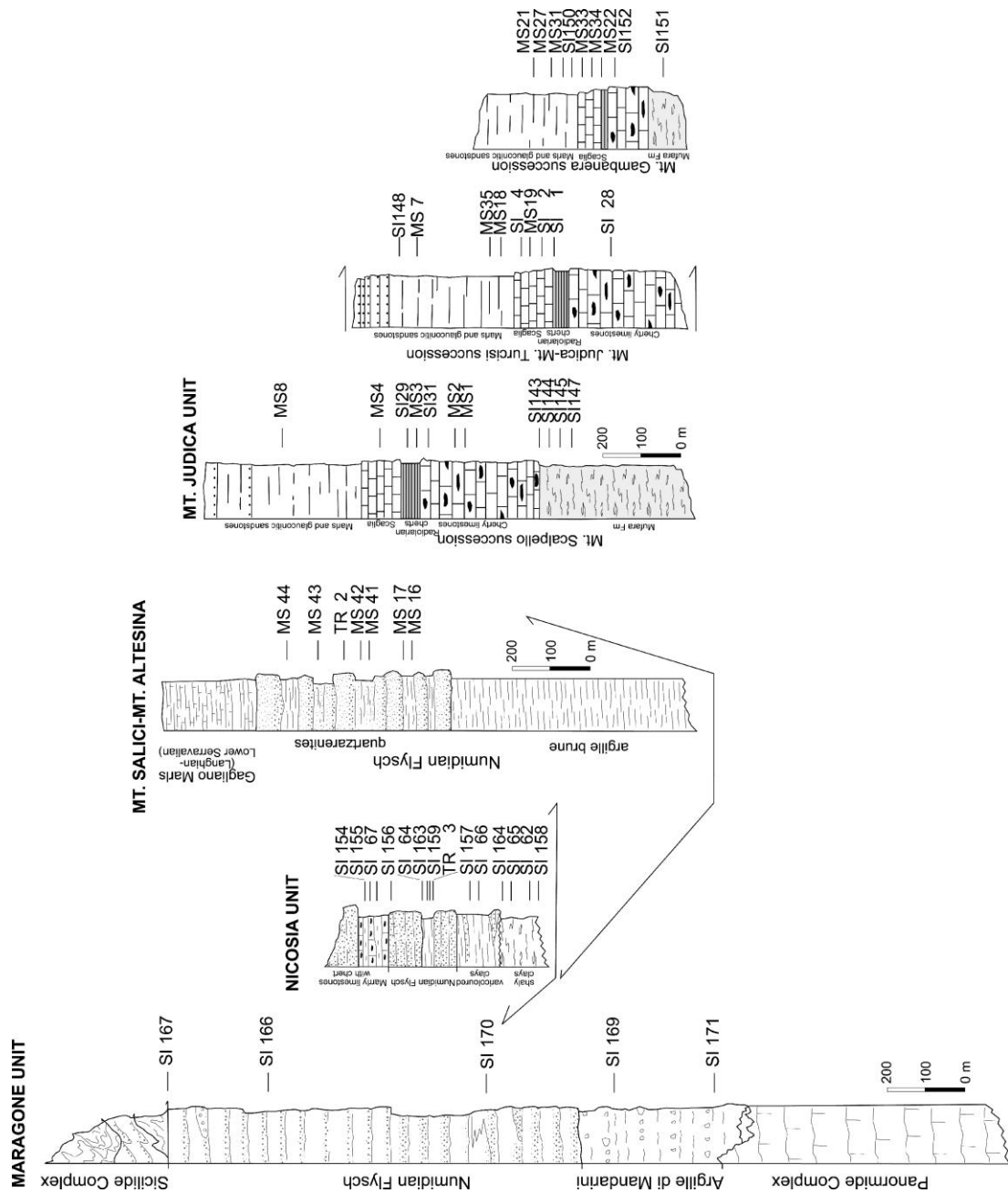


Figure 5.2 – Schematic section showing Serra del Bosco, Mt. Salici and Sicilide Units structural relations, redrawn and modified after Carbone et al. (1987).



The two more internal Numidian Flysch units are: Maragone Unit and Nicosia Unit. Maragone Unit crops out extensively in the Nebrodi Mts. (Mt. Sambughetti to the north of Nicosia, Castel di Lucio and Mistretta villages) and is intersected by Maragone1 and Pizzo Bellafontana1 wells (Fig. 5.4); it represents the Oligo-Miocene stratigraphic cover of the Panormide domain (Bianchi et al. 1987, Lentini et al. 2000). The total thickness of this unit in Maragone well is 2,350 m. From this depth to 3,250 m, the well intersects Sicilide successions and exotic of Panormide Platform carbonates. From 3,250 m to 4350 m, the well intersects limestones and dolomitic limestones related to “*Calcari di Pizzo Canna*” and “*Dolomie di Monte Quacella*” of late Triassic-Giurassic age (Grasso et al., 1978) and 50 m of Mufara Fm of Carnic age. The Numidian Flysch of this unit is made of a lower interval (1,200 m thick) made mainly of quartzarenites, followed upwards by clays and grey silty clays (150 m), an alternation of clays and quartzarenites (400 m) and 500 m of brown silty clays interbedded with quartzarenites.

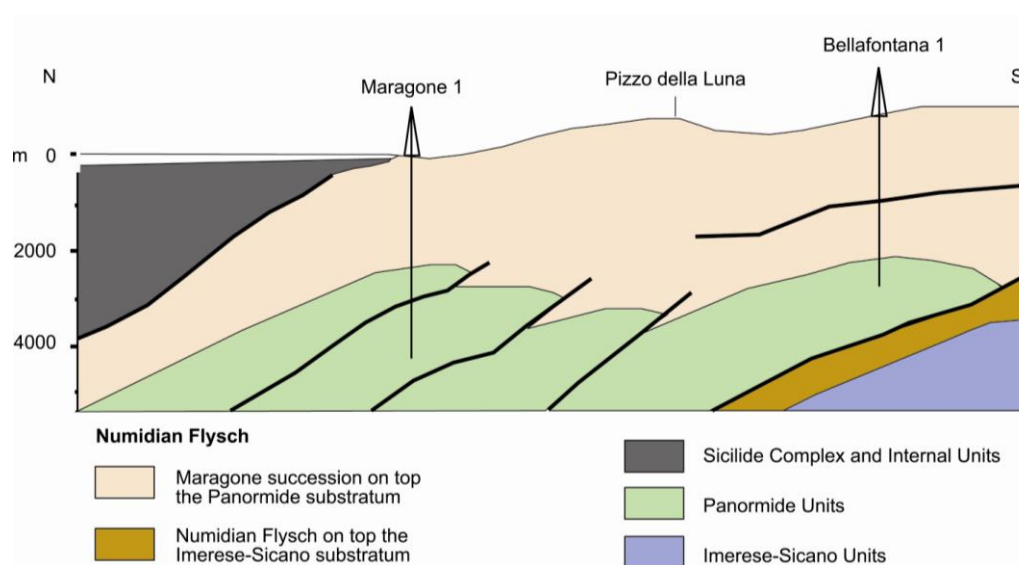


Figure 5.4 – Cross section between Maragone1 and Pizzo Bellafontana1 wells redrawn and modified after Bianchi et al. (1987).

La Manna et al., (1995) divide this unit into two minor units: Mt. Sambughetti Unit and Mt. Castelli Unit (Fig. 5.5B and C). The lower unit (Mt. Sambughetti Unit) lies above a carbonatic substratum of the Panormide domain made of “*Dolomie di Monte Quacella*” (Trias sup-Lias) and upper Cretaceous-Eocene marly limestones (“*Scaglia*”), which indicate the foundering of the margin of the carbonate platform. The thickness of this unit in outcrop is of about 1,500 m. The upper unit (Mt. Castelli Unit) cropping out in the





A partial review of their geometric relationships allowed to identify two main structural levels. A wide basal structural level made up of Gagliano, Serra del Bosco and Maragone Units and an upper structural level made up of Nicosia and Mt. Salici Units (Lentini et al. 2000 fig 5.5). Essentially, this reconstruction differs in the structural position of the Mt. Salici Unit and therefore in the paleogeographic reconstruction of the original Oligo-Miocene early foredeep basin. According to the second framework Nicosia and Mt. Salici should be more internal than Maragone, Serra del Bosco and Gagliano Units (Fig. 5.5).

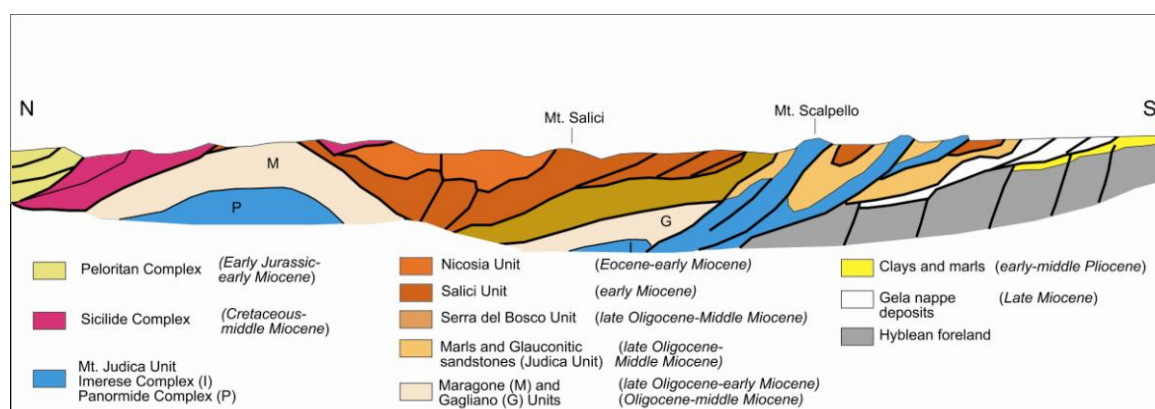


Figure 5.5– Schematic structural section of Eastern Sicily reworked and modified after Bianchi et al. (1987).

The aim of the new contribution of data provided by this thesis is to define the thermal signature of the different structural-stratigraphic units making up the Numidian flysch thrust stack and to interpret them in terms of tectonic vs. sedimentary burial.

### 5.3. Results

In this framework, a suite of 38 samples for XRD analysis, 16 samples for organic matter optical analysis and 7 samples for FTIR analysis were collected, moving from North to South, in the following stratigraphic-structural units: Maragone, Nicosia, Mt. Salici and Mt. Judica Units (Fig. 5.3 and 5.6; Table 5.1).

#### 5.3.1. Maragone Unit

The Giardinello River section was sampled between Geraci Siculo and Castel di Lucio villages. In this area the Numidian Flysch rests on the Oligocene-Early Miocene “*Argille di Portella Mandarini*”, that is unconformably lying on the Panormide Complex. Samples include the brown silty clays of the “*Argille di Portella Mandarini*” (SI 169 and SI 171) and the Numidian flysch (SI 170, SI 167, SI 168 and SI 166) (Fig. 5.3).



The I-S mixed layers correspond to ordered structures (R1) with a percentage of illite in the range of 66 and 79%.

Analyzed samples are generally scarce in organic matter, with a predominance of highly oxidized macerals and amorphous organic matter. The  $VR_o\%$  values for the Maragone Unit range from 0.28% to 0.41%.

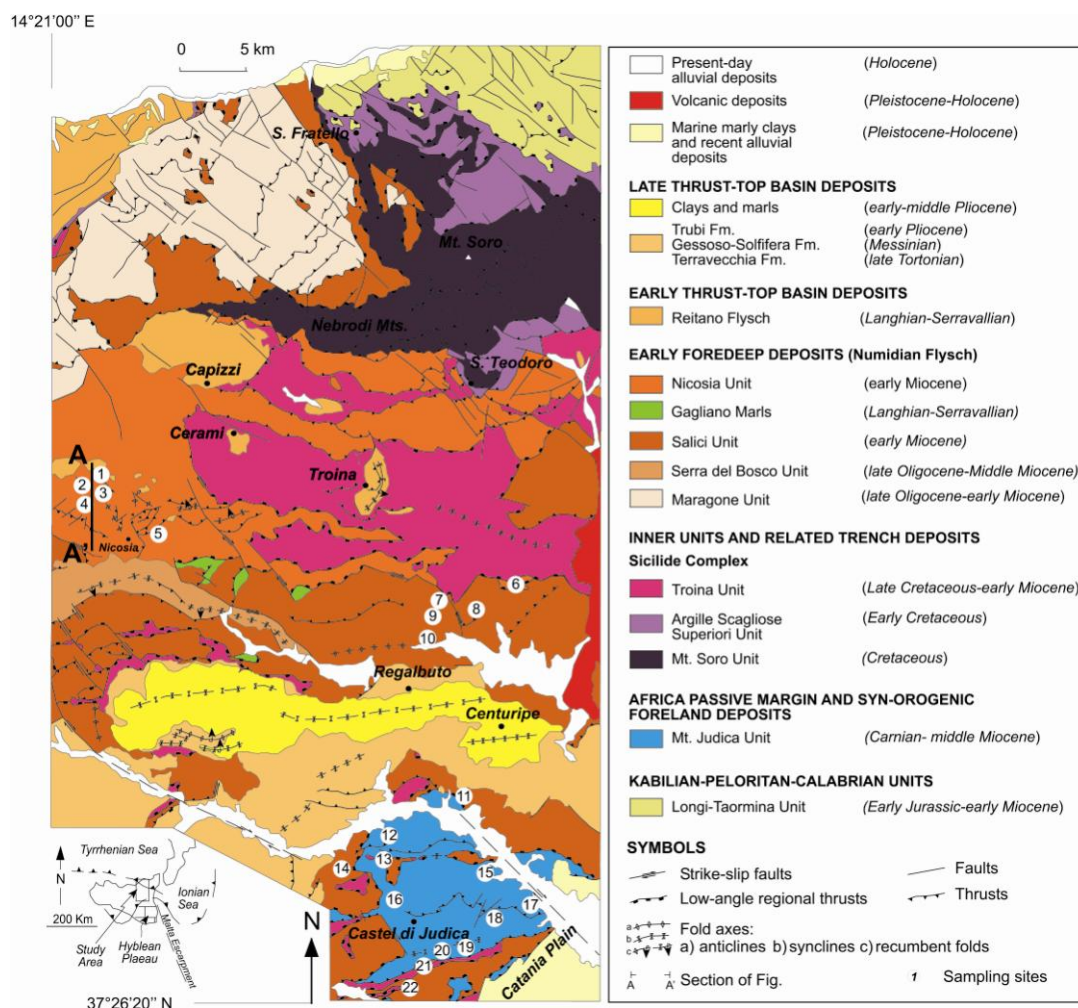


Fig. 5.6 – Geological sketch map of Eastern Sicily with sampling site, redrawn and modified after Carbone et al. (1990) and Lentini et al. (2000).

Structural Unit	Formation	Stratigraphic age	site	Samples	Locality	Lithology	%Ro ± s.d. (n.)	%I in I-S <2µm	R parameter	X-ray semi quantitative analysis (<2µm)	FTIR	
Maragone Unit	Numidian Flysch	upper Oligocene - lower Miocene		SI 166	Pastonello	Coarse-grained marls	0.27 ± 0.07 (10)	71	R1	I <sub>17</sub> -S <sub>22</sub> K <sub>67</sub> Ch <sub>4</sub>		
				SI 168		Marls	0.4± 0.09 (10)	71	R1	I <sub>23</sub> -S <sub>18</sub> K <sub>55</sub> Ch <sub>4</sub>		
	Argille di Portella Mandarini			SI 167	Silty marls	vitritine absent	67	R1	I <sub>22</sub> -S <sub>14</sub> K <sub>60</sub> Ch <sub>4</sub>			
	SI 170			Siltites	vitritine absent	66	R1	I <sub>45</sub> -S <sub>8</sub> K <sub>46</sub> Ch <sub>1</sub>				
				SI 171	Geraci	Fine-grained siltites	vitritine absent	79	R1	I <sub>22</sub> -S <sub>10</sub> K <sub>55</sub> Ch <sub>13</sub>		
				SI 169		Brown siltites	0.4± 0.07 (9)	73	R1	I <sub>28</sub> -S <sub>10</sub> K <sub>52</sub> Ch <sub>10</sub>		
Nicosia Unit			6	TR 2	Castello di Spanò	Massive sandstones		-			I <sub>26</sub> K <sub>69</sub> Ch <sub>5</sub>	
		TR 3	Brown marls			50	R0	I <sub>61</sub> -S <sub>88</sub> K <sub>24</sub> Ch <sub>2</sub>				
				SI 154		Marly limestone with chert	vitritine absent	20	R0	I <sub>19</sub> -S <sub>62</sub> K <sub>19</sub>		
			SI 155	Marly limestone with chert		0.41± 0.02 (2)						
			SI 67	Marly limestone with chert			20	R0	I <sub>36</sub> -S <sub>61</sub> K <sub>1</sub> Ch <sub>1</sub>			
			SI 156	Coarse-grained sandstones		vitritine absent						
				SI 64		Brown shales			45	R0	I <sub>18</sub> -S <sub>12</sub> K <sub>69</sub> Ch <sub>1</sub>	
				SI 163		Brown shales			35	R0	I <sub>25</sub> -S <sub>22</sub> K <sub>52</sub> Ch <sub>2</sub>	
			3	SI 159		Brown shales			40; 65	R0;R1	I <sub>9</sub> -S <sub>9</sub> K <sub>79</sub> Ch <sub>3</sub>	
			3	SI 157 OM	Sperlinga	Black shales	vitritine absent					
			SI 157 CM	Black shales		0.42 ± 0.09 (8)						
			SI 164.1 OM	Varicoloured clays		0.46 (1)	20	R0	I <sub>45</sub> -S <sub>53</sub> K <sub>2</sub>		x	
			SI 164.2 OM	Black shales		0.59 ± 0.07 (10)						
				4	SI 164.1 CM		Silty clays		50	R0	I <sub>55</sub> -S <sub>31</sub> K <sub>5</sub> Ch <sub>9</sub>	
				1	SI 62		Black shales	0.36 ± 0.04 (6)	45	R0	I <sub>26</sub> -S <sub>32</sub> K <sub>18</sub> Ch <sub>24</sub>	
					SI 65		Silty clays		40	R0	I <sub>16</sub> -S <sub>26</sub> K <sub>52</sub> Ch <sub>7</sub>	
					SI 158		Silty clays		50	R0	I <sub>22</sub> -S <sub>23</sub> K <sub>50</sub> Ch <sub>4</sub>	
	Mt. Salici Unit			10	MS 41		Grey and brown shales		50	R0	I <sub>17</sub> -S <sub>99</sub> K <sub>30</sub> Ch <sub>5</sub>	
				9	MS 42		Brown shales		55	R0	I <sub>5</sub> -S <sub>59</sub> K <sub>33</sub> Ch <sub>3</sub>	
			MS 43	Brown shales			50	R0	I <sub>3</sub> -S <sub>89</sub> K <sub>22</sub> Ch <sub>4</sub>			
			MS 44	Brown shales			55	R0	I <sub>17</sub> -S <sub>53</sub> K <sub>32</sub> Ch <sub>8</sub>			
			8	TR 1	Castel di Judica	Coarse-grained sandstones		50	R0	I <sub>9</sub> -S <sub>38</sub> K <sub>51</sub> Ch <sub>4</sub>		
			MS16	Finely laminated shales			50	R0	I <sub>6</sub> -S <sub>68</sub> K <sub>21</sub> Ch <sub>5</sub>			
			MS17	Finely laminated shales			55	R0	I <sub>1</sub> -S <sub>48</sub> K <sub>38</sub> Ch <sub>7</sub>			
			MS 24	Massive sandstones			-					
			21	MS 24		Brown shales		55	R0	I <sub>4</sub> -S <sub>88</sub> K <sub>26</sub> Ch <sub>2</sub>		
			22	MS 25		Brown and red shales		55	R0	I <sub>9</sub> -S <sub>63</sub> K <sub>26</sub> Ch <sub>2</sub>		
			22	MS 32		Brown shales		60	R1	I <sub>11</sub> -S <sub>39</sub> K <sub>46</sub> Ch <sub>4</sub>		
			14	MS 39		Brown shales						
			13	MS7	Mt. Scalpello			55	R0	I <sub>1</sub> -S <sub>88</sub> K <sub>12</sub> Ch <sub>1</sub>		
			12	MS8		Fine-grained sandstones	vitritine absent	55	R0	I <sub>3</sub> -S <sub>84</sub> K <sub>10</sub> Ch <sub>1</sub>		
			15	SI 148		Clays and marls with glauconite	vitritine absent	50	R0	I <sub>10</sub> -S <sub>13</sub> K <sub>75</sub> Ch <sub>1</sub>		
		17	MS18	Light brown and green shales			60	R0/R1	I <sub>19</sub> -S <sub>13</sub> K <sub>30</sub> Ch <sub>18</sub>			
	Marls and Glaucinitic sandstones	Oligocene - middle Miocene	16	MS35	Mt. Judica	Marls with glauconite		65	R1	I <sub>21</sub> -S <sub>18</sub> K <sub>47</sub> Ch <sub>14</sub>		
18			MS21	Brown and light brown shales			60	R1	I <sub>16</sub> -S <sub>15</sub> K <sub>57</sub> Ch <sub>12</sub>			
20			MS27	Mt. Gamberara	Brownish marls		65	R1	I <sub>22</sub> -S <sub>9</sub> K <sub>52</sub> Ch <sub>17</sub>			
MS31			Marls with glauconite			65	R1	I <sub>12</sub> -S <sub>4</sub> K <sub>64</sub> Ch <sub>20</sub>				
				19	SI 150		Clays and marls with glauconite		67	R1	I <sub>24</sub> -S <sub>29</sub> K <sub>37</sub> Ch <sub>10</sub>	
											x	

Table 5.1 –Summary of inorganic and organic thermal parameters and XRD quantitative analysis. X in the FTIR column indicate that samples have been analyzed (See Fig. 5.8 and Table 5.2 for results).

### 5.3.2. Nicosia Unit

A complete section of the Nicosia Unit was sampled in the area of Sperlinga village, where the Unit crops out in an overturned syncline (Fig. 5.7) and two samples of Numidian Flysch in the area of Castello di Spanò village. XRD and  $VR_o\%$  samples cover the whole section, while FTIR samples come from the Eocene scaly clays and interbedded black shales of the substratum and from the Oligocene varicoloured clays and interbedded black shales of the Numidian Flysch (Fig. 5.3).

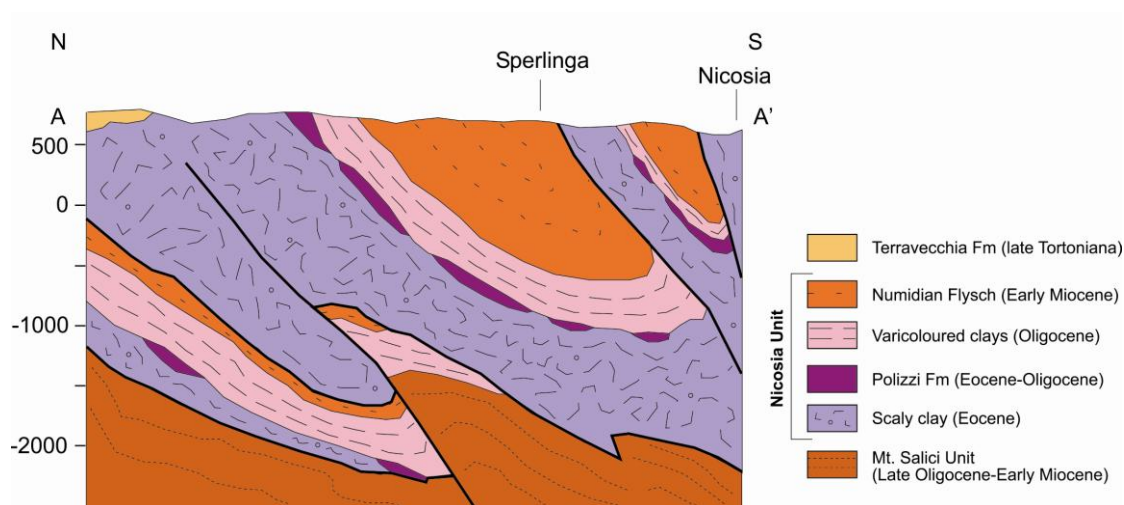


Figure 5.7 – Geological cross section between Sperlinga and Nicosia villages redrawn and modified after Carbone et al. (1990). Trace of cross section (A-A') is shown in Fig. 5.6.

XRD samples show I-S mixed layers corresponding to disordered structures (R0) with a percentage of illite ranging between 20 and 50%.

Vitrinite Reflectance values are in the range of 0.36-0.42%. In the SI 164.1 OM and SI 155 two separate clusters of  $VR_o\%$  values were recognized. The first one, characterized by lower  $VR_o\%$  values and by a less number of fragments is representative of indigenous woody fragments, whereas the second one, with higher values, is made up of highly oxidized or recycled fragments. The latter group was not taken into account for the interpretation in terms of burial/thermal evolution of the analyzed stratigraphic units.

Several Authors have demonstrated that aromaticity increase and aliphaticity decrease with increasing thermal maturity (Ganz et al., 1990; Kister et al., 1990; Lin and Ritz, 1993b; Chen et al., 1998; Lis et al., 2005).

Aromaticity and aliphaticity FTIR ratios were calculated and compared with those of the Clays and Glauconitic sandstones of the Mt. Judica Unit (Table 5.2; see data and discussion in chapter IV for Clays and Glauconitic sandstones thermal maturity).

SI 164.1OM and SI 158 spectra compared with the other spectra are characterized by lower absorbance in the 2,800-3,000  $\text{cm}^{-1}$  aliphatic CH stretching vibration region and at  $\sim 1,710 \text{ cm}^{-1}$  carbonyl/carboxyl peak (Fig. 5.8). These pieces of evidence may indicate oxidation (Calemma et. al., 1988; Sobalik et al., 1998) in agreement with the organic matter optical observations. Therefore the ratios of these samples are not taken into account for thermal maturity interpretation.

Aromaticity ratios ( $\text{Ar}_{3000-3100}/\text{Al}_{2800-3000}$ ;  $\text{Ar}_{3000-3100}/\text{Al}_{1450}$ ;  $\text{Ar}_{3000-3100}/\text{Al}_{1370}$ ;  $\text{Ar}_{1600}/\text{Al}_{2800-3000}$ ;  $\text{Ar}_{1600}/\text{Al}_{1450}$ ;  $\text{Ar}_{1600}/\text{Al}_{1375}$ ) increase from Nicosia Unit to Judica Unit. Aliphaticity ratio ( $\text{CH}_2/\text{CH}_3$ ) decreases from Nicosia Unit (values range between 2.23 and 3.09) to the Marls and Glauconitic sandstones of the Judica Unit (values of 2.03 and 2.13). Thus FTIR ratios suggest that Nicosia Unit reached a thermal maturity lower than the Marls and Glauconitic sandstones (lower than about 0.5% of vitrinite reflectance, see chapter IV for detailed data on Mt. Judica Unit).

	Formation	Site	Sample	$\text{Ar}_{3000-3100}$	$\text{Ar}_{3000-3100}$	$\text{Ar}_{3000-3100}$	$\text{Ar}_{1600}$	$\text{Ar}_{1600}$	$\text{Ar}_{1600}$	$\text{CH}_2$
				$\text{Al}_{2800-3000}$	$\text{Al}_{1450}$	$\text{Al}_{1370}$	$\text{Al}_{2800-3000}$	$\text{Al}_{1450}$	$\text{Al}_{1370}$	$\text{CH}_3$
Nicosia	Numidian Flysch	3	SI157 o	0.003	0.002	0.01	0.12	0.71	3.35	2.31
			SI157 c	0.006	0.036	0.14	0.4	2.47	9.63	3.09
	Scaly clays	4	SI164.1	—	—	—	7.09	—	—	1.81
			SI164.2	0.002	0.014	0.08	0.13	0.85	5.23	2.23
		1	SI158	0.010	0.016	—	—	—	—	2.83
Judica	Clays and glauconitic sandstones	15	SI148.1	0.010	0.072	0.21	0.6	6.33	18.72	2.03
		19	SI150.1	—	—	—	—	—	—	2.13

Table 5.2 – Aromaticity (ratios of aromatic versus aliphatic FTIR absorption values) and aliphaticity ratio ( $\text{CH}_2/\text{CH}_3$ ).

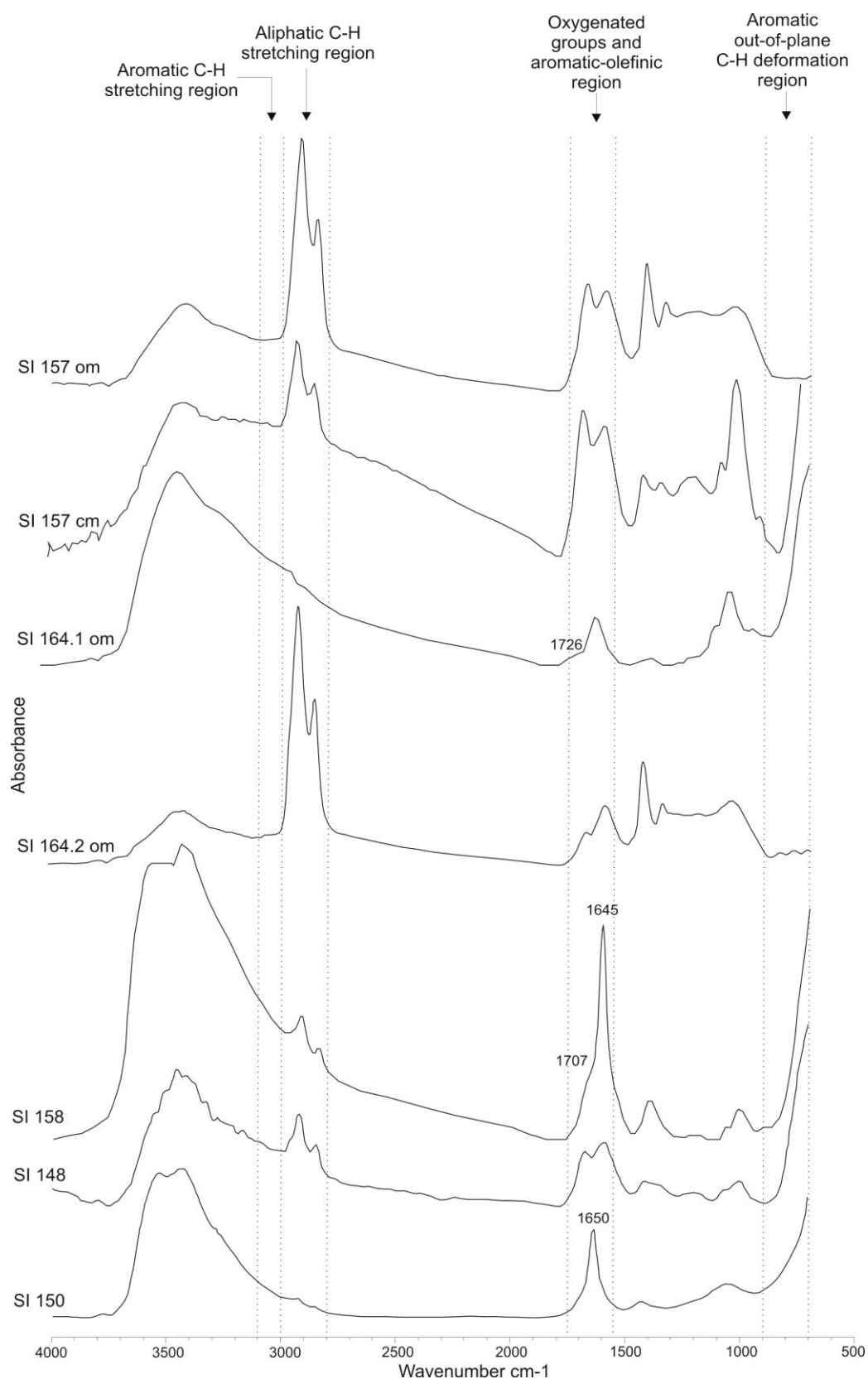


Figure 5.8 – FTIR spectra of concentrated kerogen from Oligocene-Lower Aquitanian variegated shales (SI 157 om and SI 157 cm) and Eocene scaly clays (SI 164.1 om, SI 164.2 om and SI 158) of the Nicosia Unit and from Clays and Glauconitic sandstones (148 and 150) of the Mt. Judica Unit.

### 5.3.3. Mt. Salici Unit

Five samples are from the Mt. Salici section (Fig. 5.3) and six samples are from the area of Mt. Judica. The continuity of Mt. Salici Unit is interrupted by the presence of the Tortonian-Pliocene sediments of the Leonforte thrust-top basin (Fig. 5.6). Observed I-S mixed layers correspond to disordered structures (R0) with a percentage of illite variable from 50 to 60%. Ordered structures (R1) were identified only for the MS39 sample.

Vitrinite fragments are almost absent. The only organic matter data derive from the Gagliano Marls with values of about 0.40%.

### 5.3.4. Clays and Glauconitic Sandstones of the Mt. Judica Unit

Observed I-S mixed layers correspond to disordered structures (R0) with a percentage of illite variable from 50 to 65%. Ordered structures (R1) were identified only for the SI150 sample (67% I in I-S). Vitrinite fragments are almost absent. Derived-VR<sub>o</sub> values from FTIR data correspond to about 0.5% (see chapter IV for discussion).

## **5.4. Discussion**

### **Thermal interpretation of the tectono-stratigraphic units**

#### 5.4.1. Maragone Unit

A mismatch arises from the estimated temperatures of Maragone Unit. The clay mineralogy analysis suggests higher paleotemperatures than those calculated by Barker's equations from VR<sub>o</sub>% data (about 30-50 °C). Measured vitrinite fragments are altered and therefore derived data might be slightly underestimated.

In light of this consideration, data from Maragone Unit indicate late diagenetic conditions. Nevertheless, the absence of suitable organic matter for maturity analyses prevents us from better constraining this range.

The Numidian flysch in the T. Giardinello section is 1,000 m thick. Data from Maragone and Pizzo Bellafontana1 wells drilled in northern Sicily indicate a thickness of about 2,350 m of the Unit.

The thickness of the Giardinello River section is insufficient to justify the thermal maturity indicated by clay mineralogy. Therefore the paleo-temperature estimated for the unit can be related to sedimentary load of the eroded Numidian flysch and/or tectonic burial.

#### 5.4.2. Nicosia Unit

The data indicate a very low thermal maturity and a regular trend of decreasing illite content in mixed layers I-S from pre- to syn-orogenic deposits. A good correlation between Ro, XRD and FTIR data is observed. Data suggest that the Nicosia Unit experienced low diagenetic condition in the immature stage of hydrocarbon generation.

The Sicilide type substratum of the Nicosia Unit shows a scarce maturity which differs from that observed in other studied Sicilide Units cropping out in the Nebrodi Mts. (Aldega et al. 2007; Corrado et al. 2009).

According to these Authors, Mt. Soro and Troina Units underwent severe underthrusting and sub-sequent exhumation whereas Nicosia and Antisicilidi Units were not involved in the Sicilide accretionary prism underthrusting (chapter I, section 1.4.1, Fig. 1.6).

As a matter of fact the Nicosia Unit is generally considered as the most internal portion of the early foredeep despite the fact that its pre-orogenic substratum is made up of the typical succession of the Sicilide domain.

#### 5.4.3. Mt. Salici Unit

The lack of ordered R1 structures allows to estimate paleotemperatures characteristic for the last stages of the early diagenetic zone. A lower temperature range can be established if compared to VR<sub>0</sub>%-converted temperatures for the Gagliano Marls (about 50°C).

### **5.5. Conclusion**

This study provided a data set of thermal maturity indicators for the Numidian Units.

The lowest thermal evolution was found in the Nicosia Unit which is characterized by VR<sub>0</sub>% values between 0.36 and 0.42%, FTIR data in agreement with organic matter optical analysis and illite content in I-S between 20% and 50%.

The highest percentages of illite layers in I-S (66%–79%) are found in the Maragone Unit, followed by Mt. Salici Unit (50-60%) (Fig. 5.9).

Specifically, data suggest that along the Nebrodi Mts.–Hyblean Plateau transect, the Numidian Units present an increasing thermal maturity from the uppermost structural unit (Nicosia Unit) to the lowermost one (Maragone Unit) according to the recent structural setting reconstruction in which Nicosia and Mt. Salici Units form the upper structural level of the chain (Lentini et al. 2000). They were tectonically decoupled from the

original succession and then travelled toward the foreland. This fact is already ascertained for the Nicosia Unit, that has a type sicilide substrate, while it is not verified for the Mt. Salici Unit being detached from its original substrate.

The higher thermal maturity estimated for the Maragone Unit can be related to the eroded succession which is more than double in drilled wells and/or to the tectonic load due to the Numidian internal Units and to the Sicilide Complex.

In the end, the thermal maturity of the Nicosia Unit is well constrained by the correlation of organic and inorganic independent thermal indicators. Nevertheless, the thermal maturity of the Mt. Salici and Maragone Units cannot be univocally constrained using only one type of thermal maturation data. These cases deserve a crosscheck with other independent thermal indicators to reduce the temperature ranges and better constrain the tectono-sedimentary evolution of the units.

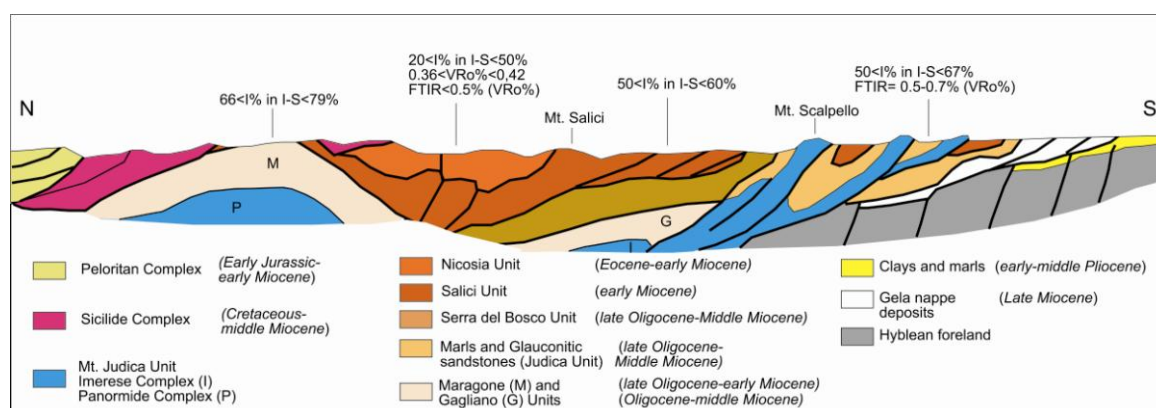


Figure 5.9 – Schematic structural section of Eastern Sicily with main paleo-thermal data, reworked and modified after Bianchi et al. (1987).



## CHAPTER VI - BURIAL AND EXHUMATION ALONG THE OROGENIC TRANSECT

The integration of organic and inorganic thermal parameters with thermo-chronological, structural and stratigraphic data performed for my PhD project on the main outcropping tectono-stratigraphic Units in Eastern Sicily (Fig. 6.1), allowed to:

1. constrain the burial and exhumation history of the Peloritani Mts. and the Apenninic-Maghrebian fold-and-thrust belt between the Nebrodi Mts. and the Hyblean Foreland,
2. create a database of thermal and thermo-chronological data including those already existing in the literature,
3. introduce the use of new techniques for the study of the thermal maturity of organic matter dispersed in sediments (e.g. FTIR).

Along the studied transect, the analysis, integration and geological contextualization of 348 samples (including samples derived from the literature; Fig. 6.2 and 6.3), corresponding to illite content in mixed layer I-S determinations (190), vitrinite reflectance measurements (95), AFT dating (45) and FTIR ratios computation (18) allowed to quantify the paleothermal conditions and maximum burial experienced by the studied tectono-stratigraphic Units and to distinguish between sedimentary and/or tectonic load.

Vitrinite reflectance data are mainly from siliciclastic sediments of the Stilo-Capo d'Orlando Formation, the Sicilide accretionary wedge, and from the thrust-top deposits. XRD analysis have been performed on the Stilo Capo d'Orlando Formation, the thrust-top deposits and on the different structural units constituting the accretionary wedge, the early foredeep and thrust-top deposits and on the Africa-passive margin unit. AFT data mainly refer to metamorphic units of the Peloritani Mts. and to the Sicilide accretionary wedge. FTIR analysis have been performed on the black shales levels of the trench and early foredeep deposits and on the Africa-passive margin unit (Fig. 6.4).

In particular, three main areas at different structural levels, corresponding to the metamorphic units of the Peloritani Mts. with related sedimentary covers and to the Meso-Cenozoic sedimentary successions of both the Sicilide Complex and the Mt. Judica Unit, record a thermal evolution in late diagenetic conditions (Fig. 6.2c and 6.3b; Fig. 6.4)

as they subducted a relevant tectonic loading (order of a few kilometers) during Miocene and then exhumed at different times according to the kinematic evolution of the chain (between late Aquitanian and Late Pliocene). In this chapter the most important results and the possible geodynamic causes of exhumation derived for these three exhumed areas will be summarized and discussed.

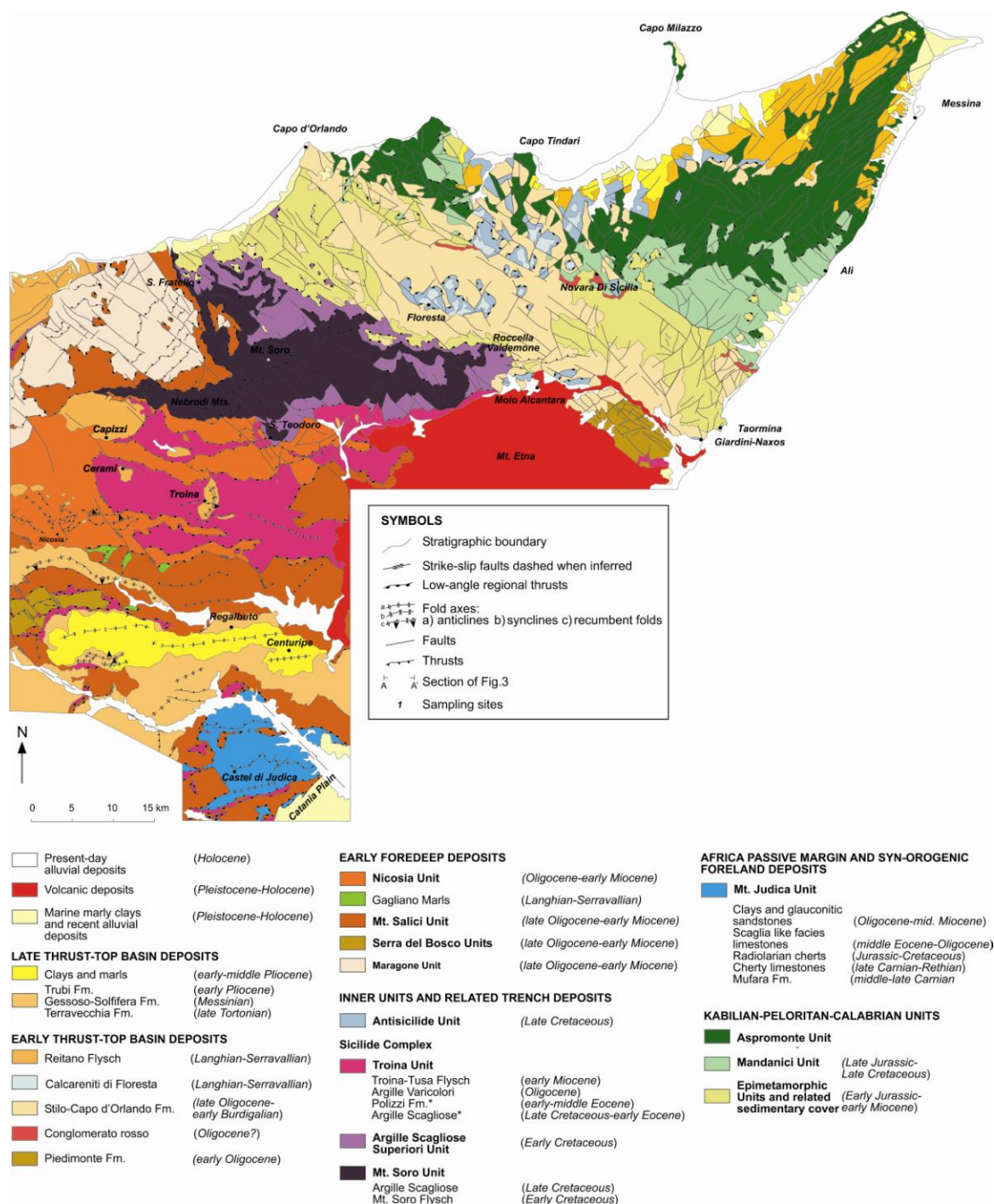


Fig. 6.1. Geological sketch map of Eastern Sicily, redrawn and modified after Carbone et al. (1990) and Lentini et al. (2000).

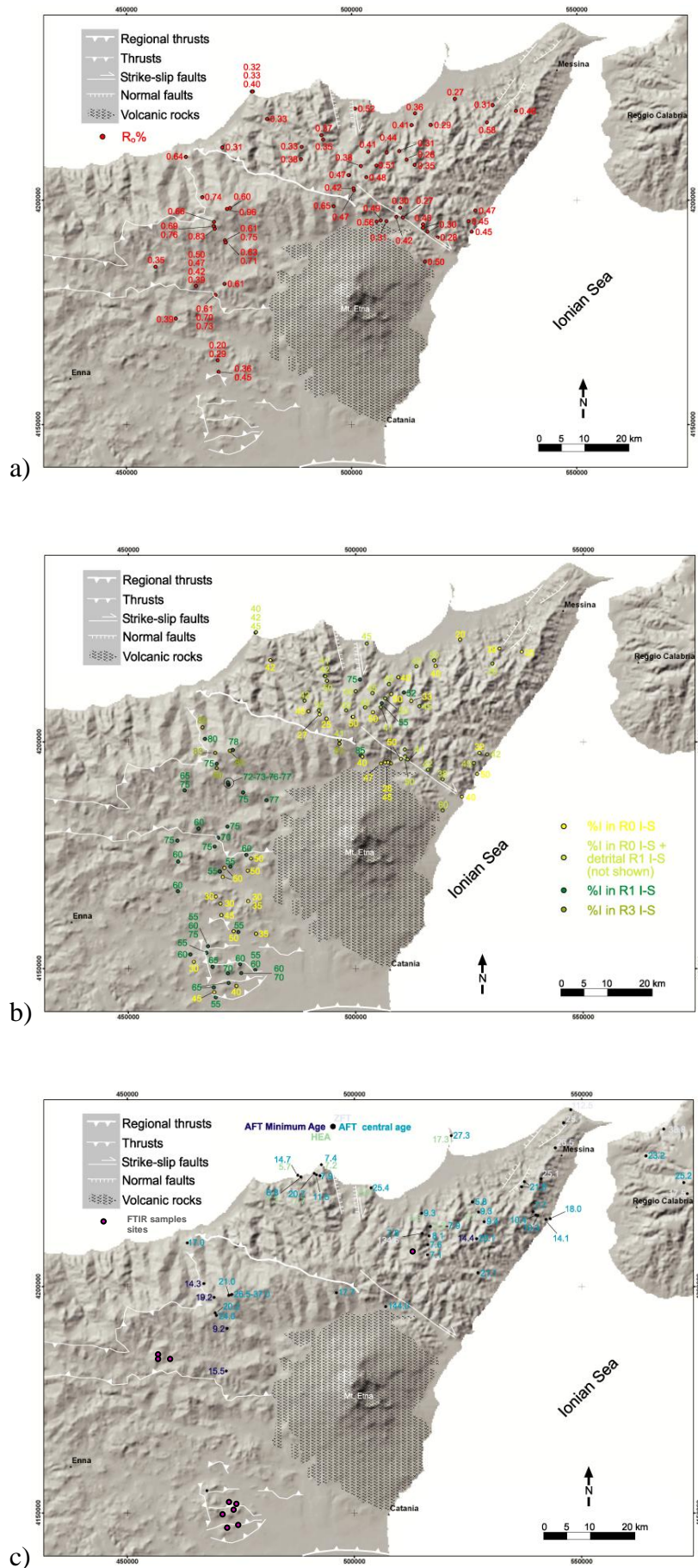


Figure 6.2 - Digital Elevation Model of the Eastern Sicily showing the distribution of: a) mean vitrinite reflectance data, b) illite content in mixed layers I-S discussed in the text, c) apatite fission track data and FTIR samples sites. Simplified main geological features from Carbone et al. (1990) and Lentini et al. (2000). Coordinates in UTM European Datum 1950.



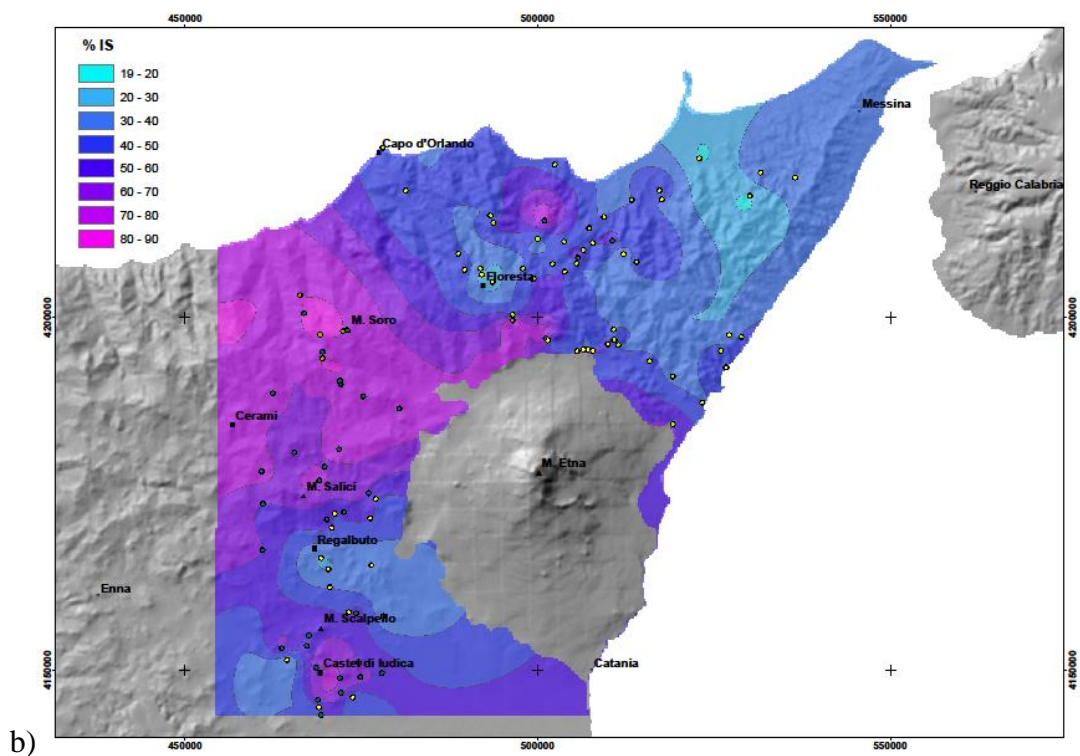
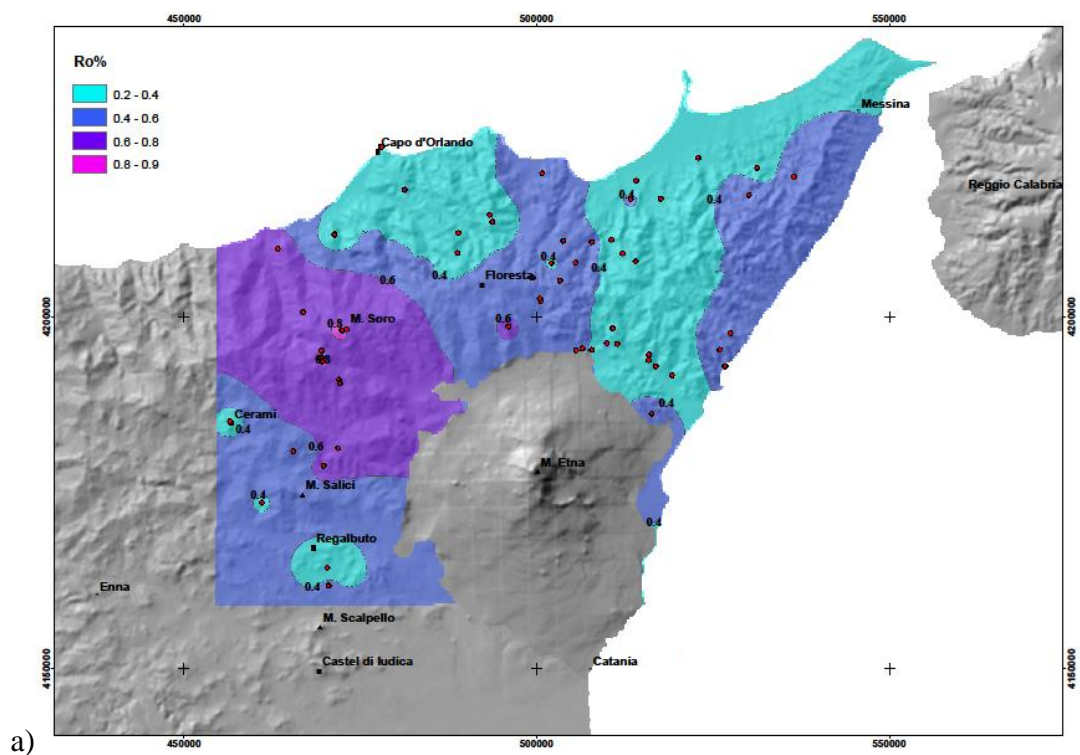


Fig. 6.3 - Digital Elevation Model of the Eastern Sicily showing contour map of: a) average vitrinite reflectance values, b) illite content in mixed layers I-S. Coordinates in UTM European Datum 1950.

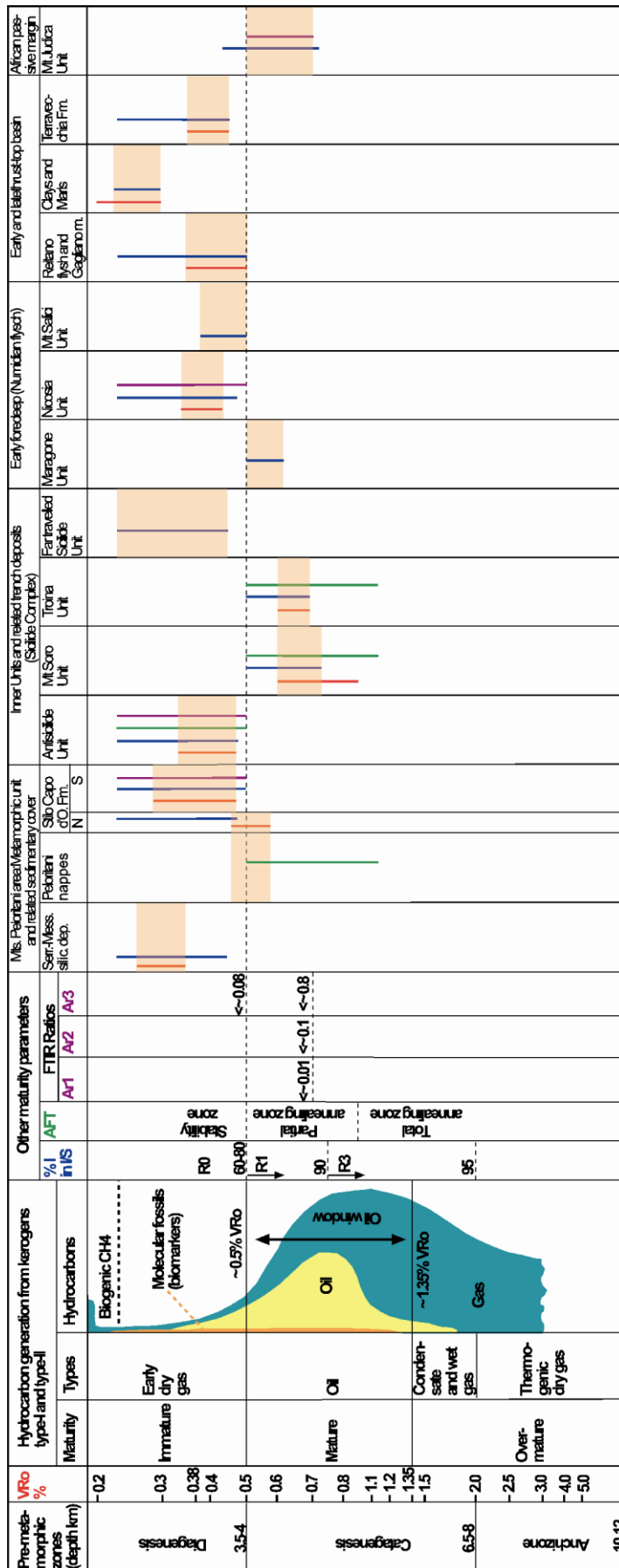


Fig. 6.4 - Relationships between metamorphic zones, VRo%, maturity phases, hydrocarbon generation, %I in I-S, AFT zones and FTIR ratios. Compiled and modified after Teichmüller (1987); Burnham and Sweeney (1989); Merriman and Frey (1999).

On the other hand, early foredeep (Numidian Flysch), early and late thrust-top deposits (Stilo-Capo d'Orlando Formation, Reitano Flysch, Terravecchia Formation and Pliocene clays and marls), and normal fault-controlled basins developed along the Tyrrhenian coast (filled with Serravallian-Messinian siliciclastics), displayed a thermal evolution in early diagenetic conditions (Fig. 6.3 and 6.4), mainly ruled by sedimentary burial alone.

In the **Peloritani Mts. area** two exhumation phases have been unraveled by low temperature thermochronology on the metamorphic nappes (Thomson, 1994; Olivetti et al., 2010, this thesis) and by a multi-disciplinary approach with thermal and structural analysis applied to the unconformably overlying siliciclastic deposits (this thesis and Aldega et al., 2011).

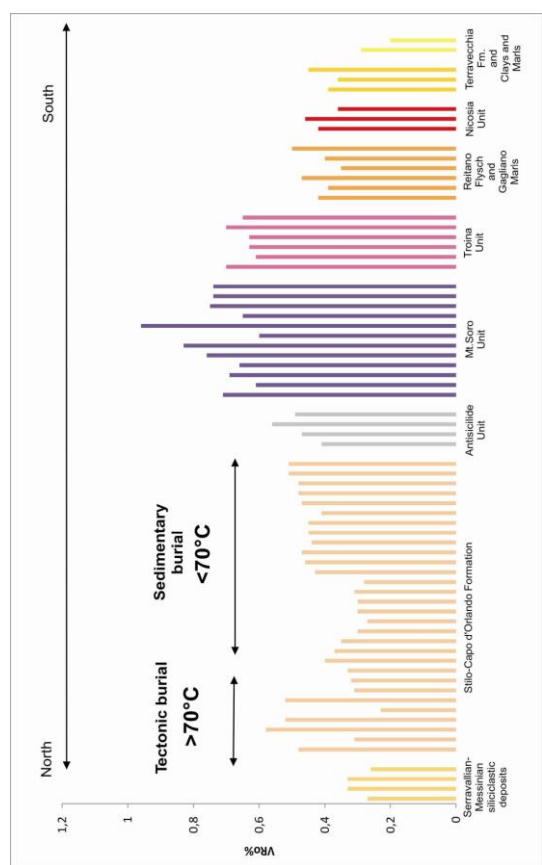
The older phase, Oligocene in age, relates to a regional cooling at shallow depths and is mainly controlled by syn orogenic extension (Cutrupia and Russo, 2005, Lentini, 1995), predating the overthrusting onto the Apenninic-Maghrebian belt in early Miocene times (Amodio-Morelli et al., 1976).

The second one, investigated with higher detail in this thesis, relates to brittle conditions after collision and is controlled by high angle extensional faults and erosion acting since Serravallian times (this thesis, Olivetti et al., 2010; Aldega et al. 2011).

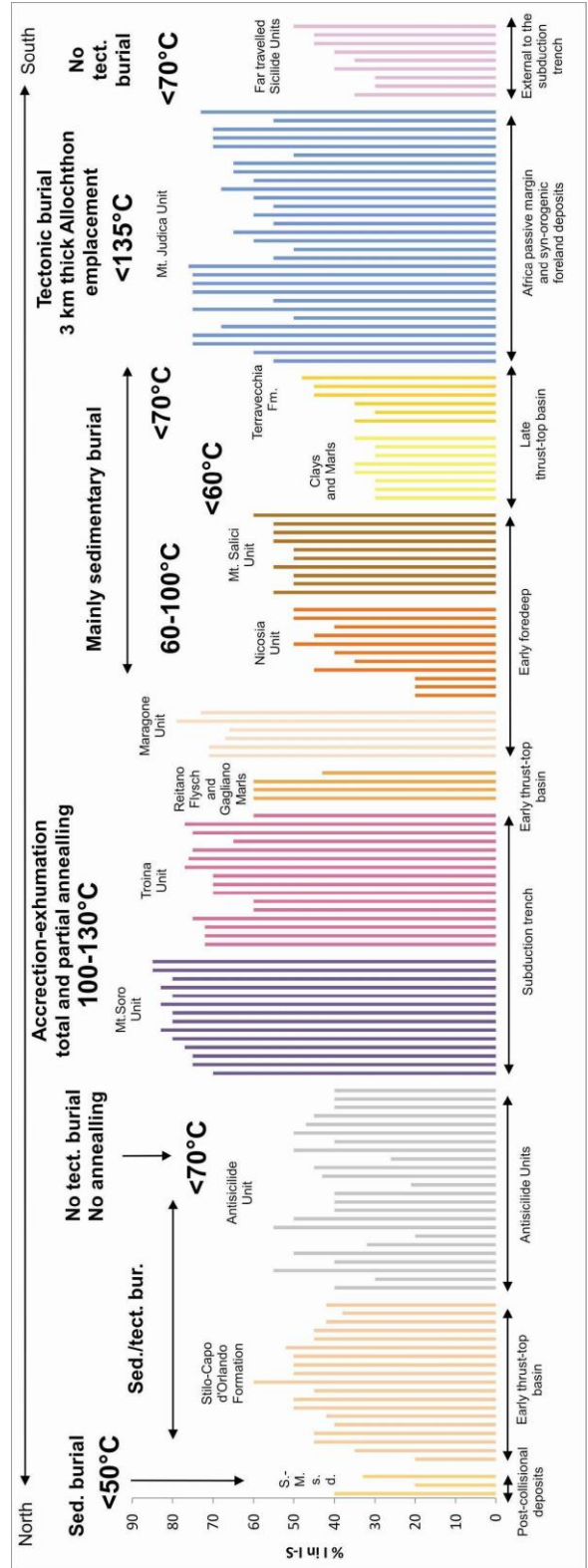
Vitrinite reflectance and mixed-layered clay minerals data from Oligo-Miocene deposits (Stilo-Capo d'Orlando Formation and Serravallian-Messinian siliciclastic deposits) lying on top the metamorphic nappes, allowed discriminating among areas affected by sedimentary and/or tectonic loads. In the Stilo-Capo d'Orlando basin depocentre, organic and inorganic thermal parameters increase as a function of depth suggesting that their evolution is ruled by sedimentary burial (from 0.28 to 0.48% and from 38 to 60% respectively, see chapter III, section 3.4; Fig. 6.5a and b of this chapter). Differently, along the northern edge of the basin, higher vitrinite reflectance values (0.46-0.58%) and annealed apatite fission tracks indicate that the thermal evolution of this area was controlled by tectonic burial related to a late Langhian-early Serravallian out-of-sequence thrust stack emplacement (Fig. 3.11 chapter III; Fig. 6.4 and 6.5a of this chapter).

The Serravallian-Messinian siliciclastic deposits record low levels of diagenesis ( $VR_o\%$  and %I in I-S data lower than 0.36% and 40% respectively) post-dating the out-of-sequence thrusting and unconformably overlying both the crystalline basement and the Stilo-Capo d'Orlando deposits.

Fig. 6.5 – a) Virinite Reflectance histogram. Distribution of the virinite reflectance (VR<sub>o</sub>%) along the Peloritani Mts.-Nebrodi-Mts.-Mt Judica area transect. b) Distribution of the illite layers in illite-smectite (I-S) along the Peloritani Mts.-Nebrodi Mts.-Mt. Judica area transect. Distinct structural units belonging to various geodynamic settings can be differentiated on the basis of the virinite reflectance and illite content in the I-S mixed layers of the <2 μm grain-size fraction.



a)



b)

In the **Sicilide accretionary prism**, Corrado et al. (2009) investigated the thermal evolution and exhumation, recognizing a warm core made up of Mt. Soro and Troina tectonic Units and two cold rims (Antisicilide and far-traveled Sicilide Units). Vitrinite reflectance data in the range of 0.60-0.96% and illite content in mixed layer I-S of 60-85% for Mt. Soro and Troina Units indicate a thermal maturity in the lower part of the late diagenetic zone with calculated maximum paleotemperatures between 100-130 °C (Fig. 6.5 and 6.6). Low temperature thermochronology data, in agreement with paleotemperature estimates from vitrinite reflectance data and clay-mineral-based geothermometers, indicate that apatite fission tracks were partially to totally annealed during wedge accretion and that the subsequent exhumation occurred mainly in Burdigalian times (starting in late Aquitanian and ending in Early Langhian; Fig. 6.7 and 6.8). The far-traveled Sicilide Units thrust to the South along the front of the fold-and-thrust belt and the Antisicilide Unit back-thrust to the North onto the Peloritani Mts.: they record low thermal conditions in early diagenetic zone and in the immature stage of hydrocarbon generation (% I in I-S 30-60% and VRo 0.35-0.50%; Fig. 6.4, 6.5, 6.7a and b). Apatite fission-track data for the Antisicilide Unit confirm low paleotemperature values as no annealed fission tracks have been recorded (Fig. 6.4).

Thus, wedge accretion took place during Aquitanian times when the Mt. Soro and Troina Units acquired a late diagenetic thermal signature (by means of thrust stacking at deep structural levels). On the other hand the Antisicilide and far-traveled Sicilide Units kept at shallow structural levels in more either internal or external positions with respect to the core of the wedge as testified by their early diagenetic signature (Fig. 6.7b)

Wedge exhumation began in late Aquitanian-early Burdigalian times for the Mt. Soro Unit and evolved in the late Burdigalian–early Langhian for the Troina Unit as a result of erosion of structurally higher accreted units (Fig. 6.7a and b). Then exhumation went on with the back-thrusting of the Antisicilide Units on the Kabilian-Peloritan-Calabrian backstop (middle Burdigalian-Langhian) as a result of the collision against the crustal ramp of the buried African rifted margin and was accompanied by gravity-driven processes which remobilized the Sicilide Units up to the frontal part of the chain.

As deformation proceeded towards the external zones, the Allochthonous tectonic Units (made up of Sicilide Complex and foredeep deposits) overthrust the **Mt. Judica succession** (chapter IV), causing a tectonic burial in the range of 2.4 – 3.2 km during Middle Miocene times (Fig. 6.7 and 6.8). Mixed-layer I-S displays a progressive increase



of the proportion of illite layers as function of depth from 55% to 76% and FTIR-derived indexes suggest a thermal maturity equivalent to  $VR_o$  values of at least 0.5-0.7% indicating maximum paleotemperature at the base of the Mt. Judica succession of about 135 °C (Fig. 6.4, 6.5b, 6.6 and 6.8).

During Late Pliocene times, the breaching phase characterized by up-thrust geometries ruled out the Mt. Judica exhumation with high amounts of shortening (in the order of 23.9 km or 45%) and thickening (4 - 5.4 km). This last tectonic phase did not overprint thermal maturity because the extent of overthrusting was negligible when compared with the magnitude of vertical movements. Moving towards west along the strike of the chain, both shortening and thickening decrease to 12.3 km or 25% and 1.4 - 3.5 km respectively. These along strike variations of the chain are mainly due to the physical and morphological along-strike changes of the Hyblean Foreland (Ben-Avraham and Grasso, 1990).

Particularly, in the recess area, the buttressing of the Mt. Judica Unit against the northern margin of the Hyblean carbonate platform caused its exhumation driven by up-thrust geometries which cut the overlying Allochthonous Units emplaced before Tortonian times (Butler et al., 1992). The bulk of deformation occurred in the Late Pliocene times, after the deposition of the Trubi Fm, giving rise to structural highs currently cropping out in the Mt. Judica area (Fig. 6.7f).

The thermal evolution of the **Early foredeep deposits** (Numidian Units, chapter V) has been mainly investigated by mixed layers clay minerals which record paleo-temperatures never exceeding 100 °C (Fig. 6.5 and 6.6). In detail, an increasing level of diagenesis has been observed from the uppermost to the lowermost tectono-stratigraphic units.

From the top to the bottom of the Numidian tectonic pile, the Nicosia Unit shows the lowest % I values in I-S mixed-layers in the range of 20-50% and vitrinite reflectance data between 0.36-0.42% in the immature stage of hydrocarbon generation (Fig. 6.4 and 6.5).

The Mt. Salici Unit displays random ordered mixed layers I-S with an illite content of 50-55%. Only one sample indicates short-range ordered I-S with an illite content of 60% (Fig. 6.5b). These data correlate to slightly higher levels of diagenesis than those recorded in the Nicosia Unit, suggesting that sedimentary burial is the main factor affecting the thermal maturity of both units (Fig. 6.4 and 6.5b).

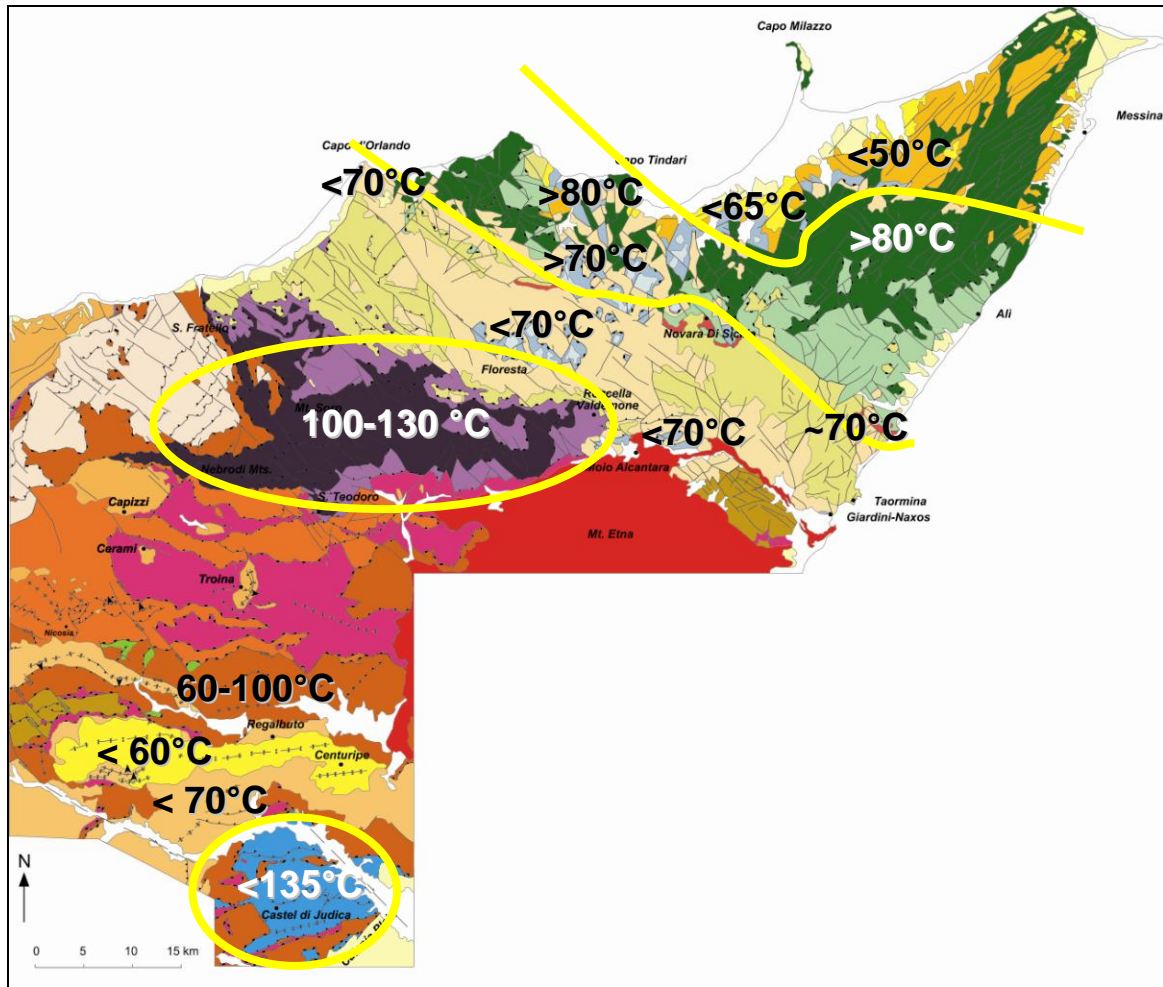


Figure 6.6 – Geological sketch map of Eastern Sicily with maximum paleo-temperatures reached by sediments, redrawn and modified after Carbone et al. (1990) and Lentini et al. (2000).

The lowermost unit of the Numidian tectonic pile (Maragone Unit) revealed mixed-layered ordered structures with % of I in I-S between 66 and 79% indicating the highest levels of thermal maturity for the Numidian Flysch (Fig. 6.4 and 6.5). The lack of thermal modeling prevents to better constrain the maximum temperatures of the Maragone Unit and to define the causes of its thermal maturity. However it cannot be excluded that both sedimentary and tectonic burial affected the Maragone Unit.

**Early and late thrust-top deposits** (Reitano Flysch, Terravecchia Formation and Pliocene clays and marls) record illite percentages in I-S values lower than 50% and vitrinite reflectance data less than 0.5% indicating early diagenetic conditions and the immature to early mature stage of hydrocarbon generation (Fig. 6.4 and 6.5). The main cause responsible for their thermal maturity is sedimentary burial (Aldega et al. 2007).

Integration of thermal information and key stratigraphic constraints derived from these deposits allowed to better define the time frame for the exhumation of the Sicilide accretionary prism and to constrain the Mt. Judica Unit deformation. As matter of fact, Reitano Flysch post-dates the exhumation of the Sicilide Units; whereas Terravecchia Fm. either pre-dates (according to Bello et al., 2000) or is coeval (according to Butler et al., 1992) to the onset of breaching of the Mt. Judica Unit.

In summary timing of deformation and exhumation for the Peloritani Mts. and Apenninic-Maghrebian fold-and-thrust belt can be traced as follows:

**Oligocene (33-23 Ma):**

Main exhumation phase of the Peloritani Mts. through low angle extensional faults and deposition of the Stilo-Capo d'Orlando Fm in a fore-arc setting.

**Aquitainian-Burdigalian (23-16 Ma):**

Continental collision between the southern edge of the Peloritani Mts. and the Hyblean plate that produced the overthrust of the metamorphic nappe on the accreted Sicilide prism. The event marked the evolution of the Stilo-Capo d'Orlando basin into a thrust top basin and the deepening of the foredeep where Numidian Flysch was deposited. During this time frame the Mt. Soro and Troina Units acquired their thermal maturity at deep structural level within the wedge and started to be exhumed mainly in Burdigalian times (Fig. 6.7a and b and 6.8). At the same time the Antisicilide Unit backthrust on top of the Stilo-Capo d'Orlando Fm and the far-travelled Sicilide Unit were demobilized at the front of the chain by gravity readjustment (Fig. 6.7b).

**Langhian-Serravallian (16-11.6 Ma):**

Emplacement of the Allochthonous Units (Numidian Flysch, Sicilide Complex and the Imerese-Sicano Unit) onto the Hyblean foreland through low angle regional thrusts (Bello et al., 2000; Fig. 6.7d).

Out-of-sequence thrusting of the Peloritani nappes in the hinterland deforming and deepening the internal margin of the Stilo-Capo d'Orlando thrust-top basin (Fig. 6.7c and 6.8).

Subsequent sea level variation and extensional tectonics controlled facies distribution and the extent of Serravallian-Messinian siliciclastic rocks which cover with a down-lap geometry the Peloritani nappes.

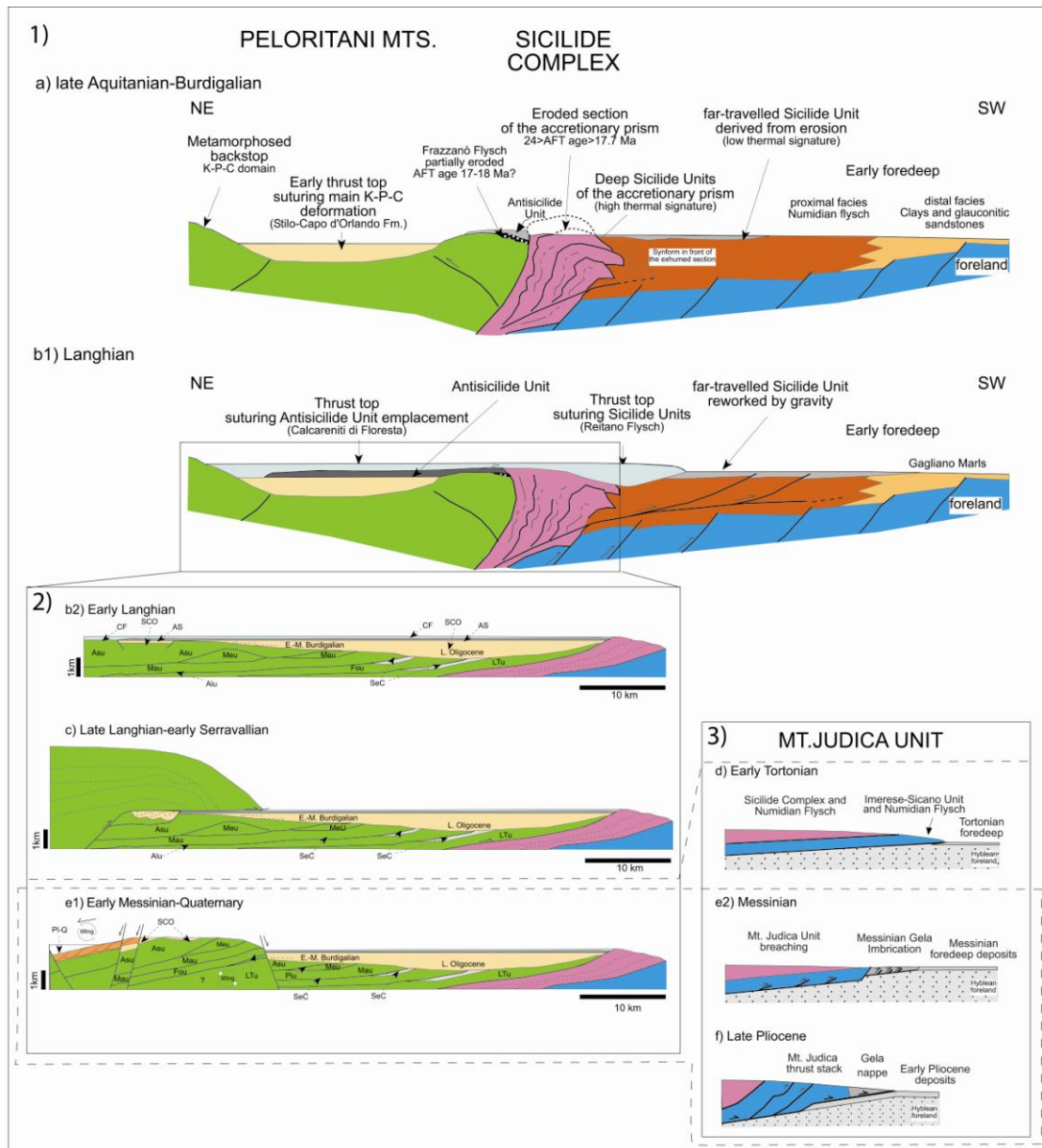


Figure 6.7 – Schematic evolution of burial-exhumation of the Apenninic-Maghrebien fold-and-thrust belt in Eastern Sicily in Aquitanian-Quaternary times redrawn and modified after 1) Corrado et al. (2009) and 2) Aldega et al. 2011 and this thesis. Panels 1) and 3) not to scale.

### Tortonian-Messinian (11.6-5.3)

The Serravallian-Messinian siliciclastics continued to be deposited in normal fault-controlled basins developed along the Northern and North-Eastern coast of Sicily while incomplete and/or condensed series sedimented on top of horst-like structures in response to the strong uplift of the Peloritani Mts. (Fig. 6.7e1; Lentini et al., 2000).

Compressive deformation affected the frontal part of the chain involving the Imerese-Sicano Unit, comprising Mt. Judica area with the development of syntectonic marine

basins (Terravecchia Fm.) and the Tortonian foredeep sediments which deformed simultaneously and created the Messinian Gela Nappe (Fig. 6.7e2).

### Late Pliocene (3.6-1.8)

Main phase of the Mt. Judica Unit stacking with up-thrusts tectonic (Bello et al., 2000), and propagation forward on top the Early Pliocene deposits (Trubi Fm.; Fig. 6.7f and 6.8). Back-thrusts tectonic in north-central Sicily (Carbone et al., 1990; Grasso et al., 1995; Sturiale et al. 2010).

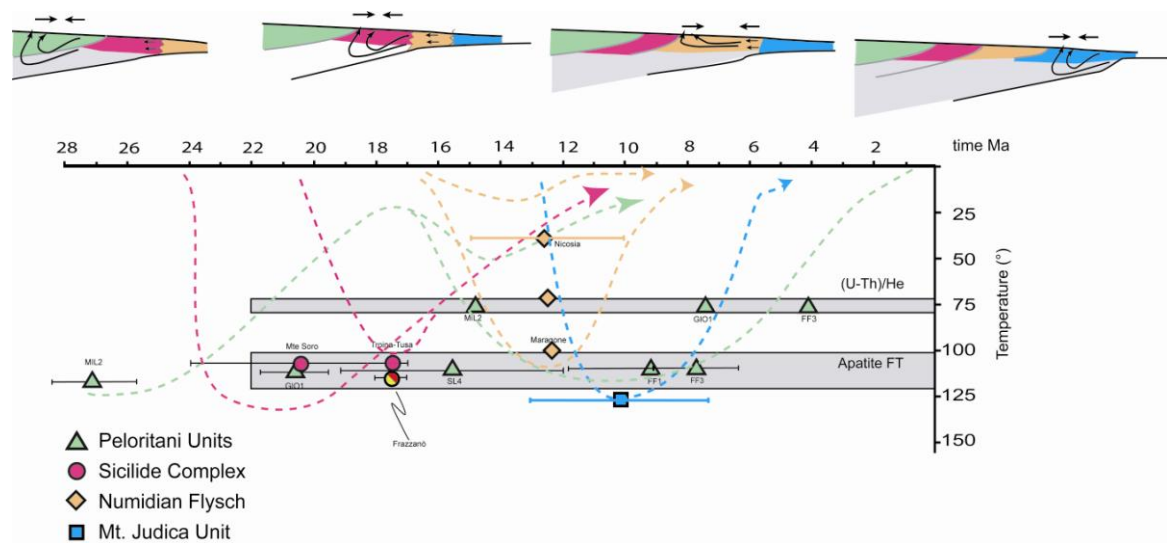


Figure 6.8 – Time-temperature path of the main tectonic Units outcropping in the Eastern Sicily transect of the Apenninic-Maghrebien orogen based on the summary of derived- AFT, AHe, VRo% and % I in I-S temperatures. Representative temperatures derived from thermochronometry on the main tectonic Units are shown (with indicated time error bars).

## REFERENCES CITED

- Accordi, B., 1958, Osservazioni preliminari sul Miocene della fascia meridionale dei Monti Nebrodi: *Boll. Soc. Geol. Ital.*, v. 77, p. 3-10.
- Adam, J., 1996, *Kinematik und Dynamic des neogenen Falten-und Deckengurtels in Sizilien. Quantifizierung neotektonischer Deformationsprozesse in der zentralmediterranen Afro-Europaischen Konvergenzzone*. PhD. Thesis, Herausgegeben von geowissenschaftlichen Instituten, Berlin, 171 pp.
- Adam, J., Reuther C.-D., 1995, Dynamics of neotectonic foreland basin deformation and inversion (Central Mediterranean Thrust Belt, Sicily). *Z. dt. Geol. Ges.*, v. 146, p. 340-354.
- Aldega, L., Corrado, S., Grasso, M., and Maniscalco, R., 2007a, Correlation of diagenetic data from organic and inorganic studies in the Apenninic-Maghrebien fold-and-thrust belt: a case study from Eastern Sicily: *The Journal of Geology*, v. 105, p. 335-353.
- Aldega, L., Botti, F., and Corrado, S., 2007b, Clay mineral assemblages and vitrinite reflectance in the Laga Basin (Central Apennines, Italy): What do they record?: *Clays and Clay Minerals*, v. 55, p. 504-518.
- Aldega, L., Corrado, C., Di Paolo, L., Somma, R., Maniscalco, R., Balestrieri, M.L., 2011, Shallow burial and exhumation of the Peloritani Mts. (NE Sicily, Italy): insight from paleo-thermal and structural indicators: *Geological Society of America Bulletin*, v. 123, p. 132-149.
- Allen, P.A., and Allen, J.R., 1993, *Basin Analysis, Principles and Application*: Oxford, Blackwell Scientific Publications, p. 1-451.
- Allerton, S., 1994, Vertical-axis rotation associated with folding and thrusting: an example from the eastern Subbetic zone of southern Spain: *Geology*, v. 22, p. 1039-1042.
- Amodio-Morelli, L., Bonardi, G., Colonna, V., Dietrich, D., Giunta, G., Ippolito, F., Liguori, V., Lorenzoni, S., Paglionico, A., Perrone, A., Piccarreta, G., Russo, M., Scandone, P., Zanettin-Lorenzoni, E., and Zuppetta, A., 1976, L'arco Calabro-peloritano nell'orogene appenninico-maghrebide: *Memorie della Società Geologica Italiana*, v. 17, p. 1-60.

- Bachman, S.B., Lewis, S.D., and Schweller, W.J., 1983, Evolution of a forearc basin, Luzon Central Valley, Philippines: American Association of Petroleum Geologists Bulletin, v. 67, p. 1143-1162.
- Baldacci, L., 1886, Descrizione geologica dell'Isola di Sicilia: Mem. Descr. Carta Geol. Ital., v. 1, p. 408.
- Balestrieri, M.L., Olivetti, V., Stuart, F.M., Vignaroli, G., Bigazzi, G., and Faccenna, C., 2008, Apatite fission-track and (U-Th)/He thermochronometry applied to constrain the exhumation history and late tectonogenic stages of Peloritani Mountains, Northern Sicily, Italy, *in* Proceedings from the 11<sup>th</sup> International Conference on thermochronometry: Anchorage, Alaska, p. 13-15.
- Barrier, P., Cravatte, J., Decis, R., Lanzafame, G., and Ott D'Estevou, P., 1987, Mise au point stratigraphique sur les relations entre la "couverture calabride miocène" et les "terrains post-orogéniques" dans la région du Déroit de Messine: Doc. et Trav. IGAL, v. 11, p. 43-53.
- Barker, C.E., and Pawlewicz, M.J., 1994, Calculation of vitrinite reflectance from thermal histories and peak temperatures, A comparison of methods, *in* Mukhopadhyay, P.K., and Dow, W.G., eds., Vitrinite Reflectance as a Maturity Parameter: Applications and Limitations: American Chemical Society Symposium Series, v. 570, p. 216-229.
- Baruah, M.K., 1986, Assignment of the i.r. absorption band at 1050 cm<sup>-1</sup> in lignite humic acid: Fuel, v. 65, p. 1756-1759.
- Basin Mod® 1-D for Windows<sup>TM</sup>, version 5.4 Software, 1996, A Basin Analysis Modelling System by Platte River Associates, Denver.
- Bello, M., Franchino, A., and Merlini, S., 2000, Structural model of eastern Sicily: Mem. Soc. Geol. Ital., v. 55, p. 61-70.
- Ben-Avraham, Z., and Grasso, M., 1990, Collisional zone segmentation in Sicily and surrounding areas in the Central Mediterranean: Special issue, v. IV, n. 2, p. 131-139.
- Benomran, O., Nairn, A. E. M., Schamel, S., 1987, Sources and dispersal of mid-Cenozoic clastic sediments in the central mediterranean Region: Mem Soc. Geol. It., v. 38, p. 47-68.
- Bianchi, F., Carbone, S., Grasso, M., Invernizzi, G., Lentini, F., Longaretti, G., Merlini, S. and Mostardini, F., 1987, Sicilia orientale: profilo geologico Nebrodi-Iblei: Mem. Soc. Geol. It., v. 38, p. 429-458.

- Billi, A., Tiberti, M.M., 2009, Possible causes of arc development in the Apennines, central Italy. *GSA Bulletin*, v. 121, p. 1409–1420.
- Billi, A., Barberi, G., Faccenna, C., Neri, G., Pepe, F., and Sulli, A., 2006, Tectonics and seismicity of the Tindari Fault System, southern Italy: Crustal deformations at the transition between ongoing contractional and extensional domains located above the edge of a subducting slab: *Tectonics*, v. 25, TC2006, doi:10.1029/2004TC001763.
- Billi, A., Presti, D., Faccenna, C., Neri, G., and Orecchio, B., 2007, Seismotectonics of the Nubia plate compressive margin in the south Tyrrhenian region, Italy: clues for subduction inception: *Journal of Geophysical Research*, v. 112, B08302, doi:10.1029/2006JB004837.
- Bonardi, G., Giunta, G., Liguori, V., Perrone, V., Russo, M., and Zuppeta A., 1976, Schema geologico dei Monti Peloritani: *Bollettino della Società Geologica Italiana*, v. 95, p. 1-26.
- Bonardi, G., Giunta, G., Perrone, V., Russo, M., Zuppeta, A., and Ciampo, G., 1980, Osservazioni sull'evoluzione dell'Arco Calabro-Peloritano nel Miocene inferiore: la Formazione di Stilo-Capo d'Orlando: *Bollettino della Società Geologica Italiana*, v. 99, p. 365-393.
- Bonardi, G., De Vivo, B., Giunta, G., and Perrone, V., 1982, I conglomerati rossi dei Monti Peloritani e considerazioni sull'Unità di Novara. *Bollettino della Società Geologica Italiana*, v. 101, p. 157-172.
- Bonardi, G., Compagnoni, R., Del Moro, A., Messina, A., and Perrone, V., 1987, Riequilibrazioni tettono-metamorfiche alpine nell'Unità dell'Aspromonte, Calabria meridionale: *Rendiconti della Società Italiana di Mineralogia e Petrologia*, v. 42, 301.
- Bonardi, G., Compagnoni, R., Messina, A., De Francesco, A.M., Del Moro, A., Perrone, V., Platt, J., and Russo, S., 1992, Sovrimpronta metamorfica alpina nell'unità dell'Aspromonte: Guida all'escursione del gruppo Paleozoico, 24-25 Settembre 1990, Gambarie-Polsi (Calabria): *Bollettino della Società Geologica Italiana*, v. 111, p. 81-108.
- Bonardi, G., Cavazza, W., Perrone, V. and Rossi, S., 2001, Calabria-Peloritani Terrane and Northern Ionian Sea, *in* Vai, G.B., and Martini, I.P., eds., *Anatomy of an Orogen: The Apennines and Adjacent Mediterranean Basins*: Dordrecht, Kluwer Academic Publishers, p. 287-306.
- Botti, F., Aldega L. and Corrado, S., 2004, Sedimentary and tectonic burial evolution of the Northern Apennines in the Modena-Bologna area: constraints from combined



- stratigraphic, structural, organic matter and clay mineral data of Neogene thrust-top basins: *Geodinamica Acta*, v. 17, p. 185-203.
- Bouillin, J.P., 1984, Nouvelle interprétation de la liaison Apennin-Maghrebides en Calabre: conséquences sur la paléogéographie téthysienne entre Gibraltar et les Alpes: *Révue Géologie Dynamique et de Géographie Physique*, v. 25, p. 321-338.
- Boyer, S.E., 1995, Sedimentary basin taper as a factor controlling the geometry and advance of thrust belts: *American Journal of Science*, v. 295, p. 1220-1254.
- Brandon, M.T., and Vance, J.A., 1992, Fission track ages of detrital zircon: implications for tectonic evolution of the Cenozoic Olympic subduction complex: *Am. Journ. Sc.*, v. 292, p. 565-636.
- Brandon, M.T., Roden-Tice, M.K., and Garver, J.I., 1998, Late Cenozoic exhumation of the Cascadia accretionary wedge in the Olympic Mountains, northwest Washington State: *Geological Society of America Bulletin*, v. 110, p. 985-1009.
- Broquet, 1970, The geology of the Madonie Mountains of Sicily, *in* *Geology and history of Sicily: Petrol. Expl. Soc. Libya*. P. 201-230.
- Broquet, P., Caire, A., Duee', G., Mascle, G., and Truillet, R., 1967, Excurcuion geologique en Sicilie. 53 ff
- Brun, J.P., and Faccenna, C., 2008, Exhumation of high-pressure rocks driven by slab rollback: *Earth and Planetary Science Letters*, v. 272, p. 1-7.
- Burnes, M.A., Burnes, W.C., Bustin, R.M., 1990, Chemistry and Diagenesis of Organic Matter in Sediments and Fossil Fuels, *in* *McIlleareath, I.A., and Morrow, D.W., eds., Diagenesis: Geoscience Canada Reprint, 4<sup>th</sup> series*, p. 189-204.
- Burnham, A.K., and Sweeney, J.J., 1989, A chemical kinetic model of vitrinite maturation and reflectance: *Geochimica and Cosmochimica Acta*, v. 53, p. 2649-2657.
- Bustin, R.M., Barnes, M.A., and Barnes, W.C., 1990, Determining levels of organic diagenesis in sediments and fossil fuels, *in* *McIlleareath, I.A., and Morrow, D.W., eds., Diagenesis: Geoscience Canada Reprint, 4<sup>th</sup> series*, p. 205-226.
- Butler, R. W. H., 1992, Hydrocarbon maturation, migration and tectonic loading in the Western Alps, *in* *England, W. A., and Fleet, A.J., eds., Petroleum migration: Geological Society of London Special Publication*, v. 59, p. 227-244.
- Butler, R. W. H., Grasso, M., La Manna, F., 1992, Origin and deformation of the Neogene-Recent Maghrebian foredeep at the Gela Nappe, SE Sicily. *Journal of the Geological Society, London*, v. 149, p. 547-556.

- Calemma, V., Rausa, R., Margarit, R. and Girardi, E., 1988, FTIR study of coal oxidation at low temperature: *Fuel*, v. 67, p. 765-769.
- Caliri, A., Carbone, S., Carveni, P., Catalano, S., Lentini, F., Strazzulla, S., Vinci, G., and Vinciguerra, G., 1993, Carta Geologica del Golfo di Patti (Sicilia settentrionale), S.EL.CA., scale 1:25,000.
- Carbone, S., Catalano, S., Grasso, M., Lentini, F., and Monaco, C., 1990, Carta geologica della Sicilia centroorientale: Università di Catania, scale 1 : 50,000.
- Carbone, S., Catalano, S., Grasso, M., Lentini, F., Monaco, C., Puglisi, D., Romeo, M., Tiralongo, P., 1987, Nota illustrativa della carta geologica della Sicilia centro-orientale (1 :50.000): *Conv. Soc. Geol. Ital. Naxos-Pergusa 22-25 aprile 1987*. p 30-31. Catania
- Carbone, S., Pedley, H.M., Grasso, M., and Lentini, F., 1993, Origin of the "Calcareni di Floresta" of NE Sicily: late orogenic sedimentation associated with a middle Miocene sea-level high stand: *Giornale di Geologia*, vol. 55/2, p. 105-116.
- Carbone, S., Lentini, F., and Vinci, G., 1998, Carta geologica del settore occidentale dei Monti Peloritani (Sicilia Nord-Orientale): S.EL.CA., scale 1:25,000.
- Carbone, S., Messina, A., and Lentini, F., 2008, Note illustrative della carta geologica d'Italia, foglio 601, Messina-Reggio di Calabria, S.EL.CA., scale 1:50,000.
- Carmisciano, R., and Puglisi, D., 1978, Caratteri petrografici delle arenarie del Flysch di Capo d'Orlando (Monti Peloritani, Sicilia Nord-Orientale): *Rendiconti Società Italiana di Mineralogia e Petrologia*, v. 34, p. 403-424.
- Carmisciano, R., and Puglisi, D., 1982, Studio sedimentologico-petrografico del Flysch di Capo d'Orlando nei Peloritani occidentali (Sicilia): *Geologica Romana*, v. 21, p.113-123.
- Carrozzo, MT., Luzio, D., Margiotta, C., Quarta, T., 1992, Gravity map of Italy Scale 1:500,000, in: *Quaderni de "La Ricerca Scientifica"* v. 114, CNR, P. F. Geodinamica (1992), p. 3.
- Catalano, S., and Di Stefano, A., 1996, Nuovi dati geologici e stratigrafici sul Flysch di Capo d'Orlando nei Peloritani orientali (Sicilia nord-orientale): *Memorie della Società Geologica Italiana*, v. 51, p. 149-164.
- Catalano, R., Di Stefano, P., Sulli, A., and Vitale, F.P., 1996, Paleogeography and structure of the central Mediterranean: Sicily and its offshore area: *Tectonophysics*, v. 260, p. 291-323.

- Catalano, S., De Guidi, G., Romagnoli, G., Torrisi, S., Tortorici, G., Tortorici, L., 2008, The migration of plate boundaries in SE Sicily: Influence on the large-scale kinematic model of the African promontory in southern Italy: *Tectonophysics*, v. 449, p. 41-62.
- Cavazza, W., Barone, M., 2010, Large-scale sedimentary recycling of tectonic mélange in a forearc setting: The Ionian basin (Oligocene -Quaternary, southern Italy): *Geological Society of America Bulletin*, v. 122, p. 1932-1949.
- Checchia-Rispoli, G., 1916, Sui terreni terziari inferiori del versante settentrionale delle Madonie: *Mem. Dscr. Carta Geol. Ital.*, v. 6, p. 109.
- Chen, J., Ping, L., and Jinchao, L., 1998, Using kerogen FTIR parameters for determination of organic facies: *Chinese Science Bulletin*, v. 43, p. 681–684.
- Chiocchini, U., Franchi, R., Guerrera, F., Ryan, W.B.F., Vannucci, S., 1980, Geologia di alcune successioni torbiditiche cretacio-terziarie appartenenti ai «Flysch Maurétaniensis» e alla «Nappe Numidienne» del Rif settentrionale (Marocco): *Studi Geol. Camerti*, v. 4, p. 37-66.
- Christy, A.A., Hopland, A.L., Barth, T., and Kvalheim, O.M., 1989, Quantitative determination of thermal maturity in sedimentary organic matter by diffuse reflectance infrared spectroscopy of asphaltenes: *Organic Geochemistry*, v. 14, p. 77–81.
- Cifelli, F., Rossetti, F., Mattei, M., Hirt, A.M., Funiciello, R., and Tortorici, L., 2004, An AMS, structural and paleomagnetic study of quaternary deformation in eastern Sicily: *Journal of Structural Geology*, v. 26, p. 29-46.
- Cifelli, F., Mattei, M., and Rossetti, F., 2007, Tectonic evolution of arcuate mountain belts on top of a retreating subduction slab: The example of the Calabrian Arc: *Journal of Geophysical research-Solid Earth*, v. 112, B09101.
- Cifelli, F., Mattei, M., and Della Seta, M., 2008, Calabrian Arc oroclinal bending: the role of subduction: *Tectonics*, v. 27, TC5001.
- Corcoran, D.V., and Doré, A.G., 2005, A review of techniques for the estimation of magnitude and timing of exhumation in offshore basins: *Earth-Science Reviews*, v. 72, p. 129-168.
- Corrado S., Aldega L., Di Leo P., Giampaolo C., Invernizzi C., Mazzoli S., and Zattin M., 2005, Thermal maturity of the axial zone of the Southern Apennines fold-and thrust-belt (Italy) from multiple organic and inorganic indicators: *Terra Nova*, v. 17 (1), p. 56-65.

- Corrado, S., Aldega, L., Balestrieri, M., Maniscalco, R., and Grasso M., 2009, Structural evolution of the sedimentary accretionary wedge of the Alpine system in Eastern Sicily: Thermal and thermochronological constraints: *Geological Society of America Bulletin*, v. 121, p. 1475-1490.
- Crespo-Blanc, A., Orozco, M., and García-Dueñas, V., 1994, Extension versus compression during the Miocene tectonic evolution of the Betic chain. Late folding of normal fault systems: *Tectonics*, v. 13, p. 78-88.
- Dahlen, F.A., Suppe, J., Davis, D., 1984, Mechanics of Fold-and-Thrust Belts and Accretionary Wedges: Cohesive Coulomb Theory. *Journ. Geoph. Res.*, v. 89, p. 10087-10101.
- Dahlen, F.A., Suppe, J., 1988, Mechanics, growth and erosion of mountain belts, in: Clark S.P., Burchfield B.C. & Suppe J. (Eds.) , “Processes in Continental Lithospheric Deformation”, *Geol. Soc. Am., spec. pap.*, v. 218, pp. 161-178.
- Dahlstrom, C.D.A., 1969, Balanced cross-sections: *Can. J. Earth Sci.*, v. 6, p. 743–757.
- Davis, D., Suppe, J., Dahlen, F.A., 1983, Mechanics of Fold-and-Thrust Belts and Accretionary Wedges. *Journ. Geoph. Res.*, v. 88, p. 1153-1172.
- De Capoa, P., Guerrera, F., Perrone, V., and Serrano, F., 1997, New biostratigraphic data on the Frazzanò Formation (Longi-Taormina Unit): consequences on defining the deformation age of the Calabria-Peloritani Arc Southern Sector: *Rivista Italiana di Paleontologia e Stratigrafia*, v. 103, p. 343-356.
- De Capoa, P., Guerrera, F., Perrone, V., Serrano, F., and Tramontana, M., 2000, The onset of the syn-orogenic sedimentation in the Flysch Basin of the Sicilian Maghrebids: State of the art and new biostratigraphic constraints: *Eclogae Geologicae Helvetiae*, v. 93, p. 65-79.
- De Capoa, P., Di Staso, A., Guerrera, F., Perrone, V., and Tramontana, M., 2004, The age of the oceanic accretionary wedge and onset of continental collision in the Sicilian Maghrebian Chain: *Geodinamica Acta*, v. 17, p. 331-348.
- Dewey, J.F., Helman, M.L., Turco, E., Hutton, D.H.W., and Knott, S.D., 1989, Kinematics of the western Mediterranean, in Coward, M.P., et al., eds., *Alpine Tectonics: Geological Society Special Publication*, v. 45, p. 265-283.
- Deweever B., Swennen, R., and Cooreman, M., 2006, Fluid flow in the Sicilian accretionary wedge: Primary geochemical signatures or recrystallization mask: *Journal of Geochemical Exploration*, v. 89, p.83-86.

- Di Stefano, A., and Lentini, F., 1995, Ricostruzione stratigrafica e significato paleotettonico dei depositi Plio-Pleistocenici del margine tirrenico tra Villafranca Tirrena e Faro (Sicilia Nord-Orientale): *Studi Geologici Camerti*, v. 1995/2, p. 219-237.
- Dodson, M.H., 1973, Closure temperature in cooling geochronological and petrological systems: *Contrib. Mineral. Petr.*, v. 40, p. 259-274.
- Doglioni, C., Fernandez, M., Gueguen, E., and Sabat, F., 1999, On the interference between the early Apennines-Maghrebides back-arc extension and the Alps-Betics orogen in the Neogene geodynamics of the Western Mediterranean: *Bollettino della Società Geologica Italiana*, v. 118, p. 75-89.
- Doré, A.G., Cartwright, J.A., Stoker, M.S., Turner, J.P., and White, N.J., 2002, Exhumation of the North Atlantic margin: introduction and background, *in* Doré, A.G., Cartwright, J.A., Stoker, M.S., Turner, J.P., White, N., eds., *Exhumation of the North Atlantic Margin: Timing, Mechanisms and Implications for Petroleum Exploration*: Geological Society, London, Special Publications, v. 196, p. 1-12.
- Dow, W.G., 1977, Kerogen studies and geological interpretation: *Journal of Geochemical Exploration*, v. 7, p. 79-99.
- Drobniak, A., and Mastalerz, M., 2006, Chemical evolution of Miocene wood: Example from the Belchatow brown coal deposit, central Poland: *International Journal of Coal Geology*, v. 66, p. 157-178.
- Durand-Delga, M., 1967, Structure and geology of the northeastern Atlas, *in* *Guide Book to the Geology and History of Tunisia*: Petroleum Exploration Society Libya, 9th Ann. Field Conf., Tripoli, p. 59-83.
- Durand, B., 1980, Sedimentary organic matter and kerogen. Definition and quantitative importance of kerogen, *in* Durand, B., ed., *Kerogen: Insoluble Organic Matter from Sedimentary Rock*: Paris, Edit. Technip, p. 13-34.
- Endignoux, L., and Wolf, S., 1990, Thermal and kinematic evolution of thrust basins: a 2D numerical model: *in* Letouzey, J., ed., *Petroleum Tectonics in mobile belts*: Paris, Edit. Technip, p. 181-192.
- Fabiani, R., and Trevisan, L., 1940, Prove dell'esistenza di uno stile tettonico a falde di ricoprimento nei monti di Palermo: *Atti R. Acc. Italia, Mem.*, v. 11, p. 435-448.
- Faccenna, C., Becker, T.W., Lucente, F.P., Jolivet, L., and Rossetti, F., 2001, History of subduction and back-arc extension in the Central Mediterranean: *Geophysical Journal International*, v. 145, p. 809-820.

- Faccenna, C., Piromallo, C., Crespo-Blanc, A., Jolivet, L., and Rossetti, F., 2004, Lateral slab deformation and the origin of the western Mediterranean arcs: *Tectonics*, v. 23, TC1012, doi:10.1029/2002TC001488.
- Flandrin, J., 1948, Contribution a L'etude stratigraphique du Nummulitique algérien: *Bull. Serv. Carte Geol. Algerie*, v. 19, p. 340.
- Fleischer, R.L., Price, P.B., and Walker, R.M., 1965, The ion explosion spike mechanism for formation of charged particle tracks: *Journ. Appl. Phy.*, v. 36, p. 3645-3652.
- Ford, M., 2005, Depositional wedge tops: interaction between low basal friction external orogenic wedges and flexural foreland basins: *Basin Research*, v.16, p. 361-375.
- Frizon de Lamotte, D., Saint Bezar, B., and Bracène, R., 2000, The two main steps of the Atlas building and geodynamics of the western Mediterranean, *Tectonics*: v. 19, p. 740-761.
- Gailbraith, R.F., 1988, Graphical display of estimates having different standard errors: *Technometrics*, v. 30, p. 271-281.
- Ganz, H., and Kalkreuth, W., 1987, Application of infrared spectroscopy to the classification of kerogen-types and the evolution of source rock and oil shale potentials: *Fuel*, v. 66, p. 708–711.
- Ganz, H.H., Kalkreuth, W., Ganz, S.N., Öner, F., Pearson, M.J., and Wehner H., 1990, Infrared analysis - State of the Art: *Berliner geowiss. Abh.*, v. 120.2, p. 1011-1026.
- Gelabert, B., Sàbat, F., and Rodríguez-Perea, A., 2002, A new proposal for the late Cenozoic geodynamic evolution of the western Mediterranean: *Terra Nova*, v. 14, p. 93-100.
- Ghisetti, F., 1979, Relazioni tra strutture e fasi trascorrenti e distensive lungo i sistemi Messina Fiumefreddo, Tindari-Letojanni e Alia-Malvagna (Sicilia nord-orientale): uno studio microtettonico: *Geologica Romana*, v. 18, p. 23-58.
- Ghisetti, F., 1992, Fault parameters in the Messina strait (southern Italy) and relations with the seismogenic source: *Tectonophysics*, v. 210, p. 117-133.
- Giunta, G., 1985, Problematiche ed ipotesi sul Bacino Numidico nelle Maghrebidi siciliane: *Boll. Soc. Geol. It.*, v. 104, p. 239-256.
- Giunta, G., and Nigro, F., 1999, Neogene tectonics in the Peloritani Thrust Belt (NE Sicily): *Annales Tectonicae*, v. 13, p.16-36.
- Gleadow, A.J.W., and Duddy, I.R., 1981, A natural long-term track annealing experiment for apatite: *Nucl. Tracks*, v. 5, p. 169-174.

- Gleadow, A.J.W., Duddy, I.R., and Lovering, J.F., 1983. Fission track analysis: a new tool for the evaluation of thermal histories and hydrocarbon potential: *Austral. Petrol. Expl. Ass. J.*, v. 23, p. 93-102.
- Grasso, M., 2001, The Appenninic-Maghrebic orogen in southern Italy, Sicily and adjacent areas. G.B. Vai and I.P. Martini (eds.), *Anatomy of an Orogen: the Apennines and Adjacent Mediterranean Basins*, 255-286. 2001 Kluwer Academic Publishers. Printed in Great Britain.
- Grasso, M., Guerrera, F., Loiacono, F., Puglisi, D., Romeo, M., Balenzano, F., Carmisciano, R., Di Pierro, M., Gonzales Donoso, J. M., Martin Algarra, A., 1987, Caratterizzazione sedimentologica, biostratigrafica e mineralogico-petrografica di "Successioni Miste" inframioceniche affioranti in Spagna (Catena betica) e in Italia meridionale (M.ti Nebrodi e Appennino lucano): *Boll. Soc. Geol. It.*, v. 106, p. 475-516.
- Grasso, M., Lentini, F., Vezzani, L., 1978, Lineamenti stratigrafico strutturali delle Madonie (Sicilia Centro-Settentrionale): *Geol. Romana* , v. XVII, p. 45-69.
- Grasso, M., Miuccio, G., Maniscalco, R., Garofalo, P., La Manna, F., and Stamilla, R., 1995, Plio-Pleistocene structural evolution of the western margin of the Hyblean Plateau and the Maghrebic foredeep, SE Sicily: implications for the deformational history of the Gela Nappe: *Ann. Tecton.*, v. 9, p. 7–21.
- Green, P.F., Duddy, I.R., Gleadow, A.J.W., Tingate, P.R., and Laslett G.M., 1986, Thermal annealing of fission tracks in apatite: 4. Quantitative modeling techniques and extension to geological scales: *Chem. Geol.*, v. 79, p. 155-182.
- Guarnieri, P., 2004, Structural evidence for deformation by block rotation in the context of transpressive tectonics, northwestern Sicily (Italy): *Journal of Structural Geology*, v. 26, p. 207–219.
- Guerrera, F., Loiacono, F., Moretti, E., Puglisi, D., 1990, La sequenza numidica nel suo contesto geotettonico: Una proposta di ordine paleogeografico: *Riv. It. Paleont. Strat.*, v. 96, p. 165-190.
- Guerrera, F., Martín-Martín M., Perrone, V., and Tramontana, M., 2005, Tectono-sedimentary evolution of the southern branch of the Western Tethys (Maghrebic Flysch Basin and Lucanian Ocean): consequences for Western Mediterranean geodynamics: *Terra Nova*, v. 17, p. 358-367.

- Guilhaumou, N., Larroque, C., Nicot, E., Roure, F., Stephan, J.F., 1994, Mineralized veins resulting from fluid flow in decollement zones of the Sicilian prism: evidence from fluid inclusions. *Bull. Soc. Geol. France* v. 165, 5, p. 425-436.
- Guo, Y., and Bustin, R.M., 1998, Micro-FTIR spectroscopy of liptinite macerals in coal: *International Journal of Coal Geology*, v. 36, p. 259–275.
- Hardebol, N.J., Callot, J.P., Bertotti, G. and Faure, J.L., 2009, Burial and temperature evolution in thrust belt systems: Sedimentary and thrust sheet loading in the SE Canadian Cordillera, *Tectonics*, v. 28, TC3003, doi:10.1029/2008TC002335.
- Hillier, S., Máttyàs, J., Matter, A., and Vasseur, G., 1995, Illite/smectite diagenesis and its variable correlation with vitrinite reflectance in the Pannonian Basin: *Clays and Clay Minerals*, v. 43, p. 174-183.
- Hoffman, J., and Hower, J., 1979, Clay mineral assemblages as low grade metamorphic geothermometers - application to the thrust faulted disturbed belt of Montana, USA, *in* Scholle, P.A., and Schluger, P.S., eds., *Aspects of Diagenesis: SEMP Special Publication*, v. 2, p. 55-79.
- Holton J., 1999, Four geologic settings dominate oil, gas fields of Italy, Sicily: *Oil & Gas Journal*, 81-84.
- Hunt, J.M., 1986, *Petroleum: McGraw-Hill Yearbook of Science and Technology*, p. 362-365.
- Iannace, A., Vitale, S., D'Errico, M., Mazzoli, S., Di Staso, A., Macaione, E., Messina, A., Reddy, S.M., Somma, R., Zamparelli, V., Zattin, M., and Bonardi, G., 2007, The carbonate tectonic units of northern Calabria (Italy): a record of Apulian paleo-margin evolution and Miocene convergence, continental crust subduction, and exhumation of HP-LT rocks: *Journal of the Geological Society*, v. 164, p. 1165-1186.
- Ibarra, J.V., Moliner, R., Bonet, A.J., 1994, FT-i.r. investigation on char formation during the early stages of coal pyrolysis: *Fuel*, v. 73, p. 918–924.
- Ibarra, J.V., Muñoz, E., Moliner, R., 1996, FTIR study of the evolution of coal structure during the coalification process: *Organic Geochemistry*, v. 24, p. 725–735.
- Iglesias, M.J., Jiménez, A., Laggoun-Défarge, F., and Suárez-Ruiz, I., 1995, FTIR study of pure vitrains and associated coals: *Energy & Fuels*, v. 9, p. 458–466.
- Kister, J., Guiliano, M., Largeau, C., Derenne, S., and Casadevall, E., 1990, Characterization of chemical structure, degree of maturation and oil potential of Torbanites (type I kerogens) by quantitative FT-i.r. spectroscopy: *Fuel*, v. 69, p. 1356–1361.



- Jagodzinski, H., 1949, Eindimensionale Fehlordnung in Kristallen Und ihr einfluss auf die röntgen interferenzen: *Acta Crystallogr.*, v. 2, p. 201-207.
- Jennings, S., and Thompson, G.R., 1986, Diagenesis of Plio-Pleistocene sediments of the Colorado River delta, southern California: *Journal of Sedimentary Petrology*, v. 56, p. 89-98.
- Jolivet, L., Frizon de Lamotte, D., Mascle, A., and Séranne, M., 1999, The Mediterranean Basins: Tertiary extension within the Alpine Orogen – an introduction: *in* Durand B., Jolivet, L., Horvath, F., and Séranne, M., eds., *The Mediterranean Basins: Tertiary extension within the Alpine Orogen*, Geological Society Special Publication, v. 156, p. 1-14.
- Jolivet, M., Labaume, P., Monié, P., Brunel, M., Arnaud, N., and Campani M., 2007, Thermochronology constraints for the propagation sequence of the south Pyrenean basement thrust system (France-Spain): *Tectonics*, v. 26, TC5007.
- Jolivet, L., Augier, R., Faccenna, C., Negro, F., Rimmele, G., Agard, P., Robin, C., Rossetti, F., and Crespo-Blanc, A., 2008, Subduction, convergence and the mode of backarc extension in the Mediterranean region: *Bulletin de la Societe Geologique de France*, v. 179, p. 525-550.
- La Manna, F., Grasso, M., Romeo, M., Maniscalco, R., Di Stefano, A., 1995, Evoluzione tettonico-sedimentaria neogenica del bordo tirrenico dei Monti Nebrodi (Sicilia settentrionale): *Studi Geologici Camerti, Volume Speciale 1995/2*, p. 293-305.
- Larroque, C., Guilhaumou, N., Stefan, J.-F., and Roure, F., 1996, Advection of fluids at the front of the Sicilian Neogene subduction complex: *Tectonophysics*, v. 254, p. 41–55.
- Lanson, B., 1997, Decomposition of experimental X-ray diffraction patterns (profile fitting): a convenient way to study clay minerals: *Clays and Clay Minerals*, v. 45, p. 132-146.
- Lentini, F. and Vezzani, L., 1978, Tentativo di elaborazione di uno schema strutturale della Sicilia orientale: *Bollettino della Società Geologica Italiana*, v. 19, p. 495-500.
- Lentini, F., Carbone, S., Catalano, S., and Monaco, C., 1991, Tettonica a thrust della catena appenninico-maghrebide: Esempi della Lucania e della Sicilia, *in* Boccaletti, M., et al., eds., *Neogene Thrust Tectonics: Studi Geologici Camerti*, v. spec., p. 19–26.
- Lentini, F., Carbone, S., Catalano, S., Di Stefano, A., Gargano, C., Romeo, M., Strazzulla, S., and Vinci, G., 1995, Sedimentary evolution in basins in mobile belts:

- examples from Tertiary terrigenous sequences of the Peloritani Mts.: *Terra Nova*, v. 7, p. 161-170.
- Lentini, F., Carbone, S., Catalano, S., and Grasso, M., 1996, Elementi per la ricostruzione strutturale della Sicilia Orientale: *Memorie della Società Geologica Italiana*, v. 51, p. 179-195.
- Lentini, F., Catalano, S., and Carbone, S., 1996, The External Thrust System in southern Italy: a target for petroleum exploration: *Petroleum Geoscience*, v. 2, p. 333-342.
- Lentini, F., Catalano, S., and Carbone, S., 2000, Carta geologica della provincia di Messina: Servizio Geologico, S.EL.CA., Provincia Regionale di Messina, Assessorato Territorio, scale 1:50,000, 3 sheets.
- Lentini, F., Grasso, M., Carbone, S., 1987, Introduzione alla geologia della Sicilia e guida all'escursione: Convegno della Società Geologica Italiana su Sistemi Avanfossa-Avampaese lungo la Catena Appenninico-Maghrebide: Naxos/Pergusa 22-25 aprile 1987.
- Levine, J.R., and Davis, A., 1989, The relationship of coal optical fabrics to Alleghanian tectonic deformation in the Central Appalachian fold-and-thrust belt, Pennsylvania: *Geol. Soc. Am. Bull.*, v. 101, p. 1333-1347.
- Lickorish, W.H., Grasso, M., Butler, R.W.H., Argnani, A., and Maniscalco, R., 1999, Structural styles and regional tectonic setting of the "Gela Nappe" and frontal part of the Maghrebian thrust belt in Sicily: *Tectonics*, v. 18, p. 655–668, doi: 10.1029/1999TC900013.
- Lin, R., and Ritz, G.P., 1993a, Reflectance FT-IR microspectroscopy of fossil algae contained in organic-rich shales: *Applied Spectroscopy*, v. 47, p. 265–271.
- Lin, R., and Ritz, G.P., 1993b, Studying individual macerals using i.r. microspectroscopy, and implications on oil versus gas/condensate proneness and "low-rank" generation: *Organic Geochemistry*, v. 20, p. 695–706.
- Lis, G.P., Mastalerz, M., and Schimmelmann A., Lewan, M.D., Stankiewicz B.A., 2005, FTIR absorption indices for thermal maturity in comparison with vitrinite reflectance R<sub>0</sub> in type-II kerogens from Devonian black shales: *Organic Geochemistry*, v. 36, p. 1533-1552.

- Lis, G.P., Mastalerz, M., and Schimmelmann A., 2008, Increasing maturity of kerogen type II reflected by alkylbenzene distribution from pyrolysis-gas chromatography–mass spectrometry: *Organic Geochemistry*, v. 39, p. 440-449.
- Lugeon, M. and Argand, E., 1906a, Sur l'existence de grands phénomènes de charriage an Sicile : *Comptes Rendus Académie des Sciences*, v. 142, p. 966.
- Lugeon, M. and Argand, E., 1906b, Sur la grande nappe de recouvrement de la Sicile: *Comptes Rendus Académie des Sciences*, v. 142, p. 3.
- Malinverno, A., and Ryan, W.B.F., 1986, Extension in the Tyrrhenian Sea and shortening in the Apennines as result of arc migration driven by sinking of the lithosphere: *Tectonics*, v. 5, p. 227- 254.
- Mantovani, E., Albarello, D., Tamburelli C., and Babbucci, B., 1996, Evolution of the Tyrrhenian basin and surrounding regions as a result of the Africa-Eurasia convergence: *Journal of Geodynamics*, v. 21, p. 35-72.
- Mariotti, G., and Doglioni C., 2000, The dip of the foreland monocline in the Alps and Apennines: *Earth Planet. Sc. Lett.*, v. 181, p. 191-202.
- Marshak, S., 1988, Kinematics of orocline and arc formation in thin-skinned orogens: *Tectonics*, v. 7, p. 73–86.
- Marshak, S., 2004, Salients, recesses, arcs, oroclines, and syntaxes -A review of ideas concerning the formation of map-view curves in fold-thrust belts, *in* McClay, K.R., ed., *Thrust Tectonics and Hydrocarbon Systems: American Association of Petroleum Geologists (AAPG) Memoir v. 82*, pp. 131–156.
- Martín-Algarra, A., Messina, A., Perrone, V., Russo, S., Maaté A., and Martín-Martín, M., 2000, A lost realm in the internal domains of the Betic-Rif Orogen (Spain and Morocco): Evidence from conglomerates and consequences for alpine geodynamic evolution: *Journal of Geology*, v. 108, p. 447-467.
- Martín-Algarra, A., and Vera, J.A., 2004, La Cordillera Bética y las Baleares en el contexto del Mediterráneo Occidental, *in* Vera, J.A., ed., *Geología de España: Sociedad Geológica de España-Instituto Geológico y Minero de España, Madrid*, p. 352-354.
- Mastalerz, M., and Bustin, R.M., 1993, Variation in maceral chemistry within and between coals of varying rank: an electron microprobe and micro-Fourier transform infra-red investigation: *Journal of Microscopy*, v. 171, p. 153–166.
- Mastalerz, M., and Bustin, R.M., Application of reflectance micro-Fourier Transform infrared analysis to the study of coal macerals: an example from the Late Jurassic to

- Early Cretaceous coals of the Mist Mountain Formation, British Columbia, Canada: *International Journal of Coal Geology*, v. 32, p. 55-67.
- Merriman, R.J., and Frey, M., 1999, Patterns of very low-grade metamorphism in metapelitic rocks, *in* Frey, M., and Robinson, D., eds., *Low grade metamorphism*: Oxford, Blackwell, p. 61-107.
- Messina, A., Russo, S., and Stagno, F., 1996, The crystalline basements of the Calabrian-Peloritani Arc: 6<sup>th</sup> field Meeting IGCP project n°276, v. 6, p. 94.
- Messina, A., Somma, R., Careri, G., Carbone, G., and Macaone, E. 2004, Peloritani continental crust composition (southern Italy): geological and petrochemical evidences: *Bollettino della Società Geologica Italiana*, v. 123, p. 405-441.
- Miller, S., and Macdonald, D.I.M., 2004, Metamorphic and Thermal History of a Fore-Arc Basin: the Fossil Bluff Group, Alexander Island, Antarctica: *Journal of Petrology*, v. 45, p. 1453-1465.
- Mitra, G., 1997, Evolution of salients in a fold-and-thrust belt: the effects of sedimentary basin geometry, strain distribution and critical taper, *in* *Evolution of Geological Structures in Micro-and Macro-Scales*, Sengupta, S., ed., pp. 59-90. Chapman & Hall, London.
- Monaco, C., and De Guidi, G., 2006, Structural evidence for Neogene rotations in the eastern Sicilian fold and thrust belt: *Journal of Structural Geology*, v. 28, p. 561-574.
- Monthieux, M., and Landais, P., 1988, Natural and artificial maturations of coal series: infrared spectrometry study: *Energy & Fuels*, v. 2, p. 794–801.
- Moore, D.M., and Reynolds, R.C., Jr., 1997, X-Ray diffraction and the identification and analysis of clay minerals: Oxford, Oxford University Press, p. 1-378.
- Mukhopadhyay, P.K., 1994, Vitrinite reflectance as maturity parameter: petrographic and molecular characterization and its applications to basin modeling: *in* Mukhopadhyay, P.K., and Dow, W.G., eds., *Vitrinite reflectance as a maturity parameter: applications and limitations*: American Chemical Society Symposium Series v. 570, p. 1-24.
- Nicolich, R., 2001, Deep Seismic Transect, *in* *Anatomy of an Orogen: The Apennines and Adjacent Mediterranean Basins*. Kluwer Academic Publishing, Great Britain, pp. 47-52.
- Nigro, F., Renda, P., 2001, Late Miocene-Quaternary stratigraphic record in the Sicilian Belt (Central Mediterranean): tectonics versus eustasy. *Boll. Soc. Geol. It.*, v. 120, p. 151-164.

- Oberlin, A., Boulmier, J.L., and Villey, M., 1980, Electron microscopic study of kerogen microtexture. Selected criteria for determining the evolution path and evolution stage of kerogen. *In*: (Durand B., ed.), *Kerogen*, Editions Technip, Paris, p. 191-242.
- Ogniben, L., 1960, Nota illustrativa dello Schema geologico della Sicilia Nord-orientale. *Riv. Min. Sic*, v. 11(64-65), p. 183-212.
- Ogniben, L., 1969, Schema introduttivo alla geologia del confine Calabro-Lucano: *Memorie della Società Geologica Italiana*, v. 8, p. 453-763.
- Oldow, J.S., Channell, J.E.T., and Catalano, R., 1990, Contemporaneous thrusting and large-scale rotations in the western Sicilian fold and thrust belt: *Tectonics*, v. 9, p. 661-681.
- Olivetti, V., Balestrieri, M, L, Faccenna, C, Finlay, M. S., and Vignaroli, G., 2010, Middle Miocene out-of-sequence thrusting and successive exhumation in the Peloritani Mountains, Sicily: Late stage evolution of an orogen unraveled by apatite fission track and (U-Th)/He thermochronometry: *Tectonics*, v. 29, TC2005, doi:10.1029/2009TC002659.
- Painter, P.C., Snyder, R.W., Starsinic, M., Coleman, M.M., Kuehn, D.W., and Davis, A., 1981: Concerning the application of FT-IR to the study of coal: A critical assessment of band assignments and the application of spectral analysis programs: *Applied Spectroscopy*, v. 35, p. 475–485.
- Painter, P.C., Starsinic, M., Squires, E., and Davis, A.A., 1983, Concerning the 1600 cm<sup>-1</sup> region in the i.r. spectrum of coal: *Fuel*, v. 62, p. 742–744.
- Paulsen, T., and Marshak, S., 1999, Origin of the Uinta recess, Sevier fold–thrust belt, Utah: influence of basin architecture on fold–thrust belt geometry: *Tectonophysics*, v. 312 (2-4), p. 203-216.
- Pepe, F., Bertotti, G., Cella, F., and Marsella, E., 2000, Rifted margin formation in the South Tyrrhenian Sea: a high-resolution seismic profile across the North Sicily passive continental margin: *Tectonics*, v. 19, p. 241-257.
- Perrone, V., Martín-Algarra, A., Critelli, S., Decandia, F.A., D’Errico, M., Estevez, A., Iannace, A., Lazzarotto, A., Martín-Martín, M., Martín-Rojas, I., Mazzoli, S., Messina, A., Mongelli, G., Vitale, S., and Zaghloul, M.N., 2006, “Verrucano” and “Pseudoverrucano” in the central-western Mediterranean Alpine chains: paleogeographical evolution and geodynamic significance, *in* Chalouan, A., and Moratti, G., eds., *Tectonics of the Western Mediterranean and North Africa: Geological Society, London, Special Publications*, v. 262, p. 1-43.

- Platt, J.P., and Compagnoni, R., 1990, Alpine ductile deformation and metamorphism in a Calabrian basement nappe (Aspromonte, south Italy): *Eclogae Geologicae Helvetiae*, v. 83, p. 41-58.
- Platzman, E., Platt, J.P., and Oliver, P., 1993, Palaeomagnetic rotations and fault kinematics in the Rif Arc of Morocco: *Journal of the Geological Society, London*, v. 8, p. 707-718.
- Pollastro, R.M., 1990, The illite/smectite geothermometer - concepts, methodology and application to basin history and hydrocarbon generation, *in* Nuccio, F., and Barker, C.E., eds., *Application of thermal maturity studies to energy exploration: SEPM Rocky Mountains section*, p. 1-18.
- Pollastro, R.M., 1993, Consideration and applications of the illite/smectite geothermometer in hydrocarbon-bearing rocks of Miocene to Mississippian age: *Clays and Clay Minerals*, v. 41, p. 119-133.
- Pradier, B., Landais, P., Rochdi, A., and Davis, A., 1992, Chemical basis of fluorescence alteration of crude oils and kerogens-II, Fluorescence and infrared micro-spectrometric analysis of vitrinite and liptinite: *Org. Geochem.*, v. 18, p. 241-248.
- Riesser, B., Starsinic, M., Squires, E., Davis, A., and Painter, P.C., 1984, Determination of aromatic and aliphatic CH groups in coal by FT-i.r. 2. Studies of coals and vitrinite concentrates: *Fuel*, v. 63, p. 1253-1261.
- Ring, U., Brandon, M.T., Willett, S.D., and Lister, G.S., 1999, Exhumation processes, *in* Ring, U., Brandon, M.T., Lister, G.S., Willett, S.D., eds., *Exhumation Processes: Normal Faulting, Ductile Flow and Erosion: Geological Society Special Publication*, v. 154, p. 1-27.
- Robl, T.L., and Davis, B.H., 1993, Comparison of the HF-HCl and HF-BF<sub>3</sub> maceration techniques and the chemistry of resultant organic concentrates: *Organic Geochemistry*, v. 20, p. 249-255.
- Roca, E., Frizon de Lamotte, D., Mauffret, A., Bracène, R., Vergés, J., Benaouali, N., Fernández, M., Muñoz, J.A., and Zeyen, H., 2004, TRANSMED Transect II, *in* Cavazza, W., Roure, F., Spakman, W., Stampfli, G.M., and Ziegler, P.A., eds., *The TRANSMED Atlas. The Mediterranean Region from Crust to Mantle: Geological and Geophysical Framework*, Springer, Berlin Heidelberg, CD Rom.
- Rossetti, F., Faccenna, C., Goffé, B., Monié, P., Argentieri, A., Funicello, R., and Mattei, M., 2001, Alpine structural and metamorphic signature of the Sila Piccola Massif

- nappe stack (Calabria, Italy): Insights for the tectonic evolution of the Calabrian Arc: *Tectonics*, v. 20, p. 112-133.
- Rottura, A., Bargossi, M.G., Caironi, V., Del Moro, A., Maccarrone, E., Macera, P., Paglionico, A., Petrini, R., Piccarreta, G., and Poli, G., 1990, Petrogenesis of contrasting Hercynian granitoids from the Calabrian Arc, southern Italy: *Lithos*, v. 24, p. 97-119.
- Roure, F., Howell, D.G., Müller, C., and Moretti, I., 1990, Late Cenozoic subduction complex of Sicily: *Journal of Structural Geology*, v. 12, p. 259-266.
- Rouxhet, P.G., and Robin, P.L., 1978, Infrared study of the evolution of kerogens of different origins during catagenesis and pyrolysis: *Fuel* v. 57, p. 533–540.
- Schenk, H.J., Witte, E.G., Littke, R., and Schwochau, K., 1990, Structural modifications of vitrinite and alginite concentrates during pyrolytic maturation at different heating rates. A combined infrared, <sup>13</sup>C NMR and microscopical study: *Organic Geochemistry*, v. 16, p. 943–950.
- Schimmelmann, A., Lewan, M.D., and Wintsch, R.P., 1999, D/H isotope ratio of kerogen, bitumen, oil, and water in hydrous pyrolysis of source rocks containing kerogen types I, II, IIS, and III: *Geochimica et Cosmochimica Acta*, v. 63, p. 3751–3766.
- Schmidt Di Friedberg, P., Barbieri, F., and Giannini, C., 1960, La geologia del gruppo montuoso delle Madonie (Sicilia centro- settentrionale): *Boll. Serv. Geol. Ital.*, v. 81, p. 73-140.
- Sclater, J.G., and Christie, P.A.F., 1980, Continental stretching: an explanation of post-Mid Cretaceous subsidence on the Central North Sea Basin: *Journal of Geophysical Research*, v. 85, p. 3711-3739.
- Scotti, P., 2003, Thermal constraints from the organic matter: *Atti Ticinensi di Scienze della Terra*, v. 9, Serie Speciale, p. 23-32.
- Selli, R., 1957, Sulla trasgressione del Miocene nell'Italia meridionale: *Giornale Geologia*, v. 26, p. 1-54.
- Selli, R., 1978, Geologia e sismotettonica dello stretto di Messina: *Atti dell'Accademia Nazionale dei Lincei*, Roma, Abstracts, v. 43, p. 119-154.
- Sequenza, G., 1873, Brevissimi cenni intorno la serie terziaria della provincia di Messina: *Boll. R. Comit. Ital.*, v. 4, p. 231-238, p. 259-270.

- Sobalík, Z., Čejka, J., and Kříbek, B., 1998, Continuous monitoring of the oxidation of algal- and humic-type kerogen in a heated FTIR flow cell: *Org. Geochem.*, v. 28, n. 11, p. 767-772.
- Sobkowiak, M., and Painter, P., 1992, Determination of the aliphatic and aromatic CH contents of coals by FT-i.r.: studies of coal extracts: *Fuel*, v. 71, p. 1105–1125.
- Somma, R., Messina, A., and Mazzoli, S., 2005a, Syn-orogenic extension in the Peloritani Alpine Thrust Belt (NE Sicily, Italy): evidence from the Alì Unit: *Compte Rendus Geoscience Paris*, v. 337, p. 861-871.
- Somma, R., Messina, A., and Perrone, V., 2005b, The Cambrian to Aquitanian geological record of the Longi-Taormina Unit (Calabria-Peloritani Arc, southern Italy): geodynamic implications: *Geodinamica Acta*, v. 18, p. 417-430.
- Somma, R., 2006, The south-western side of the Calabrian Arc (Peloritani Mountains): geological, structural and AMS evidence for passive clockwise rotations: *Journal of Geodynamics*, v. 41, p. 422-439.
- Speranza, F., Villa, I.M., Sagnotti, L., Florindo, F., Cosentino, D., Cipollari, P., and Mattei, M., 2002, Age of the Corsica-Sardinia rotation and Liguro-Provençal Basin spreading: new paleomagnetic and Ar/Ar evidence: *Tectonophysics*, v. 347, p. 231-251.
- Speranza, F., Maniscalco, R., and Grasso M., 2003, Pattern of orogenic rotations in central-eastern Sicily: implications for the timing of spreading in the Ttrrhénian Sea: *Journal of the Geological Society, London*, vol. 160, p. 183-195.
- Stach, E., Mackowsky, M.Th., Teichmüller, M., Taylor, G.H., Chandra, D., and Teichmüller, R., 1982, *in* Gebrüder Borntraeger, ed., *Stach's Textbook of Coal Petrology*: Berlin, p. 535.
- Sturiale, G., Maniscalco, R., De Guidi, G., Pedley, M., Grasso, M., 2010, Geological map of the Corvillo and Mandre Basins (Central Sicily). Explanatory notes, 316-326.
- Sussman, A.J., Weil, A.B., eds., 2004, *Orogenic Curvature: Integrating Paleomagnetic and Structural Analyses*: Geological Society of America Special Paper v. 383, p. 271.
- Sweeney, J.J., and Burnham, A.K., 1990, Evaluation of a simple model of vitrinite reflectance based on chemical kinetics: *American Association of Petroleum Geologists Bulletin*, v. 74, p. 1559-1570.
- Teichmüller, M., 1987, Organic material and very low-grade metamorphism, *in* Frey, M., ed., *Low Temperature Metamorphism*: Glasgow and London, Blackie, p. 114-161.



- Thomson, S.N., 1994, Fission track analysis of the crystalline basement rocks of the Calabrian Arc, southern Italy: evidence of Oligo-Miocene late orogenic extension and erosion: *Tectonophysics*, v.238, p. 331-352.
- Thomson, S.N., 1998, Assessing the nature of tectonic contacts using fission-track thermochronology: an example from the Calabrian Arc, southern Italy: *Terra Nova*, v. 10, p. 32-36.
- Truillet, R., 1969, Etude géologique des Péloritains orientaux (Sicile): Thèse Doct. Sci. Nat. Univ. de Paris, p. 547.
- Underwood, M.B., Fulton, D.A., and McDonald, K.W., 1988, Thrust control on thermal maturity of the frontal Ouachita Mountains, Central Arkansas, USA: *Journal of Petroleum Geology*, v. 11, p. 325-340.
- Vai, G.B., and Martini I.P., 2001, Anatomy of an Orogen: the Apennines and adjacent Mediterranean basins.
- Van Hinte, J.E., 1978, Geohistory analysis - Application of micropaleontology in exploration geology: *AAPG Bull.*, v. 62, p. 201-222.
- Vera, J.A., 2004, Geología de España: Sociedad Geológica de España-Instituto Geológico y Minero de España, Madrid, 1-890.
- Vezzani L., 1972, Carta geologica d'Italia 1:50.000, foglio 611, Mistretta. Ser. Geol. It., Roma.
- Vignaroli, G., Rossetti, F., Theye, T., and Faccenna, C., 2008, Styles and regimes of orogenic thickening in the Peloritani Mountains (Sicily, Italy): new constraints on the tectono-metamorphic evolution of the Apennine belt: *Geological Magazine*, v. 145, p. 552-569.
- Wallis, S.R., Platt, J.P., and Knott, S.D., 1993, Recognition of sin-convergent extension in accretionary wedges with example from the Calabrian arc and the eastern Alps: *American Journal of Science*, v. 293, p. 463-495.
- Wagner, G.A., and Reimer, G.M., 1972, Fission track tectonics: the tectonic interpretation of fission track apatite ages: *Earth Pl. Sci. Lett.*, v. 14, p. 263-268.
- Wagner, G.A., and Van de Haute, P., 1992, Fission-track dating: Kluwer, Dordrecht, p. 286.
- Wang, S.-H., and Griffiths, P.R., 1985, Resolution enhancement of diffuse reflectance i.r. spectra of coals by Fourier-self deconvolution. 1. C-H stretching and bending modes: *Fuel*, v. 64, p. 229-236.
- Wezel, F.C., 1970, Geologia del Flysch Numidico della Sicilia Nord-Orientale: Mem

- Soc. Geol. It v.9, p. 225-280 Pisa.
- Wortel, M.J.R., and Spakman, W., 2000, Subduction and slab detachment in the Mediterranean-Carpathian Region: *Science*, v. 290, p. 1910-1917.
- Yellin-Dror, A., Grasso, M., Ben-Avraham, Z., Tibor, G., 1997, The subsidence history of the northern Hyblean plateau margin, southeastern Sicily. *Tectonophysics* v. 282, p. 277-289.
- Zattin, M., Picotti, V., and Zuffa, G.G., 2002, Fission-track reconstruction of the front of the Northern Apennine thrust wedge and overlying Ligurian Unit: *American Journal of Science*, v. 302, p. 346-379.
- Zattin, M., 2003, Apatite fission-track analysis and the thermochronology of sedimentary Successions: *Atti Ticinensi di Scienze della Terra - special series*, v. 9, p. 33-42.

## APPENDIX

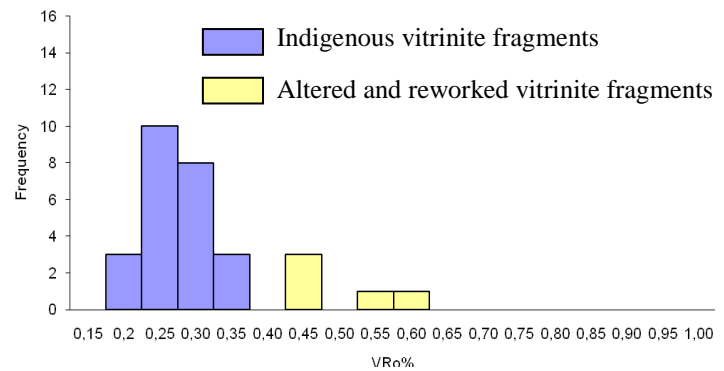
<b>LEGEND</b>	<b>144</b>
<b>SECTION I - INTERNAL ZONE (PELORITANI MTS.)</b>	<b>145</b>
<i>Serravallian-Messinian siliciclastic deposits</i>	146
SI81.1 (7)	146
SI83.1cm (15)	147
SI84.1 (8)	148
SI 87.1 (30)	149
<b>Antisicilide Unit</b>	150
SI 106.1 (11)	150
SI 82.1 (14a)	151
SI 82.2 (14b)	152
SI 85.1 (16a)	153
SI 85.2 (16a)	154
SI 96.1 (17)	155
SI 122.1 (37a)	156
SI 122.2 (37b)	157
SI 137.1 (41)	158
SI 111.1 (45a)	159
<i>Stilo-Capo d'Orlando Formation</i>	160
SI 116.1 (1a)	160
SI 114.1 (1)	160
SI 112.1 (1b)	161
SI 113.1 (1c)	162
SI 115.1 (1d)	163
SI 117.1 (1e)	164
SI 130.1 (3)	165
SI 131.1 (4)	166
SI 102.1 (5)	166
SI 103.1 (6)	166
SI 105.1 (10)	167
SI 140.1 (18)	167
SI 95.1 (12)	168
SI 107.1 (13)	169
SI 132.1 (20a)	170
SI 142.2 (22)	170
SI 133.1 (20b)	171
SI 128.1 (23)	171
SI 134.1 (21)	172
SI 98.1 (28)	173
SI 101.1 (25)	174
SI 97.1 (26)	175
SI 86.1 (27)	176
SI 88.1 OM (31a)	177
SI 88.1 CM (31b)	178
SI 129.1 (32)	179
SI 100.1 (33)	180
SI 135.1 (34)	181
SI 121.1 (40)	181
SI 139.1 (36)	182
SI 118.1 (43)	183
SI 126.1 (48)	183
SI 119.1 (44)	184
SI 110.1 (46b)	185

SI 108.1 (46a)	185
SI 127.1 (47)	186
SI 91.1 (49)	187
SI 125.1 (50)	188
SI 94.1 (51)	189
SI 90.1 (55)	190
SI 123.1 (56)	191
SI 92.1 (59)	191
SI 124.1 (57)	192
SI 93.1 (58)	193
SI 89.1 (60)	194
SI 172.1	195
<b>SECTION II - EXTERNAL ZONE (MT. JUDICA UNIT)</b>	<b>196</b>
<i>Clays and glauconitic sandstones</i>	197
SI 148.1 (11)	197
SI 150.1 (23)	198
<i>Cherty limestones</i>	199
SI 152.1 (20)	199
<i>Mufara Fm</i>	200
SI 143.1 (4a)	200
SI 144.1 (4b)	201
SI 145.1 (4c)	202
SI 146.1 OM (5)	202
SI 147.1 (6a)	203
SI 147.2 (6b)	204
SI 151.1 CM (24a)	205
SI 151.1 OM (24b)	206
<b>SECTION III - EARLY FOREDEEP DEPOSITS (NUMIDIAN FLYSCH)</b>	<b>207</b>
<b>Maragone Unit</b>	<b>208</b>
<i>Numidian Flysch</i>	208
SI 166.1	208
SI 167.1	208
SI 168.1	209
SI 170.1	209
<i>Argille di Portella Mandarinini</i>	210
SI 169.1	210
SI 171.1	210
<b>Nicosia Unit</b>	<b>211</b>
<i>Numidian Flysch</i>	211
SI 154.1 (2)	211
SI 155.1 (2)	211
SI 163.1 (5)	211
SI 159.1 OM (3)	212
<i>Argille Varicolori</i>	213
SI 157.1 OM (3)	213
SI 157.1 CM (3)	214
<i>Argille Scagliose</i>	215
SI 164.1 OM (4)	215
SI 164.1 CM (4)	216
SI 164.2 OM (4)	216
SI 158.1 (1)	217

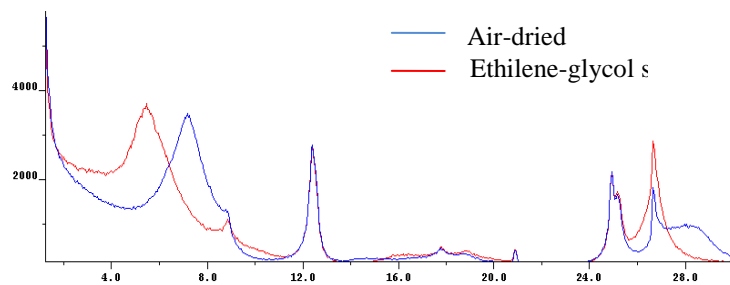
## Legend

**Sample name (site)**

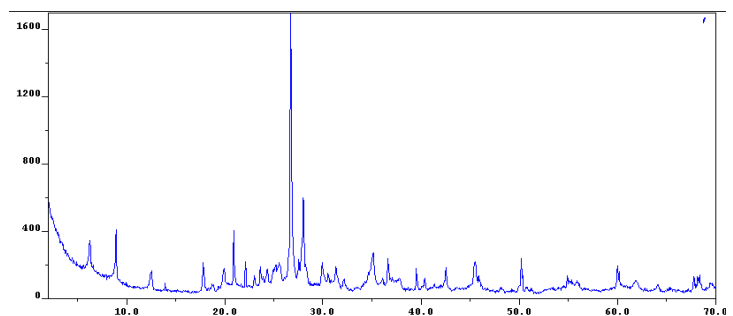
Vitrinite reflectance histogram.



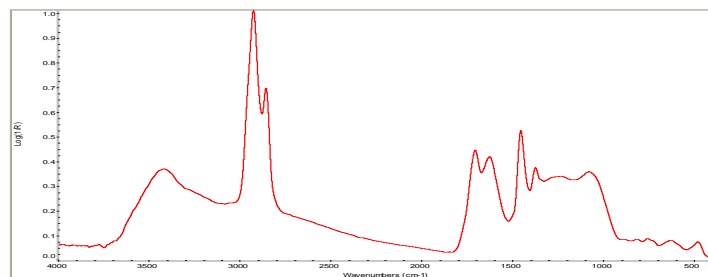
Diffraction patterns in the <2- $\mu$ m grain-size fraction.



Whole rock diffraction pattern.



FTIR spectrum



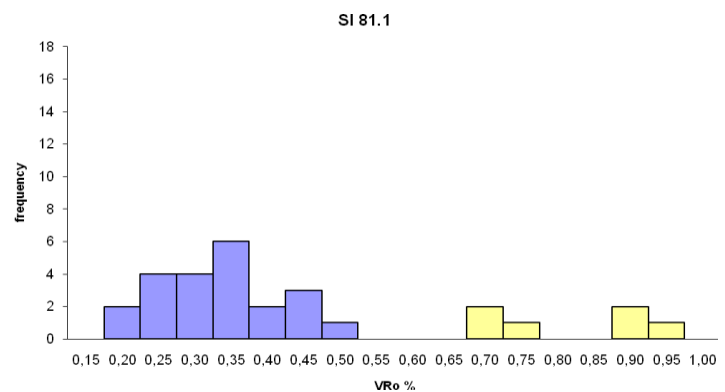
**SECTION I -  
INTERNAL ZONE  
(PELORITANI  
MTS.)**

**Serravallian-  
Messinian  
siliciclastic deposits  
SI81.1 (7)**

Outcrop photo



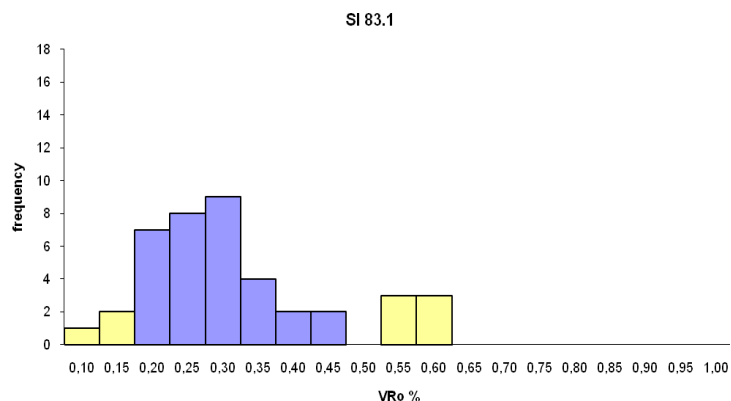
Vitrinite reflectance  
histogram.  
 $VR_o\%$  (n.  
measurements):  
 $0.36 \pm 0.08$  (22)



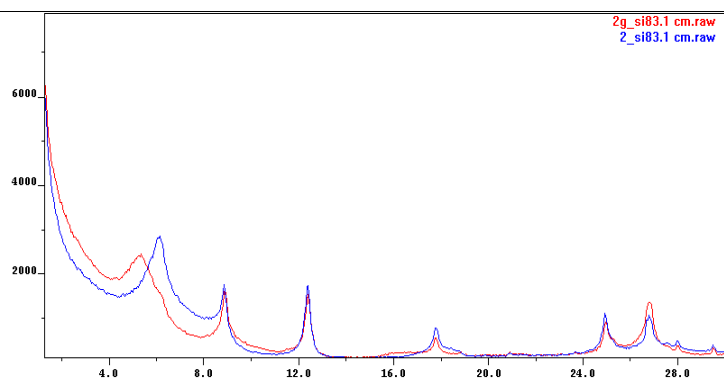
# SI83.1cm (15)

Vitrinite reflectance  
histogram.

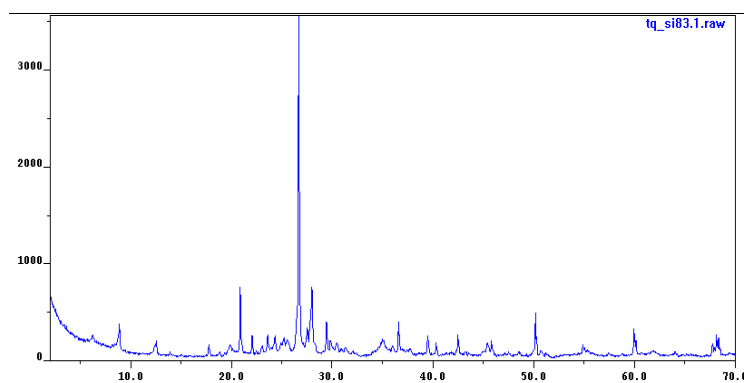
VR<sub>o</sub>% (n.  
measurements):  
0.30±0.06 (22)



Diffraction patterns in  
the <2-μm grain-size  
fraction.  
% I in I/S (R parameter):  
40 (R0)



Whole rock diffraction  
pattern

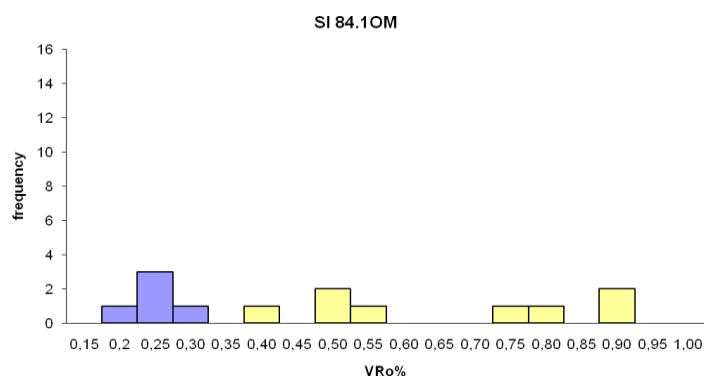




# SI84.1 (8)

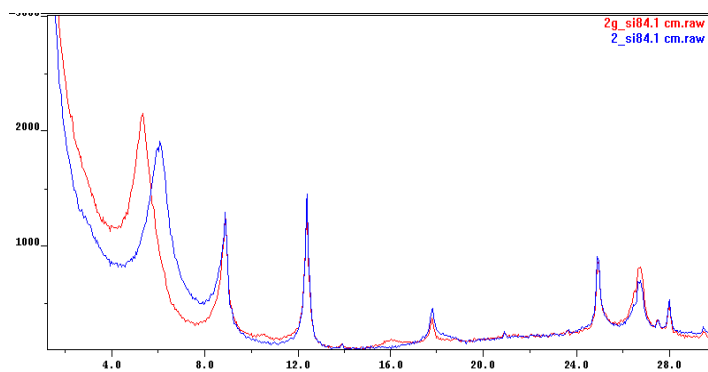
Vitrinite reflectance  
histogram.

VR<sub>o</sub>% (n.  
measurements):  
0.27±0.05(5)

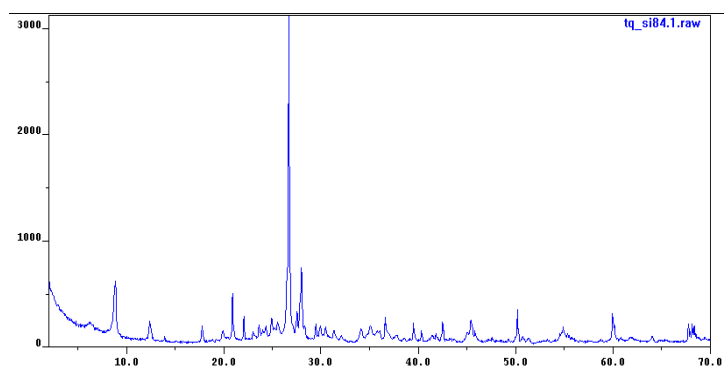


Diffraction patterns in  
the <2-μm grain-size  
fraction.

% I in I/S (R parameter):  
20 (R0)



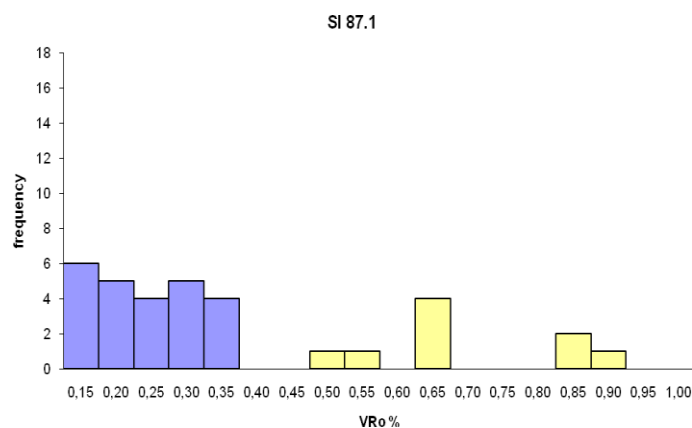
Whole rock diffraction  
pattern



# SI 87.1 (30)

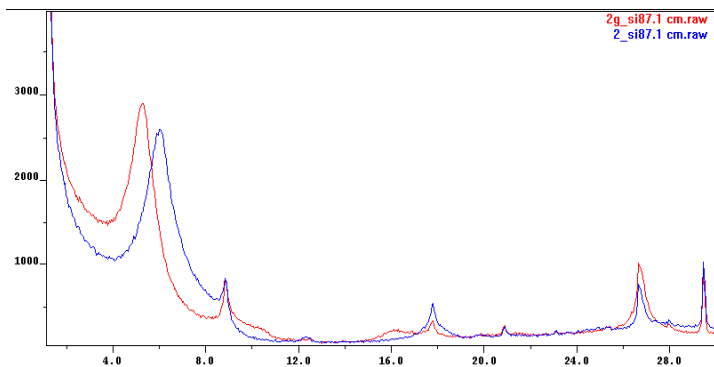
Vitrinite reflectance  
histogram.

VR<sub>0</sub>% (n.  
measurements):  
0.26±0.07(24)

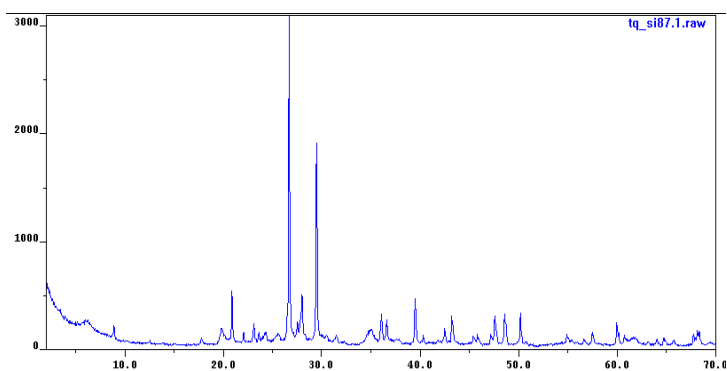


Diffraction patterns in  
the <2-μm grain-size  
fraction.

% I in I/S (R parameter):  
33 (R0)



Whole rock diffraction  
pattern

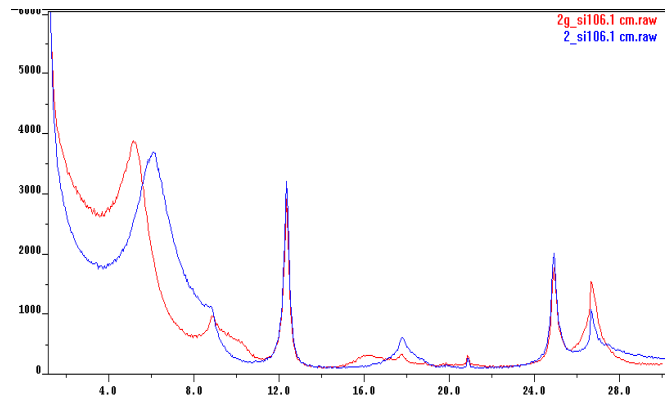


## Antisicilide Unit

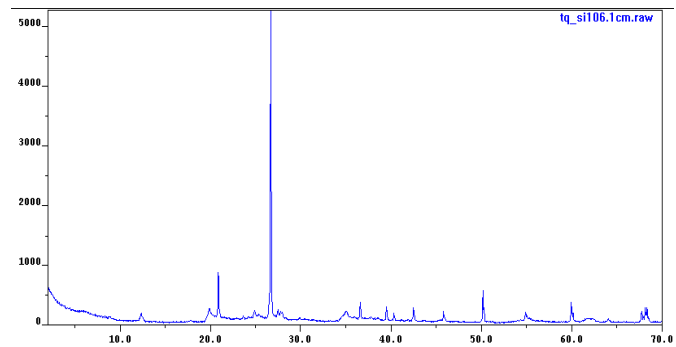
### SI 106.1 (11)

Diffraction patterns in  
the <2- $\mu$ m grain-size  
fraction.

% I in I/S (R parameter):  
30 (R0)



Whole rock diffraction  
pattern

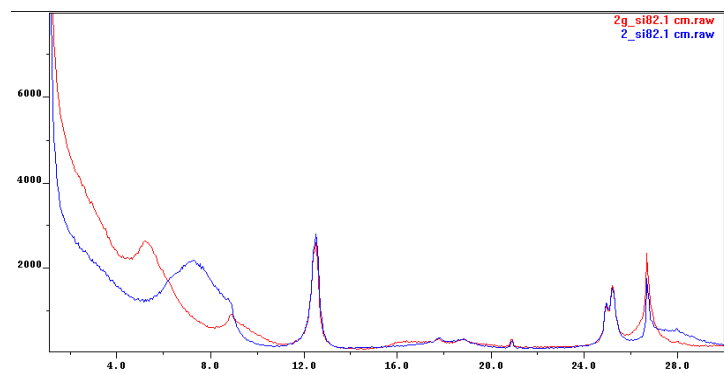


**SI 82.1 (14a)**

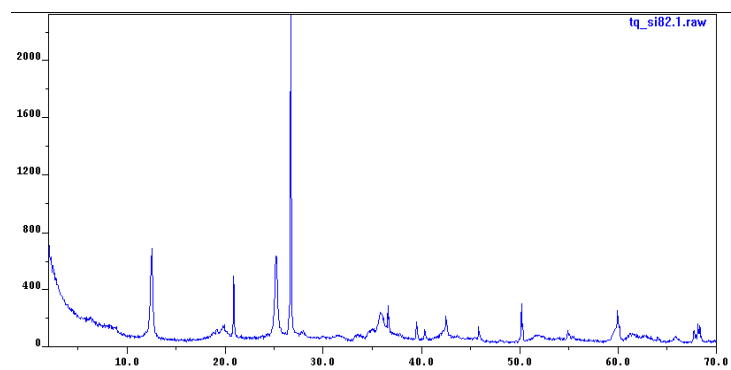
Outcrop photo



Diffraction patterns in  
the <2- $\mu$ m grain-size  
fraction.  
% I in I/S (R parameter):  
50;55 (R0;R1)



Whole rock diffraction  
pattern

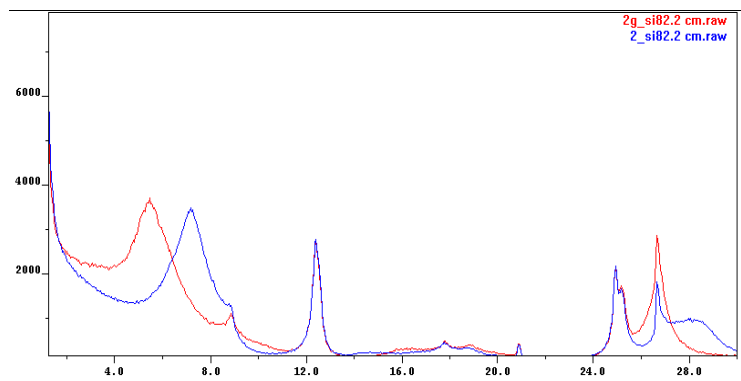


**SI 82.2 (14b)**

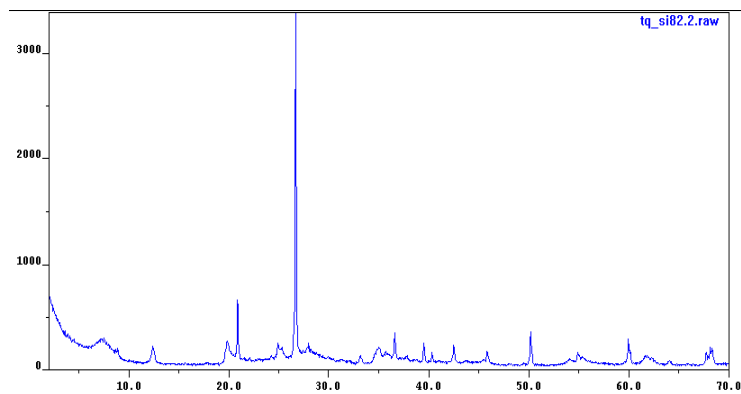
Outcrop photo



Diffraction patterns in  
the <2- $\mu$ m grain-size  
fraction.  
% I in I/S (R parameter):  
50;55 (R0;R1)



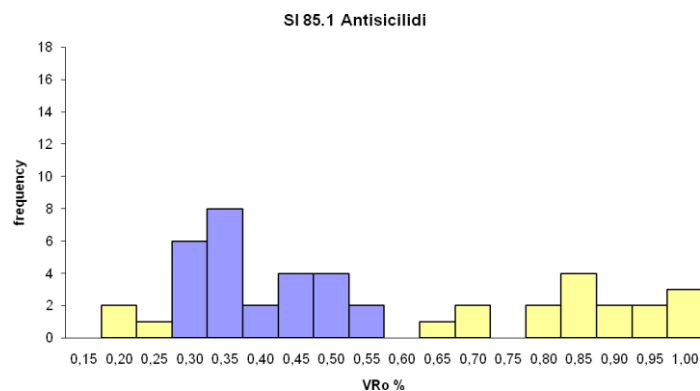
Whole rock diffraction  
pattern



## SI 85.1 (16a)

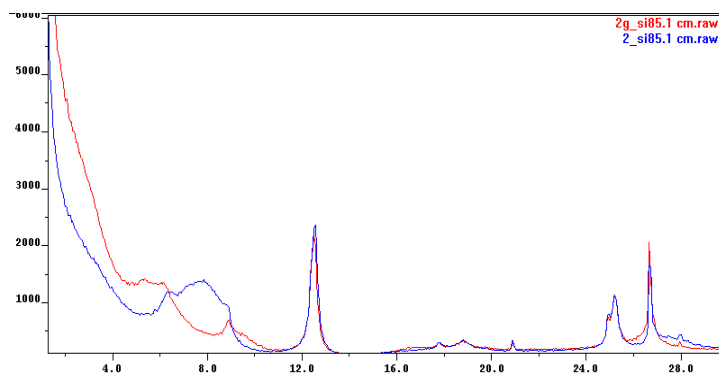
Vitrinite reflectance  
histogram.

VR<sub>o</sub>% (n.  
measurements):  
0.41±0.09(26)

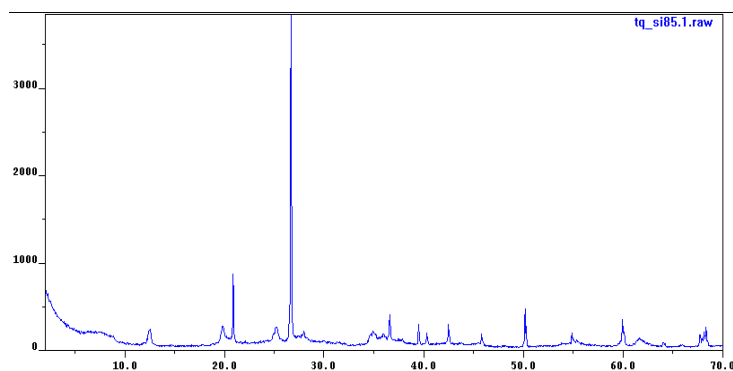


Diffraction patterns in  
the <2-μm grain-size  
fraction.

% I in I/S (R parameter):  
40; 60 (R0; R1)



Whole rock diffraction  
pattern

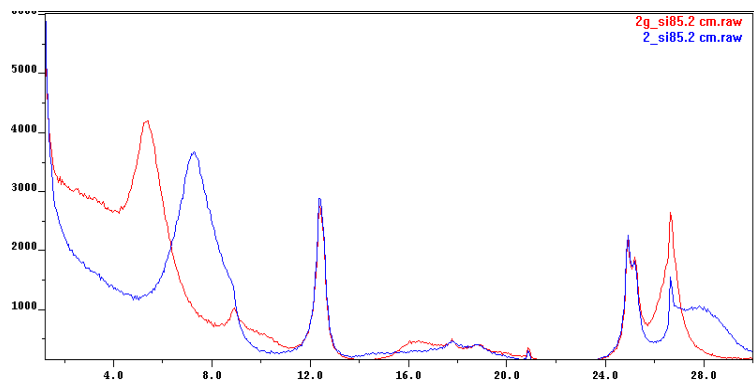


**SI 85.2 (16a)**

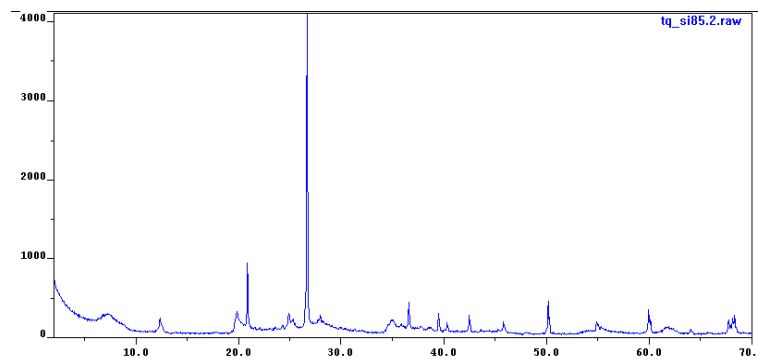
Outcrop photo



Diffraction patterns in  
the <2- $\mu$ m grain-size  
fraction.  
% I in I/S (R parameter):  
40; 60 (R0; R1)



Whole rock diffraction  
pattern

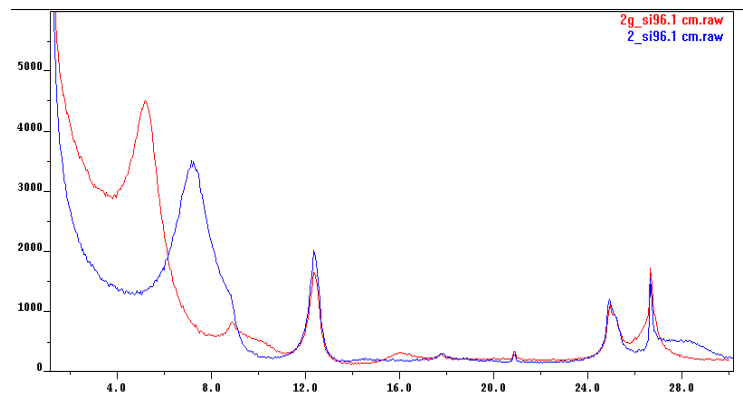


**SI 96.1 (17)**

Outcrop photo



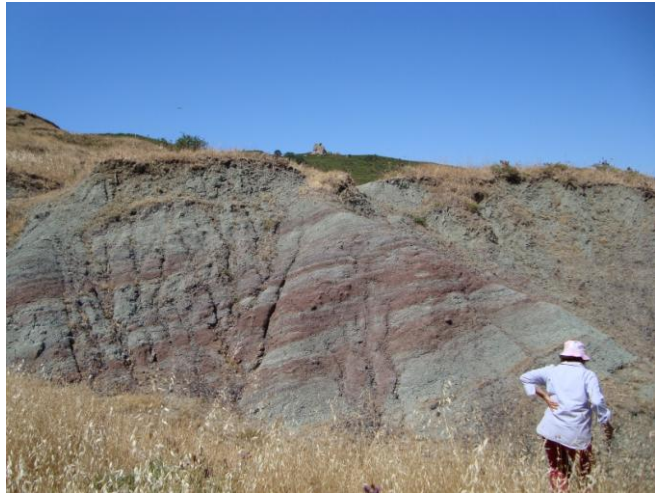
Diffraction patterns in  
the <2- $\mu$ m grain-size  
fraction.  
% I in I/S (R parameter):  
40 (R0)



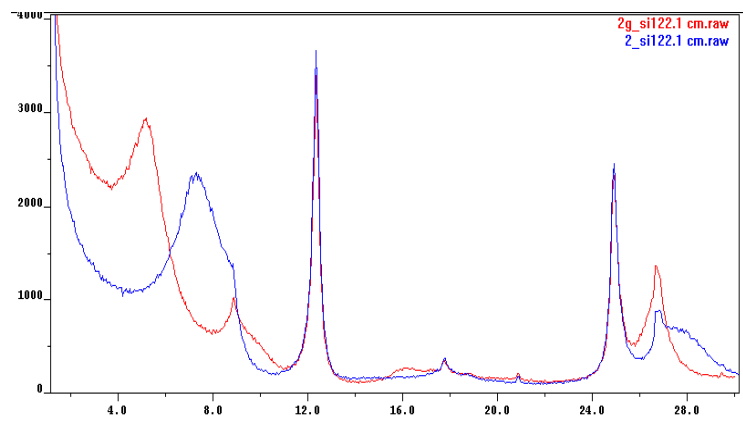


**SI 122.1 (37a)**

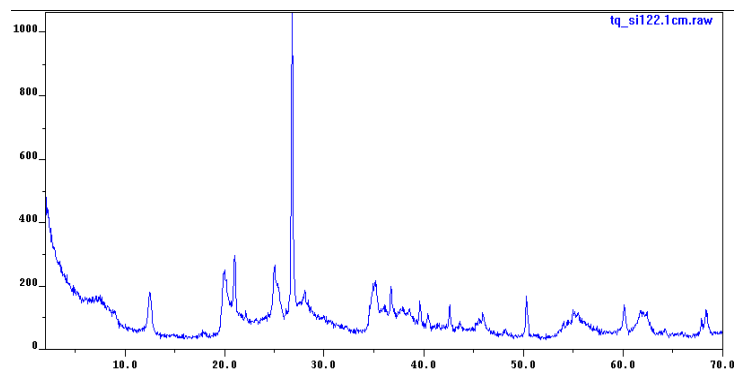
Outcrop photo



Diffraction patterns in  
the <2- $\mu$ m grain-size  
fraction.  
% I in I/S (R parameter):  
40 (R0)

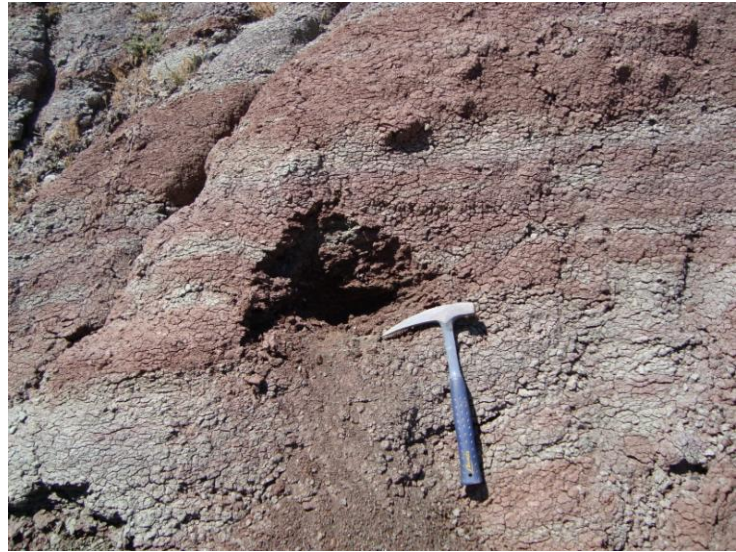


Whole rock diffraction  
pattern

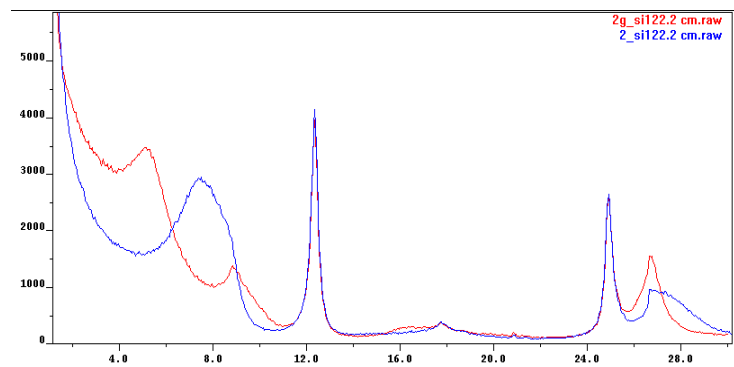


**SI 122.2 (37b)**

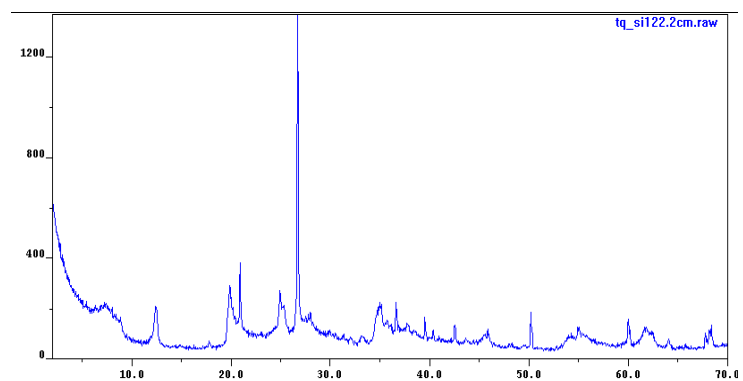
Outcrop photo



Diffraction patterns in  
the <2- $\mu$ m grain-size  
fraction.  
% I in I/S (R parameter):  
40 (R0)



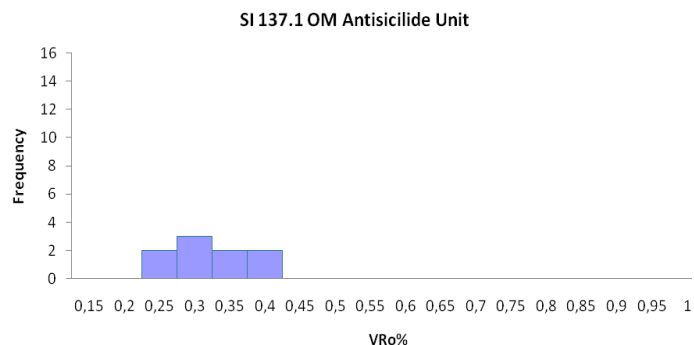
Whole rock diffraction  
pattern



## SI 137.1 (41)

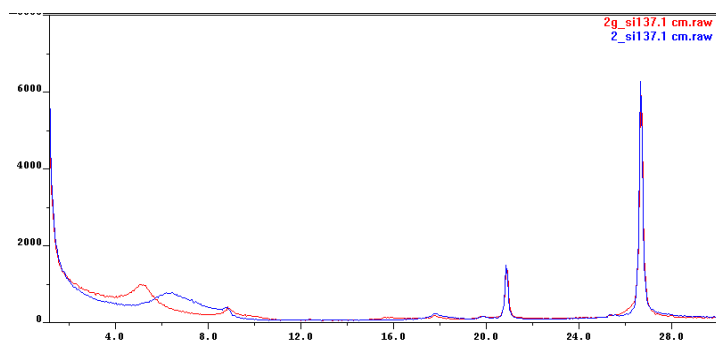
Vitrinite reflectance  
histogram.

VR<sub>o</sub>% (n.  
measurements):  
0.35±0.05(9)

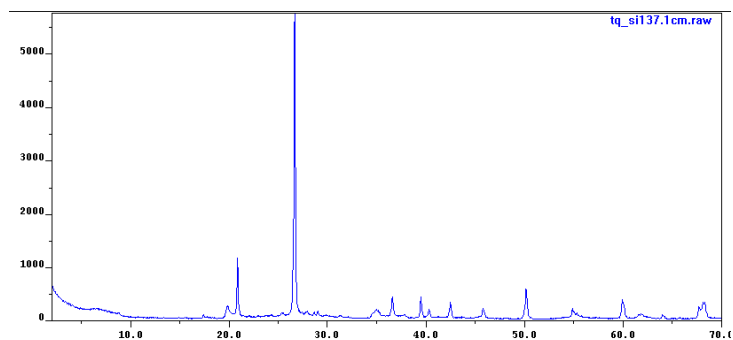


Diffraction patterns in  
the <2-μm grain-size  
fraction.

% I in I/S (R parameter):  
27 (R0)



Whole rock diffraction  
pattern

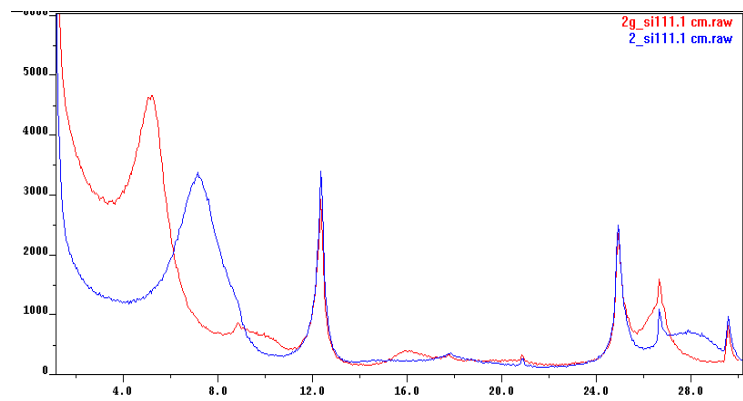


**SI 111.1 (45a)**

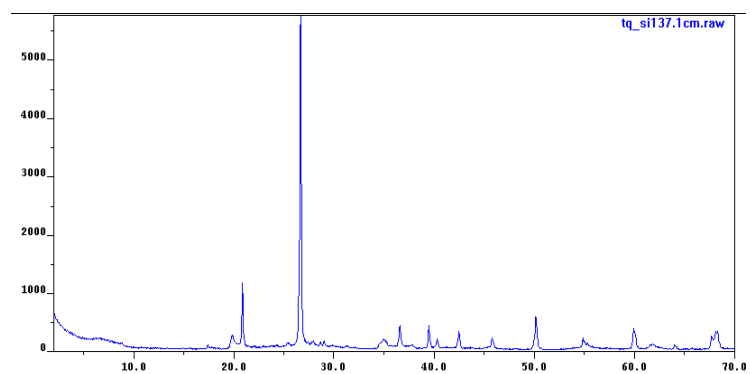
Outcrop photo



Diffraction patterns in  
the <2- $\mu$ m grain-size  
fraction.  
% I in I/S (R parameter):  
32 (R0)

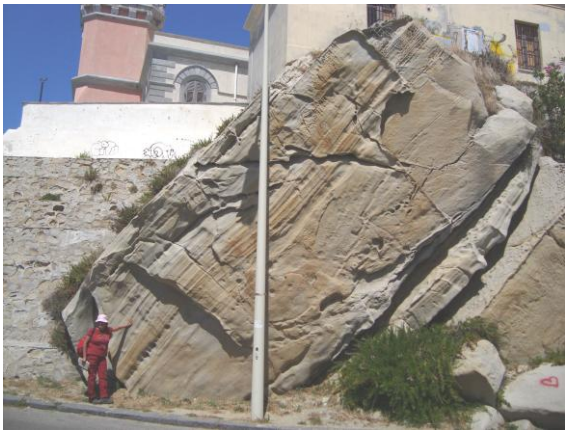


Whole rock diffraction  
pattern

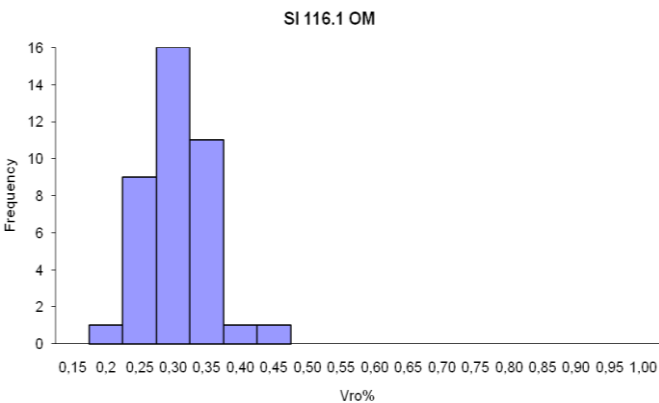


**Stilo-Capo  
d'Orlando  
Formation  
SI 116.1 (1a)**

Outcrop photo

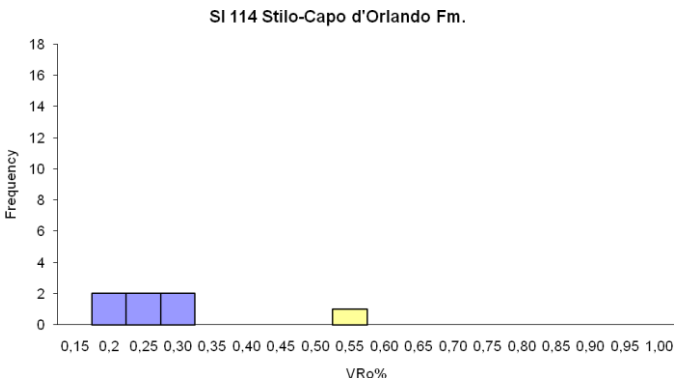


Vitrinite reflectance  
histogram.  
VR<sub>o</sub>% (n.  
measurements):  
0.33±0.04(39)



**SI 114.1 (1)**

Vitrinite reflectance  
histogram.  
VR<sub>o</sub>% (n.  
measurements):  
0.29±0.07 (6)

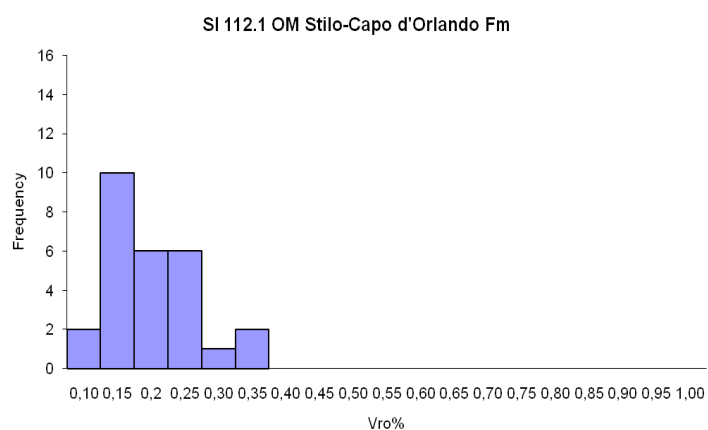


**SI 112.1 (1b)**

Outcrop photo



Vitrinite reflectance  
histogram.  
 $VR_o\%$  (n.  
measurements):  
 $0.22 \pm 0.07(27)$



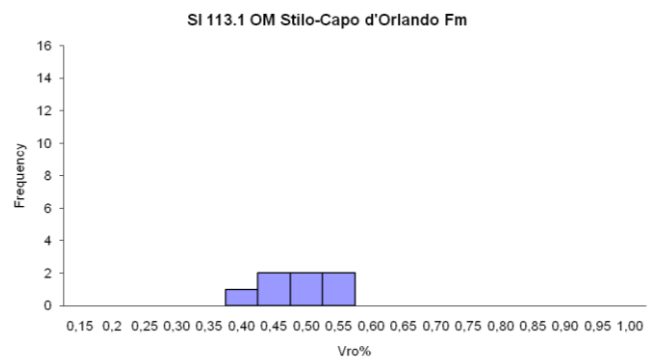
**SI 113.1 (1c)**

Outcrop photo



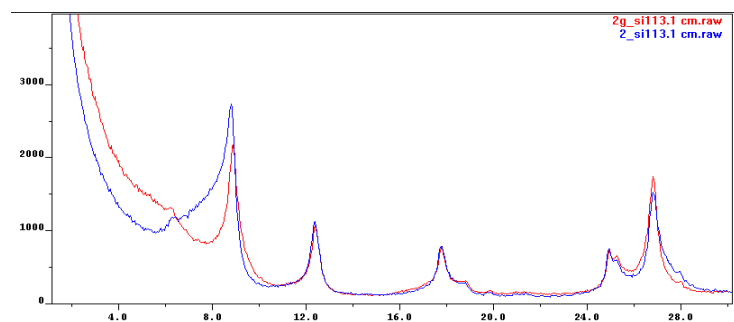
Vitrinite reflectance histogram.

VR<sub>0</sub>% (n. measurements):  
0.52±0.05(7)

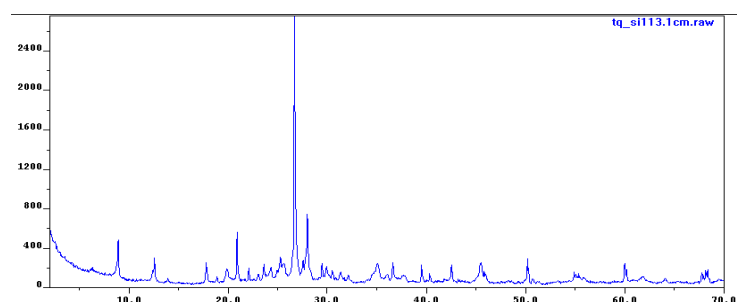


Diffraction patterns in the <2-μm grain-size fraction.

% I in I/S (R parameter):  
45; 76 (R0; R1)



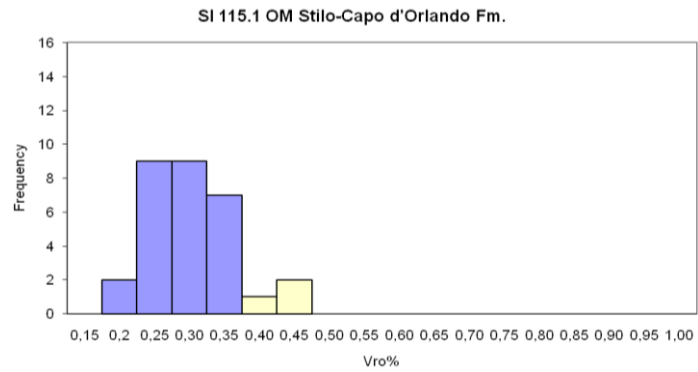
Whole rock diffraction pattern



# SI 115.1 (1d)

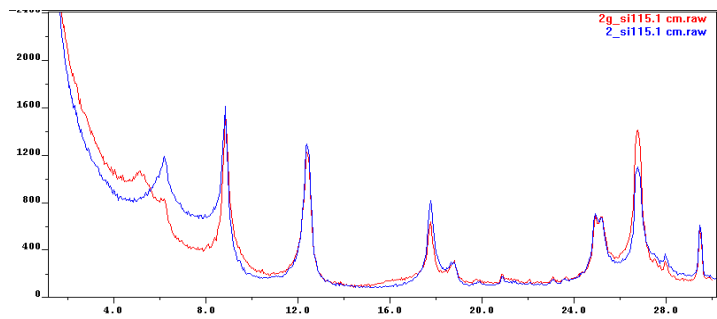
Vitrinite reflectance  
histogram.

VR<sub>o</sub>% (n.  
measurements):  
0.32±0.04(27)

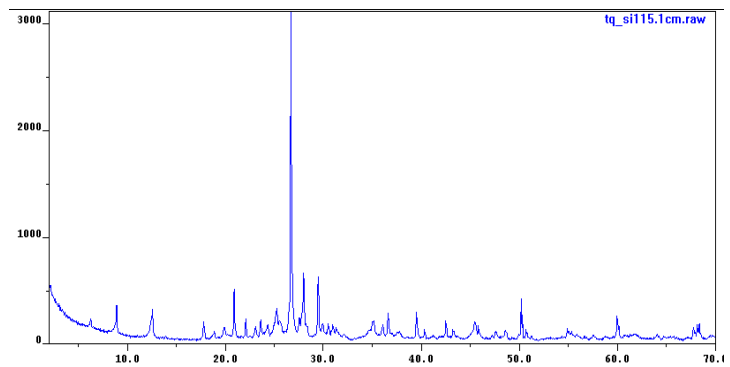


Diffraction patterns in  
the <2-μm grain-size  
fraction.

% I in I/S (R parameter):  
42; 78 (R0; R1)



Whole rock diffraction  
pattern

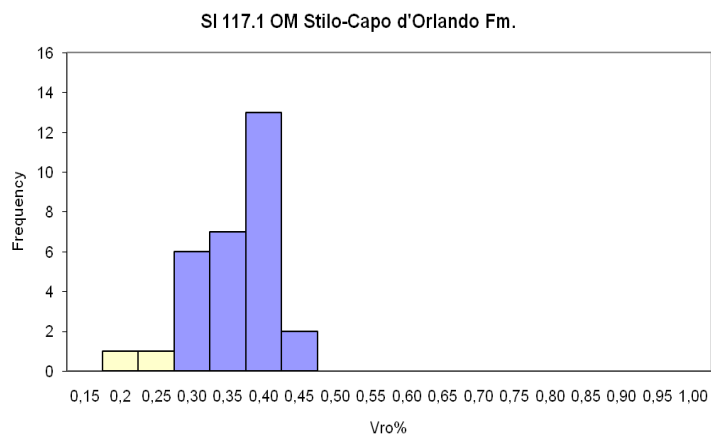




### SI 117.1 (1e)

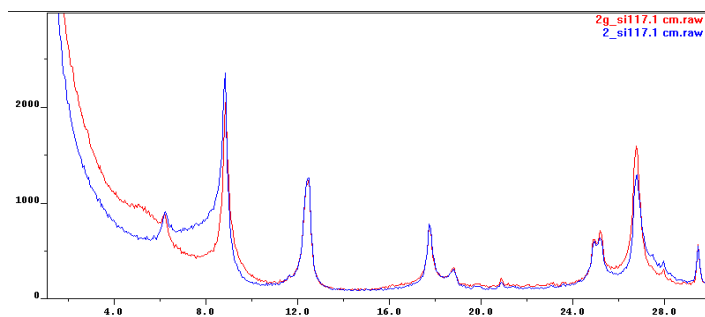
Vitrinite reflectance  
histogram.

VR<sub>o</sub>% (n.  
measurements):  
0.40±0.05(28)

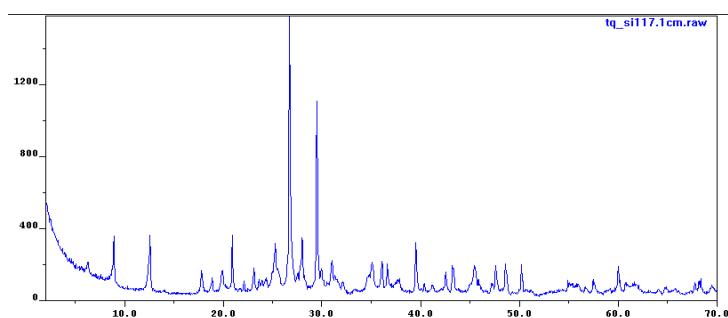


Diffraction patterns in  
the <2-μm grain-size  
fraction.

% I in I/S (R parameter):  
42; 80 (R0; R1)



Whole rock diffraction  
pattern

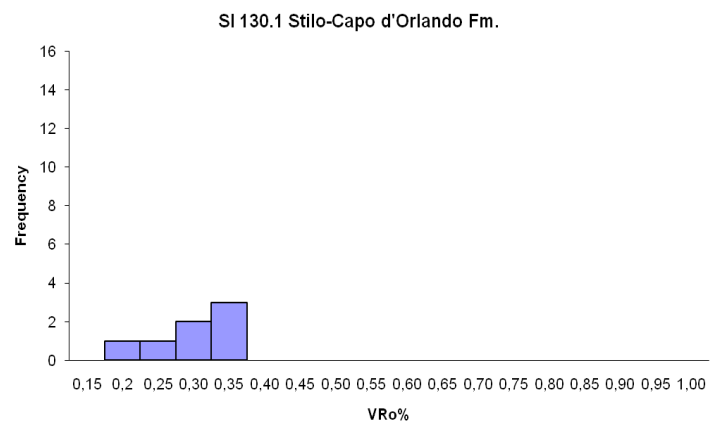


**SI 130.1 (3)**

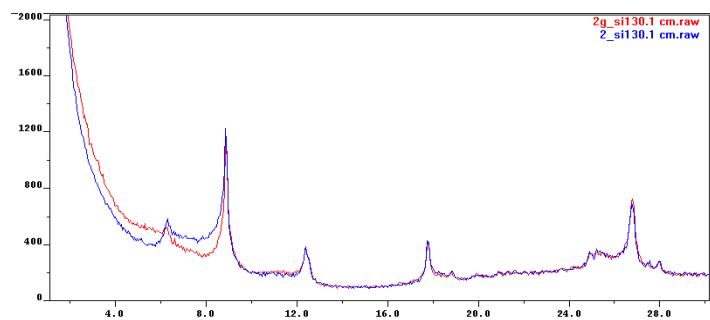
Outcrop photo



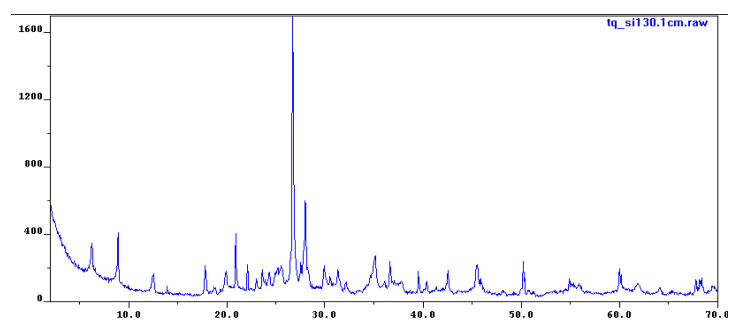
Vitrinite reflectance  
histogram.  
VR<sub>o</sub>% (n.  
measurements):  
0.33±0.06(7)



Diffraction patterns in  
the <2-μm grain-size  
fraction.  
% I in I/S (R parameter):  
42 (R0)

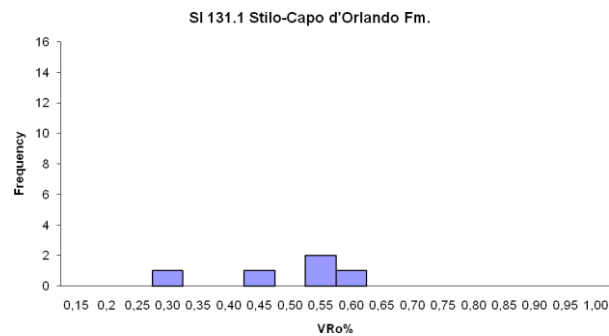


Whole rock diffraction  
pattern



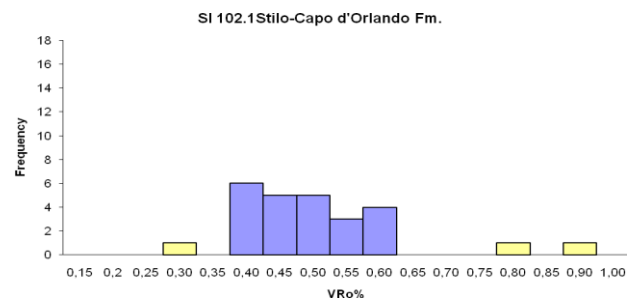
### SI 131.1 (4)

Vitrinite reflectance  
histogram.  
VR<sub>o</sub>% (n.  
measurements):  
N.D.



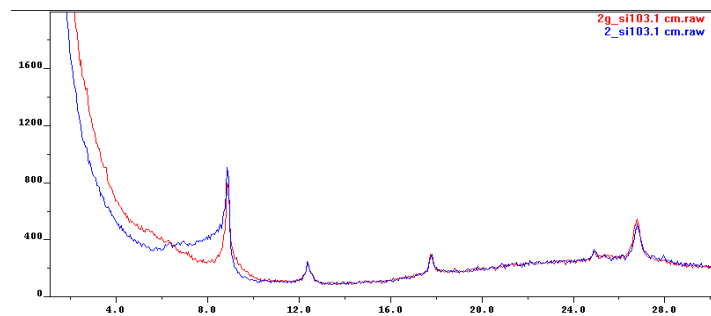
### SI 102.1 (5)

Vitrinite reflectance  
histogram.  
VR<sub>o</sub>% (n.  
measurements):  
0.52±0.07(23)

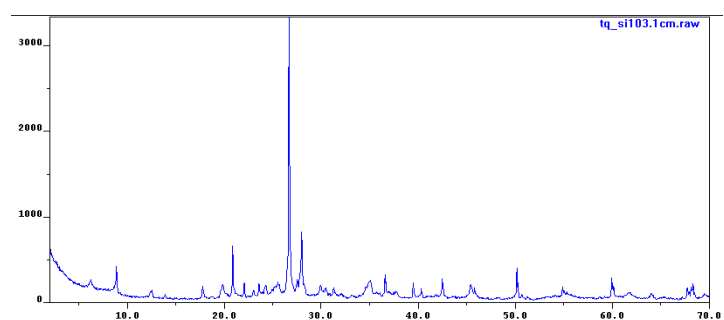


### SI 103.1 (6)

Diffraction patterns in  
the <2-μm grain-size  
fraction.  
% I in I/S (R parameter):  
425; 75 (R0; R1)



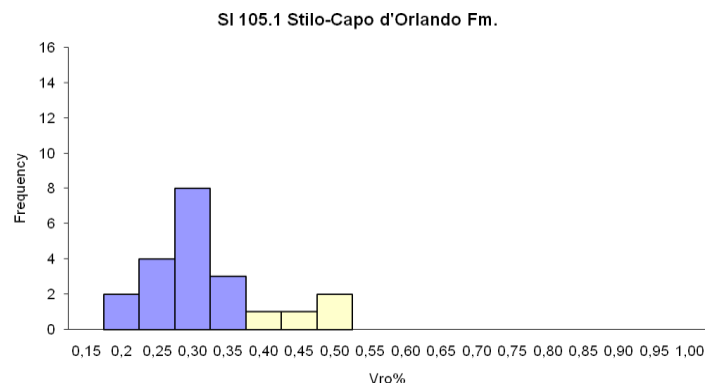
Whole rock diffraction  
pattern



### SI 105.1 (10)

Vitrinite reflectance  
histogram.

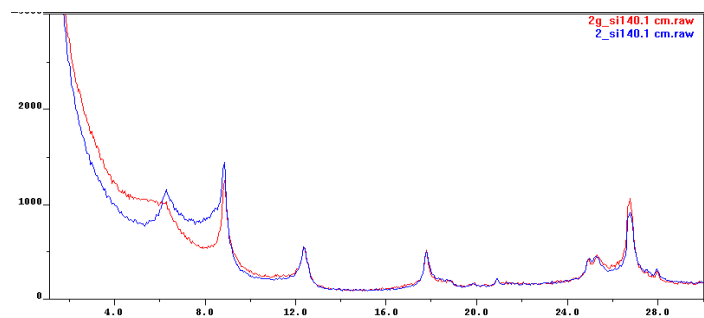
VR<sub>o</sub>% (n.  
measurements):  
0.31±0.05(19)



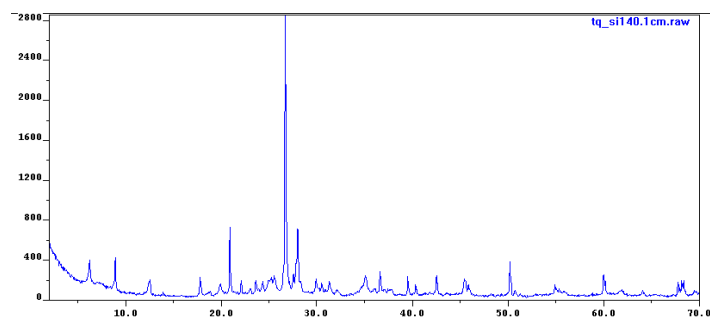
### SI 140.1 (18)

Diffraction patterns in  
the <2-μm grain-size  
fraction.

% I in I/S (R parameter):  
45; 78 (R0; R1)



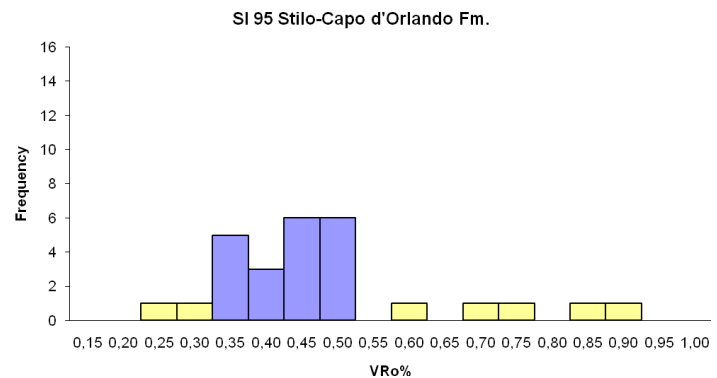
Whole rock diffraction  
pattern



## SI 95.1 (12)

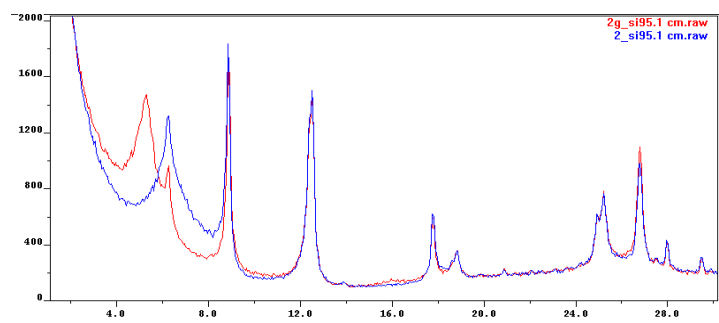
Vitrinite reflectance  
histogram.

VR<sub>0</sub>% (n.  
measurements):  
0.46±0.06 (20)

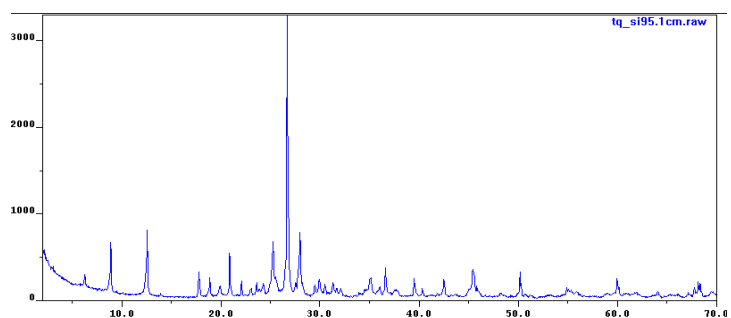


Diffraction patterns in  
the <2-μm grain-size  
fraction.

% I in I/S (R parameter):  
35 (R0)



Whole rock diffraction  
pattern



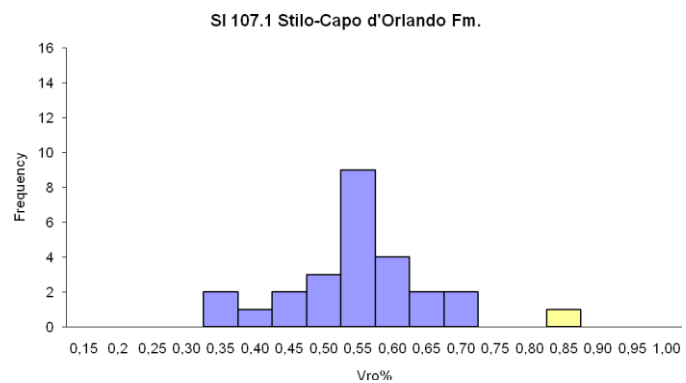
## SI 107.1 (13)

Outcrop photo



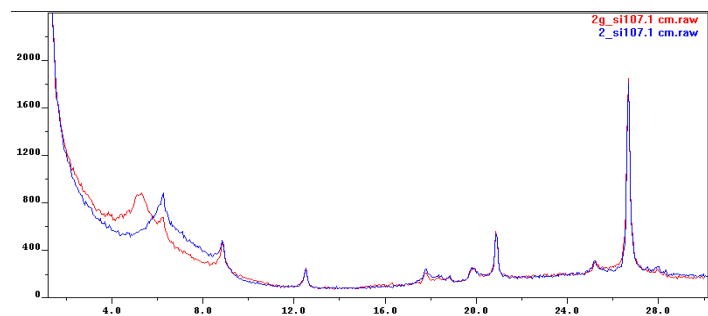
Vitrinite reflectance  
histogram.

$VR_o\%$  (n.  
measurements):  
 $0.58 \pm 0.08$  (22)

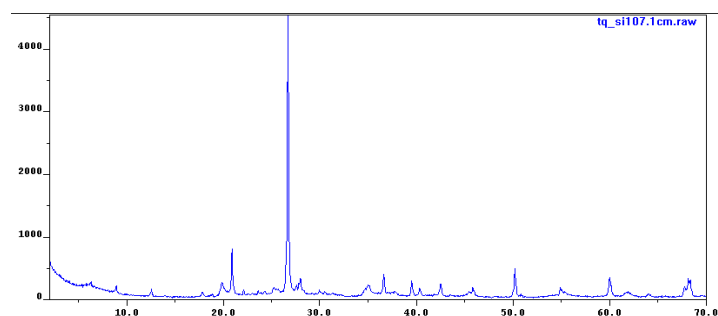


Diffraction patterns in  
the <2- $\mu$ m grain-size  
fraction.

% I in I/S (R parameter):  
20; 70 (R0; R1)



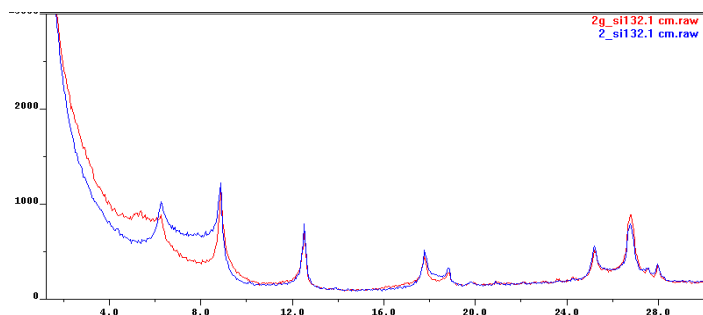
Whole rock diffraction  
pattern



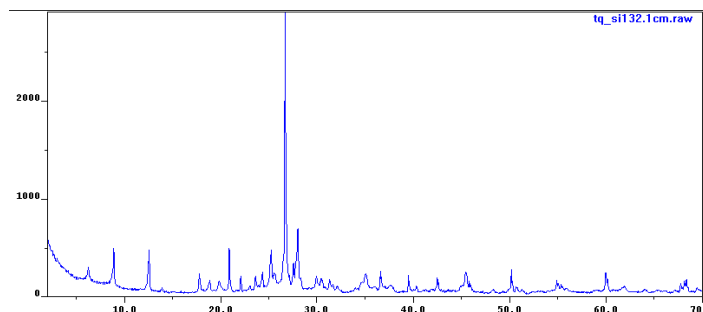
### SI 132.1 (20a)

Diffraction patterns in the <2- $\mu$ m grain-size fraction.

% I in I/S (R parameter):  
42; 78 (R0; R1)



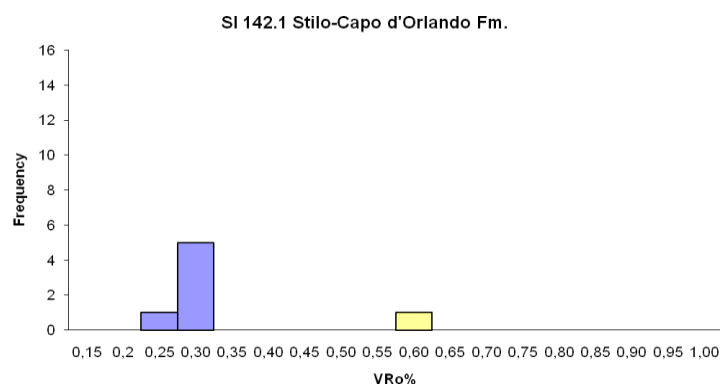
Whole rock diffraction pattern



### SI 142.2 (22)

Vitrinite reflectance histogram.

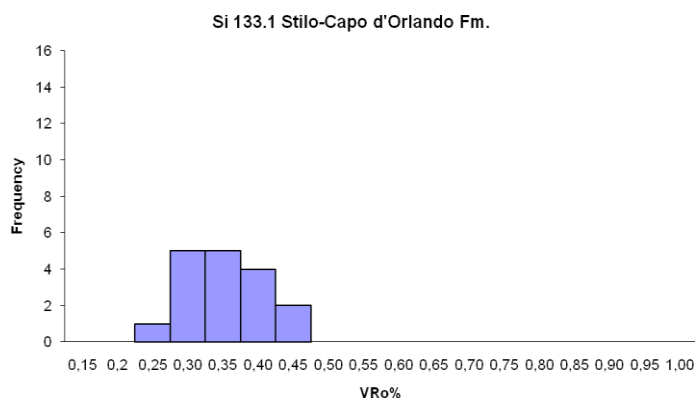
VR<sub>o</sub>% (n.  
measurements):  
0.31 $\pm$ 0.03 (6)



### SI 133.1 (20b)

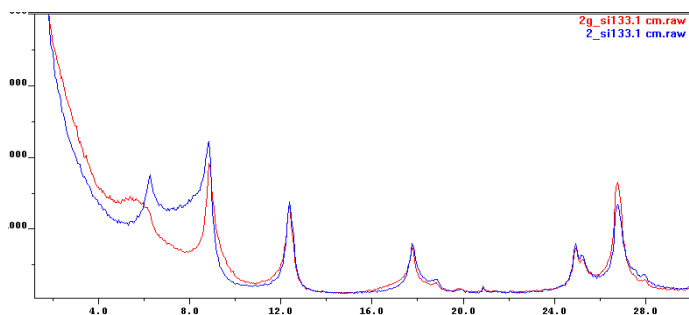
Vitrinite reflectance  
histogram.

VR<sub>o</sub>% (n.  
measurements):  
0.37±0.06 (17)



Diffraction patterns in  
the <2-μm grain-size  
fraction.

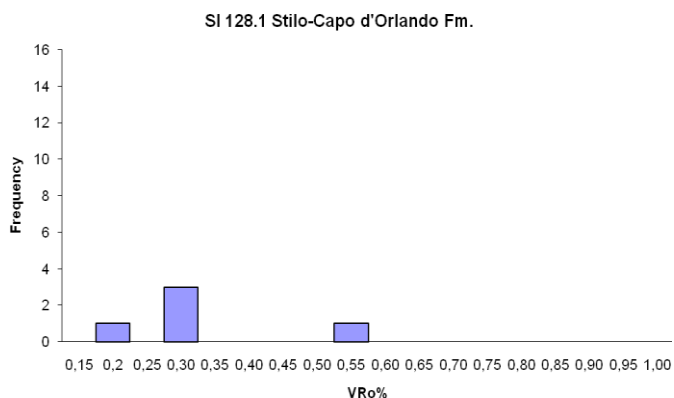
% I in I/S (R parameter):  
41; 80 (R0; R1)



### SI 128.1 (23)

Vitrinite reflectance  
histogram.

VR<sub>o</sub>% (n.  
measurements):  
0.33±0.004 (3)





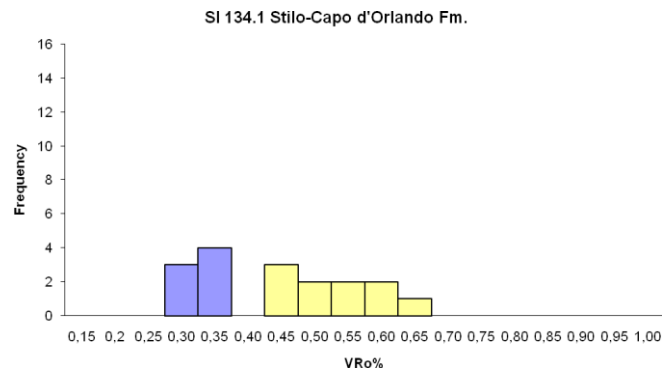
**SI 134.1 (21)**

Outcrop photo



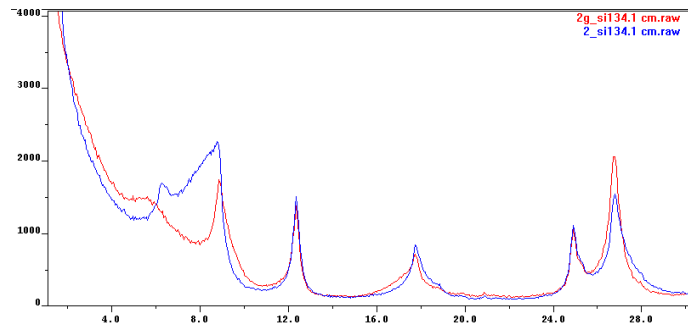
Vitrinite reflectance histogram.

VR<sub>o</sub>% (n. measurements):  
0.35±0.03 (7)

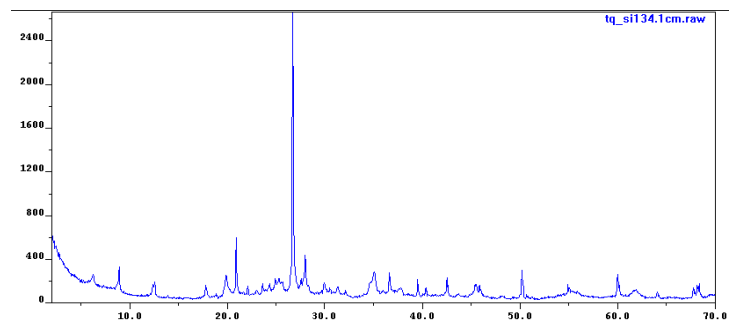


Diffraction patterns in the <2-μm grain-size fraction.

% I in I/S (R parameter):  
50; 80 (R<sub>0</sub>; R<sub>1</sub>)

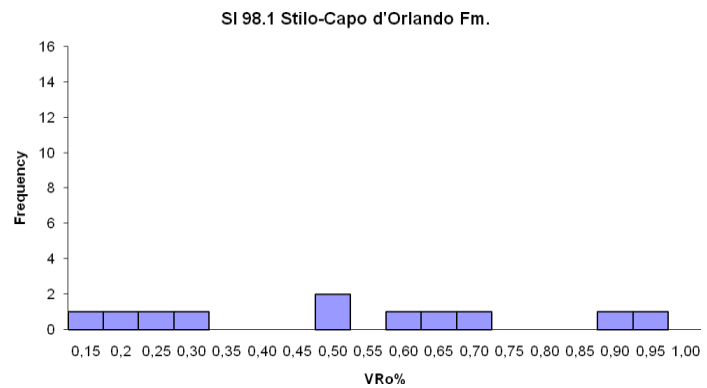


Whole rock diffraction pattern

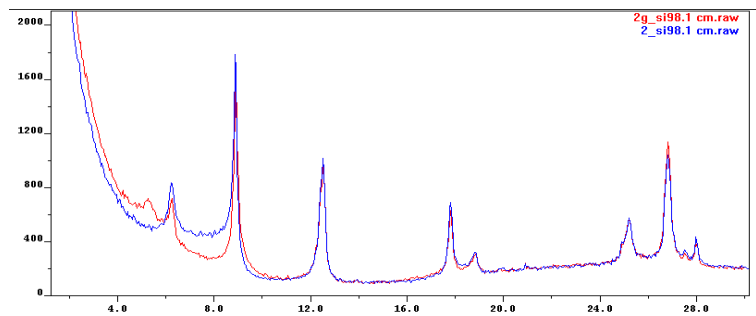


**SI 98.1 (28)**

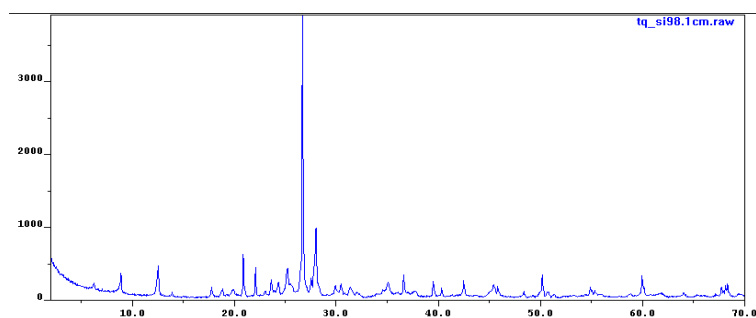
Vitrinite reflectance  
histogram.  
VR<sub>o</sub>% (n.  
measurements):  
N.D.



Diffraction patterns in  
the <2- $\mu$ m grain-size  
fraction.  
% I in I/S (R parameter):  
50; 80 (R0; R1)



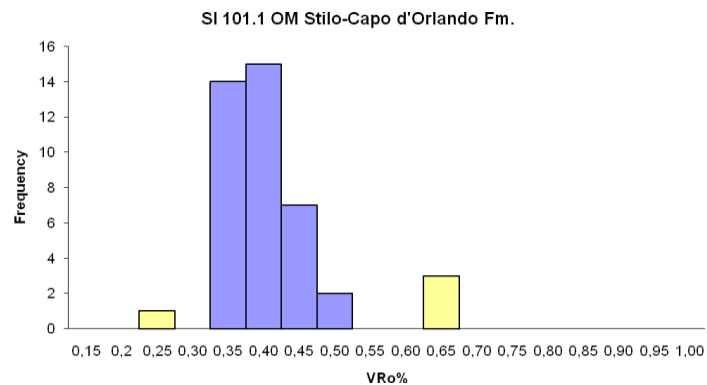
Whole rock diffraction  
pattern



## SI 101.1 (25)

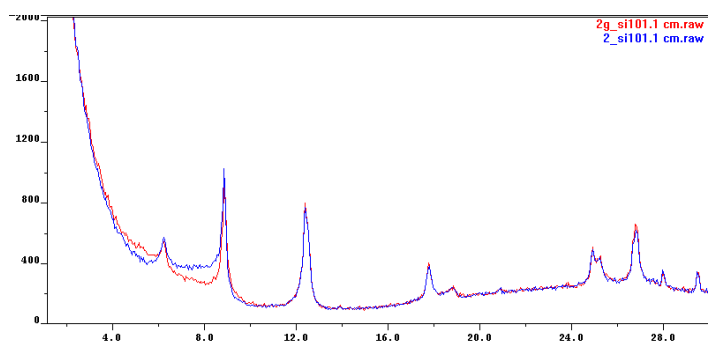
Vitrinite reflectance  
histogram.

VR<sub>o</sub>% (n.  
measurements):  
0.41±0.05 (38)

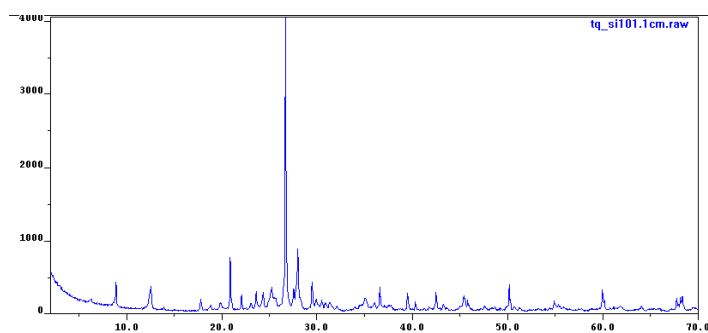


Diffraction patterns in  
the <2-μm grain-size  
fraction.

% I in I/S (R parameter):  
45; 60 (R0; R1)



Whole rock diffraction  
pattern

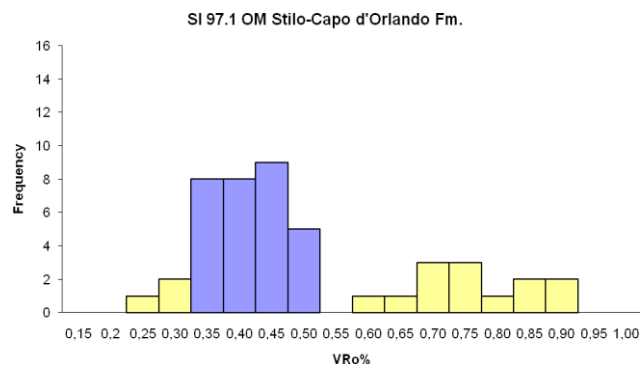


**SI 97.1 (26)**

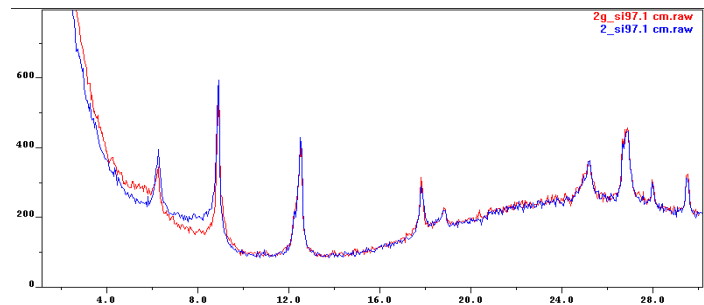
Outcrop photo



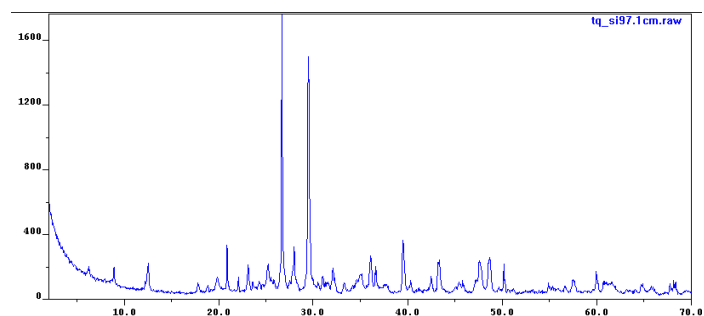
Vitrinite reflectance histogram.  
VR<sub>o</sub>% (n. measurements):  
0.44±0.05 (30)



Diffraction patterns in the <2-μm grain-size fraction.  
% I in I/S (R parameter):  
45; 60 (R0; R1)



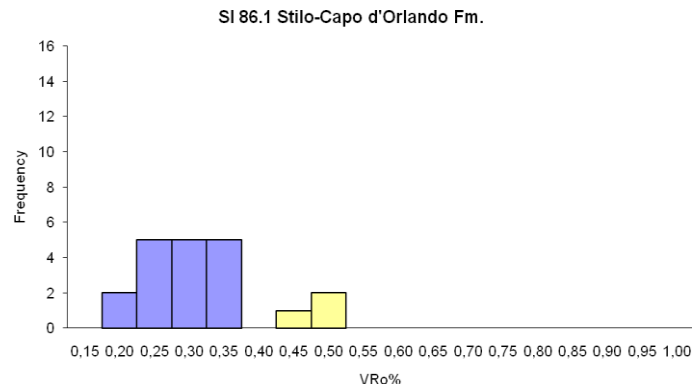
Whole rock diffraction pattern



**SI 86.1 (27)**

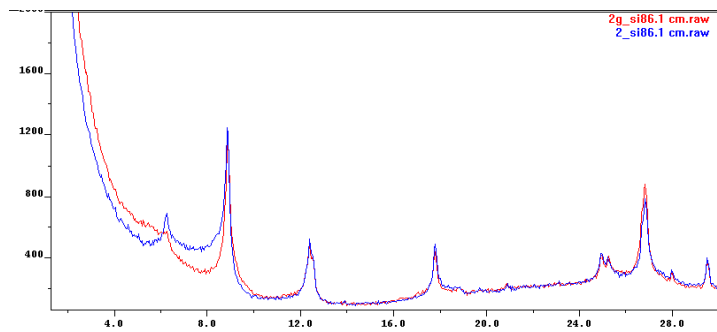
Vitrinite reflectance  
histogram.

VR<sub>o</sub>% (n.  
measurements):  
0.31±0.05 (17)

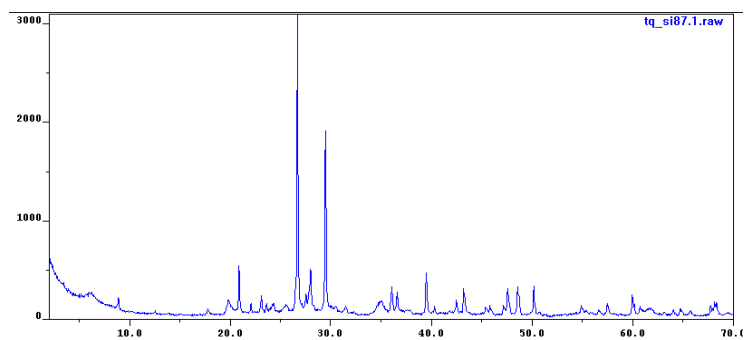


Diffraction patterns in  
the <2-μm grain-size  
fraction.

% I in I/S (R parameter):  
52 (R0)



Whole rock diffraction  
pattern



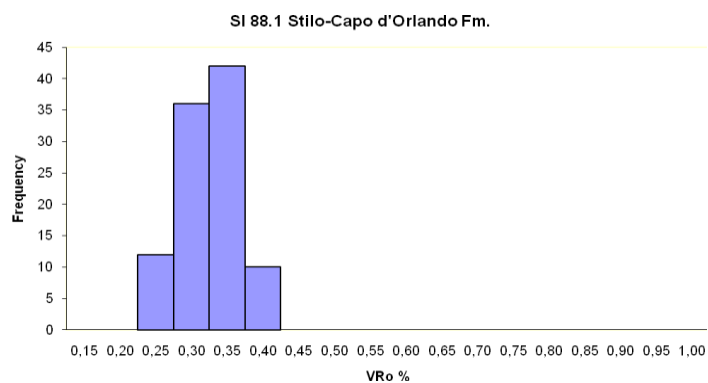
**SI 88.1 OM (31a)**

Outcrop photo

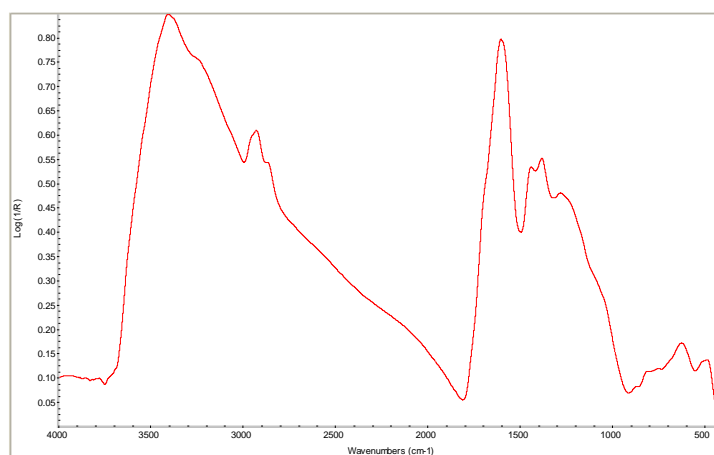


Vitrinite reflectance  
histogram.

VR<sub>o</sub>% (n.  
measurements):  
0.35±0.04 (100)



FTIR spectrum

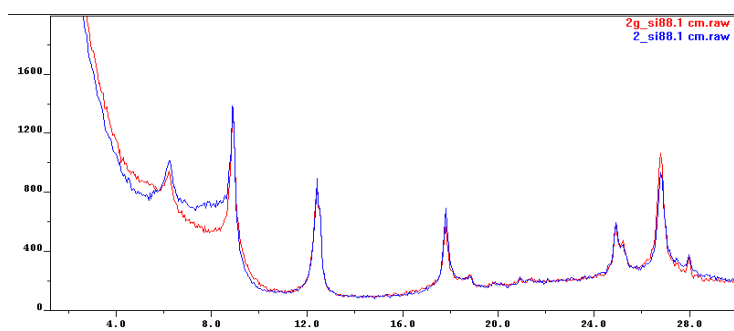


**SI 88.1 CM (31b)**

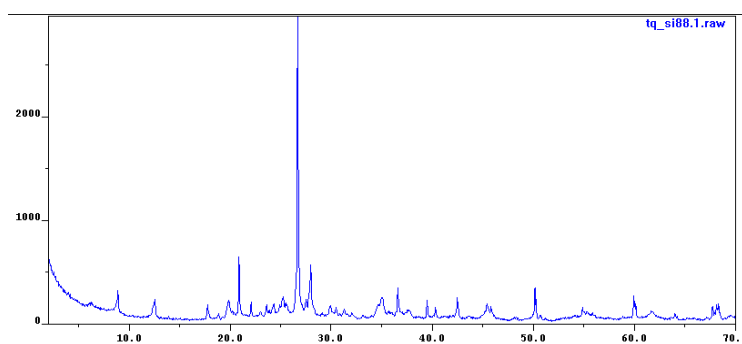
Outcrop photo



Diffraction patterns in  
the <2- $\mu$ m grain-size  
fraction.  
% I in I/S (R parameter):  
52 (R0)



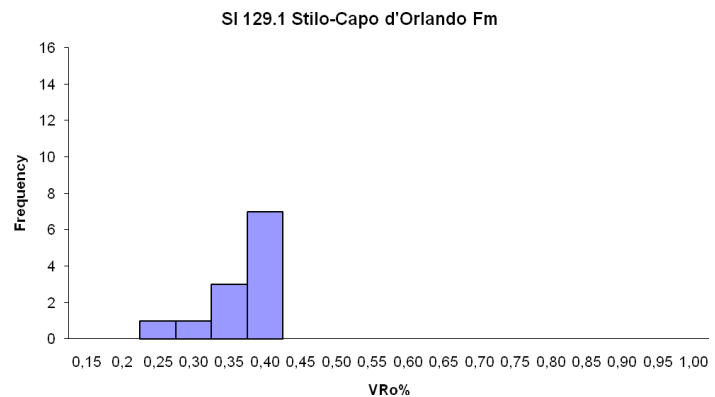
Whole rock diffraction  
pattern



## SI 129.1 (32)

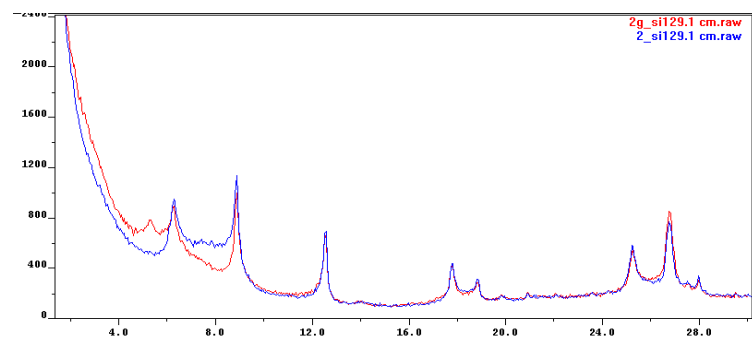
Vitrinite reflectance  
histogram.

VR<sub>0</sub>% (n.  
measurements):  
0.38±0.05 (12)

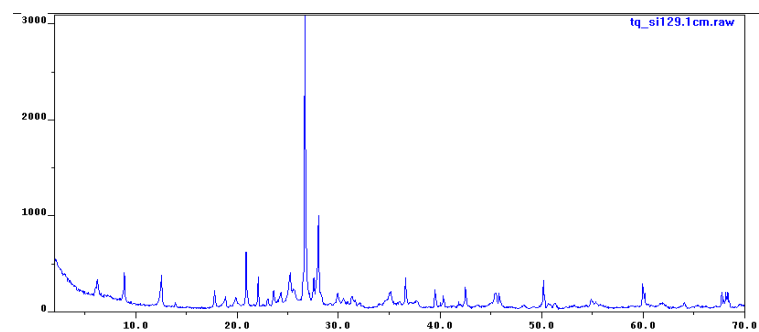


Diffraction patterns in  
the <2-μm grain-size  
fraction.

% I in I/S (R parameter):  
42; 80 (R0; R1)



Whole rock diffraction  
pattern





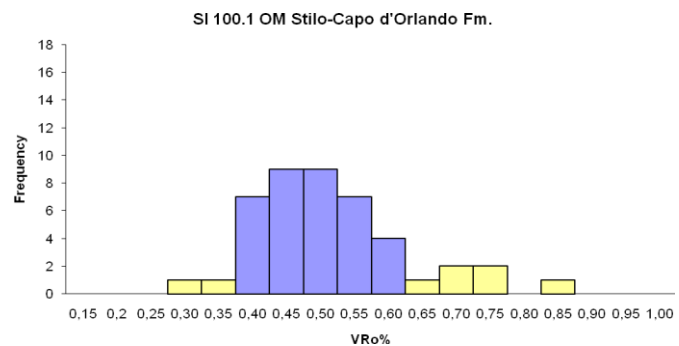
**SI 100.1 (33)**

Outcrop photo



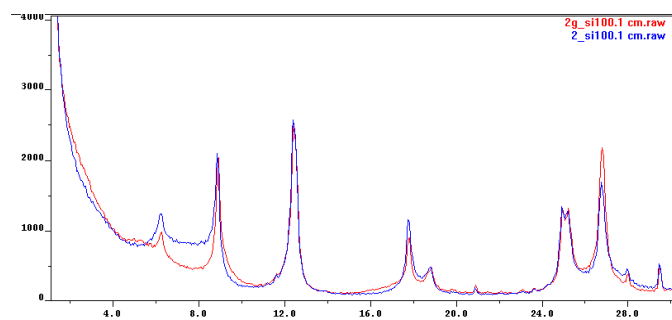
Vitrinite reflectance  
histogram.

VR<sub>o</sub>% (n.  
measurements):  
0.51±0.06 (36)

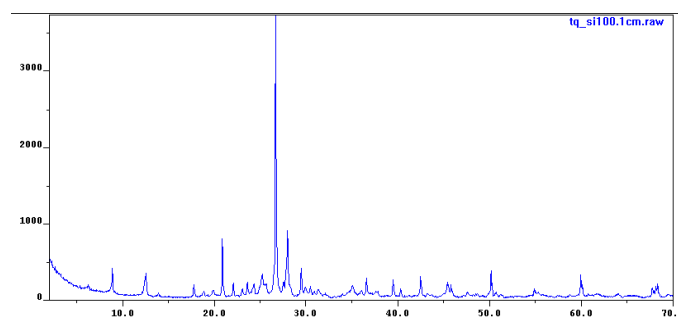


Diffraction patterns in  
the <2-μm grain-size  
fraction.

% I in I/S (R parameter):  
41; 83 (R0; R1)



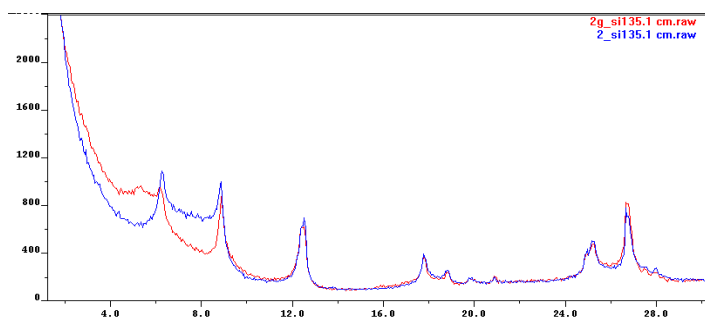
Whole rock diffraction  
pattern



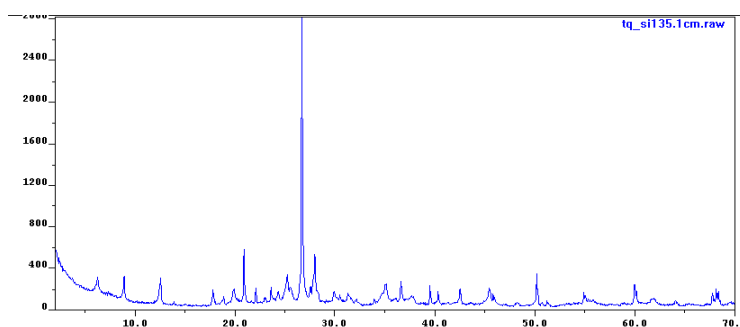
### SI 135.1 (34)

Diffraction patterns in the <2- $\mu$ m grain-size fraction.

% I in I/S (R parameter):  
35; 80 (R0; R1)



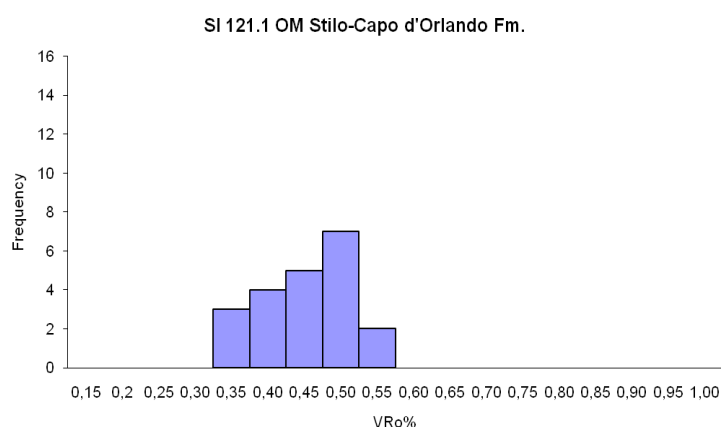
Whole rock diffraction pattern



### SI 121.1 (40)

Vitrinite reflectance histogram.

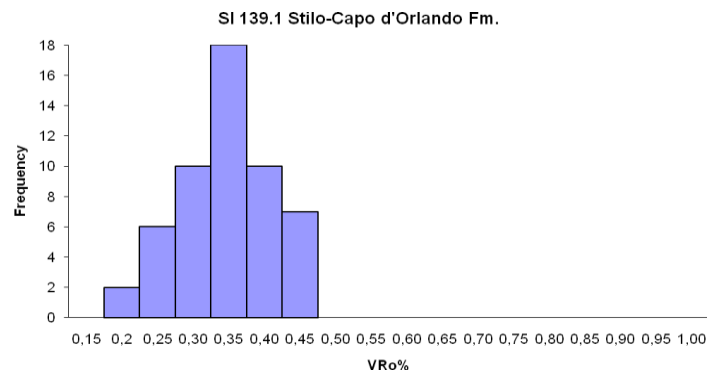
VR<sub>o</sub>% (n.  
measurements):  
0.48 $\pm$ 0.06 (21)



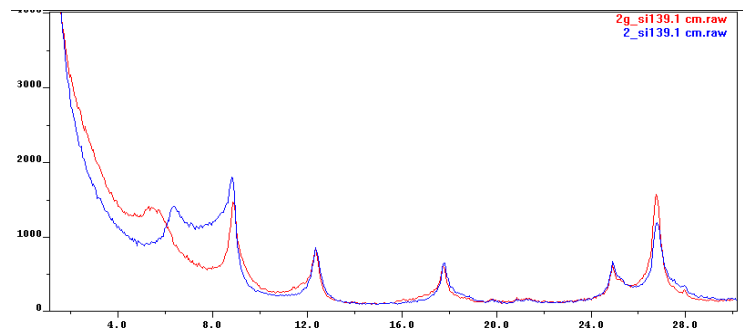
# SI 139.1 (36)

Vitrinite reflectance  
histogram.

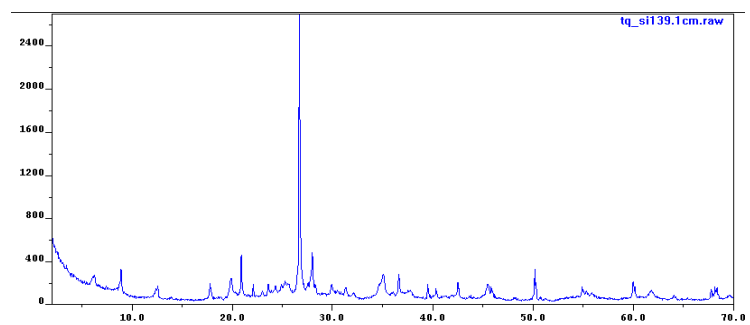
VR<sub>o</sub>% (n.  
measurements):  
0.48±0.06 (21)



Diffraction patterns in  
the <2-μm grain-size  
fraction.  
% I in I/S (R parameter):  
45; 80 (R0; R1)



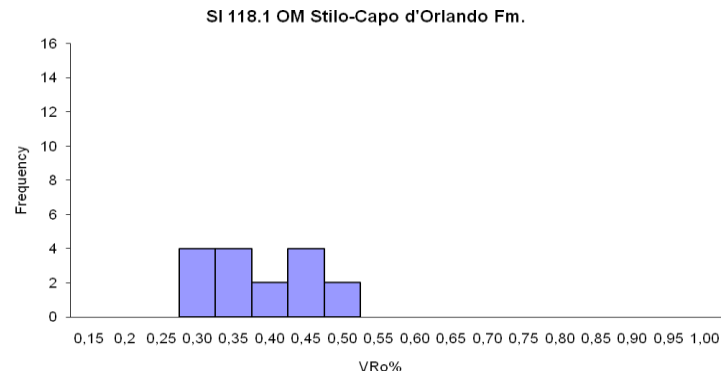
Whole rock diffraction  
pattern



### SI 118.1 (43)

Vitrinite reflectance  
histogram.

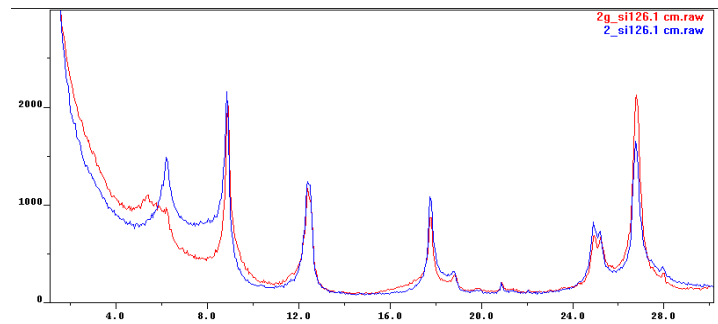
VR<sub>o</sub>% (n.  
measurements):  
0.42±0.07 (16)



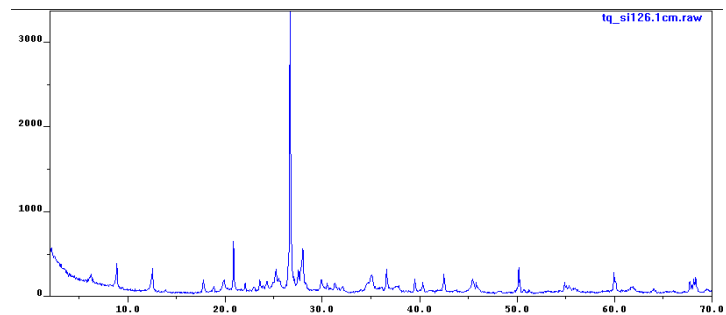
### SI 126.1 (48)

Diffraction patterns in  
the <2-μm grain-size  
fraction.

% I in I/S (R parameter):  
50; 80 (R0; R1)



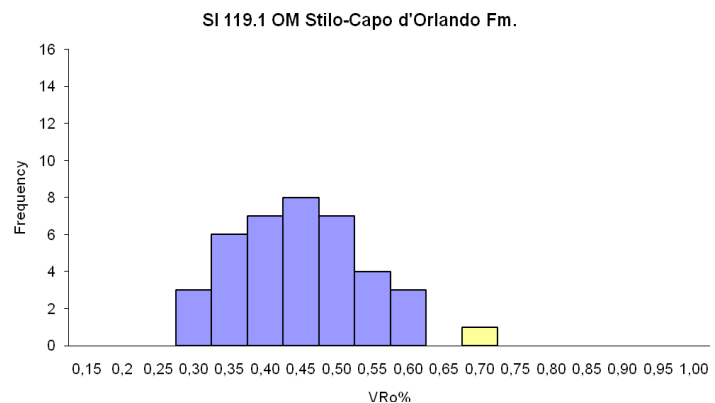
Whole rock diffraction  
pattern



## SI 119.1 (44)

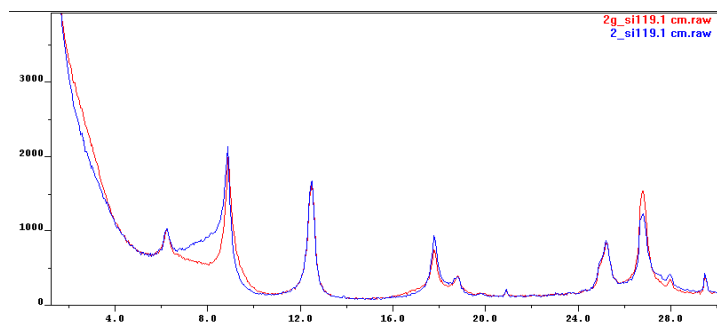
Vitrinite reflectance  
histogram.

VR<sub>o</sub>% (n.  
measurements):  
0.47±0.08 (39)

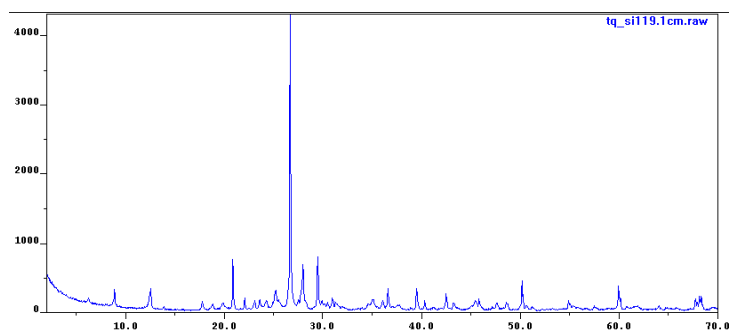


Diffraction patterns in  
the <2-μm grain-size  
fraction.

% I in I/S (R parameter):  
60 (R1)



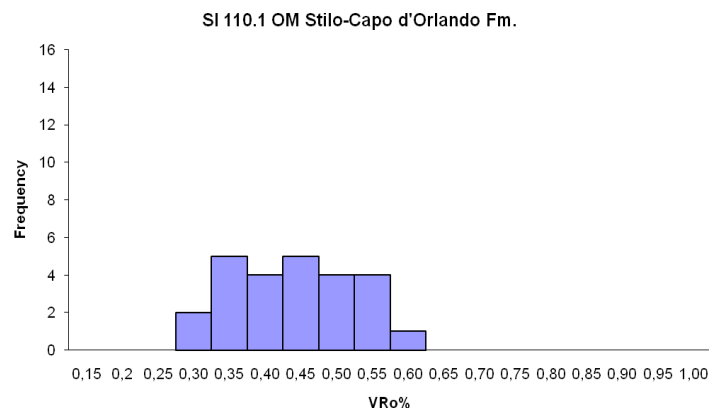
Whole rock diffraction  
pattern



### SI 110.1 (46b)

Vitrinite reflectance  
histogram.

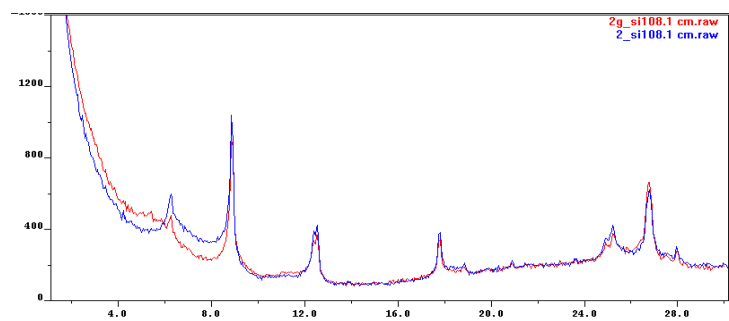
VR<sub>o</sub>% (n.  
measurements):  
0.47±0.09 (25)



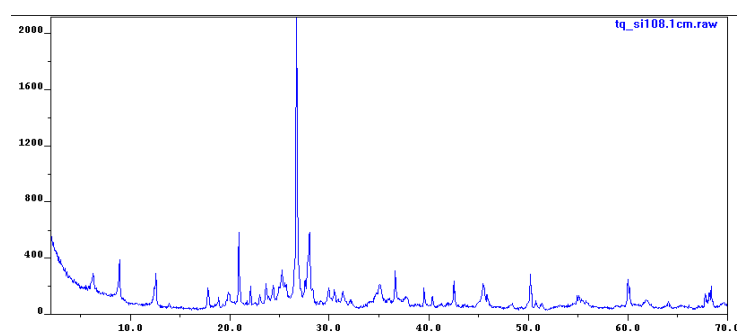
### SI 108.1 (46a)

Diffraction patterns in  
the <2-μm grain-size  
fraction.

% I in I/S (R parameter):  
42; 75 (R0; R1)



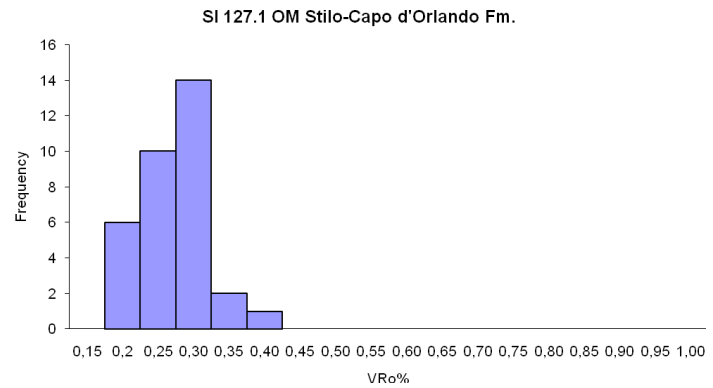
Whole rock diffraction  
pattern



## SI 127.1 (47)

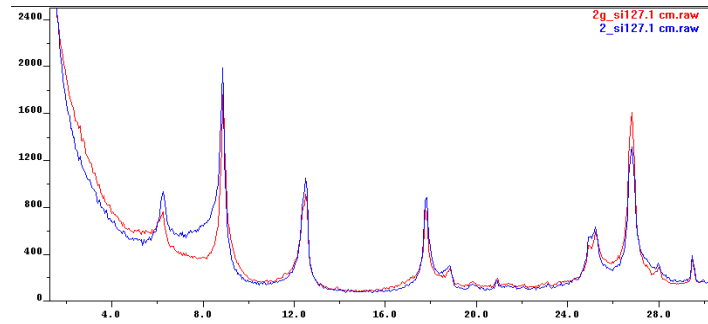
Vitrinite reflectance  
histogram.

VR<sub>o</sub>% (n.  
measurements):  
0.30±0.05 (33)

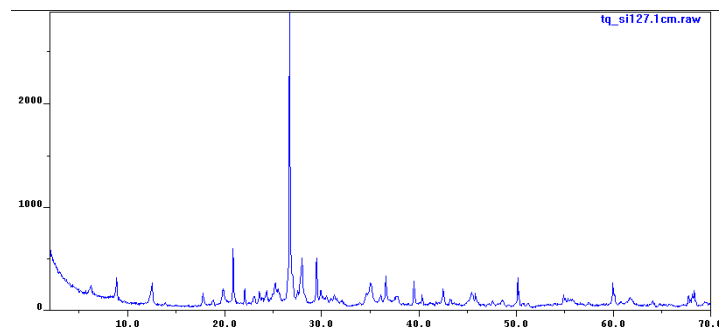


Diffraction patterns in  
the <2-μm grain-size  
fraction.

% I in I/S (R parameter):  
41; 78 (R0; R1)



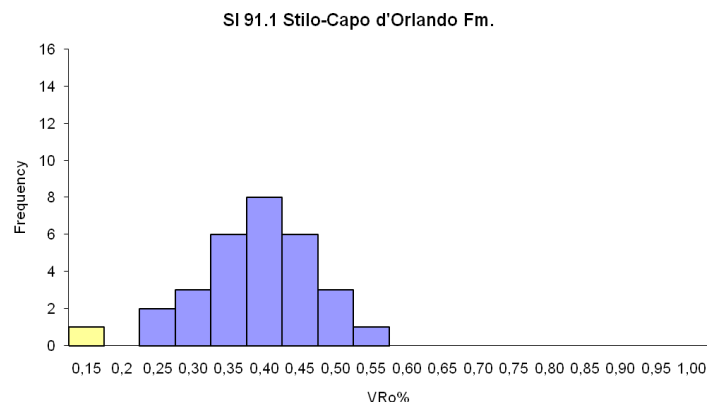
Whole rock diffraction  
pattern



## SI 91.1 (49)

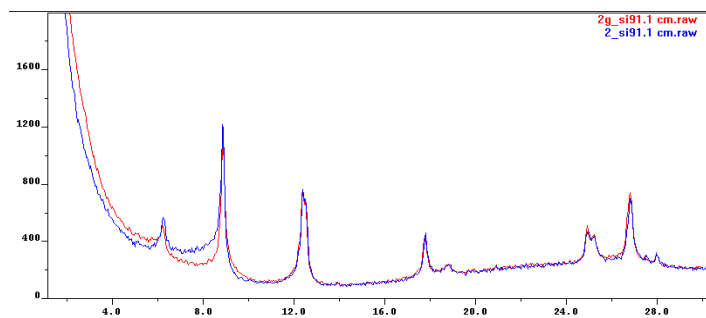
Vitrinite reflectance  
histogram.

VR<sub>o</sub>% (n.  
measurements):  
0.42±0.06 (29)

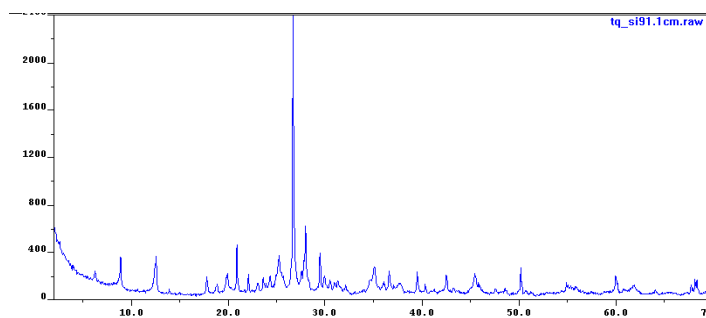


Diffraction patterns in  
the <2-μm grain-size  
fraction.

% I in I/S (R parameter):  
50 (R0)



Whole rock diffraction  
pattern

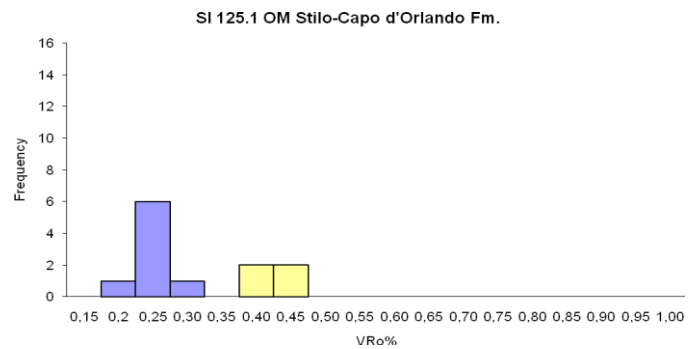




## SI 125.1 (50)

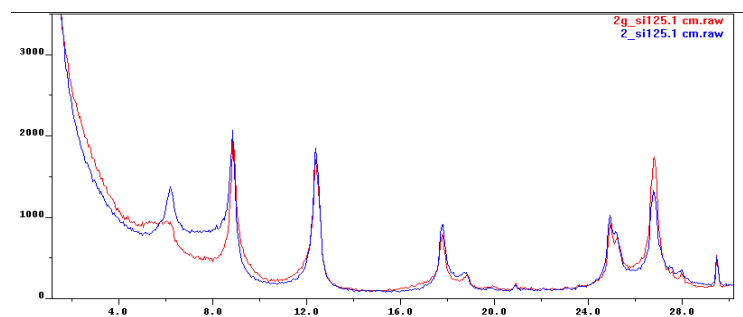
Vitrinite reflectance  
histogram.

VR<sub>0</sub>% (n.  
measurements):  
0.27±0.02 (8)

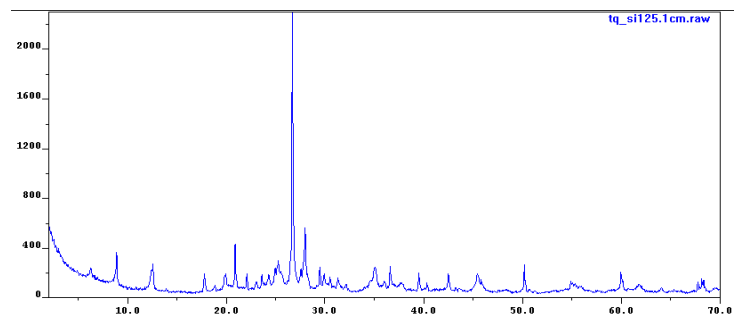


Diffraction patterns in  
the <2-μm grain-size  
fraction.

% I in I/S (R parameter):  
41; 78 (R0; R1)



Whole rock diffraction  
pattern



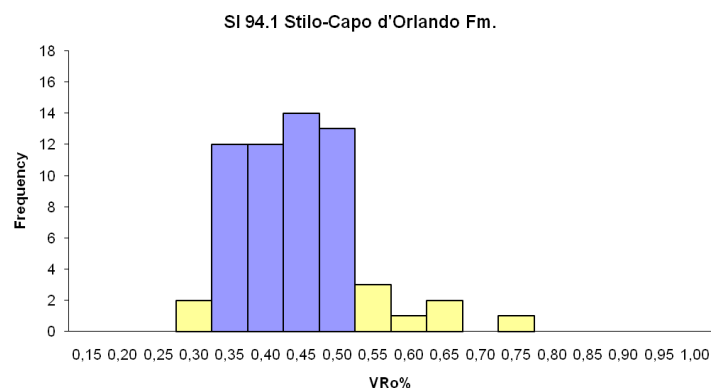
**SI 94.1 (51)**

Outcrop photo



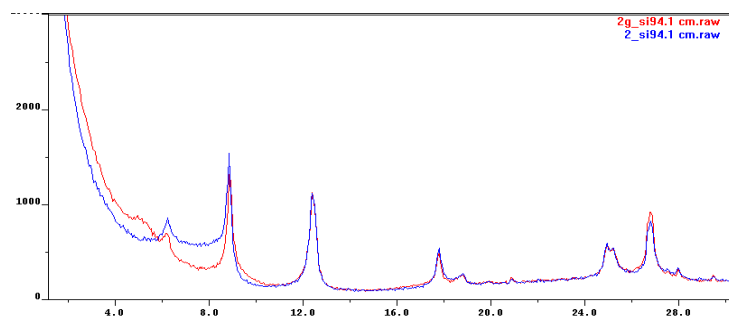
Vitrinite reflectance  
histogram.

VR<sub>o</sub>% (n.  
measurements):  
0.45±0.05 (51)

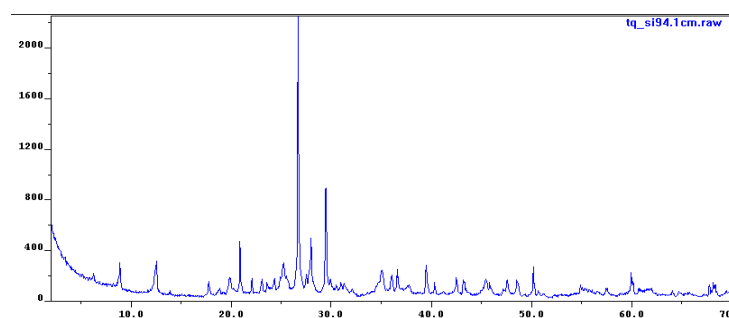


Diffraction patterns in  
the <2-μm grain-size  
fraction.

% I in I/S (R parameter):  
45; 75 (R0; R1)



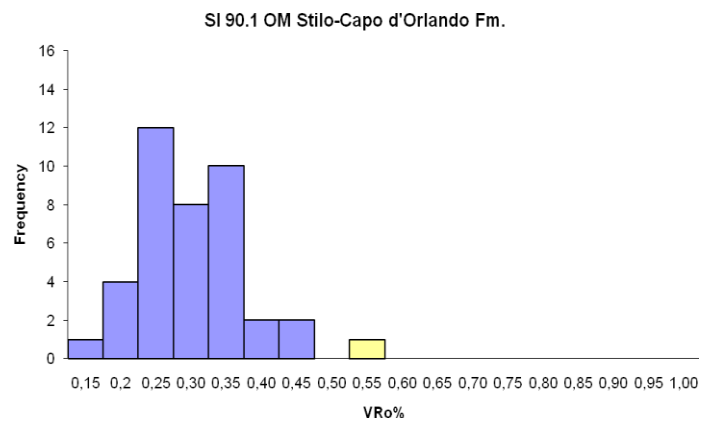
Whole rock diffraction  
pattern



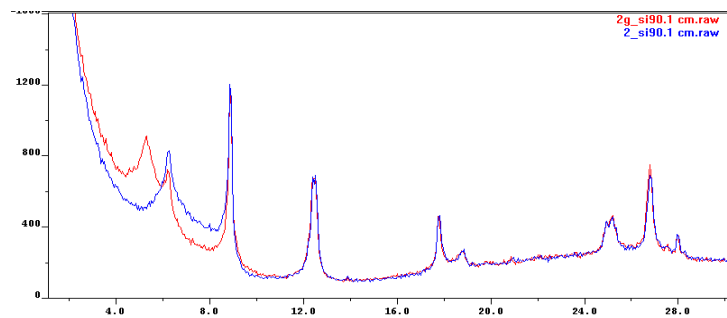
## SI 90.1 (55)

Vitrinite reflectance  
histogram.

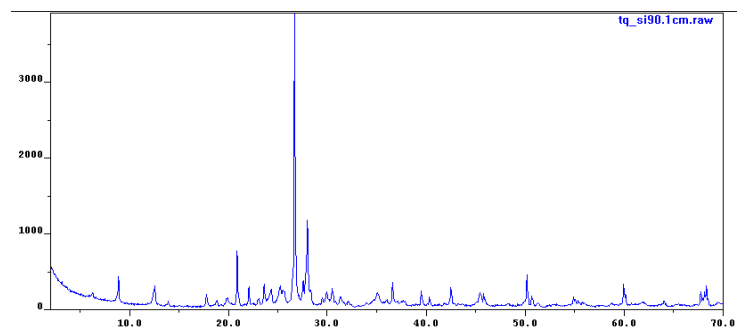
VR<sub>o</sub>% (n.  
measurements):  
0.31±0.05 (39)



Diffraction patterns in  
the <2-μm grain-size  
fraction.  
% I in I/S (R parameter):  
50 (R0)



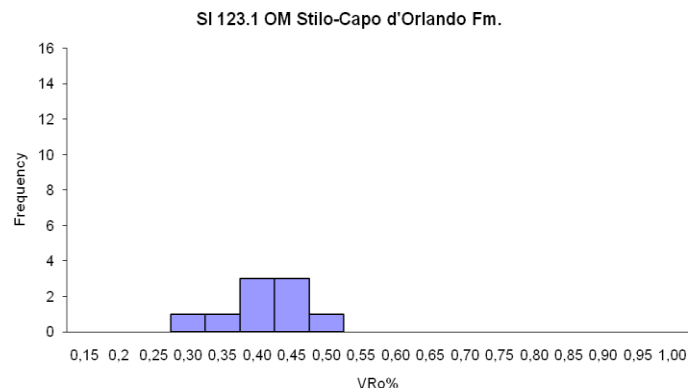
Whole rock diffraction  
pattern



**SI 123.1 (56)**

Vitrinite reflectance  
histogram.

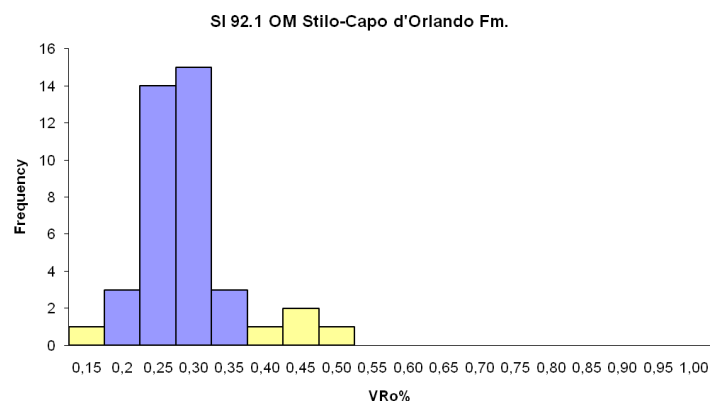
VR<sub>o</sub>% (n.  
measurements):  
0.43±0.06 (9)



**SI 92.1 (59)**

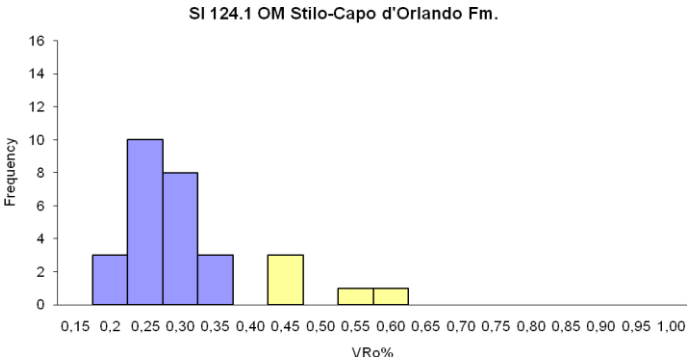
Vitrinite reflectance  
histogram.

VR<sub>o</sub>% (n.  
measurements):  
0.30±0.04 (30)

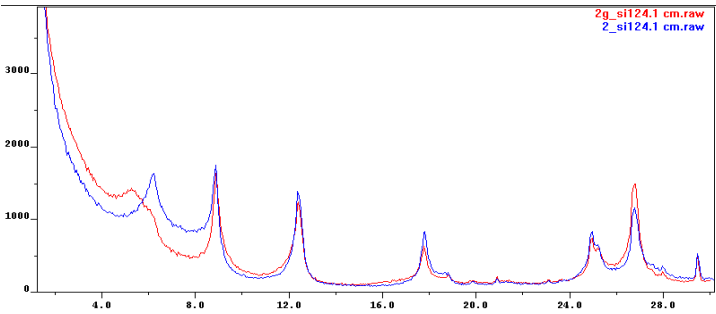


SI 124.1 (57)

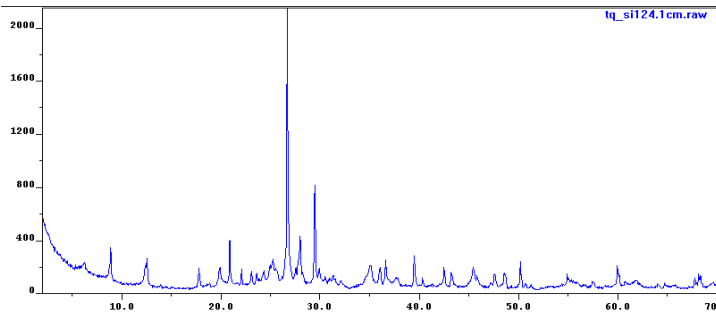
Vitrinite reflectance  
histogram.  
VR<sub>o</sub>% (n.  
measurements):  
0.30±0.04 (24)



Diffraction patterns in  
the <2-μm grain-size  
fraction.  
% I in I/S (R parameter):  
42; 76 (R0; R1)



Whole rock diffraction  
pattern

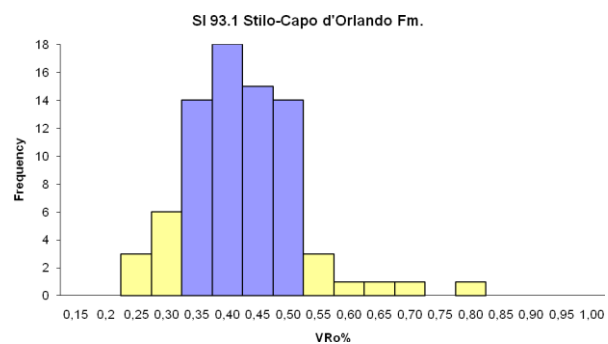


**SI 93.1 (58)**

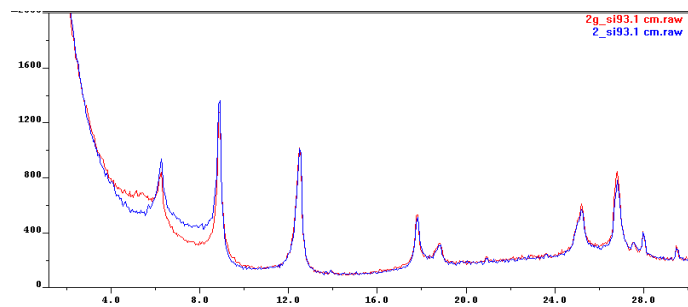
Outcrop photo



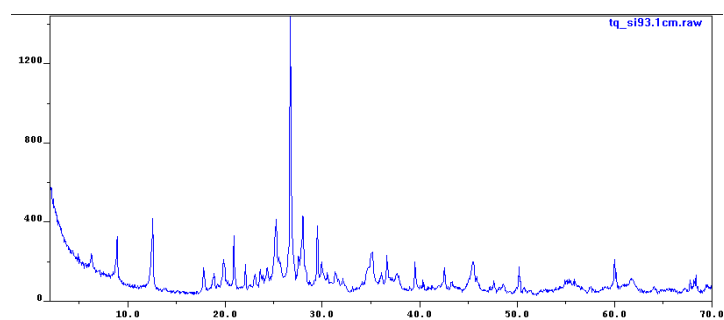
Vitrinite reflectance  
histogram.  
VR<sub>o</sub>% (n.  
measurements):  
0.45±0.05 (61)



Diffraction patterns in  
the <2-μm grain-size  
fraction.  
% I in I/S (R parameter):  
50 (R0)



Whole rock diffraction  
pattern

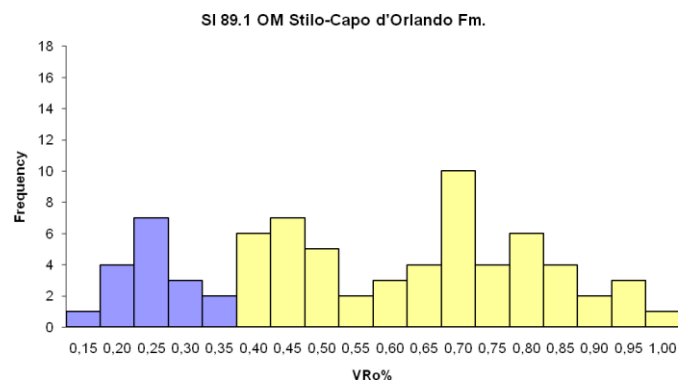


**SI 89.1 (60)**

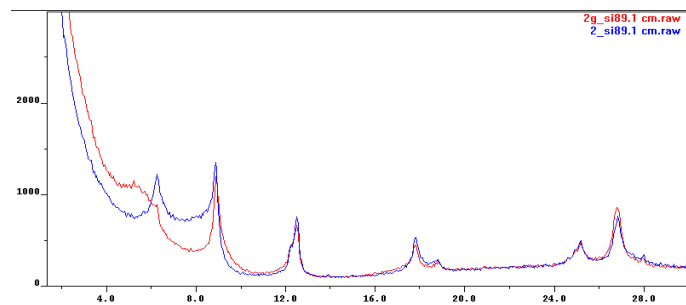
Outcrop photo



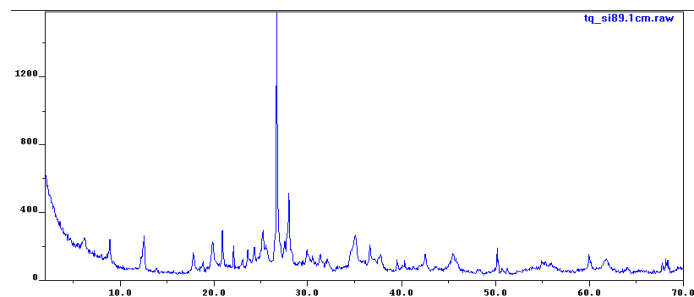
Vitrinite reflectance  
histogram.  
 $VR_o\%$  (n.  
measurements):  
 $0.28 \pm 0.06$  (17)



Diffraction patterns in  
the <2- $\mu$ m grain-size  
fraction.  
% I in I/S (R parameter):  
38; 70 (R0; R1)



Whole rock diffraction  
pattern



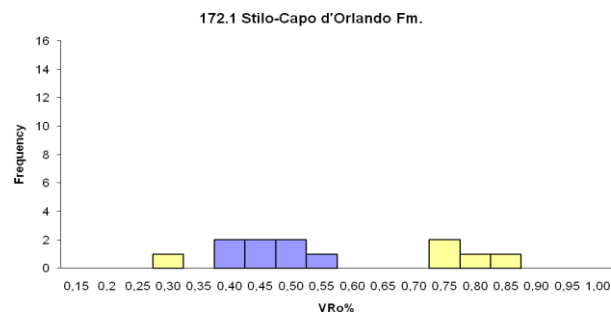
**SI 172.1**

Outcrop photo



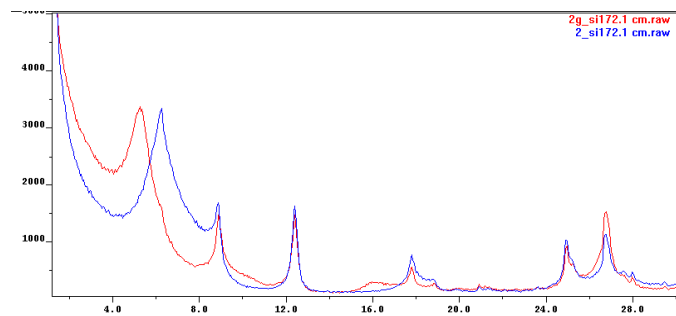
Vitrinite reflectance  
histogram.

VR<sub>o</sub>% (n.  
measurements):  
0.49±0.06 (7)

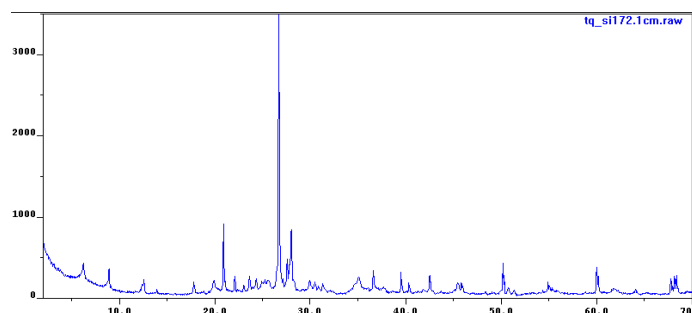


Diffraction patterns in  
the <2-μm grain-size  
fraction.

% I in I/S (R parameter):  
35 (R0)



Whole rock diffraction  
pattern



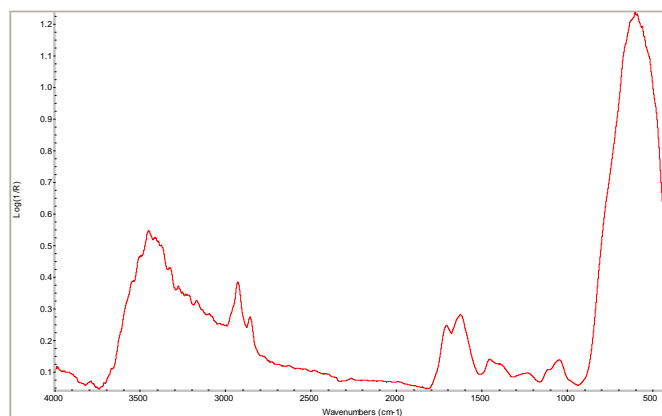


**SECTION II -  
EXTERNAL ZONE  
(MT.JUDICA UNIT)**

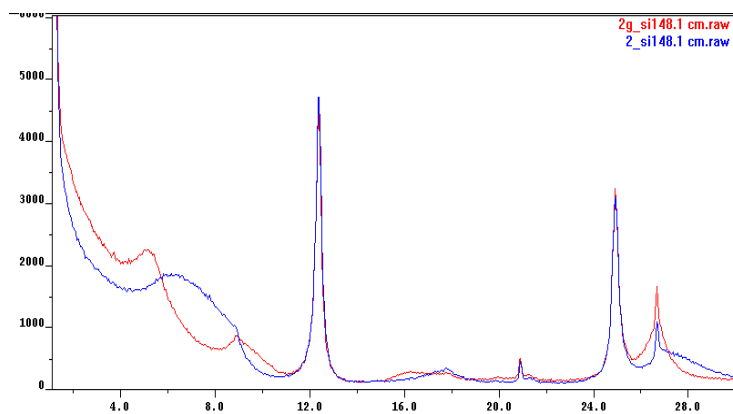
## Clays and glauconitic sandstones

SI 148.1 (11)

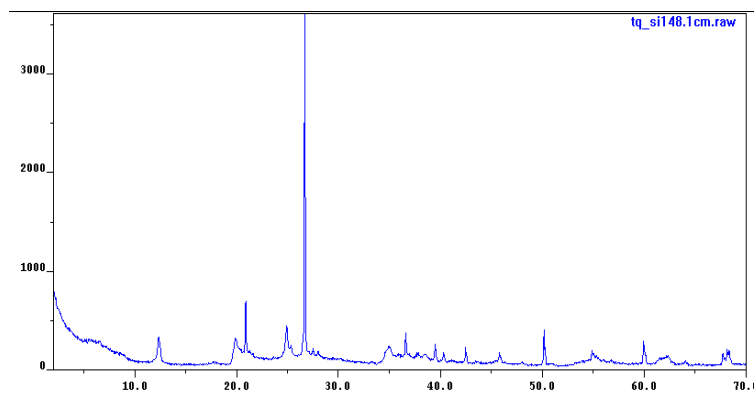
FTIR spectrum



Diffraction patterns in  
the <2- $\mu$ m grain-size  
fraction.  
% I in I/S (R parameter):  
50 (R0)

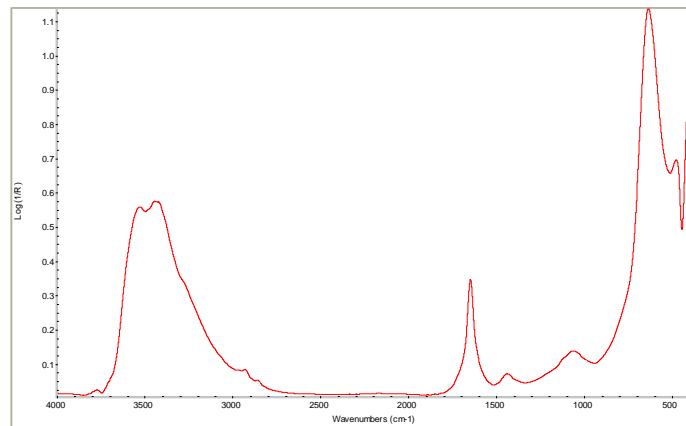


Whole rock diffraction  
pattern

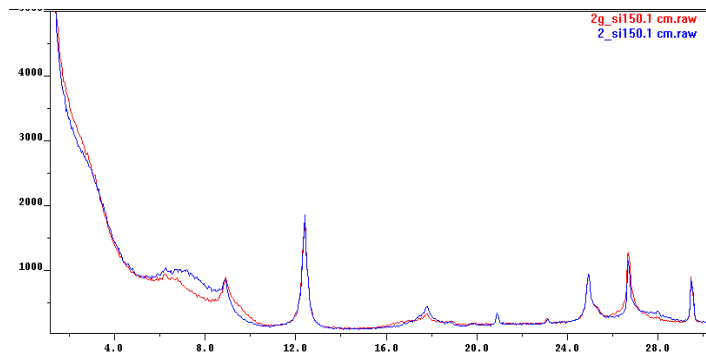


**SI 150.1 (23)**

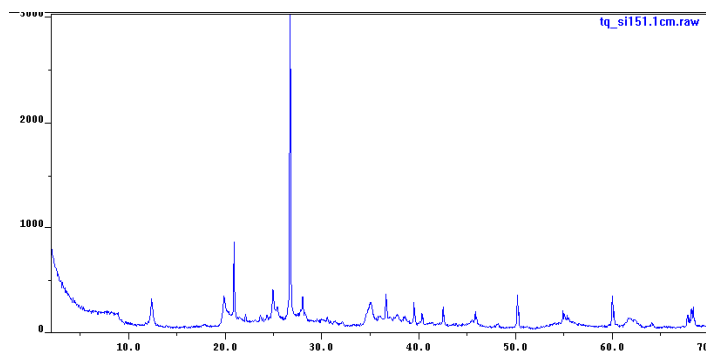
FTIR spectrum



Diffraction patterns in  
the <2- $\mu$ m grain-size  
fraction.  
% I in I/S (R parameter):  
67 (R1)



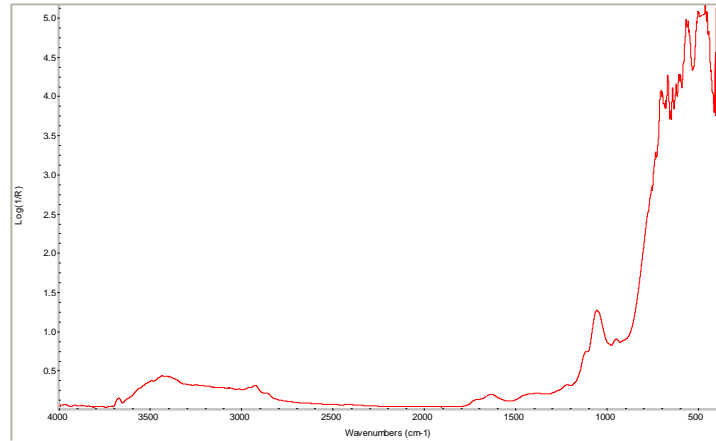
Whole rock diffraction  
pattern



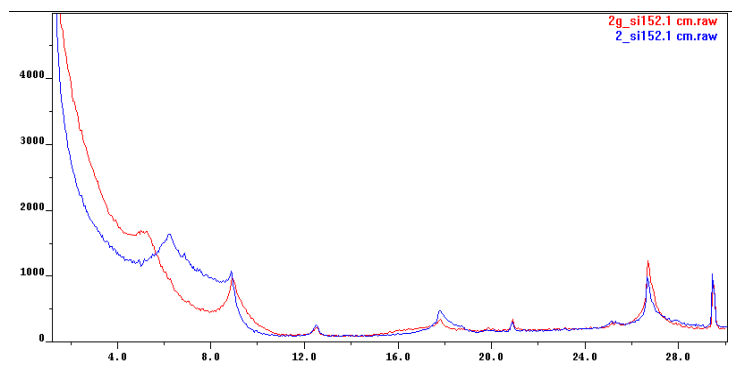
## Cherty limestones

SI 152.1 (20)

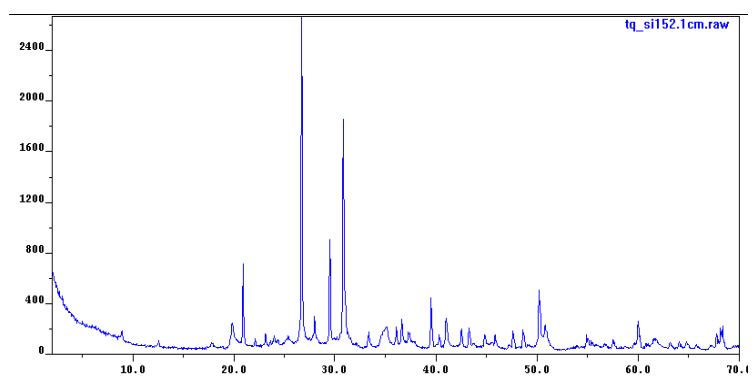
FTIR spectrum



Diffraction patterns in  
the <2- $\mu$ m grain-size  
fraction.  
% I in I/S (R parameter):  
55 (R0/R1)



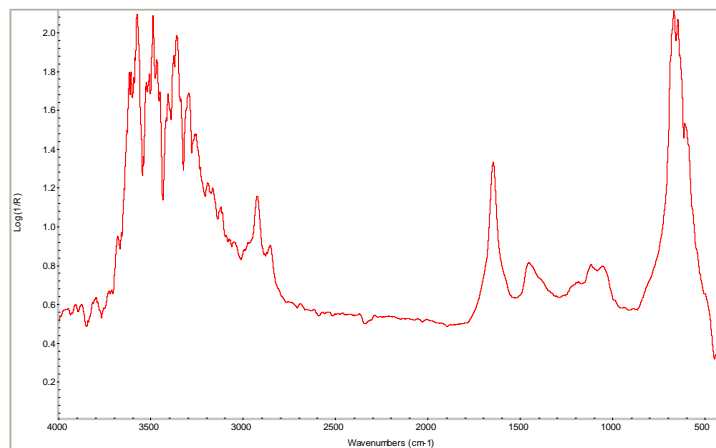
Whole rock diffraction  
pattern



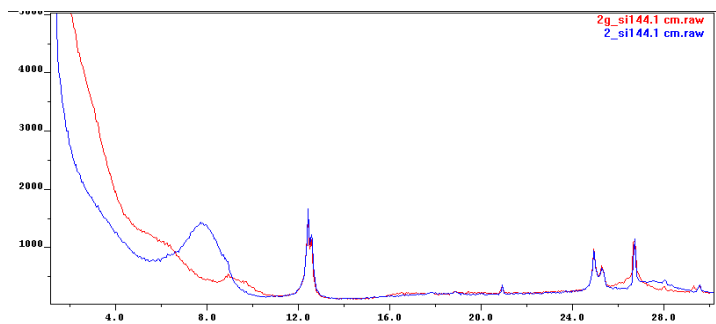
## Mufara Fm

### SI 143.1 (4a)

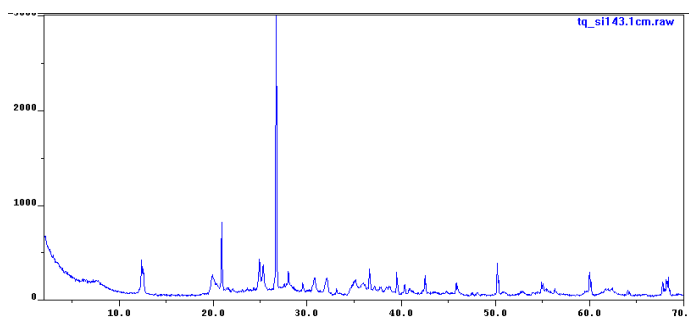
FTIR spectrum



Diffraction patterns in  
the <2- $\mu$ m grain-size  
fraction.  
% I in I/S (R parameter):  
55 (R0/R1)



Whole rock diffraction  
pattern

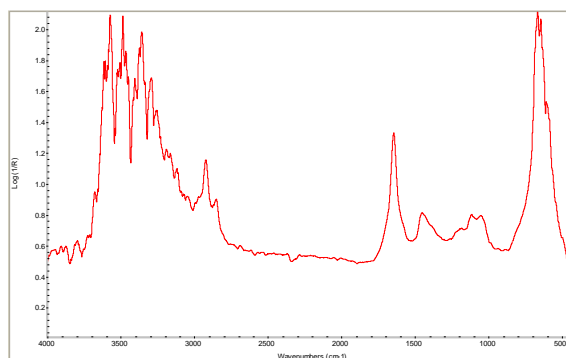


SI 144.1 (4b)

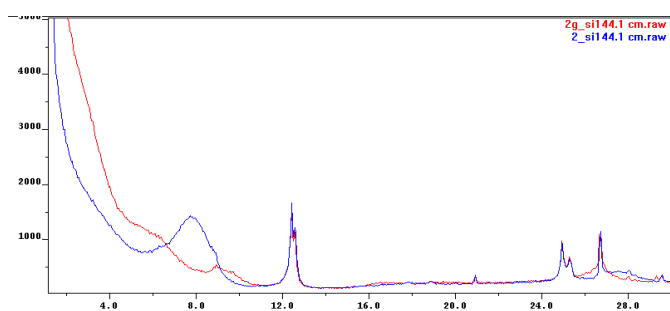
Outcrop photo



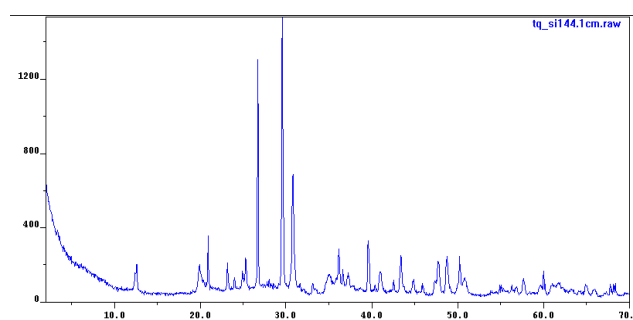
FTIR spectrum



Diffraction patterns in  
the <2- $\mu$ m grain-size  
fraction.  
% I in I/S (R parameter):  
75 (R1)

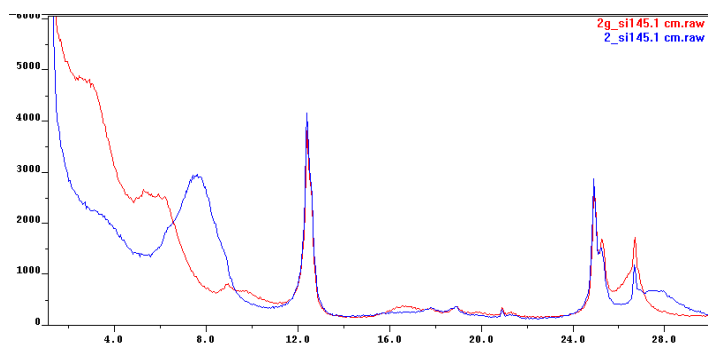


Whole rock diffraction  
pattern

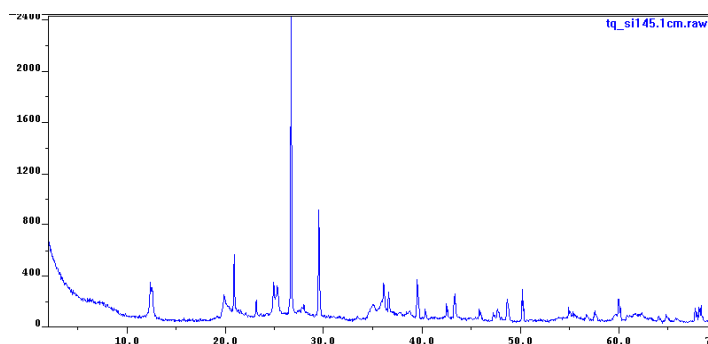


### SI 145.1 (4c)

Diffraction patterns in  
the <2- $\mu$ m grain-size  
fraction.  
% I in I/S (R parameter):  
75 (R1)

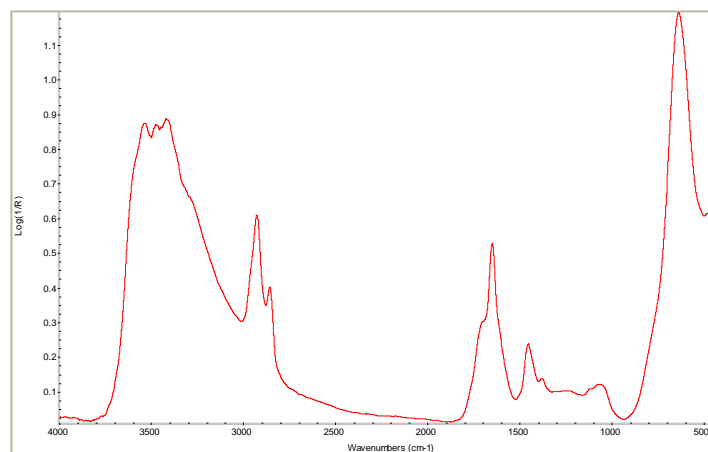


Whole rock diffraction  
pattern



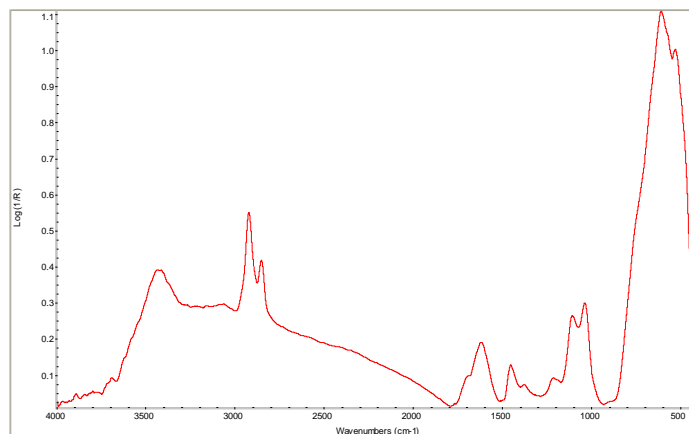
### SI 146.1 OM (5)

FTIR spectrum

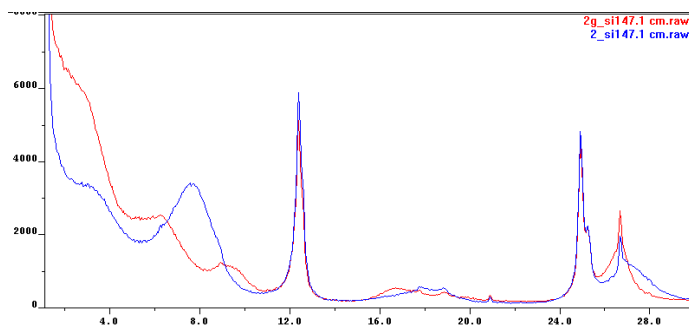


SI 147.1 (6a)

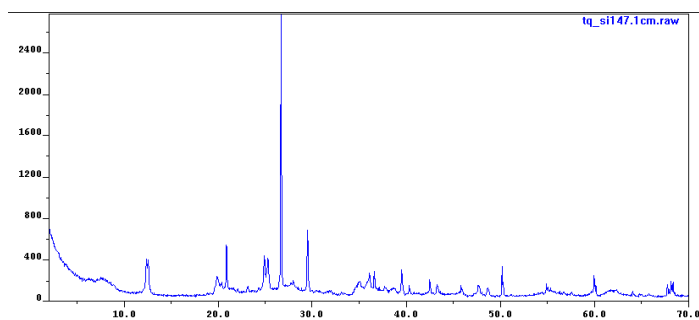
FTIR spectrum



Diffraction patterns in  
the <2- $\mu$ m grain-size  
fraction.  
% I in I/S (R parameter):  
76 (R1)



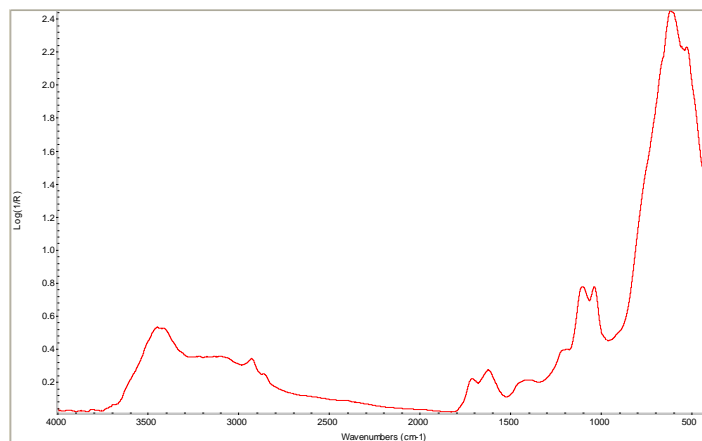
Whole rock diffraction  
pattern



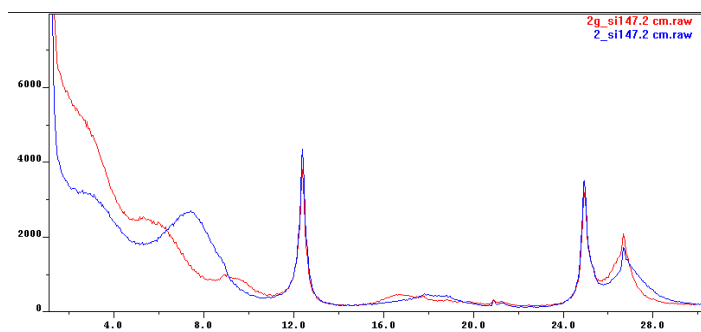


SI 147.2 (6b)

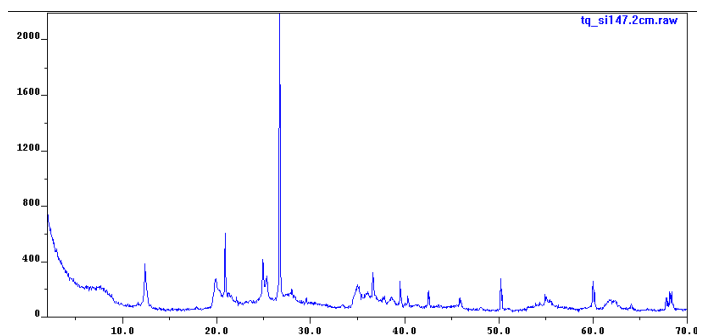
FTIR spectrum



Diffraction patterns in  
the <2- $\mu$ m grain-size  
fraction.  
% I in I/S (R parameter):  
76 (R1)

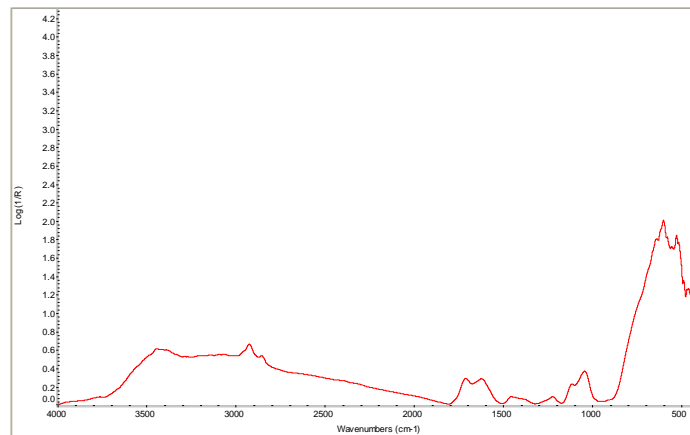


Whole rock diffraction  
pattern

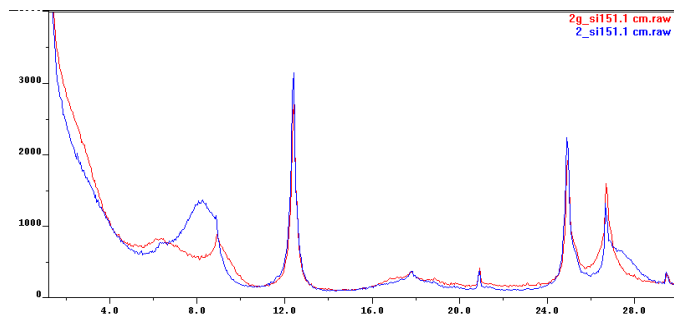


SI 151.1 CM (24a)

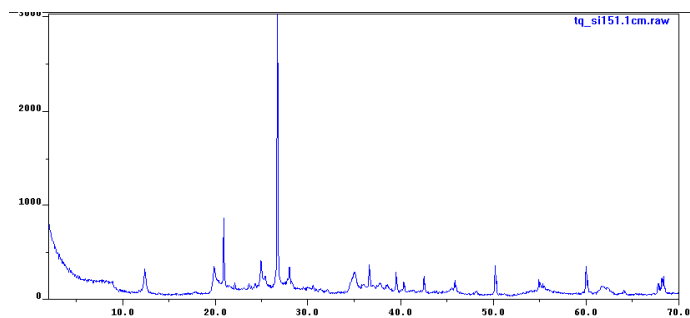
FTIR spectrum



Diffraction patterns in  
the <2- $\mu$ m grain-size  
fraction.  
% I in I/S (R parameter):  
73 (R1)

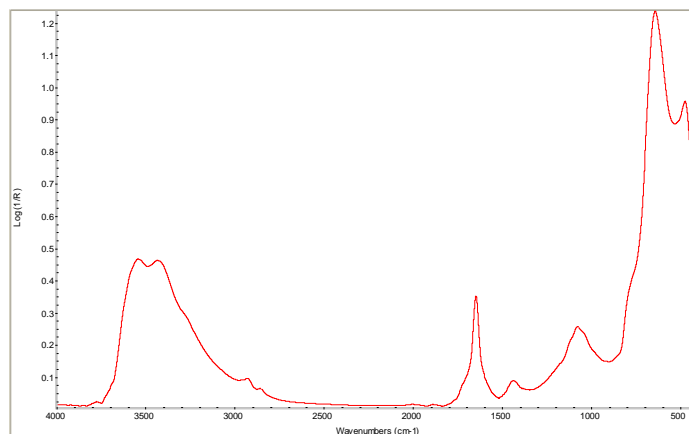


Whole rock diffraction  
pattern

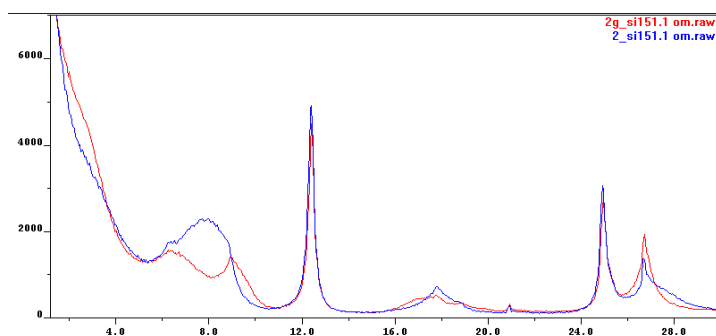


## SI 151.1 OM (24b)

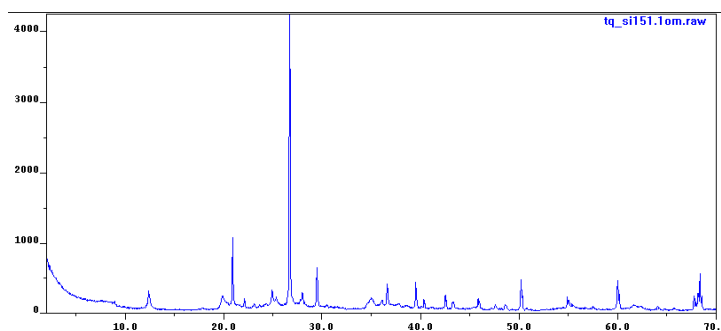
FTIR spectrum



Diffraction patterns in  
the <2-μm grain-size  
fraction.  
% I in I/S (R parameter):  
76 (R1)



Whole rock diffraction  
pattern



**SECTION III -  
EARLY  
FOREDEEP  
DEPOSITS  
(NUMIDIAN  
FLYSCH)**

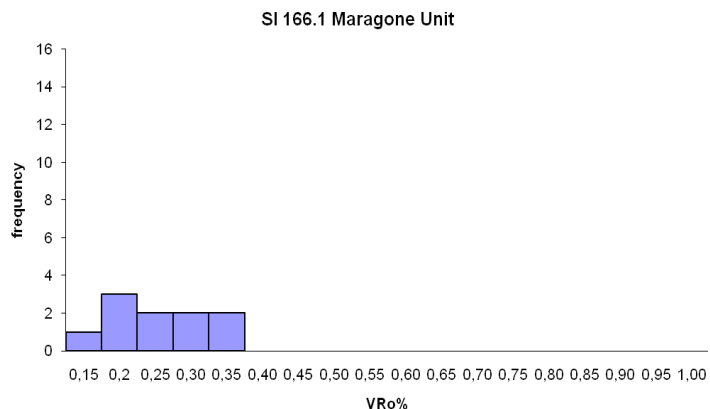
## Maragone Unit

### Numidian Flysch

#### SI 166.1

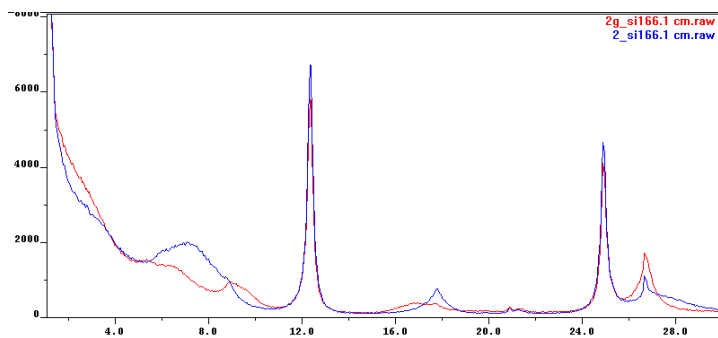
Vitrinite reflectance  
histogram.

VR<sub>o</sub>% (n.  
measurements):  
0.27±0.07 (10)



Diffraction patterns in  
the <2-μm grain-size  
fraction.

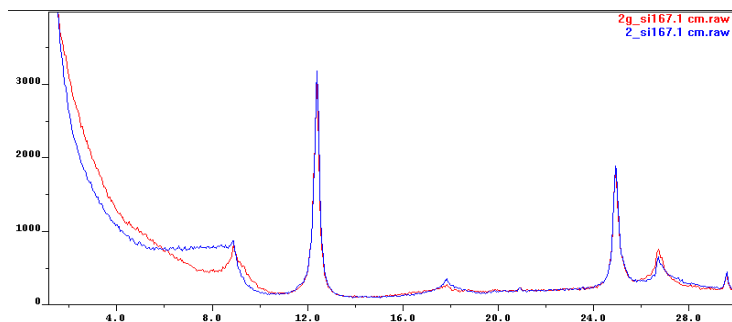
% I in I/S (R parameter):  
71 (R1)



#### SI 167.1

Diffraction patterns in  
the <2-μm grain-size  
fraction.

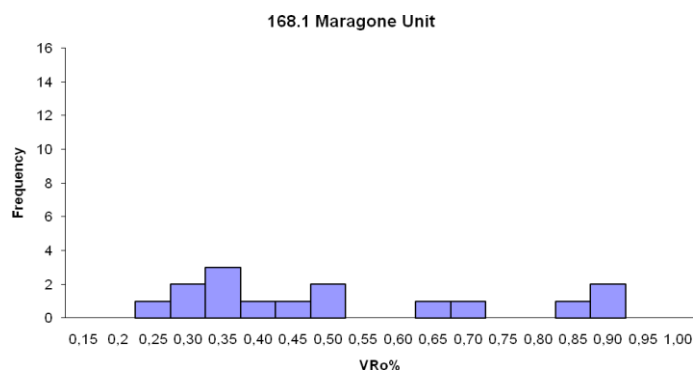
% I in I/S (R parameter):  
67 (R1)



### SI 168.1

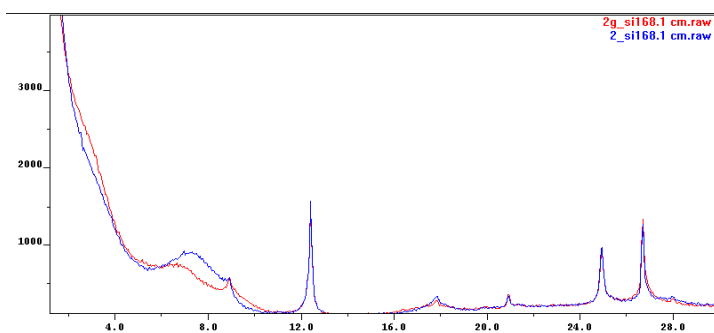
Vitrinite reflectance  
histogram.

VR<sub>o</sub>% (n.  
measurements):  
0.40±0.09 (10)



Diffraction patterns in  
the <2-μm grain-size  
fraction.

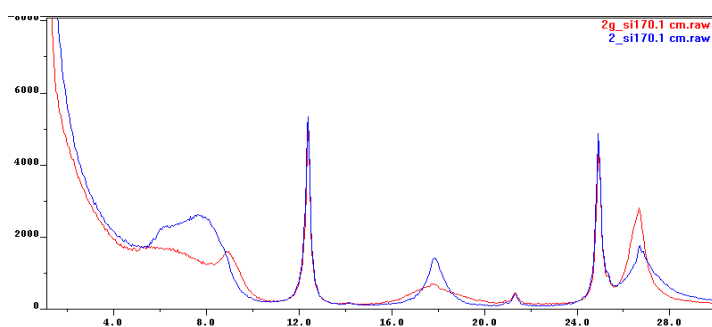
% I in I/S (R parameter):  
71 (R1)



### SI 170.1

Diffraction patterns in  
the <2-μm grain-size  
fraction.

% I in I/S (R parameter):  
66 (R1)

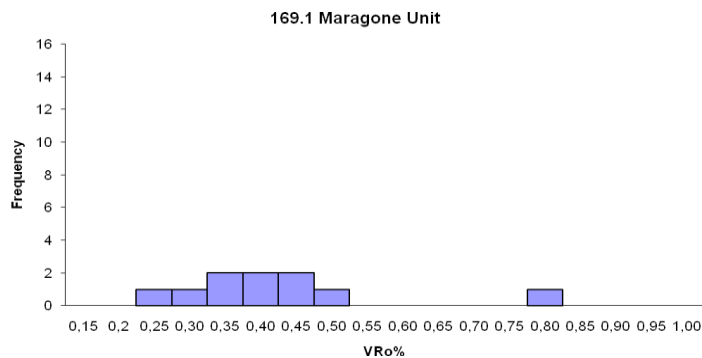


**Argille di Portella  
Mandarinini**

**SI 169.1**

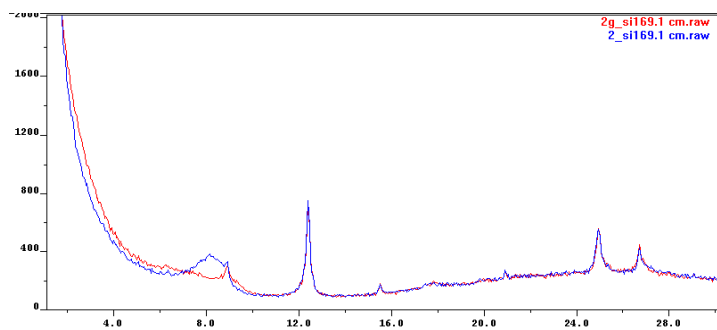
Vitrinite reflectance  
histogram.

VR<sub>o</sub>% (n.  
measurements):  
0.40±0.07 (9)



Diffraction patterns in  
the <2-μm grain-size  
fraction.

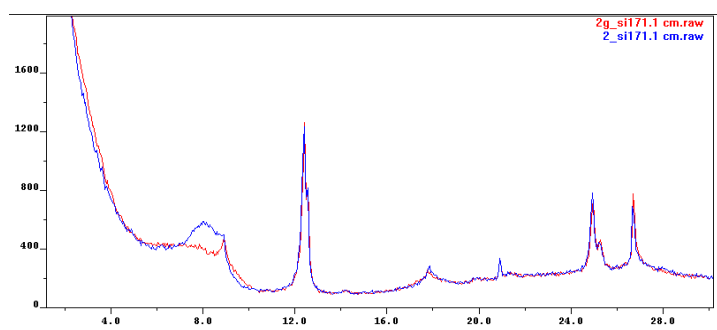
% I in I/S (R parameter):  
71 (R1)



**SI 171.1**

Diffraction patterns in  
the <2-μm grain-size  
fraction.

% I in I/S (R parameter):  
79 (R1)

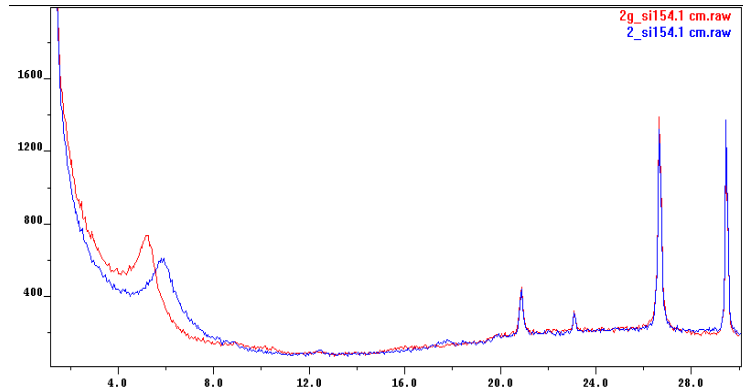


## Nicosia Unit

### Numidian Flysch

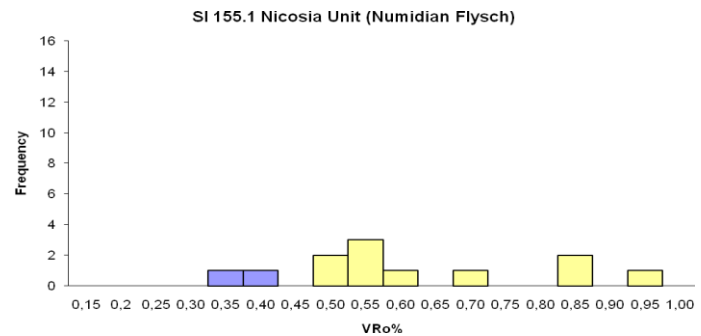
#### SI 154.1 (2)

Diffraction patterns in  
the <2- $\mu$ m grain-size  
fraction.  
% I in I/S (R parameter):  
20 (R0)



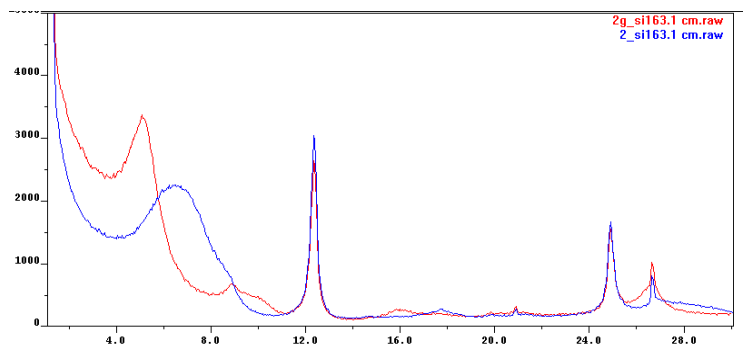
#### SI 155.1 (2)

Vitrinite reflectance  
histogram.  
VR<sub>0</sub>% (n.  
measurements):  
0.41±0.02 (2)



#### SI 163.1 (5)

Diffraction patterns in  
the <2- $\mu$ m grain-size  
fraction.  
% I in I/S (R parameter):  
35 (R0)



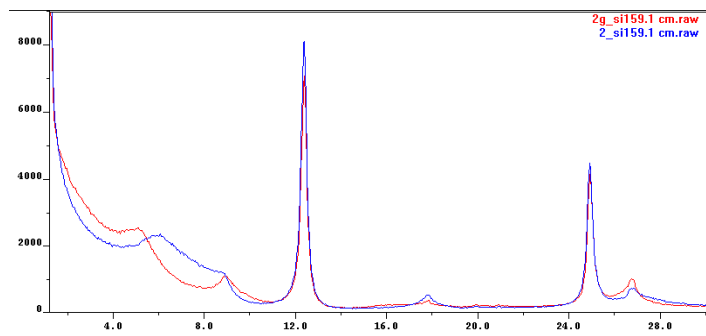


**SI 159.1 OM (3)**

Outcrop photo



Diffraction patterns in  
the <2- $\mu$ m grain-size  
fraction.  
% I in I/S (R parameter):  
40; 65 (R0; R1)



## Argille Varicolori

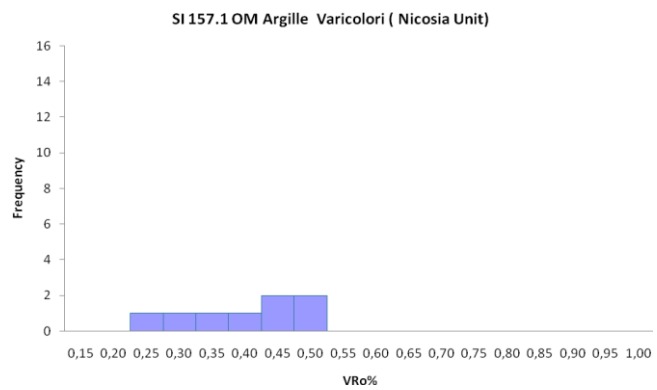
### SI 157.1 OM (3)

Outcrop photo

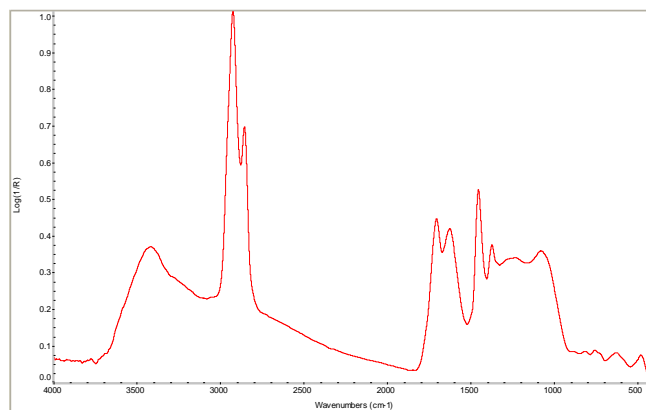


Vitrinite reflectance  
histogram.

VR<sub>o</sub>% (n.  
measurements):  
0.42±0.09 (8)



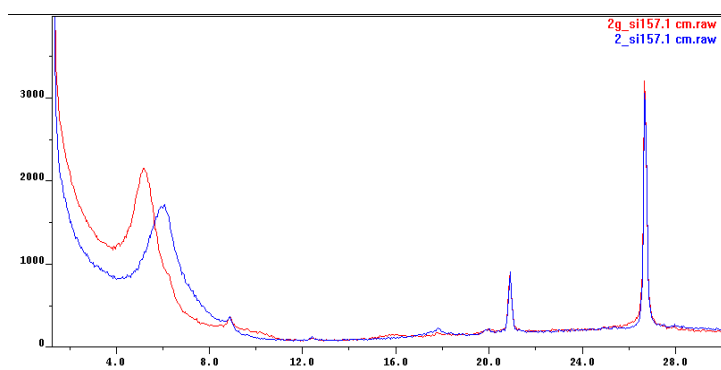
FTIR spectrum



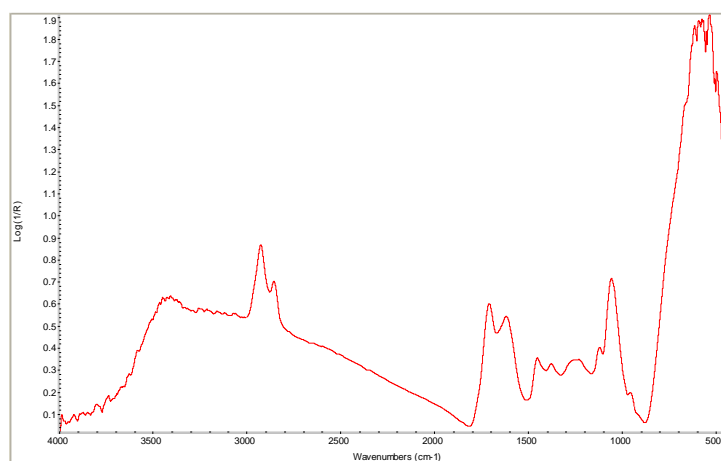
### SI 157.1 CM (3)

Diffraction patterns in  
the <2- $\mu\text{m}$  grain-size  
fraction.

% I in I/S (R parameter):  
40; 65 (R0; R1)



### FTIR spectrum



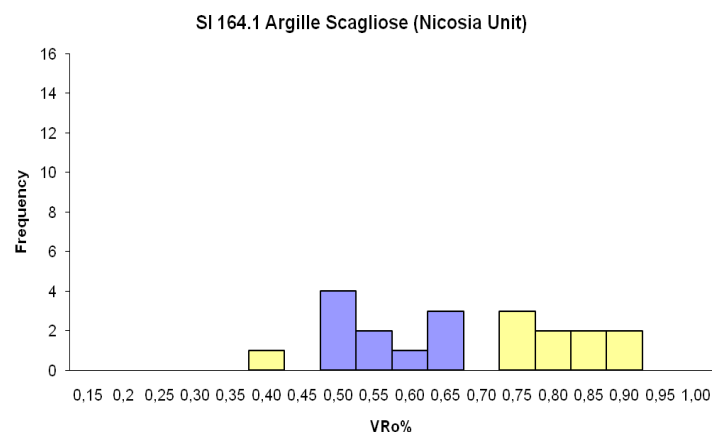
## Argille Scagliose

### SI 164.1 OM (4)

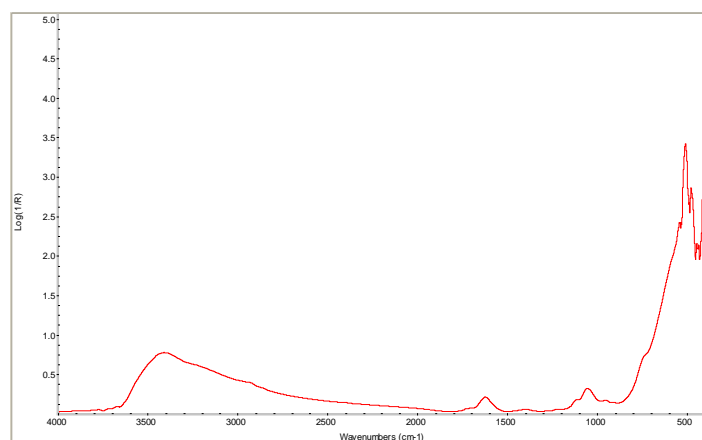
Outcrop photo



Vitrinite reflectance  
histogram.  
VR<sub>o</sub>% (n.  
measurements):  
0.59±0.07 (10)



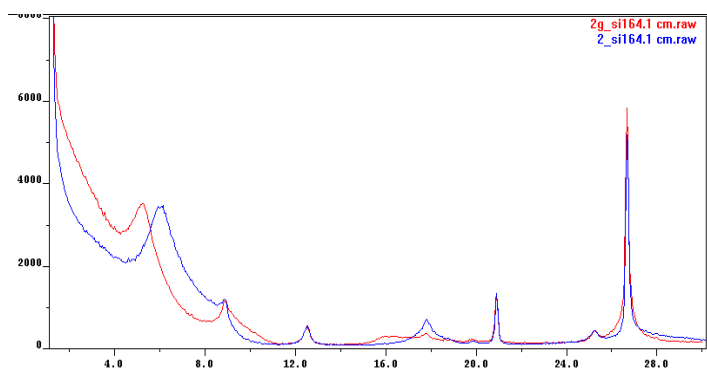
FTIR spectrum



### SI 164.1 CM (4)

Diffraction patterns in the <2- $\mu$ m grain-size fraction.

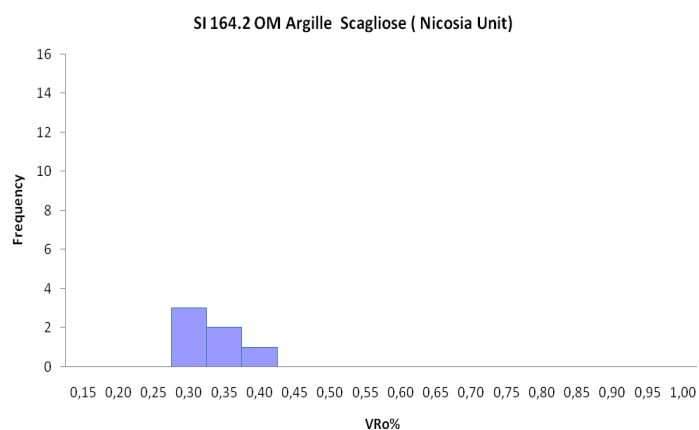
% I in I/S (R parameter):  
50 (R0)



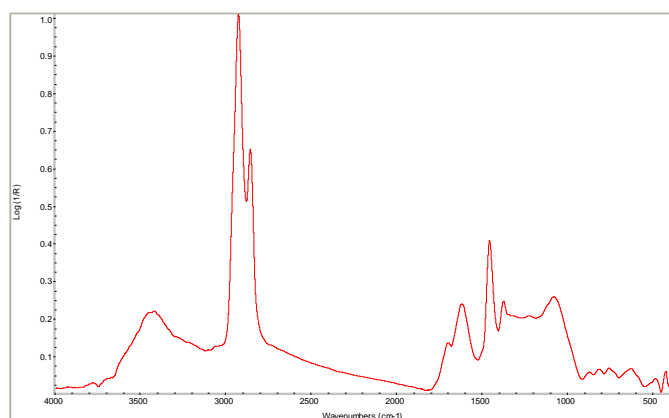
### SI 164.2 OM (4)

Vitrinite reflectance histogram.

VR<sub>o</sub>% (n.  
measurements):  
0.36±0.04 (6)



### FTIR spectrum

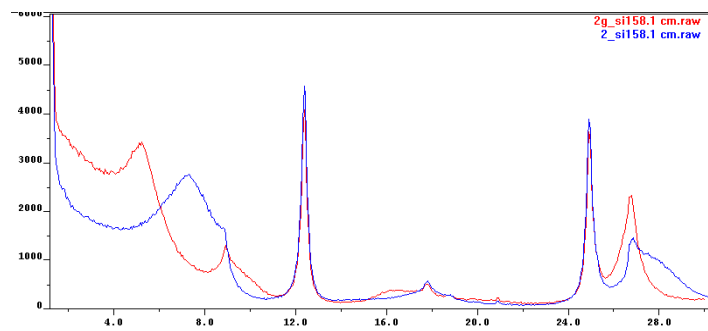


SI 158.1 (1)

Outcrop photo



Diffraction patterns in  
the <2- $\mu$ m grain-size  
fraction.  
% I in I/S (R parameter):  
50 (R0)



FTIR spectrum

